VARYING MASS MISSILE DYNAMICS, GUIDANCE & CONTROL

A THESIS SUBMITTED TO
THE GRADUATE SCHOOL OF NATURAL AND APPLIED SCIENCES
OF
MIDDLE EAST TECHNICAL UNIVERSITY

BY

YAKUP GÜNBATAR

IN PARTIAL FULFILLMENT OF THE REQUIREMENTS FOR THE DEGREE
OF
MASTER OF SCIENCE
IN
ELECRICAL and ELECTRONICS ENGINEERING

SEPTEMBER 2007

Approval of the thesis:

VARYING MASS MISSILE DYNAMICS, GUIDANCE & CONTROL

submitted by YAKUP GÜNBATAR in partial fulfillment of the requirements for the degree of **Master of Science in Electrical and Electronics Engineering Department, Middle East Technical University** by,

Prof. Dr. Canan Özgen _____
Dean, Graduate School of **Natural and Applied Sciences**

Prof. Dr. İsmet ERKMEN _____
Head of the Department, **Electrical and Electronics Engineering**

Prof. Dr. Kemal Leblebicioğlu _____
Supervisor, **Electrical and Electronics Engineering Dept., METU**

Examining Committee Members:

Prof. Dr. Ersin Tulunay _____
Electrical and Electronics Engineering Dept., METU

Prof. Dr. Kemal Leblebicioğlu _____
Electrical and Electronics Engineering Dept., METU

Prof. Dr. Uğur Halıcı _____
Electrical and Electronics Engineering Dept., METU

Assoc. Prof. Volkan Nalbantoğlu _____
Aerospace Engineering Dept., METU

Assist. Prof. Dr. Ilkay Ulusoy _____
Electrical and Electronics Engineering Dept., METU

Date: _____

I hereby declare that all information in this document has been obtained and presented in accordance with academic rules and ethical conduct. I also declare that, as required by these rules and conduct, I have fully cited and referenced all material and results that are not original to this work.

Name, Last name : Yakup, GÜNBATAR

Signature :

ABSTRACT

VARYING MASS MISSILE DYNAMICS, GUIDANCE & CONTROL

Günbatar, Yakup

M.S., Department of Electrical and Electronics Engineering

Supervisor: Prof. Dr. Kemal Leblebicioğlu

September 2007, 150 pages

The focus of this study is to be able to control the air-to-surface missile throughout the entire flight, with emphasis on the propulsion phase to increase the impact range of the missile.

A major difficulty in controlling the missile during the propulsion phase is the important change in mass of the missile. This results in sliding the center of gravity (cg) point and changing inertias. Moreover, aerodynamic coefficients and stability derivatives are not assumed to be constant at predetermined ranges; conversely, they depend on Mach number, angle of attack, and side slip angle. Consequently, as the change of missile mass, cg point, inertia terms, and stability and aerodynamic coefficients come together apart from flight operation stages**,** a great number of points need to be taken into account when designing the controller. This makes controlling the missile all the more complicated.

In this thesis, first the equations of motion are derived, in which, mass of the missile is not assumed constant. Thus, not only the variation of mass but also the variation of inertias is incorporated in the equations of motion. From the derived

equations of motion, a nonlinear inverse dynamics controller that can achieve desired guidance for a conceptually developed air-to-surface missile has been designed, tested and verified for a modeled missile with six degrees of freedom. For brevity of the study, conceptual design and aerodynamic calculations are not given in detail. Nevertheless, improvements for conceptual design are suggested.

As a result, it is shown that the controller works efficiently: the missile is able to hit the target with less than 12 m circular error of probability (CEP). Finally, studies and improvements are proposed.

Keywords: Guidance, control, missile

ÖZ

DEĞİŞKEN KÜTLELİ FÜZENİN DİNAMİĞİ, GÜDÜMÜ & KONTROLÜ

Günbatar, Yakup

M.S., Department of Electrical and Electronics Engineering

Supervisor : Prof. Dr. Kemal Leblebicioğlu

Eylül 2007, 150 sayfa

Bu çalışmanın konusu, havadan yere füzenin tüm uçusu boyunca, özellikle motor yanması aşamasında kontrolünü sağlamak ve bu şekilde hedefi imha edebileceği olası alanı genişletmektir.

Motorun yanması aşamasında füzenin kontrolünde karşılaşılan temel zorluk, bu sırada kütlede meydana gelen önemli değişimdir. Bunun sonucu olarak füzenin ağırlık merkezi ve eylemsizlik momentleri değişmektedir. Ayrıca, aerodinamik katsayılar ve denge türevleri belirlenen aralıklarda sabit kabül edilmeyip, tersine Mach sayısına, hücum açısına ve yana kayma açısına bağlı olarak değişmektedir. Sonuçta uçuş aşamalarına ek olarak, kütle, ağırlık merkezi, aerodinamik katsayılar ve denge terimleri değişimleri bir araya geldiğinde, kontrol ünitesi dizaynında yüksek sayıda aralığın hesaba katılması gerekmektedir. Bu islem füzenin kontrolünün daha karmaşık hale getirir.

Bu tezde, ilk olarak kütle değişimi ihmal edilmeden hareket denklemleri türetilmiştir. Böylece, kütlenin değişiminin yanında eylemsizlik momentlerinin değişimi de hareket denklemlerinde yerini almaktadır. Türetilen hareket denklemlerinden, tasarlanan havadan karaya füze için arzu edilen güdümü başaran,

doğrusal olmayan, kontrol ünitesi test edilmekte ve onaylanmaktadır. Füzenin modellemesi alti serbestlik dereceli olarak yapılmaktadır. Tezin sadeliği ve odak noktasının kontrol ünitesi olması nedeni ile füzenin kavramsal tasarımı ve aerodinamik katsayıların hesaplanmasında ayrıntıya girilmemiştir. Fakat, kavramsal tasarımla ilgili değerlendirmeler ve iyileştirme tavsiyeleri verilmektedir.

Ulaşılan sonuçlarda görülmektedir ki kontrol ünitesi etkili şekilde çalışmakta akabinde füze, hedefi 12 metreden daha az hata ile vurabilmektedir. Sonuç olarak gerekli iyileştirmeler ve çalışmalar önerilmektedir.

Anahtar Kelimeler: Güdüm, kontrol, füze

To my family, SADIK, AYTEN, SELÇUK, and SERCAN

ACKNOWLEDGEMENTS

I express sincere appreciation to my supervisor Prof. Dr. Kemal Leblebicioğlu for his guidance and support throughout this study. I would like to thank Assoc. Prof. Dr. Uğur Halıcı, Prof. Dr. Ersin Tulunay, Assoc. Prof. Volkan Nalbantoğlu , and Assist. Prof. Dr. Ilkay Ulusoy for serving on my committee.

I would like to thank Kerem Hacıkamiloğlu for helping on three dimensional graphic design of the missile, to Taner Budak for helping on calculating mass properties of the missile, to Bülent Özkan for his comments on missile control methods, and to my ex-coworkers Bayındır Kuran, Dilek Başaran, Deniz Kaya and Kenan Bozkaya for their help and support throughout this thesis.

.

TABLE OF CONTENTS

LIST OF TABLES

LIST OF FIGURES

NOMENCLATURE

b	Span
c	Chord
C_D	Drag coefficient
C_{D_o}	Drag coefficient at zero lift coefficient
C_{D_α}	$\partial C_D / \partial \alpha$
$C_{D_{\dot{\alpha}}}$	$(\partial C_D / \partial \dot{\alpha})(2V_\infty / c)$
$C_{D_{\delta_e}}$	$(\partial C_D / \partial \delta_e)$
C_{D_u}	$\partial C_D / \partial (u / V_\infty)$
C_F	Force coefficient
C_l	Rolling moment coefficient
C_{l_o}	Rolling moment coefficient for zero sideslip angle and zero control surface deflections
C_{l_v}	$(\partial C_l / \partial v)$
C_{l_β}	$(\partial C_l / \partial \beta)$
C_{l_p}	$(\partial C_l / \partial p)(2V_\infty / b)$
C_{l_r}	$(\partial C_l / \partial r)(2V_\infty / b)$
$C_{l_{\delta_r}}$	$(\partial C_D / \partial \delta_r)$

$C_{l_{\delta_a}}$	$\left(\partial C_D / \partial \delta_a\right)$
C_{L_o}	Lift coefficient for zero angle of attack
$C_{L_{\delta_e}}$	$\left(\partial C_L / \partial \delta_e\right)$
C_L	Lift coefficient
C_{L_u}	$\partial C_L / \partial \left(u / V_\infty\right)$
C_{L_α}	$\partial C_L / \partial \alpha$
$C_{L_{\dot{\alpha}}}$	$\left(\partial C_L / \partial \dot{\alpha}\right)\left(2V_\infty / c\right)$
C_{L_q}	$\left(\partial C_L / \partial q\right)\left(2V_\infty / c\right)$
$C_{L_{\max}}$	Maximum lift coefficient
$C_{L_{trim}}$	Trim lift coefficient
C_m	Pitching moment coefficient
C_{m_o}	Pitching moment coefficient for zero angle of attack
C_{m_u}	$\partial C_m / \partial \left(u / V_\infty\right)$
C_{m_w}	$\partial C_m / \partial w$
$C_{m_{\dot{w}}}$	$\partial C_m / \partial \dot{w}$
C_{m_q}	$\left(\partial C_m / \partial q\right)\left(2V_\infty / c\right)$
$C_{m_{\delta_e}}$	$\left(\partial C_m / \partial \delta_e\right)$
C_n	Yawing moment coefficient

C_{n_o} Yawing moment coefficient for zero sideslip angle and zero control surface deflections

C_{n_v} $\left(\partial C_n / \partial v\right)$

C_{n_β} $\left(\partial C_n / \partial \beta\right)$

C_{n_p} $\left(\partial C_n / \partial p\right)\left(2V_\infty / b\right)$

C_{n_r} $\left(\partial C_n / \partial r\right)\left(2V_\infty / b\right)$

$C_{n_{\delta_a}}$ $\left(\partial C_n / \partial \delta_a\right)$

$C_{n_{\delta_r}}$ $\left(\partial C_n / \partial \delta_r\right)$

C_X Force coefficient along X_B axis

C_{x_o} Force coefficient along X_B axis for zero angle of attack

C_{x_α} $\partial C_x / \partial \alpha$

$C_{x_{\dot\alpha}}$ $\left(\partial C_x / \partial \dot\alpha\right)\left(2V_\infty / c\right)$

C_{x_u} $\partial C_x / \partial \left(u / V_\infty\right)$

C_{x_w} $\partial C_x / \partial w$

$C_{x_{\dot w}}$ $\left(\partial C_x / \partial \dot w\right)\left(2V_\infty / c\right)$

$C_{x_{\delta_e}}$ $\left(\partial C_x / \partial \delta_e\right)$

C_y Side force coefficient

C_{y_o} Side force coefficient for zero sideslip angle and zero control surface deflections

C_{y_v} $\left(\partial C_y / \partial v\right)$

C_{y_β} $\left(\partial C_y / \partial \beta\right)$

C_{y_p} $\left(\partial C_y / \partial p\right)\left(2V_\infty / b\right)$

C_{y_r} $\left(\partial C_y / \partial r\right)\left(2V_\infty / b\right)$

$C_{y_{\delta_r}}$ $\left(\partial C_y / \partial \delta_r\right)$

$C_{y_{\delta_a}}$ $\left(\partial C_y / \partial \delta_a\right)$

C_{z} Force coefficient along Z_B-axis

C_{z_o} Force coefficient along Z_B-axis for zero angle of attack

C_{z_α} $\partial C_z / \partial \alpha$

$C_{z_{\dot\alpha}}$ $\left(\partial C_z / \partial \dot\alpha\right)\left(2V_\infty / c\right)$

C_{z_u} $\partial C_z / \partial \left(u / V_\infty\right)$

C_{z_w} $\partial C_z / \partial w$

$C_{z_{\dot w}}$ $\left(\partial C_z / \partial \dot w\right)\left(2V_\infty / c\right)$

C_{z_q} $\left(\partial C_z / \partial q\right)\left(2V_\infty / c\right)$

$C_{z_{\delta_e}}$ $\left(\partial C_z / \partial \delta_e\right)$

D_O Time derivative operator for the frame $F_O(O)$

D_b	Time derivative operator for the frame $F_b(C)$
$F_{A_x}, F_{A_y}, F_{A_z}$	Aerodynamic force components along $X_B Y_B Z_B$
$F_{T_x}, F_{T_y}, F_{T_z}$	Thrust force components along $X_B Y_B Z_B$
$F_o(O)$	Earth-fixed frame
$F_b(C)$	Body-fixed frame
$\vec{F}$	Force
$\vec{g}$	Acceleration of gravity
h	Altitude
$\breve{\mathrm{J}}_{\mathrm{c}}$	Inertia tensor about center of mass
I_{xx}, I_{yy}, I_{zz}	Aircraft moments of inertia about $X_B Y_B Z_B$
I_{zx}	Aircraft product of inertia about $X_B Y_B Z_B$
$\vec{l}$	Distance vector from aircraft to center of a restricted area
L_A, M_A, N_A	Aerodynamic moment components about $X_B Y_B Z_B$
L_T, M_T, N_T	Thrust moment components about $X_B Y_B Z_B$
m	Aircraft mass
$\vec{M}$	Moment
n	Load factor, the ratio of an external load to the weight of the aircraft
$n_{structural}$	Structural load factor
P, Q, R	Aircraft angular velocity components about $X_B Y_B Z_B$
p, q, r	Perturbed values of P, Q, R

P_{PC}	Pilot command penalty function
P_{CC}	Controller command penalty function
$\vec{r}$	Vector which defines the position of any mass element dm with respect to body-fixed frame
$\vec{r}_p$	Vector which defines the position of any mass element dm with respect to Earth-fixed frame
$\vec{r}_c$	Vector which defines the position of center of the gravity of the aircraft with respect to Earth-fixed frame
r_t	Target radius
q_∞	Dynamic pressure, $q_\infty = 0.5\rho V_\infty^{\ 2}$
R_T	Radius of restricted zone
S	Area
U, V, W	Velocity components of aircraft along $X_B Y_B Z_B$
U_w, V_w, W_w	Wind velocity components along $X_B Y_B Z_B$
u, v, w	Perturbed values of U, V, W
V_∞	Free stream velocity
$\vec{V}_{wind}$	Wind linear velocity
$\vec{V}_{AC}$	Aircraft velocity with respect to inertial frame
$X_E Y_E Z_E$	Earth-fixed frame axes set
$X_B Y_B Z_B$	Body-fixed frame axes set

XY_D	Distance from missile to target on XY plane of Earth-fixed frame
$(X_m, Y_m, Z_m)_E$	Missile coordinates in inertial frame
$(X_t, Y_t, Z_t)_E$	Target coordinates in inertial frame

Greek Symbols

α	Angle of attack
$\dot{\alpha}$	Rate of change of angle of attack
β	Sideslip angle
$\dot{\beta}$	Rate of change of sideslip angle
δ_a	Actual aileron deflection angle
δ_{a_cnd}	Commanded aileron deflection angle
δ_e	Actual elevator deflection angle
δ_{e_cnd}	Commanded elevator deflection angle
δ_r	Actual rudder deflection angle
δ_{r_cnd}	Commanded rudder deflection angle
ρ	Air density
φ	Bank angle command
γ	Flight path angle
γ_{ins}	Instantaneous flight path angle
γ_{des}	Desired flight path angle
Θ	Pitch angle

Φ	Roll angle
Ψ	Yaw angle
$\Psi_{desired}$	Desired yaw angle
Ψ_{ins}	Instantaneous yaw angle

CHAPTER 1

INTRODUCTION

In missile design, especially in the propulsion unit, usage of solid propellant will provide missile with high acceleration, as well as a simpler propulsion unit. Less complex propulsion sections are very important due to the fact that they reduce both the cost and the size of the missile. However, they come out with non-negligible rate of change of missile mass unless the solid propellant has a low burn rate.

Moreover, guided missiles have naturally nonlinear dynamics because of inertial coupling, aerodynamic effects, and gravitational forces. Therefore, linear autopilots which are designed on linearized dynamics of the vehicle face the nonlinearities that significantly influence these dynamics.

For coherence with the methods, it is necessary to begin with a discussion of a second difficulty, the nonlinear dynamics of the missiles. Much of the studies in literature apply the liner robust control methods with gain scheduling to deal with nonlinearities [1-7]. Implementation of gain scheduling methodology to autopilot design is based on determination of the group of constant operating points, designing a family of linear autopilots corresponding to each constant operating point, and finally building a gain scheduled autopilot that linearizes to the proper linear autopilot. This can actually be called a nonlinear control since the outcome is a nonlinear closed loop feedback system. The use of a nonlinear controller to cope with nonlinearities was encouraged in the early 1980's by Hunt, Su, and Meyer who showed the successful execution of dynamic inversion for flight control [8]. In this study, dynamic inversion was used to get feedback linearization of the nonlinear system. Lane and Stengel developed flight controllers for maneuvers via several sets of desired output variables that were based on dynamic inversion [9]. Moreover, Azam and Singh designed a nonlinear controller for simultaneous lateral and longitudinal

maneuvers [10]. In the early 1990's, studies on nonlinear control designs accelerated. Many studies have since been conducted, some of which are based on nonlinear optimal control method by using the solutions to Hamilton-Jacobi-Bellman (HJB) and Hamilton-Jacobi-Isaacs (HJI) equations [11,12]. In the later study mentioned feedback controllers are designed by full nonlinear dynamics of the system. There is no linearization involved and optimal controllers are acquired by the numerical solution of the Hamilton-Jacobi-Bellman equation. The main contribution of the use of a nonlinear controller is to widen the stability boundaries and to improve the precision.

The first challenge, rate of change of mass of the missile, explained previously can be taken into account via various different approaches. One of these is the initiation of the autopilot after burn-out. This is a very common method and extensively used. The main disadvantage of this method comes to light when the target is at a distance shorter than burn-out distance. For a 2.75" anti-tank missile burn-out distance is about 1.5 km. For a stand-off missile with 100 km range it can be approximated from 40-60 km. What is obvious from these burn-out distances is that these two missiles are not capable of hitting the targets at a distance less than corresponding burn-out distances unless they are fired exactly towards the targets with the assumption that their paths are not disturbed. Another approach is generating a huge family of linear autopilots from an immense collection of point designs for every flight condition and for a series of predetermined mass ranges each of which has a different mass, center of gravity and moment of inertias.

To avoid large numbers of operating points, to broaden the stability borders and to get better the accuracy, a nonlinear dynamic inversion controller is designed and implemented using PID dynamics in this study. The design of the nonlinear controller is similar to the one in [13, 14]. In order to deal with the mass variation, equations of motions are derived without assuming the mass of the vehicle is constant.

In this thesis, equations of motion for the missile are derived that include the rate of change of missile, and inertias. This derivation is explicated in CHAPTER 2. CHAPTER 3 covers the acquiring stability and aerodynamic coefficients via

MISSILE DATCOM. This chapter also gives a brief explanation about the stability derivatives. CHAPTER 4 explores the target, missile, and the guidance section of the study. The following chapter articulates the theory and implementation of the controller that serves for guidance. Nonlinear inverse dynamic controller is derived and implemented by PID controller in this chapter. CHAPTER 6 consists of the simulation results for 6 different cases which are arc, two cruises, and two diving trajectories and one case with moving target. Simulations are carried out in the MATLAB Environment with some of the symbolic derivations are obtained using MAPLE 9.

CHAPTER 2

EQUATIONS OF MOTION

2.1 Equations of motion in general aspect

With the aim of getting a general understanding of aircrafts, equations of motion are first derived for an aircraft and then modified for the missile involved in this research. Newton's Second law is applied to the aircraft given in the Figure 2-1. In this law, it is stated that time derivative of linear momenta is equal to the externally applied forces, and the time derivative of angular momenta is equal to the externally applied moments.

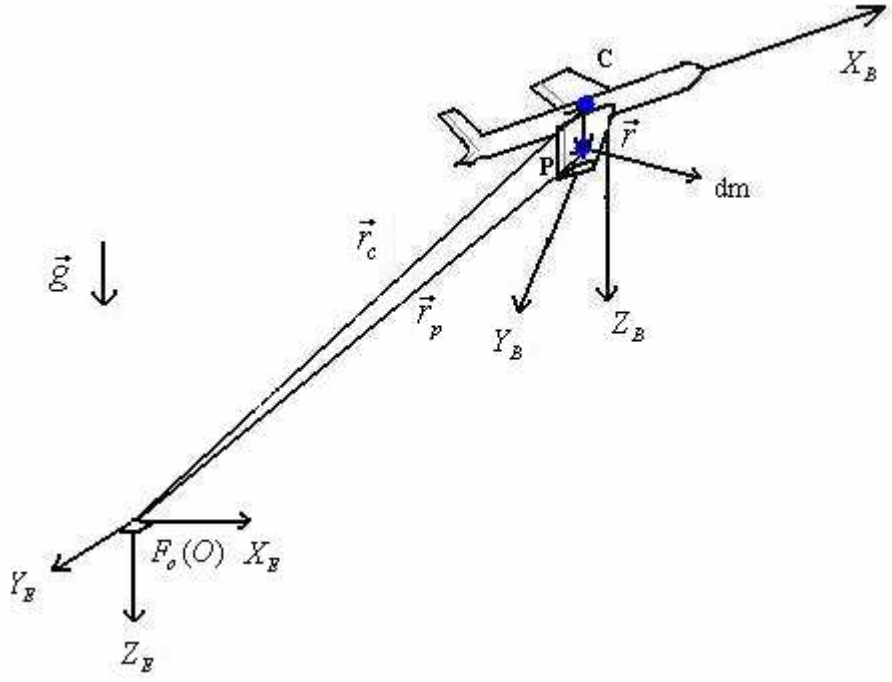

Figure 2-1 Earth and body fixed coordinate systems

where:

- $X_E Y_E Z_E$ is Earth-Fixed axis system
- $X_B Y_B Z_B$ is Body-Fixed axis system

2.1.1 Force Equation

In Figure 2-1, $\vec{r}_p$ connects the origin of $X_E Y_E Z_E$ with each mass element, dm. In the case of aircraft these mass elements hold their distance relative to each other except for the mass elements which are part of rotating machines or part of the fuel. Every mass element is subject to the acceleration of gravity $\vec{g}$ and as seen in Figure 2-1 the vector $\vec{g}$ is directed along the positive Z_E axis. This states the flat Earth assumption. It is convenient to use $\vec{r}$ and $\vec{r}_c$ which form $\vec{r}_p$ as given in Equation(2.1).

$$\vec{r}_p = \vec{r}_c + \vec{r} \tag{2.1}$$

Here, $\vec{r}_p$ is the vector which defines the position of any mass element, dm, with respect to Earth-fixed frame, $X_E Y_E Z_E$, and can alternatively be written as $\vec{r}_{p/o}$. Also, $\vec{r}_c$ is the vector which defines the position of center of the gravity of the aircraft with respect to Earth-fixed frame, $X_E Y_E Z_E$, and can alternatively be written as $\vec{r}_{c/o}$. Additionally, $\vec{r}$ is the vector which defines the position of any mass element, dm, with respect to body-fixed frame, $X_B Y_B Z_B$, and can alternatively be written as $\vec{r}_{p/c}$.

In the time of application of Newton's Second Law, the time derivative of $\vec{r}_p$ is needed. As a result, it is better to find the time derivative of $\vec{r}_p$ with respect to the frame $F_O(O)$.

$$\vec{r}_{p/o} = \vec{r}_{c/o} + \vec{r}_{p/c} \tag{2.2}$$

$$D_O \vec{r}_p = D_O \vec{r}_{c/o} + D_O \vec{r}_{p/c} \tag{2.3}$$

$$D_O \vec{r}_p = \vec{V}_p = \vec{V}_c + D_b \vec{r}_{p/c} + \vec{\omega}_{c/o} \times \vec{r}_{p/c} \tag{2.4}$$

Where D_O and D_b are the time derivative operators for the frame $F_O(O)$ and $F_b(C)$ respectively. $\vec{V}_p$ is the velocity of the point p (mass element, dm) on the aircraft, $\vec{V}_c$ is the velocity of the CG (center of gravity) point of the aircraft, and $\vec{\omega}_{c/o}$ the angular velocity of $F_b(C)$ with respect to $F_O(O)$. Since the mass of the aircraft changes with time:

$$D_b \vec{r}_{p/c} \neq 0 \tag{2.5}$$

then:

$$\vec{V}_p = \vec{V}_c + \vec{\omega}_{c/o} \times \vec{r}_{p/c} + \dot{\vec{r}}_{p/c} = \vec{V}_c + \vec{\omega} \times \vec{r} + \dot{\vec{r}} \tag{2.6}$$

$$\vec{V}_p = \frac{d}{dt}(\vec{r}_p) = D_O \vec{r}_{p/o} \tag{2.7}$$

Newton's Second Law states that [15]:

$$\frac{\mathrm{d}}{\mathrm{dt}}(\text{Angular Momenta}) = \text{Externally Applied Moments} \tag{2.8}$$

$$\frac{\mathrm{d}}{\mathrm{dt}}(\text{Linear Momenta}) = \text{Externally Applied Forces} \tag{2.9}$$

Equation (2.10) can be expanded as follows:

$$\frac{d}{dt}\left[\int_v \vec{V}_p \rho dv\right] = \int_v \rho \vec{g} dv + \int_S \vec{F} ds \tag{2.11}$$

Where, $\int_v dv$ and $\int_S ds$ are volume integral and surface integral respectively and $\vec{F}$ is the combination of aerodynamic and thrust force to which the aircraft is exposed:

$$\vec{F} = \vec{F}_A + \vec{F}_T \tag{2.12}$$

When Equations (2.2) and (2.7) are inserted in to Equation (2.11), the left hand side of the Equation (2.11) becomes:

$$\frac{d}{dt}\left(\int_v \frac{d}{dt}(\vec{r}_c + \vec{r})\rho dv\right) = \frac{d}{dt}\frac{d}{dt}\left[\int_v \vec{r}_c \rho dv + \int_v \vec{r} \rho dv\right] \tag{2.13}$$

Where $\int_v \vec{r}\,\rho dv = 0$, since the point C is the center of mass. Therefore, Equation (2.13) yields:

$$\frac{d}{dt}\left(\int_v \frac{d}{dt}(\vec{r}_c)\rho dv\right) = \frac{d}{dt}\left[\int_v \frac{d}{dt}(\vec{r}_c)\,\rho dv\right] \tag{2.14}$$

then:

$$\frac{d}{dt}\left[m\vec{V}_c\right] = m\dot{\vec{V}}_c + \dot{m}\vec{V}_c \tag{2.15}$$

The left hand side of the Equation (2.11) can be written as follows:

$$\int_v \rho\vec{g}dv + \int_S \vec{F}ds = m\vec{g} + \vec{F}_A + \vec{F}_T \tag{2.16}$$

Finally, as Equations (2.15) and (2.16) are put into (2.11) Equation (2.17) is obtained:

$$\boxed{m\dot{\vec{V}}_c + \dot{m}\vec{V}_c = m\vec{g} + \vec{F}_A + \vec{F}_T} \tag{2.17}$$

2.1.2 Moment equation

In this section, the moment equation is derived via Equation(2.8). The left hand side of this equation is equal to:

$$\frac{d}{dt}\left(Angular\ Momenta\right) = \frac{d}{dt}\left[\int_v (\vec{r}_c + \vec{r})\times\rho\vec{V}_p dv\right] \tag{2.18}$$

$$\frac{d}{dt}\left(Angular\ Momenta\right) = \frac{d}{dt}\left[\int_v \vec{r}_c\times\vec{V}_p\rho dv + \int_v \vec{r}\times\vec{V}_p\rho dv\right] \tag{2.19}$$

where:

$$\vec{V}_p = \vec{V}_c + \frac{d}{dt}\vec{r} \quad D_O\vec{r} = \frac{d}{dt}\vec{r} \tag{2.20}$$

Then, Equation (2.19) takes the form:

$$\frac{d}{dt}\left(Angular\ Momenta\right) = \frac{d}{dt}\left[\int_v \vec{r}_c\times\vec{V}_p\rho dv\right] + \frac{d}{dt}\left[\int_v \vec{r}\times\left(\vec{V}_c + \frac{d}{dt}\vec{r}\right)\rho dv\right] \tag{2.21}$$

$\vec{V}_c$ is independent of the integral since C is the center of mass. Change of angular momentum would then yield the equation as below:

$$\frac{d}{dt}\left[\int_v \vec{r}_c \times \vec{V}_p \rho dv\right] + \frac{d}{dt}\left[\left(\int_v \vec{r}\,\rho dv\right)\times \vec{V}_c + \int_v \vec{r} \times \frac{d}{dt}\vec{r}\,\rho dv\right] \tag{2.22}$$

$$\int_v \vec{r}\,\rho dv = 0 \tag{2.23}$$

Therefore, the left hand side of Equation (2.8) takes the form as given in Equation (2.24).

$$\frac{d}{dt}\left(\textit{Angular Momenta}\right) = \frac{d}{dt}\left[\int_v \vec{r}_c \times \vec{V}_p \rho dv\right] + \frac{d}{dt}\left[\int_v \vec{r} \times \frac{d}{dt}\vec{r}\,\rho dv\right] \tag{2.24}$$

Meanwhile, the right hand side of Equation (2.8)

$$\text{Externally Applied Moments} = \int_v \vec{r}_p \times \rho \vec{g} dv + \int_S \vec{r}_p \times \vec{F} ds \tag{2.25}$$

When Equation (2.1) is placed into Equation (2.25) the following equation is obtained:

$$\vec{r}_c \times \int_v \rho \vec{g} dv + \left(\int_v \vec{r}\,\rho dv\right)\times \vec{g} + \vec{r}_c \times \int_S \vec{F} ds + \int_S \vec{r} \times \vec{F} ds \tag{2.26}$$

After solving Equation (2.11) for $\int_S \vec{F} ds$ and using Equation (2.23), the right hand side of Equation (2.8) takes the form as given in Equation (2.27).

$$\text{Externally Applied Moments} = \frac{d}{dt}\left[\int_v \vec{r}_c \times \vec{V}_p \rho dv\right] + \int_S \vec{r} \times \vec{F} ds \tag{2.27}$$

Placing Equations (2.24) and (2.27) into Equation (2.8) results in:

$$\boxed{\frac{d}{dt}\left[\int_v \vec{r} \times \frac{d}{dt}\vec{r}\,\rho dv\right] = \int_S \vec{r} \times \vec{F} ds = \vec{M}_A + \vec{M}_T} \tag{2.28}$$

Where $\vec{M}_A$ and $\vec{M}_T$ are total aerodynamic moment vector and total thrust moment vector respectively.

2.1.3 Orientation and position of the aircraft

As seen in the Figure 2-1, the aircraft's orientation and position are given relative to the Earth-fixed frame F_O. Orientation of the aircraft from Earth-fixed

frame F_O to Body-fixed frame F_b is provided by Euler angles composed of three consecutive rotations whose order is (3,2,1) as given in Figure 2-2 and in Equation (2.29). There, F_m and F_n are intermediate frames. Where $\vec{u}_1^{(r)}$ corresponds to the x axis of the F_r frame and $\vec{u}_2^{(r)}$ and $\vec{u}_3^{(r)}$ corresponds to y and z axes respectively of the F_r frame.

$$\begin{array}{ccccccc} & \vec{u}_3^{(o)} & & \vec{u}_2^{(m)} & & \vec{u}_1^{(n)} & \\ F_O & \rightarrow & F_m & \rightarrow & F_n & \rightarrow & F_b \\ & \Psi & & \Theta & & \Phi & \end{array} \tag{2.29}$$

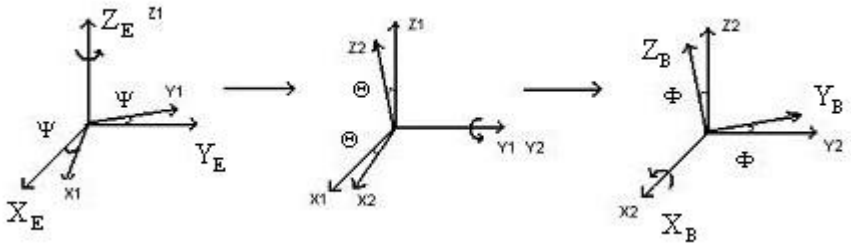

Figure 2-2 Aircraft orientation with Euler angles

First rotation is the rotation of $X_E Y_E Z_E$ coordinate system about its Z_E axis through an angle **Ψ,** called the heading (azimuth) angle. After this rotation, the coordinate system is renamed as $X1Y1Z1$ coordinate system.

Second rotation is the rotation of $X1Y1Z1$ coordinate system about its $Y1$ axis through an angle **Θ,** called the pitch attitude angle. After this rotation, the coordinate system is renamed as $X2Y2Z2$ coordinate system.

Third rotation is the rotation of $X2Y2Z2$ coordinate system about its $X2$ axis through an angle **Φ,** called the roll (or bank) angle. After this rotation, the coordinate system is renamed as $X3Y3Z3$ coordinate system.

There is a problem in using Euler angles when $\Theta = \pm 90°$ since in this case **Φ** bank angle looses its meaning. Also in steady rotation, rolling time variation of **Φ** is discontinuous.

This situation can be overcome by Quaternion method instead of Euler angles. The reason why Euler angles would be used is that they give a more physical picture of the aircraft attitude than the other methods.

Direct cosine matrix is used to transform a vector from one frame to another. Direct cosine matrix from frame F_O to F_m is given as:

$$\hat{C}^{(o,m)} = \begin{bmatrix} \cos\Psi & -\sin\Psi & 0 \\ \sin\Psi & \cos\Psi & 0 \\ 0 & 0 & 1 \end{bmatrix} = e^{\tilde{u}_3\Psi} \tag{2.30}$$

Direct cosine matrix from frame F_m to F_n is given as:

$$\hat{C}^{(m,n)} = \begin{bmatrix} \cos\Theta & 0 & \sin\Theta \\ 0 & 1 & 0 \\ -\sin\Theta & 0 & \cos\Theta \end{bmatrix} = e^{\tilde{u}_2\Theta} \tag{2.31}$$

Direct cosine matrix from frame F_n to F_O is given as:

$$\hat{C}^{(n,b)} = \begin{bmatrix} 1 & 0 & 0 \\ 0 & \cos\Phi & -\sin\Phi \\ 0 & \sin\Phi & \cos\Phi \end{bmatrix} = e^{\tilde{u}_1\Phi} \tag{2.32}$$

Hence, direct cosine matrix from Earth-fixed frame F_O to body-fixed frame F_b is obtained from the multiplication of these three direct cosine matrices: $\hat{C}^{(o,m)}\hat{C}^{(m,n)}\hat{C}^{(n,b)}$ (see Ref.16 for detailed exponential matrix representation). Then overall direct cosine matrix is

$$\hat{C}^{(o,b)} = \begin{bmatrix} \cos\Theta\cos\Psi & \sin\Phi\sin\Theta\cos\Psi - \cos\Phi\sin\Psi & \cos\Phi.\sin\Theta\cos\Psi + \sin\Phi\sin\Psi \\ \cos\Theta\sin\Psi & \sin\Phi\sin\Theta\sin\Psi + \cos\Phi\cos\Psi & \cos\Phi.\sin\Theta\sin\Psi - \sin\Phi\cos\Psi \\ -\sin\Theta & \sin\Phi\cos\Theta & \cos\Phi\cos\Theta \end{bmatrix} \tag{2.33}$$

Position of the aircraft with respect to the earth-fixed frame is determined by the vector $\vec{r}_c$. In order to track the flight path of the aircraft relative to earth-fixed frame, velocity components in Earth-fixed frame need to be acquired. Consequently, this is achieved by taking the time derivative, $\vec{r}_c$ in inertial frame (Earth-fixed frame) through direct cosine matrix $\hat{C}^{(o,b)}$.

$$\left\{D_o \vec{r}_c\right\}^{(o)} = \hat{C}^{(o,b)} \left\{D_o \vec{r}_c\right\}^{(b)} \tag{2.34}$$

Then:

$$\dot{\vec{r}}_c{}^{(0)} = \begin{bmatrix} \dot{X}_E \\ \dot{Y}_E \\ \dot{Z}_E \end{bmatrix} = \hat{C}^{(o,b)} \dot{\vec{r}}_c{}^{(b)} = \hat{C}^{(o,b)} \dot{\vec{r}}_c{}^{(b)} \tag{2.35}$$

where:

$$\dot{\vec{r}}_c{}^{(b)} = \begin{bmatrix} U \\ V \\ W \end{bmatrix} \tag{2.36}$$

Then, the final equation is:

$$\begin{bmatrix} \dot{X}_E \\ \dot{Y}_E \\ \dot{Z}_E \end{bmatrix} = \begin{bmatrix} \begin{bmatrix} \cos\Theta\cos\Psi & \sin\Phi\sin\Theta\cos\Psi - \cos\Phi\sin\Psi & \cos\Phi\sin\Theta\cos\Psi + \sin\Phi\sin\Psi \\ \cos\Theta\sin\Psi & \sin\Phi\sin\Theta\sin\Psi + \cos\Phi\cos\Psi & \cos\Phi\sin\Theta\sin\Psi - \sin\Phi\cos\Psi \\ -\sin\Theta & \sin\Phi\cos\Theta & \cos\Phi\cos\Theta \end{bmatrix} \end{bmatrix} \begin{bmatrix} U \\ V \\ W \end{bmatrix} \tag{2.37}$$

Its alternative form is:

$$\begin{aligned} \dot{X}_E &= U\left(\cos\Theta\cos\Psi\right) + V\left(\sin\Phi\sin\Theta\cos\Psi - \cos\Phi\sin\Psi\right) + w\left(\cos\Phi\sin\Theta\cos\Psi + \sin\Phi\sin\Psi\right) \\ \dot{Y}_E &= U\left(\cos\Theta\sin\Psi\right) + V\left(\sin\Phi\sin\Theta\sin\Psi + \cos\Phi\cos\Psi\right) + w\left(\cos\Phi\sin\Theta\sin\Psi - \sin\Phi\cos\Psi\right) \\ \dot{Z}_E &= U\left(-\sin\Theta\right) + V\left(\sin\Phi\cos\Theta\right) + W\left(\cos\Phi\cos\Theta\right) \end{aligned} \tag{2.38}$$

2.1.4 Body-axis system's forces, moments and velocities

Force equations can be written in any frame desired; nonetheless, it is preferred to be expressed in Body-fixed Frame. Due to the fact that Equation (2.28) involves the derivative of angular momentum which contains the moments and products of inertia with respect to any axes system chosen. Picking the axes system to be fixed relative to inertial space results in varying inertia terms in the equations. This is most undesirable and can be avoided by writing the equations in the frame F_b, in which all the inertias are constant except the period in which the propellant burns.

All the velocity vectors seen in the Figure 2-3 are defined in Table 2-1.

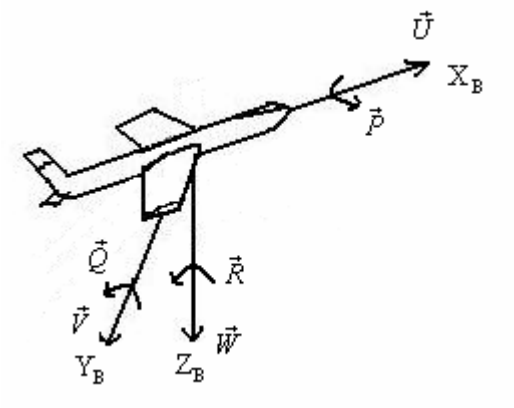

Figure 2-3 Angular and linear velocity components in body-fixed frame

Table 2-1 Velocity vectors in body-fixed frame

$\vec{U}$	Along-track velocity component in body-fixed frame
$\vec{V}$	Side velocity component in body-fixed frame
$\vec{W}$	Downward velocity component in body-fixed frame
$\vec{P}$	Roll rate in body-fixed frame
$\vec{Q}$	Pitch rate in body-fixed frame
$\vec{R}$	Yaw rate in body-fixed frame

Aerodynamic and thrust forces and moments are seen in Figure 2-4.

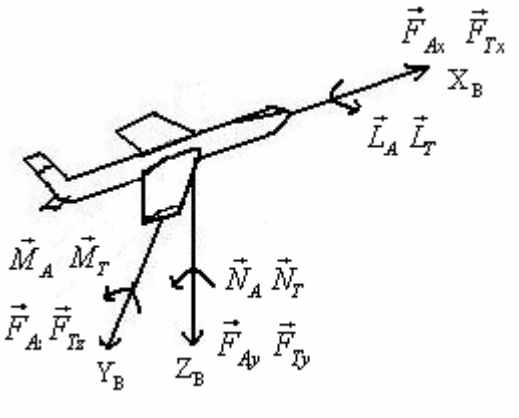

Figure 2-4 Aerodynamic and thrust forces and moments exposed on the aircraft in Body-fixed frame.

Aerodynamic forces and moments are expanded in Table 2-2

Table 2-2 Aerodynamic and thrust forces and moments

Aerodynamic force	$\vec{F}_A = \vec{F}_{Ax} + \vec{F}_{Ay} + \vec{F}_{Az}$
Thrust force	$\vec{F}_T = \vec{F}_{Tx} + \vec{F}_{Ty} + \vec{F}_{Tz}$
Aerodynamic moment	$\vec{M}_A = \vec{L}_A + \vec{M}_A + \vec{N}_A$
Thrust moment	$\vec{M}_T = \vec{L}_T + \vec{M}_T + \vec{N}_T$

To write moment and force equations in Body-fixed frame, the time derivative of $\vec{V}_c$ and acceleration of gravity $\vec{g}$ should be expressed in this frame (see Figure 2-1). All the steps to acquire the time derivative of $\vec{V}_c$ in body-fixed frame are summarized from Equations (2.39) to (2.51).

$$\dot{\vec{V}}_c = \left\{ D_o \vec{V}_c \right\}^{(o)} = \hat{C}^{(o,b)} \left\{ D_o \vec{V}_c \right\}^{(b)} \tag{2.39}$$

Where, $\hat{C}^{(o,b)}$ is the direct cosine matrix obtained in section 2.1.3 and $\overline{V}_c^{(o)}$ is :

$$\overline{V}_c^{(o)} = \hat{C}^{(o,b)}\overline{V}_c^{(b)} \tag{2.40}$$

Then, the time derivative of Equation (2.39) yields:

$$\dot{\overline{V}}_c^{(o)} = \dot{\hat{C}}^{(o,b)}\overline{V}_c^{(b)} + \hat{C}^{(o,b)}\dot{\overline{V}}_c^{(b)} \tag{2.41}$$

This can be written as:

$$\dot{\overline{V}}_c^{(o)} = \hat{C}^{(o,b)}\left[\hat{C}^{(b,o)}\dot{\hat{C}}^{(o,b)}\overline{V}_c^{(b)} + \dot{\overline{V}}_c^{(b)}\right] \tag{2.42}$$

where:

$$\hat{C}^{(b,o)}\dot{\hat{C}}^{(o,b)} = \tilde{\omega}_{b/o} \tag{2.43}$$

Then:

$$\dot{\overline{V}}_c^{(o)} = \hat{C}^{(o,b)}\left[\dot{\overline{V}}_c^{(b)} + \tilde{\omega}_{b/o}\overline{V}_c^{(b)}\right] \tag{2.44}$$

Equation (2.44) can be expressed in the form as follows:

$$\left\{D_o\vec{V}_c\right\}^{(o)} = \hat{C}^{(o,b)}\left\{D_b\vec{V}_c + \vec{\omega}_{b/o}\times\vec{V}_c\right\}^{(b)} \tag{2.45}$$

$$D_o\vec{V}_c = D_b\vec{V}_c + \vec{\omega}_{b/o}\times\vec{V}_c \tag{2.46}$$

Thus,

$$\left\{D_o\vec{V}_c\right\}^{(b)} = \left\{D_b\vec{V}_c + \vec{\omega}_{b/o}\times\vec{V}_c\right\}^{(b)} \tag{2.47}$$

where:

$$\left\{\vec{\omega}_{b/o}\right\}^{(b)} = \begin{bmatrix}\vec{P}\\ \vec{Q}\\ \vec{R}\end{bmatrix} \tag{2.48}$$

$$\left\{\vec{V}_c\right\}^{(b)} = \begin{bmatrix}\vec{U}\\ \vec{V}\\ \vec{W}\end{bmatrix} \tag{2.49}$$

$$\left\{D_b\vec{V}_c\right\}^{(b)} = \begin{bmatrix} \dot{\vec{U}} \\ \dot{\vec{V}} \\ \dot{\vec{W}} \end{bmatrix} \tag{2.50}$$

For that reason time derivative of $\vec{V}_c$ in body-fixed frame becomes:

$$\dot{\vec{V}}_c = \begin{bmatrix} \dot{U} \\ \dot{V} \\ \dot{W} \end{bmatrix} + \begin{bmatrix} QW - VR \\ UR - PW \\ PV - UQ \end{bmatrix} \tag{2.51}$$

Next step is to express acceleration of gravity $\vec{g}$ in body-fixed frame.

$$\left\{\vec{g}\right\}^{(b)} = \hat{C}^{(b,o)}\left\{\vec{g}\right\}^{(o)} \tag{2.52}$$

where:

$$\hat{C}^{(b,o)} = \left(\hat{C}^{(o,b)}\right)^{-1} \tag{2.53}$$

$$\overline{g}^{(b)} = \hat{C}^{(b,o)}\overline{g}^{(o)} \tag{2.54}$$

The vector $\vec{g}$ is directed along the positive z_e axis in earth-fixed frame (see Figure 2-1) and z_e axis can be expressed with $\overline{u}_3$ axis. Then:

$$\overline{g}^{(b)} = \hat{C}^{(b,o)} g(\overline{u}_3) \tag{2.55}$$

where:

$$\hat{C}^{(b,o)} = e^{-\tilde{u}_1\Phi}e^{-\tilde{u}_2\Theta}e^{-\tilde{u}_3\Psi} \tag{2.56}$$

Then:

$$\overline{g}^{(b)} = e^{-\tilde{u}_1\Phi}e^{-\tilde{u}_2\Theta}e^{-\tilde{u}_3\Psi}\overline{u}_3 g \tag{2.57}$$

$$\overline{g}^{(b)} = (-\overline{u}_1 \sin\Theta + \overline{u}_2 \cos\Theta \sin\Phi + \overline{u}_3 \cos\Theta \cos\Phi) g \tag{2.58}$$

Therefore, the representation of acceleration of gravity $\vec{g}$ in body-fixed frame is found as:

$$\vec{g}^{(b)} = \begin{bmatrix} -g \sin\Theta \vec{u}_1 \\ g \cos\Theta \sin\Phi \vec{u}_2 \\ g \cos\Theta \cos\Phi \vec{u}_3 \end{bmatrix} \tag{2.59}$$

Now writing force equation (2.17) in body-fixed frame via Equations (2.51) and (2.59) in scalar form results in:

$$\boxed{\dot{m}\begin{bmatrix} U \\ V \\ W \end{bmatrix} + m\begin{bmatrix} \dot{U} + QW - VR \\ \dot{V} + UR - PW \\ \dot{W} + PV - UQ \end{bmatrix} = \begin{bmatrix} -mg\sin\Theta + F_{Ax} + F_{Tx} \\ mg\cos\Theta\sin\Phi + F_{Ay} + F_{Ty} \\ mg\cos\Theta\cos\Phi + F_{Az} + F_{Tz} \end{bmatrix}} \tag{2.60}$$

The moment equation obtained in Section 2.1.2 needs to be expanded. From Equations (2.4) and (2.20) the left-hand side of the moment Equation (2.28) takes the form:

$$\frac{d}{dt}\left[\int_v \vec{r}\times\frac{d}{dt}\vec{r}\,\rho dv\right] = \frac{d}{dt}\left[\int_v \vec{r}\times(D_o\vec{r})\rho dv\right] \tag{2.61}$$

then:

$$\frac{d}{dt}\left[\int_v \vec{r}\times(D_o\vec{r})\rho dv\right] = \frac{d}{dt}\int_v \vec{r}\times(D_b\vec{r} + \vec{\omega}_{b/o}\times\vec{r})\rho dv \tag{2.62}$$

where:

$$D_b\vec{r} = 0 \tag{2.63}$$

$$\frac{d}{dt}\int_v \vec{r}\times(\vec{\omega}_{b/o}\times\vec{r})\rho dv = \frac{d}{dt}\vec{H}_c \tag{2.64}$$

Where, $\vec{H}_c$ is the angular momentum about center of mass and defined as:

$$\vec{H}_c = \int_v \vec{r}\times(\vec{\omega}_{b/o}\times\vec{r})\rho dv = \int_m \vec{r}\times(\vec{\omega}_{b/o}\times\vec{r})dm \tag{2.65}$$

$$\vec{r}\times(\vec{\omega}_{b/o}\times\vec{r}) = \tilde{r}\tilde{\omega}\bar{r} \tag{2.66}$$

Where, the cap ~ denotes skew symmetric matrix.

$$\left\{\vec{r}\times(\vec{\omega}_{b/o}\times\vec{r})\right\}^{(b)} = \tilde{r}^{(b)}\tilde{\omega}^{(b)}\bar{r}^{(b)} = -\tilde{r}^2\bar{\omega} \tag{2.67}$$

where:

$$\tilde{r}^{(b)} = \tilde{r}, \tilde{\omega}^{(b)} = \tilde{\omega} \tag{2.68}$$

then:

$$-\tilde{r}^2\bar{\omega} = \left[\bar{r}\bar{r}^t - \bar{r}^t\bar{r}\hat{I}\right]\bar{\omega} = \left[r^2\hat{I} - \bar{r}\bar{r}^t\right]\bar{\omega} \tag{2.69}$$

then:

$$\vec{H}_c = \int_m \left[r^2 \breve{I} - \vec{r}\vec{r} \right] \vec{\omega} dm = \int_m \left(r^2 \breve{I} - \vec{r}\vec{r} \right) \vec{\omega} dm = \breve{J}_c \vec{\omega} \tag{2.70}$$

Where, $\breve{J}_c$ is inertia tensor about center of mass and defined as:

$$\breve{J}_c = \int_m \left(r^2 . \breve{I} - \vec{r} . \vec{r} \right) . dm \tag{2.71}$$

$$\vec{H}_c = \breve{J}_c \vec{\omega} \tag{2.72}$$

The right hand-side of the Equation (2.64) can be written as in Equation (2.78) through Equations (2.73) to (2.77).

$$\frac{d}{dt} \vec{H}_c = D_o \vec{H}_c = D_b \vec{H}_c + \vec{\omega}_{b/o} \times \vec{H}_c = \sum \vec{M}_c \tag{2.73}$$

$$D_o \vec{H}_c = D_b \left(\breve{J}_c . \vec{\omega} \right) + \vec{\omega}_{b/o} \times \left(\breve{J}_c . \vec{\omega} \right) \tag{2.74}$$

$$D_o \vec{H}_c = \left(D_b \breve{J}_c \right) \left(\vec{\omega} \right) + \left(\breve{J}_c \right) \left(D_b \vec{\omega} \right) + \vec{\omega} \times \left(\breve{J}_c \vec{\omega} \right) \tag{2.75}$$

$$D_o \vec{H}_c = \dot{\breve{J}}_c \vec{\omega} + \breve{J}_c \dot{\vec{\omega}} + \vec{\omega} \times \left(\breve{J}_c \vec{\omega} \right) \tag{2.76}$$

$$\frac{d}{dt} \vec{H}_c = D_o \vec{H}_c = D_b \vec{H}_c + \vec{\omega}_{b/o} \times \vec{H}_c = \sum \vec{M}_c \tag{2.77}$$

$$\begin{bmatrix} \sum M_1 \\ \sum M_2 \\ \sum M_3 \end{bmatrix} = \begin{bmatrix} \dot{J}_{11} & \dot{J}_{12} & \dot{J}_{13} \\ \dot{J}_{21} & \dot{J}_{22} & \dot{J}_{23} \\ \dot{J}_{31} & \dot{J}_{32} & \dot{J}_{33} \end{bmatrix} \begin{bmatrix} \vec{\omega}_1 \\ \vec{\omega}_2 \\ \vec{\omega}_3 \end{bmatrix} + \begin{bmatrix} J_{11} & J_{12} & J_{13} \\ J_{21} & J_{22} & J_{23} \\ J_{31} & J_{32} & J_{33} \end{bmatrix} \begin{bmatrix} \dot{\vec{\omega}}_1 \\ \dot{\vec{\omega}}_2 \\ \dot{\vec{\omega}}_3 \end{bmatrix} + \begin{bmatrix} 0 & -\omega_3 & \omega_2 \\ \omega_3 & 0 & -\omega_1 \\ -\omega_2 & \omega_1 & 0 \end{bmatrix} \begin{bmatrix} J_{11} & J_{12} & J_{13} \\ J_{21} & J_{22} & J_{23} \\ J_{31} & J_{32} & J_{33} \end{bmatrix} \begin{bmatrix} \vec{\omega}_1 \\ \vec{\omega}_2 \\ \vec{\omega}_3 \end{bmatrix} \tag{2.78}$$

Where:

$$\begin{bmatrix} \vec{\omega}_1 \\ \vec{\omega}_2 \\ \vec{\omega}_3 \end{bmatrix} = \begin{bmatrix} \vec{P} \\ \vec{Q} \\ \vec{R} \end{bmatrix} \tag{2.79}$$

$$\begin{bmatrix} J_{11} & J_{12} & J_{13} \\ J_{21} & J_{22} & J_{23} \\ J_{31} & J_{32} & J_{33} \end{bmatrix} = \begin{bmatrix} I_{xx} & -I_{xy} & -I_{xz} \\ -I_{yx} & I_{yy} & -I_{yz} \\ -I_{zx} & -I_{zy} & I_{zz} \end{bmatrix} \tag{2.80}$$

$$\begin{bmatrix} \sum M_1 \\ \sum M_2 \\ \sum M_3 \end{bmatrix} = \begin{bmatrix} L_A + L_T \\ M_A + M_T \\ N_A + N_T \end{bmatrix} \tag{2.81}$$

$$\begin{bmatrix} \dot{J}_{11} & \dot{J}_{12} & \dot{J}_{13} \\ \dot{J}_{21} & \dot{J}_{22} & \dot{J}_{23} \\ \dot{J}_{31} & \dot{J}_{32} & \dot{J}_{33} \end{bmatrix} = \begin{bmatrix} \dot{I}_{xx} & -\dot{I}_{xy} & -\dot{I}_{xz} \\ -\dot{I}_{yx} & \dot{I}_{yy} & -\dot{I}_{yz} \\ -\dot{I}_{zx} & -\dot{I}_{zy} & \dot{I}_{zz} \end{bmatrix} \tag{2.82}$$

$$I_{xx} = \int \left(y^2 + z^2 \right) dm \tag{2.83}$$

$$I_{yy} = \int \left(x^2 + z^2 \right) dm \tag{2.84}$$

$$I_{zz} = \int \left(x^2 + y^2 \right) dm \tag{2.85}$$

$$I_{xy} = I_{yx} = \int xy dm \tag{2.86}$$

$$I_{xz} = I_{zx} = \int xz dm \tag{2.87}$$

$$I_{yz} = I_{zy} = \int yz dm \tag{2.88}$$

Equations (2.82) through (2.88) are defined such that I_{xx}, I_{yy}, and I_{zz} are moments of inertia about $X_B Y_B Z_B$ and I_{xy}, I_{yz}, and I_{xz} are products of inertia about $X_B Y_B Z_B$ .Therefore, the final form of the moment equation is:

$$\begin{aligned} &\dot{I}_{xx}P - \dot{I}_{xy}Q - \dot{I}_{xz}R + I_{xx}\dot{P} - I_{yz}\left(Q^2 - R^2\right) - I_{zx}\left(\dot{R} + PQ\right) - I_{xy}\left(\dot{Q} - RP\right) - \left(I_{yy} - I_{zz}\right)RQ = L_A + L_T \\ &\dot{I}_{yy}Q - \dot{I}_{yx}P - \dot{I}_{yz}R + I_{yy}\dot{Q} - I_{zx}\left(R^2 - P^2\right) - I_{xy}\left(\dot{P} + QR\right) - I_{yz}\left(\dot{R} - PQ\right) - \left(I_{zz} - I_{xx}\right)RP = M_A + M_T \\ &\dot{I}_{zz}R - \dot{I}_{zx}P - \dot{I}_{zy}Q + I_{zz}\dot{R} - I_{xy}\left(P^2 - Q^2\right) - I_{yz}\left(\dot{Q} + RP\right) - I_{zx}\left(\dot{P} - QR\right) - \left(I_{xx} - I_{yy}\right)PQ = N_A + N_T \end{aligned} \tag{2.89}$$

2.1.5 Kinematics equations

The aircraft has an angular velocity which can be represented in the body-fixed frame as well as the inertial frame. Thus the angular velocity in the body-fixed frame can be stated via rates of Euler angles. This is actualized along the Equations (2.90) to (2.97).

$$\vec{\omega} = \begin{bmatrix} \vec{P} \\ \vec{Q} \\ \vec{R} \end{bmatrix} = \dot{\Psi}\vec{u}_3^{(o)} + \dot{\Theta}\vec{u}_2^{(m)} + \dot{\Phi}\vec{u}_1^{(n)} = \dot{\Psi}\vec{u}_3^{(o)} + \dot{\Theta}\vec{u}_2^{(m)} + \dot{\Phi}\vec{u}_1^{(b)} \tag{2.90}$$

$$\overline{\omega}^{(b)} = \begin{bmatrix} P \\ Q \\ R \end{bmatrix} = \dot{\Psi}\overline{u}_3^{(0/b)} + \dot{\Theta}\overline{u}_2^{(m/b)} + \dot{\Phi}\overline{u}_1^{(n/b)} \tag{2.91}$$

$$\overline{\omega}^{(b)} = \dot{\Psi}\hat{C}^{(b,o)}\overline{u}_3 + \dot{\Theta}\hat{C}^{(b,m)}\overline{u}_2 + \dot{\Phi}\hat{C}^{(b,n)}\overline{u}_1 \tag{2.92}$$

$$\overline{\omega}^{(b)} = \dot{\Psi}e^{-\tilde{u}_1\Phi}e^{-\tilde{u}_2\Theta}e^{-\tilde{u}_3\Psi}\overline{u}_3 + \dot{\Theta}e^{-\tilde{u}_1\Phi}e^{-\tilde{u}_2\Theta}\overline{u}_2 + \dot{\Phi}e^{-\tilde{u}_1\Phi}\overline{u}_1 \tag{2.93}$$

$$\overline{\omega}^{(b)} = \dot{\Psi}e^{-\tilde{u}_1\Phi}\left(\overline{u}_3\cos\Theta - \overline{u}_1\sin\Theta\right) + \dot{\Theta}\left(\overline{u}_2\cos\Phi - \overline{u}_3\sin\Phi\right) + \dot{\Phi}\overline{u}_1 \tag{2.94}$$

$$\overline{\omega}^{(b)} = \dot{\Psi}\left(\cos\Theta\left(\overline{u}_3\cos\Phi + \overline{u}_2\sin\Phi\right) - \overline{u}_1\sin\Theta\right) + \dot{\Theta}\overline{u}_2\cos\Phi - \dot{\Theta}\overline{u}_3\sin\Phi + \dot{\Phi}\overline{u}_1 \tag{2.95}$$

$$\overline{\omega}^{(b)} = \overline{u}_1\left(\dot{\Phi} - \dot{\Psi}\sin\Theta\right) + \overline{u}_2\left(\dot{\Theta}\cos\Phi + \dot{\Psi}\cos\Theta\sin\Phi\right) + \overline{u}_3\left(\dot{\Psi}\cos\Theta\cos\Phi - \dot{\Theta}\sin\Phi\right) \tag{2.96}$$

$$\boxed{\begin{bmatrix} P \\ Q \\ R \end{bmatrix} = \begin{bmatrix} -\sin\Theta & 0 & 1 \\ \cos\Theta\sin\Phi & \cos\Phi & 0 \\ \cos\Theta\cos\Phi & -\sin\Phi & 0 \end{bmatrix}\begin{bmatrix} \dot{\Psi} \\ \dot{\Theta} \\ \dot{\Phi} \end{bmatrix}} \tag{2.97}$$

Through equation (2.97) it is obvious to define the rates of Euler angles as in Equation (2.98).

$$\boxed{\begin{aligned} \dot{\Psi} &= \left(R\cos\Phi + Q\sin\Phi\right)\sec\Theta \\ \dot{\Theta} &= Q\cos\Phi - R\sin\Phi \\ \dot{\Phi} &= P + \left(R\cos\Phi + Q\sin\Phi\right)\tan\Theta \end{aligned}} \tag{2.98}$$

2.1.6 Summary of the equations of motion

Up to this point, 3 force equations, 3 moment equations and 3 angular velocity equations in the body-fixed frame, as well as 3 linear velocity equations of the center of mass in the Earth-fixed frame and 3 differential equations for Euler angles are derived. Mass change of aircraft resulted in change in force and moment equations compared differently from constant mass aircraft.

$$\dot{m}U + m\left(\dot{U} + QW - VR\right) = -mg\sin\Theta + F_{Ax} + F_{Tx} \tag{2.99}$$

$$\dot{m}V + m\left(\dot{V} + UR - PW\right) = mg\cos\Theta\sin\Phi + F_{Ay} + F_{Ty} \tag{2.100}$$

$$\dot{m}W + m\left(\dot{W} + PV - UQ\right) = mg\cos\Theta\cos\Phi + F_{Az} + F_{Tz} \tag{2.101}$$

$$\begin{aligned}&\dot{I}_{xx}P - \dot{I}_{xy}Q - \dot{I}_{xz}R + I_{xx}\dot{P} - I_{yz}\left(Q^2 - R^2\right) - I_{zx}\left(\dot{R} + PQ\right) - I_{xy}\left(\dot{Q} - RP\right)\\&-\left(I_{yy} - I_{zz}\right)RQ = L_A + L_T\end{aligned} \tag{2.102}$$

$$\begin{aligned}&\dot{I}_{yy}Q - \dot{I}_{yx}P - \dot{I}_{yz}R + I_{yy}\dot{Q} - I_{zx}\left(R^2 - P^2\right) - I_{xy}\left(\dot{P} + QR\right) - I_{yz}\left(\dot{R} - PQ\right)\\&-\left(I_{zz} - I_{yy}\right)RP = M_A + M_T\end{aligned} \tag{2.103}$$

$$\begin{aligned}&\dot{I}_{zz}R - \dot{I}_{zx}P - \dot{I}_{zy}Q + I_{zz}\dot{R} - I_{xy}\left(P^2 - Q^2\right) - I_{yz}\left(\dot{Q} + RP\right) - I_{zx}\left(\dot{P} - QR\right)\\&-\left(I_{xx} - I_{yy}\right)PQ = N_A + N_T\end{aligned} \tag{2.104}$$

$$P = \dot{\Phi} - \dot{\Psi}\sin\Theta \tag{2.105}$$

$$Q = \dot{\Theta}\cos\Phi + \dot{\Psi}\cos\Theta\sin\Phi \tag{2.106}$$

$$R = \dot{\Psi}\cos\Theta\cos\Phi - \dot{\Theta}\sin\Phi \tag{2.107}$$

$$\begin{aligned}&\dot{X}_E = U\left(\cos\Theta\cos\Psi\right) + V\left(\sin\Phi\sin\Theta\cos\Psi - \cos\Phi\sin\Psi\right)\\&+W\left(\cos\Phi\sin\Theta\cos\Psi + \sin\Phi\sin\Psi\right)\end{aligned} \tag{2.108}$$

$$\begin{aligned}&\dot{Y}_E = U\left(\cos\Theta\sin\Psi\right) + V\left(\sin\Phi\sin\Theta\sin\Psi + \cos\Phi\cos\Psi\right)\\&+W\left(\cos\Phi\sin\Theta\sin\Psi - \sin\Phi\cos\Psi\right)\end{aligned} \tag{2.109}$$

$$\dot{Z}_E = U\left(-\sin\Theta\right) + V\left(\sin\Phi\cos\Theta\right) + W\left(\cos\Phi\cos\Theta\right) \tag{2.110}$$

$$\dot{\Psi} = \left(R\cos\Phi + Q\sin\Phi\right)\sec\Theta \tag{2.111}$$

$$\dot{\Theta} = Q\cos\Phi - R\sin\Phi \tag{2.112}$$

$$\dot{\Phi} = P + \left(R\cos\Phi + Q\sin\Phi\right)\tan\Theta \tag{2.113}$$

2.2 Equations of motion for variable mass missile

The baseline missile is given in Figure 2-5. This missile has two fin sets first of which can be also called the wing section of the missile and the second fin set can called the tail fin set. The first fin of the wing section is placed on fuselage at 0°, second one is at 90°, third one is at 180°, and fourth one is at 270°. The tail fin set

(second fin set) arrangement is similar to the first fin set. Second and third fins of the first set are movable, and all fins of the second fin set are movable to provide the missile with automatic control systems. Necessary thrust is accommodated by virtue of the motor section, which uses end burning type solid propellant. The body of the missile includes also a guidance section, electronic parts, and a warhead.

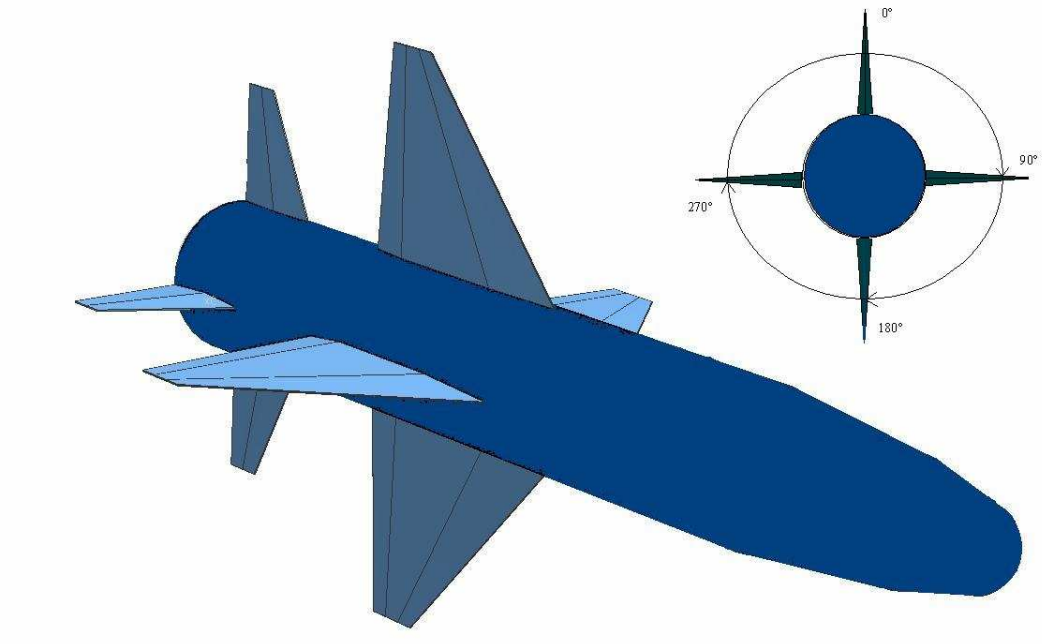

Figure 2-5 Baseline missile

It is obvious from the Figure 2-5 that the missile is axisymmetric, thence the missile products of inertia about $X_B Y_B Z_B$ are zero and moment of inertia terms about Y and Z axes are equal:

$$I_{xy} = 0 \tag{2.114}$$

$$I_{xz} = 0 \tag{2.115}$$

$$I_{yz} = 0 \tag{2.116}$$

$$I_{yy} = I_{zz} \tag{2.117}$$

During the burning period of the motor propellant, it is assumed that rate of change of mass of propellant and rate of change of mass of the missile is constant. Due to the fact that, the propulsion unit has a constant rate end burning type propellant. As a result of this, provided thrust from the motor section is constant and the thrust vector is assumed to be directed in the X_B axis of the body-fixed frame. Hence apart from $\vec{F}_{Tx}$, other components of the thrust vectors are zero. Owing to the fact that X_B, Y_B, and Z_B axes intersect in the center of missile there is no moment caused by the thrust vector; so all the moments on account of the thrust vector are zero. The consequences of this are:

$$\vec{F}_{Ty} = 0 \tag{2.118}$$

$$\vec{F}_{Tz} = 0 \tag{2.119}$$

$$\vec{L}_T = 0 \tag{2.120}$$

$$\vec{M}_T = 0 \tag{2.121}$$

$$\vec{N}_T = 0 \tag{2.122}$$

Consequently, missile equations of motion are obtained as follows:

$$\dot{m}U + m\left(\dot{U} + QW - VR\right) = -mg\sin\Theta + F_{Ax} + F_{Tx} \tag{2.123}$$

$$\dot{m}V + m\left(\dot{V} + UR - PW\right) = mg\cos\Theta\sin\Phi + F_{Ay} \tag{2.124}$$

$$\dot{m}W + m\left(\dot{W} + PV - UQ\right) = mg\cos\Theta\cos\Phi + F_{Az} \tag{2.125}$$

$$\dot{I}_{xx}P + I_{xx}\dot{P} = L_A \tag{2.126}$$

$$\dot{I}_{yy}Q + I_{yy}\dot{Q} - \left(I_{zz} - I_{xx}\right)RP = M_A \tag{2.127}$$

$$\dot{I}_{zz}R + I_{zz}\dot{R} - \left(I_{xx} - I_{yy}\right)PQ = N_A \tag{2.128}$$

$$P = \dot{\Phi} - \dot{\Psi}\sin\Theta \tag{2.129}$$

$$Q = \dot{\Theta}\cos\Phi + \dot{\Psi}\cos\Theta\sin\Phi \tag{2.130}$$

$$R = \dot{\Psi}\cos\Theta\cos\Phi - \dot{\Theta}\sin\Phi \tag{2.131}$$

$$\dot{X}_E = U\left(\cos\Theta\cos\Psi\right) + V\left(\sin\Phi\sin\Theta\cos\Psi - \cos\Phi\sin\Psi\right) + W\left(\cos\Phi\sin\Theta\cos\Psi + \sin\Phi\sin\Psi\right) \tag{2.132}$$

$$\dot{Y}_E = U\left(\cos\Theta\sin\Psi\right) + V\left(\sin\Phi\sin\Theta\sin\Psi + \cos\Phi\cos\Psi\right) + W\left(\cos\Phi\sin\Theta\sin\Psi - \sin\Phi\cos\Psi\right) \tag{2.133}$$

$$\dot{Z}_E = U\left(-\sin\Theta\right) + V\left(\sin\Phi\cos\Theta\right) + W\left(\cos\Phi\cos\Theta\right) \tag{2.134}$$

$$\dot{\Psi} = \left(R\cos\Phi + Q\sin\Phi\right)\sec\Theta \tag{2.135}$$

$$\dot{\Theta} = Q\cos\Phi - R\sin\Phi \tag{2.136}$$

$$\dot{\Phi} = P + \left(R\cos\Phi + Q\sin\Phi\right)\tan\Theta \tag{2.137}$$

CHAPTER 3

STABILITY DERIVATIVES

3.1 Survey of stability derivatives

The forces and moments presented in CHAPTER 2 can be represented by stability derivatives. The general force term (F) is formulated in terms of force coefficient (C_F), dynamic pressure (q_∞), and cross-sectional area, (S) (see Equation(3.1)). The general moment term (M) is formulated in terms of moment coefficient (C_M), dynamic pressure, cross-sectional area, and c which is either mean geometric chord or diameter of the fuselage (nacelle) (see Equation(3.2)). On account of the fact that the missile is concerned in this study, c is taken as the diameter of the missile.

$$F = C_F q_\infty S \tag{3.1}$$

$$M = C_M q_\infty S c \tag{3.2}$$

where, q_∞ and S are formulated as:

$$q_\infty = \frac{1}{2}\rho V_\infty^{\,2} \tag{3.3}$$

$$S = \frac{1}{4}\pi d^2 \tag{3.4}$$

Where, ρ is the air density, d is the diameter of the missile and V_∞ is the velocity of the center of mass of the missile and it is represented as follows:

$$V_\infty = \sqrt{(U+u)^2 + (V+v)^2 + (W+w)^2} \tag{3.5}$$

In Equations (3.6)-(3.11) aerodynamic forces and moments are written with respect to their coefficients:

$$F_{A_x} = C_x q_\infty S \tag{3.6}$$

$$F_{A_y} = C_y q_\infty S \tag{3.7}$$

$$F_{A_z} = C_z q_\infty S \tag{3.8}$$

$$L_A = C_l q_\infty S b \tag{3.9}$$

$$M_A = C_m q_\infty S c \tag{3.10}$$

$$N_A = C_n q_\infty S b \tag{3.11}$$

Aerodynamic coefficients can be expanded via their derivatives $u, v, w, p, q, r, \dot{w}$ and control deflections consisting of aileron, elevator and rudder.

$$C_x = C_{x_o} + C_{x_u} u + C_{x_w} w + C_{x_{\dot{w}}} \dot{w} + C_{x_{\delta_e}} \delta_e \tag{3.12}$$

$$C_y = C_{y_o} + C_{y_v} v + C_{y_p} p + C_{y_r} r + C_{y_{\delta_a}} \delta_a + C_{y_{\delta_r}} \delta_r \tag{3.13}$$

$$C_z = C_{z_o} + C_{z_u} u + C_{z_w} w + C_{z_{\dot{w}}} \dot{w} + C_{z_q} q + C_{z_{\delta_e}} \delta_e \tag{3.14}$$

$$C_l = C_{l_o} + C_{l_v} v + C_{l_p} p + C_{l_r} r + C_{l_{\delta_a}} \delta_a + C_{l_{\delta_r}} \delta_r \tag{3.15}$$

$$C_m = C_{m_o} + C_{m_u} u + C_{m_w} w + C_{m_{\dot{w}}} \dot{w} + C_{m_q} q + C_{m_{\delta_e}} \delta_e \tag{3.16}$$

$$C_n = C_{n_o} + C_{n_v} v + C_{n_p} p + C_{n_r} r + C_{n_{\delta_a}} \delta_a + C_{n_{\delta_r}} \delta_r \tag{3.17}$$

The aerodynamic coefficients, C_x, C_y, C_z, C_l, C_m, and C_n depend on velocity perturbations, their derivatives and control deflections. Thrust force is directed along X_B axis of body-fixed frame and it is constant during flight in which propellant burns. That is, it does not change, so there is no need to formulate thrust force.

Relation of aerodynamic coefficients with angle of attack, side slip angle and with their derivatives can be observed as attack and side slip angle are examined. Angle of attack is given by:

$$\alpha = \arctan\left(\frac{W+w}{U+u}\right) \tag{3.18}$$

resulting in:

$$w = \tan(\alpha)(U+u) - (W) \tag{3.19}$$

Moreover, the sideslip angle is:

$$\beta = \arctan\left(\frac{V+v}{\sqrt{(U+u)^2 + (W+w)^2}}\right) \approx \arctan\left(\frac{V+v}{U+u}\right) \tag{3.20}$$

resulting in:

$$v = \tan(\beta)(U+u) - (V) \tag{3.21}$$

Hence:

$$\dot{\alpha} = \frac{\frac{(\dot{w})}{(U+u)} - \frac{(W+w)\dot{u}}{(U+u)^2}}{1 + \frac{(W+w)^2}{(U+u)^2}} \tag{3.22}$$

and

$$\dot{\beta} = \frac{\frac{(\dot{v})}{(U+u)} - \frac{(V+v)\dot{u}}{(U+u)^2}}{1 + \frac{(V+v)^2}{(U+u)^2}} \tag{3.23}$$

then:

$$C_{x_w} = \frac{\partial C_x}{\partial w} = \frac{\partial C_x}{\partial \alpha}\frac{\partial \alpha}{\partial w} = C_{x_\alpha}\frac{1}{(U+u)\left(1 + \frac{(W+w)^2}{(U+u)^2}\right)} \tag{3.24}$$

$$C_{x_w} \cong \frac{1}{U+u} C_{x_\alpha} \tag{3.25}$$

Since:

$$(U+u)^2 >> (W+w)^2 \tag{3.26}$$

and

$$(U+u)^2 >> (V+v)^2 \tag{3.27}$$

one obtains $\dot{w}$ and $\dot{v}$ as:

$$\dot{w} = \dot{\alpha}(U+u) \tag{3.28}$$

and

$$\dot{v} = \dot{\beta}(U+u) \tag{3.29}$$

With the same procedure, stability derivatives take the following forms:

$$C_{y_v} = \frac{1}{U+u} C_{y_\beta} \tag{3.30}$$

$$C_{z_w} = \frac{1}{U+u} C_{z_\alpha} \tag{3.31}$$

$$C_{x_{\dot{w}}} = \frac{1}{U+u} C_{x_{\dot{\alpha}}} \tag{3.32}$$

$$C_{z_{\dot{w}}} = \frac{1}{U+u} C_{z_{\dot{\alpha}}} \tag{3.33}$$

$$C_{l_v} = \frac{1}{U+u} C_{l_\beta} \tag{3.34}$$

$$C_{n_v} = \frac{1}{U+u} C_{n_\beta} \tag{3.35}$$

$$C_{m_w} = \frac{1}{U+u} C_{m_\alpha} \tag{3.36}$$

$$C_{m_{\dot{w}}} = \frac{1}{U+u} C_{m_{\dot{\alpha}}} \tag{3.37}$$

The stability derivatives $C_{x_{\dot{\alpha}}}$, $C_{z_{\dot{\alpha}}}$, C_{z_q}, C_{m_q}, $C_{m_{\dot{\alpha}}}$, C_{y_p}, C_{y_r}, C_{l_p}, C_{l_r}, C_{n_p}, and C_{n_r} are made nondimensional by being divided by $\frac{d}{2V_\infty}$. Whereas nondimensional C_{x_u} C_{m_u} and C_{z_u} are obtained by dividing the derivatives by $1/V_\infty$.

subsequently:

$$C_x = C_{x_o} + C_{x_u}\frac{u}{V_\infty} + \frac{1}{U+u} C_{x_\alpha}\left(\tan\alpha(U+u) - W\right) + C_{x_{\dot{\alpha}}}\dot{\alpha}\frac{c}{2V_\infty} + C_{x_{\delta_e}}\delta_e \tag{3.38}$$

$$C_y = C_{y_o} + \frac{1}{U+u} C_{y_\beta} \left(\tan\beta (U+u) - V \right) + C_{y_p} p \frac{b}{2V_\infty} + C_{y_r} r \frac{b}{2V_\infty} + C_{y_{\delta_a}} \delta_a + C_{y_{\delta_r}} \delta_r \quad (3.39)$$

$$C_z = C_{z_o} + C_{z_u} \frac{u}{V_\infty} + \frac{1}{U+u} C_{z_\alpha} \left(\tan\alpha (U+u) - W \right) + C_{z_{\dot\alpha}} \dot\alpha \frac{c}{2V_\infty} + C_{z_q} q \frac{c}{2V_\infty} + C_{z_{\delta_e}} \delta_e \quad (3.40)$$

$$C_l = C_{l_o} + \frac{1}{U+u} C_{l_\beta} \left(\tan\beta (U+u) - V \right) + C_{l_p} p \frac{b}{2V_\infty} + C_{l_r} r \frac{b}{2V_\infty} + C_{l_{\delta_a}} \delta_a + C_{l_{\delta_r}} \delta_r \quad (3.41)$$

$$C_m = C_{m_o} + C_{m_u} \frac{u}{V_\infty} + \frac{1}{U+u} C_{m_\alpha} \left(\tan\alpha (U+u) - W \right) + C_{m_{\dot\alpha}} \dot\alpha \frac{c}{2V_\infty} + C_{m_q} q \frac{c}{2V_\infty} + C_{m_{\delta_e}} \delta_e \quad (3.42)$$

$$C_n = C_{n_o} + \frac{1}{U+u} C_{n_\beta} \left(\tan\beta (U+u) - V \right) + C_{n_p} p \frac{b}{2V_\infty} + C_{n_r} r \frac{b}{2V_\infty} + C_{n_{\delta_a}} \delta_a + C_{n_{\delta_r}} \delta_r \quad (3.43)$$

For small α and β, as a matter of experience and convenience the following approximations can be reached:

$$\frac{1}{U+u} C_{x_\alpha} \left(\tan\alpha (U+u) - W \right) = C_{x_\alpha} \alpha \quad (3.44)$$

$$\frac{1}{U+u} C_{y_\beta} \left(\tan\beta (U+u) - V \right) = C_{y_\beta} \beta \quad (3.45)$$

$$\frac{1}{U+u} C_{z_\alpha} \left(\tan\alpha (U+u) - W \right) = C_{z_\alpha} \alpha \quad (3.46)$$

$$\frac{1}{U+u} C_{l_\beta} \left(\tan\beta (U+u) - V \right) = C_{l_\beta} \beta \quad (3.47)$$

$$\frac{1}{U+u} C_{m_\alpha} \left(\tan\alpha (U+u) - W \right) = C_{m_\alpha} \alpha \quad (3.48)$$

$$\frac{1}{U+u} C_{n_\beta} \left(\tan\beta (U+u) - V \right) = C_{n_\beta} \beta \quad (3.49)$$

Therefore, Equations (3.38) to (3.43) turn out to be:

$$C_x = C_{x_o} + C_{x_u} \frac{u}{V_\infty} + C_{x_\alpha} \alpha + C_{x_{\dot\alpha}} \dot\alpha \frac{d}{2V_\infty} + C_{x_{\delta_e}} \delta_e \quad (3.50)$$

$$C_y = C_{y_o} + C_{y_\beta} \beta + C_{y_p} p \frac{d}{2V_\infty} + C_{y_r} r \frac{d}{2V_\infty} + C_{y_{\delta_a}} \delta_a + C_{y_{\delta_r}} \delta_r \quad (3.51)$$

$$C_z = C_{z_o} + C_{z_u} \frac{u}{V_\infty} + C_{z_\alpha} \alpha + C_{z_{\dot\alpha}} \dot\alpha \frac{d}{2V_\infty} + C_{z_q} q \frac{d}{2V_\infty} + C_{z_{\delta_e}} \delta_e \quad (3.52)$$

$$C_l = C_{l_o} + C_{l_\beta}\beta + C_{l_p} p\frac{d}{2V_\infty} + C_{l_r} r\frac{d}{2V_\infty} + C_{l_{\delta_a}}\delta_a + C_{l_{\delta_r}}\delta_r \tag{3.53}$$

$$C_m = C_{m_o} + C_{m_u}\frac{u}{V_\infty} + C_{m_\alpha}\alpha + C_{m_{\dot\alpha}}\dot\alpha\frac{d}{2V_\infty} + C_{m_q} q\frac{d}{2V_\infty} + C_{m_{\delta_e}}\delta_e \tag{3.54}$$

$$C_n = C_{n_o} + C_{n_\beta}\beta + C_{n_p} p\frac{d}{2V_\infty} + C_{n_r}\mathrm{r}\frac{d}{2V_\infty} + C_{n_{\delta_a}}\delta_a + C_{n_{\delta_r}}\delta_r . \tag{3.55}$$

Dynamic pressure includes airspeed. Therefore, aerodynamic forces and moments ought to include the deviation of dynamic pressure with respect to the velocity components in the body-fixed frame. The effects of the vertical and the side velocity components are included mainly in angle of attack and sideslip angle. On the other hand, changes in the forward velocity should be included as perturbations in the magnitude of the velocity; as a result in variations of dynamic pressure. Following equations show the effect forward velocity perturbations:

$$\frac{\partial F_{A_x}}{\partial\left(\frac{U}{V_\infty}\right)} = C_{x_u} q_\infty S + C_{x_o} q_{\infty_u} S V_\infty \tag{3.56}$$

$$\frac{\partial F_{A_x}}{\partial\left(\frac{U}{V_\infty}\right)} = C_{z_u} q_\infty S + C_{z_o} q_{\infty_u} S V_\infty \tag{3.57}$$

$$\frac{\partial M_A}{\partial\left(\frac{U}{V_\infty}\right)} = C_{m_u} q_\infty S + C_{m_o} q_{\infty_u} S V_\infty \tag{3.58}$$

where:

$$q_{\infty_u} = \rho U \tag{3.59}$$

$$\rho U V_\infty \approx 2 q_\infty \tag{3.60}$$

Then:

$$\frac{\partial F_{A_x}}{\partial\left(\frac{U}{V_\infty}\right)} = C_{x_u} q_\infty S + 2 C_{x_o} q_\infty S . \tag{3.61}$$

$$\frac{\partial F_{A_z}}{\partial\left(\frac{U}{V_\infty}\right)} = C_{z_u} q_\infty S + 2C_z q_\infty S \tag{3.62}$$

$$\frac{\partial M_A}{\partial\left(\frac{U}{V_\infty}\right)} = C_{m_u} q_\infty S + 2C_m q_\infty S \,. \tag{3.63}$$

Finally aerodynamic force and moment terms can be written as:

$$F_{A_x} = \left[C_{x_o} + \left(C_{x_u} + 2C_{x_0}\right)\frac{u}{V_\infty} + C_{x_\alpha}\alpha + C_{x_{\dot\alpha}}\dot\alpha\frac{d}{2V_\infty} + C_{x_{\delta_e}}\delta_e \right] q_\infty S \tag{3.64}$$

$$F_{A_y} = \left[C_{y_o} + C_{y_\beta}\beta + C_{y_p}\, p\frac{d}{2V_\infty} + C_{y_r}\, r\frac{d}{2V_\infty} + C_{y_{\delta_a}}\delta_a + C_{y_{\delta_r}}\delta_r \right] q_\infty S \tag{3.65}$$

$$F_{A_z} = \left[C_{z_o} + \left(C_{z_u} + 2C_{z_0}\right)\frac{u}{V_\infty} + C_{z_\alpha}\alpha + C_{z_{\dot\alpha}}\dot\alpha\frac{d}{2V_\infty} + C_{z_q}\, q\frac{d}{2V_\infty} + C_{z_{\delta_e}}\delta_e \right] q_\infty S \tag{3.66}$$

$$L_A = \left[C_{l_o} + C_{l_\beta}\beta + C_{l_p}\, p\frac{d}{2V_\infty} + C_{l_r}\, r\frac{d}{2V_\infty} + C_{l_{\delta_a}}\delta_a + C_{l_{\delta_r}}\delta_r \right] q_\infty S d \tag{3.67}$$

$$M_A = \left[C_{m_o} + \left(C_{m_u} + 2C_{m_0}\right)\frac{u}{V_\infty} + C_{m_\alpha}\alpha + C_{m_{\dot\alpha}}\dot\alpha\frac{d}{2V_\infty} + C_{m_q}\, q\frac{d}{2V_\infty} + C_{m_{\delta_e}}\delta_e \right] q_\infty S d \tag{3.68}$$

$$N_A = \left[C_{n_o} + C_{n_\beta}\beta + C_{n_p}\, p\frac{d}{2V_\infty} + C_{n_r}\, r\frac{d}{2V_\infty} + C_{n_{\delta_a}}\delta_a + C_{n_{\delta_r}}\delta_r \right] q_\infty S d \tag{3.69}$$

3.2 Analysis of stability derivatives and perturbation for the missile

The representation of forces and moments with respect to stability derivatives is accomplished in the previous sections. This section investigates the perturbations on variables and control surfaces: forward velocity, lateral velocity, downward velocity, roll rate, pitch rate, yaw rate, rate of change of sideslip angle, rate of change of angle of attack, and aileron, elevator, and rudder surfaces.

Aerodynamic characteristics of aircraft are dominated by wings. Thus, stability derivatives are formed by wings and can be assumed constant at a specific

flight condition, such as approach, and cruise condition as long as the aircraft does not stall. However, this is not the case for missiles. Aerodynamic characteristics of missiles are dominated by the body. Besides the velocity range of the missile in this study is 0.4 M to 2 M. This states that airflow around the missile changes importantly in this range and so do stability derivatives. This is also important for military aircraft flying at supersonic velocity.

Therefore in this research assuming the stability derivatives constant at a specific flight condition is avoided.

Each stability derivative depends on velocity, angle of attack and sideslip angle. Via MISSILE DATCOM stability derivatives are obtained at different speed, angle of attack, and sideslip angle. The ranges corresponding to velocity (Mach number), angle of attack and sideslip angle are given in Table 3-1.

Table 3-1 Mach number, angle of attack, and sideslip angle ranges

M	0.4	0.6	0.8	0.9	0.9	1	1.1	1.2	1.4	1.6	1.8				
α (deg)	-21	-18	-15	-12	-9	-6	-3	0	3	6	9	12	15	18	21
β (deg)	-12	-10	-8	-6	-4	-2	0	2	4	6	8	10	12		

For that reason, C_{x_o}, C_{y_o}, C_{z_o}, C_{l_o}, C_{m_o}, and C_{n_o} cover the variation of velocity (C_{x_u} C_{m_u} and C_{z_u}), variation of angle of attack (C_{x_α}, C_{m_α}, and C_{z_α}) and sideslip variation (C_{y_β}, C_{l_β}, and C_{n_β}).

Perturbations on variables are briefly explained below [17].

3.2.1 Along track velocity (forward velocity) perturbation, u:

Forward speed perturbation results in change in dynamic pressure, q_∞, and Mach number, M; consequently, change in longitudinal aerodynamic forces and moment: F_{A_x}, F_{A_z}, and M_A. Corresponding stability derivatives to these forces and

moments are C_{x_u} , C_{z_u} , and C_{m_u} . As acknowledged previously, theses terms are included in C_{x_o} , C_{y_o} , and C_{z_o} terms. Forward speed perturbation's effects in lateral force and moments, $\mathrm{F_{A_y}}$, $\mathrm{L_A}$, and $\mathrm{N_A}$, are negligible.

3.2.2 Side velocity (lateral velocity) perturbation, v:

The relation ship between sideslip angle and lateral velocity is formulated in Equation (3.21). Lateral speed perturbation results in change in lateral aerodynamic force and moments: F_{A_y} , L_A, and N_A. Corresponding stability derivatives to these forces and moments are C_{y_β} , C_{l_β} , and C_{n_β} which are already involved in C_{y_o} , C_{l_o} , and C_{n_o} . Lateral speed perturbation's effects on longitudinal forces and moment are negligible as long as the sideslip angle is small. The effect of lateral velocity perturbation in dynamic pressure $\mathrm{q_\infty}$ can be ignored.

3.2.3 Downward speed perturbation, w:

The relation ship between angle of attack and downward speed is formulated in Equation (3.19). Downward speed perturbation results in change in longitudinal aerodynamic forces and moment: F_{A_x} , F_{A_z} , and M_A . Corresponding stability derivatives to these forces and moments are C_{x_α} , C_{z_α} and C_{m_α} . Downward speed's effects in lateral force and moments, F_{A_y} , L_A and N_A, are neglected. The effect of downward velocity perturbation in dynamic pressure q_∞ is negligible. Downward speed perturbation's effects in lateral forces and moments are negligible as long as the angle of attack is small. Besides, effect of α is negligible on $\mathrm{C_x}$ for the missile. This assumption is made based on the data obtained from MISSILE DATCOM.

3.2.4 Roll rate perturbation, p:

Small perturbations in roll rate cause non-symmetrical changes in local angles of attacks over wing set and tail fin set surfaces. It is assumed that there are negligible

effects on longitudinal aerodynamic moment and forces, F_{A_x}, F_{A_z}, and M_A, owing to changes in local angles of attacks which take place in an anti-symmetrical manner. Roll rate perturbation results in change in lateral aerodynamic force and moments: F_{A_y}, L_A, and N_A. Corresponding stability derivatives to these forces and moments are C_{y_p}, C_{l_p}, and C_{n_p}.

3.2.5 Pitch rate perturbation, q:

Pitch rate perturbation can cause a symmetrical, local angle of attack changes over fuselage, wing and tail fin sets. Pitch rate perturbation results in change in longitudinal aerodynamic forces and moment, F_{A_x}, F_{A_z}, and M_A. Corresponding stability derivatives to these forces and moments are C_{x_q}, C_{z_q}, and C_{m_q}. Pitch rate perturbation's effects in lateral force and moments, F_{A_y}, L_A, and N_A, are neglected:. Moreover, stability derivative, C_{x_q} is neglected according to the literature and MISSILE DATCOM. For the reason that this program does not give this stability derivative as outputs.

3.2.6 Yaw rate perturbation, r:

Yaw rate perturbation not only causes a non-symmetrical changes in the local velocities of wing and tail fin sets but also to cause a non-symmetrical change in local angle of attacks over tail fins. Yaw rate perturbation results in change in lateral aerodynamic forces and moments, F_{A_y}, L_A, and N_A. Corresponding stability derivatives to these forces and moments are C_{y_r}, C_{l_r}, and C_{n_r}.

3.2.7 Rate of change of angle of attack, $\dot{\alpha}$:

When the angle of attack changes with time, wing set produces a vortex which, changes with time also and this results in a significant effect on the tail fin set. Nevertheless, since this missile is a long range air to surface missile, it does not face

an important rate of change of alpha; as a result, its fin set does not produce a significant vortex field. On account of those reasons, it is possible to neglect the effect of rate of change of angle of attack $\dot{\alpha}$.

3.2.8 Rate of change of sideslip angle, $\dot{\beta}$:

That the sideslip angle changes with time, and that wing-fuselage combination produce a vortex which changes with time, have a significant effect on the tail fin set, especially vertical on vertical ones. Nevertheless, since this missile is a long range air-to-surface missile, it does not face an important rate of change of sideslip angle; as a result, its fin set does not generate a significant vortex field. On account of those reasons, it is possible to neglect the effect of rate of change of sideslip angle $\dot{\beta}$.

3.2.9 Control surface perturbations, δ_e, δ_a, and δ_r:

It is assumed that control surface deflections, δ_a, and δ_r, affect lateral moments and force, F_{A_y}, L_A, and, N_A but not longitudinal forces and moments. Corresponding derivatives are, $C_{l_{\delta_a}}$, $C_{l_{\delta_r}}$, $C_{n_{\delta_a}}$, $C_{n_{\delta_r}}$, $C_{y_{\delta_a}}$, and $C_{y_{\delta_r}}$. And It is assumed that longitudinal control surface deflection δ_e affects longitudinal moment and forces, F_{A_x}, F_{A_z}, and M_A.but not lateral force and moments. Corresponding derivatives are, $C_{x_{\delta e}}$, $C_{z_{\delta e}}$, and $C_{m_{\delta e}}$.

Finally, with regard of these resulting stability derivatives Equations through (3.50)-(3.55) and (3.64)-(3.69) result in:

$$C_x = C_{x_o} + C_{x_{\delta_e}} \delta_e \tag{3.70}$$

$$C_y = C_{y_o} + C_{y_p} p \frac{d}{2V_\infty} + C_{y_r} r \frac{d}{2V_\infty} + C_{y_{\delta_a}} \delta_a + C_{y_{\delta_r}} \delta_r \tag{3.71}$$

$$C_z = C_{z_o} + C_{z_{\dot{\alpha}}} \dot{\alpha} \frac{d}{2V_\infty} + C_{z_q} q \frac{d}{2V_\infty} + C_{z_{\delta_e}} \delta_e \tag{3.72}$$

$$C_l = C_{l_o} + C_{l_p} p \frac{d}{2V_\infty} + C_{l_r} r \frac{d}{2V_\infty} + C_{l_{\delta_a}} \delta_a + C_{l_{\delta_r}} \delta_r \tag{3.73}$$

$$C_m = C_{m_o} + C_{m_{\dot{\alpha}}}\dot{\alpha}\frac{d}{2V_\infty} + C_{m_q} q\frac{d}{2V_\infty} + C_{m_{\delta_e}}\delta_e \tag{3.74}$$

$$C_n = C_{n_o} + C_{n_p} p\frac{d}{2V_\infty} + C_{n_r}\mathrm{r}\frac{d}{2V_\infty} + C_{n_{\delta_a}}\delta_a + C_{n_{\delta_r}}\delta_r . \tag{3.75}$$

$$F_{A_x} = \left[C_{x_o} + C_{x_{\delta_e}}\delta_e\right] q_\infty S \tag{3.76}$$

$$F_{A_y} = \left[C_{y_o} + C_{y_p} p\frac{d}{2V_\infty} + C_{y_r} r\frac{d}{2V_\infty} + C_{y_{\delta_a}}\delta_a + C_{y_{\delta_r}}\delta_r\right] q_\infty S \tag{3.77}$$

$$F_{A_z} = \left[C_{z_o} + C_{z_{\dot{\alpha}}}\dot{\alpha}\frac{d}{2V_\infty} + C_{z_q} q\frac{d}{2V_\infty} + C_{z_{\delta_e}}\delta_e\right] q_\infty S \tag{3.78}$$

$$L_A = \left[C_{l_o} + C_{l_p} p\frac{d}{2V_\infty} + C_{l_r} r\frac{d}{2V_\infty} + C_{l_{\delta_a}}\delta_a + C_{l_{\delta_r}}\delta_r\right] q_\infty Sd \tag{3.79}$$

$$M_A = \left[C_{m_o} + C_{m_{\dot{\alpha}}}\dot{\alpha}\frac{d}{2V_\infty} + C_{m_q} q\frac{d}{2V_\infty} + C_{m_{\delta_e}}\delta_e\right] q_\infty Sd \tag{3.80}$$

$$N_A = \left[C_{n_o} + C_{n_p} p\frac{d}{2V_\infty} + C_{n_r} r\frac{d}{2V_\infty} + C_{n_{\delta_a}}\delta_a + C_{n_{\delta_r}}\delta_r\right] q_\infty Sd \tag{3.81}$$

CHAPTER 4

TARGET, MISSILE AND GUIDANCE

This part covers the missile's characteristics, potential targets, and the approach of guidance that shapes the basis of controller design. It is apparent that the target constructs the scenario, missile type and its features or vice-versa. At this point, guidance achieves the path of scenario ending at target in a way that terminates the path with best accuracy. Therefore, starting with the target would not be a bad choice at all.

4.1 Target

A chief goal of this missile is to shatter enemy's fore-defense barrier before the attacking force, especially military aircraft, reach the zone. In other words, mission is to destroy high-value, well defended or heavily defended land targets. A target can be a military base, an airport or a communication station. Actually, ships, or any relocatable system can be a target. More information about the target is definitely required, especially for warhead design; nonetheless, this is adequate at this point for this study.

To sum up, in this study the target is assumed to be a fixed circle on the Earth's surface with 50 m radius. Its altitude is assumed the same as sea level.

4.2 Missile

As stated in the previous part, the aim of this missile is to wipe out an opponent's defensive line. Approximate necessary range for this missile is about 80 km +/- 20 km. These kinds of missiles are called stand off missiles as well as short range ballistic missiles. They are like guided glide bombs. Nevertheless they have some form of propulsion systems, such as air-breathing engines or rocket motors. The most common propulsion systems for air-breathing engines are turbojet, ramjet, and

scramjet. Solid propellant and liquid propellant type rocket motors are the most common systems for rocket motors. Although air-breathing engines provide missiles with more stand-off distance, they cost quite a bit more than rocket motors. Consequently, as long as the aimed range can be obtained by a rocket motor, cost effectiveness of the rocket motors is an adequate basis on which to make the design decision of propulsion unit.

In this study, the missile propulsion system is assumed to be a solid propellant rocket motor. Since it has simple structure, high reliability, and high density over and above that they are low cost systems. Furthermore, they are easy to operate. That's why solid propellant rockets compose the majority of the missiles on the market.

End burning solid propellant with constant burning rate is used as in this research. Therefore, constant thrust is acquired throughout the burning period. This period takes about 116 seconds. The propellant's weight is approximately 35 % of the missile. A basic scheme of the end burning type propellant is figured in Figure 4-1.

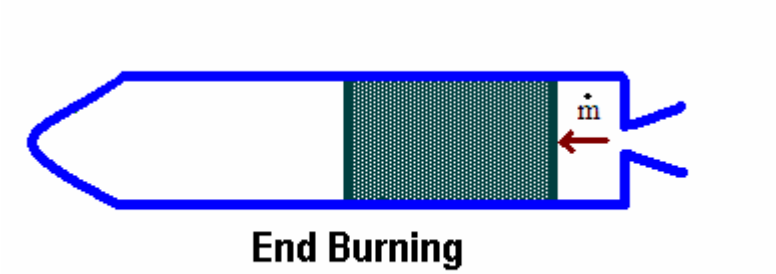

Figure 4-1 End burning propellant

As a result, the rate of change of center of gravity of the missile depends on the rate of change of mass of the propellant, $\dot{m}$. In addition, change of center of gravity results in change in inertia terms. This is taken into account at seen equations of motion in CHAPTER 2 .

A missile can be launched from an air vehicle and in this case it is called as an air-to-surface missile, whereas it is a surface-to-surface missile is lunched from a surface unit. Modifying the missile with essential hardware and software may enable it to be able to accomplish an air-to-surface and surface-to-surface mission. A major advantage of air-to-surface missiles over surface-to-surface ones is the standoff distance they provide. This permits them to launch the artillery outside the most intense air defenses around the target location.

In this study, an air-to-surface type launcher is selected. Thus, the missile's flight initiates at a specified altitude. It may need to be capable of achieving different trajectories such as arc, cruise, glide to cruise, and diving trajectory (see Figure 4-2, Figure 4-3, Figure 4-4, and Figure 4-5).

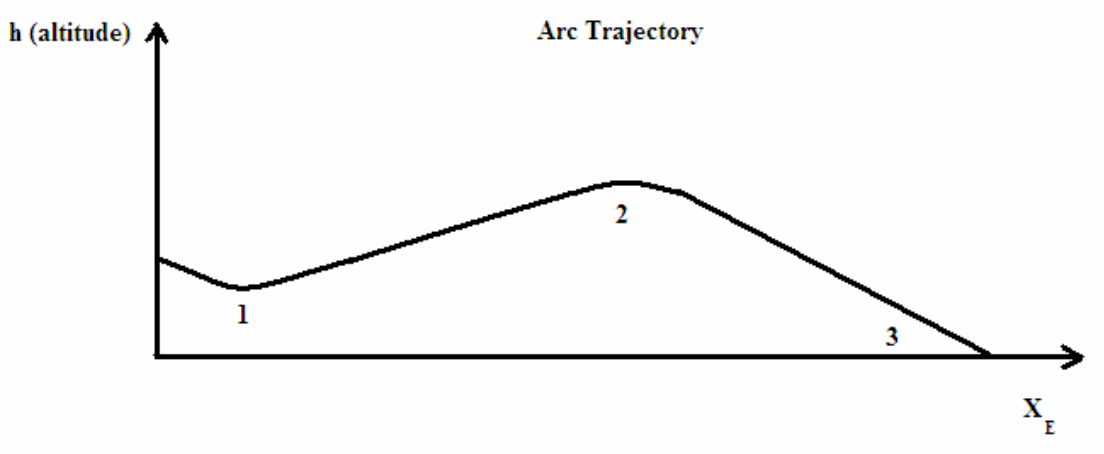

Figure 4-2 Arc trajectory

In Figure 4-2, phase 1 defines the initiation of propulsion, phase 2 defines the burn-out, and phase 3 defines termination. The stage between 1 and 2 shows the thrust-powered flight. The stage after this one is the gravity-powered flight.

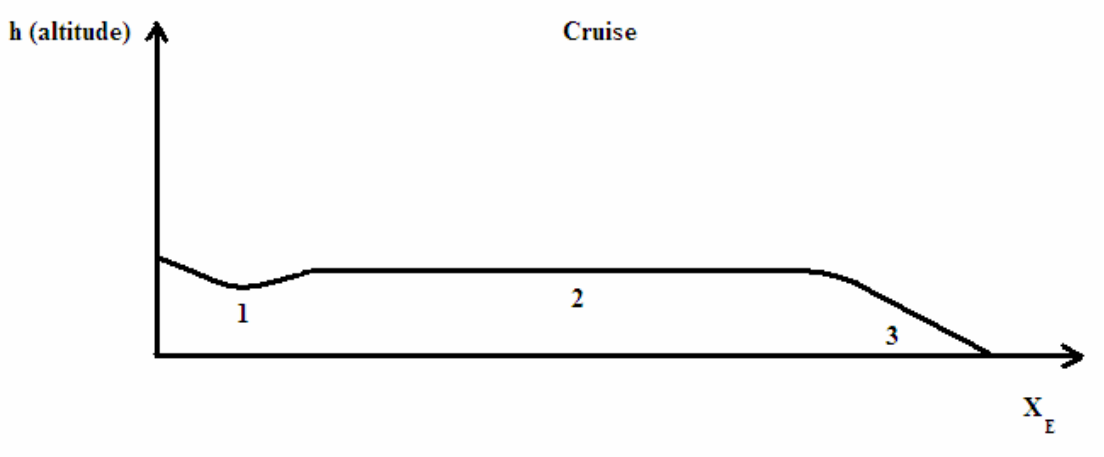

Figure 4-3 Cruise trajectory

In Figure 4-3, phase 1 defines the initiation of propulsion, phase 2 defines cruise stage, and phase 3 defines termination. The burn-out stage takes place towards the end of cruise. When the velocity of the missile drops to a point which results in lift less than weight of the missile, missile starts to loose altitude and cruise stage ends. Thrust-powered flight is the largest component of cruise. The stage after cruise is the gravity-powered flight that ends at the target.

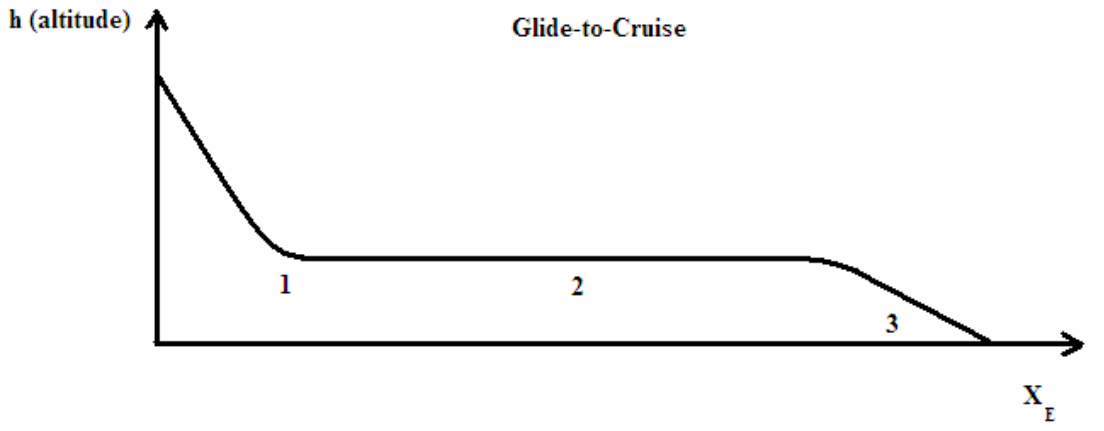

Figure 4-4 Glide-to-cruise trajectory

In Figure 4-4, phase 1 defines the initiation of propulsion, phase 2 defines cruise stage, and phase 3 defines termination. As the separation of missile from aircraft takes place, the missile begins to glide to cruise altitude by the help of gravity. The burn-out stage takes place towards the end of cruise. When the velocity of the missile falls to a point which results in lift less than weight of the missile, it starts to loose altitude and cruise stage ends. The last stage is the gravity-powered flight towards the target.

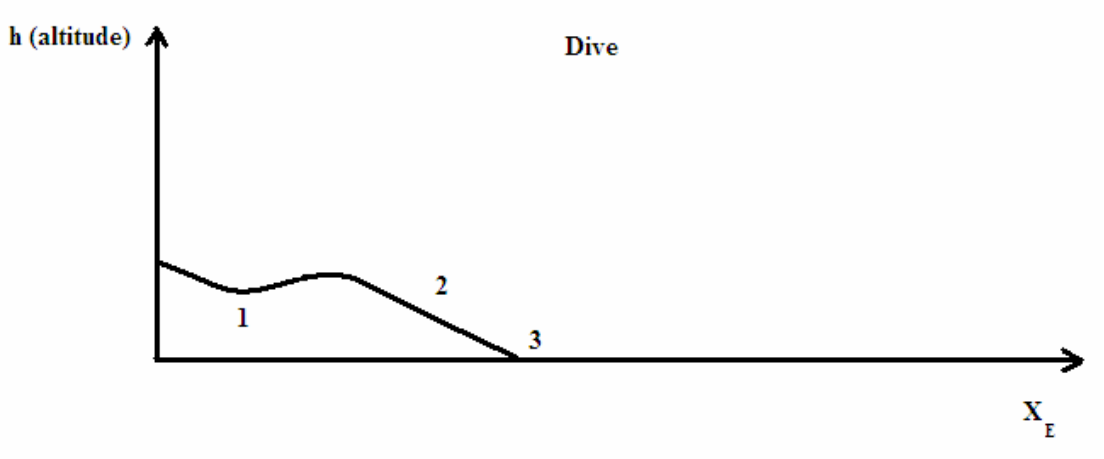

Figure 4-5 Dive trajectory

In Figure 4-5, phase 1 defines the initiation of propulsion, phase 2 defines the dive stage, and phase 3 defines termination. The burn-out stage does not take place in this trajectory. Actually, achieving especially this kind of trajectory is the goal of this study, since termination happens before burn-out. In other words, guidance of the missile via active control that commences just after separation and lasts to the blast.

Details about trajectories are studied in the next section, and comprehensive design of controller of the missile is studied in the next chapter.

Design of the missile is conducted via searching competitors, first guess sizing, airfoil and geometry selection, propulsion and fuel system integration, aerodynamics, weight and balance, stability and control, performance and flight mechanics. Dynamics, control and guidance of the missile is the focus of this study.

However, it is crucial to understand missile geometry and aerodynamics since appreciating them builds a bridge to flight mechanics and control. Hence, it is helpful to concentrate on the missile geometry and its control surfaces somewhat. Not to divert the object of this thesis, brevity is kept though. Figure 4-6 illustrates the fin sets and control surfaces of the missile. Control surfaces are indicated in red. Second and fourth panels of fin set 1 are used as the aileron unit to provide roll moment. Corresponding rotation is seen in Figure 4-7. Second and fourth panels of fin set 2 are used as elevator to provide pitch moment. Its rotation is given in Figure 4-8. Yaw moment is provided by the panels 1 and 3 and their rotation direction is available in Figure 4-9. In the figures, positive deflections are illustrated.

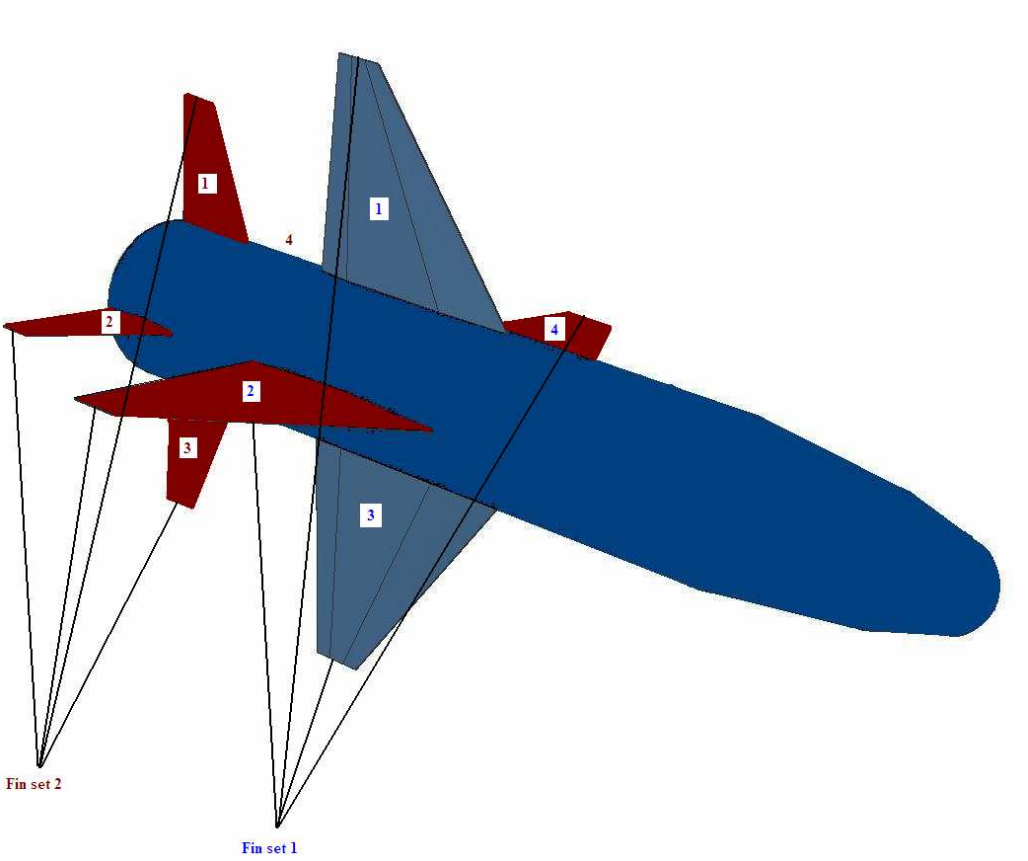

Figure 4-6 Control surfaces

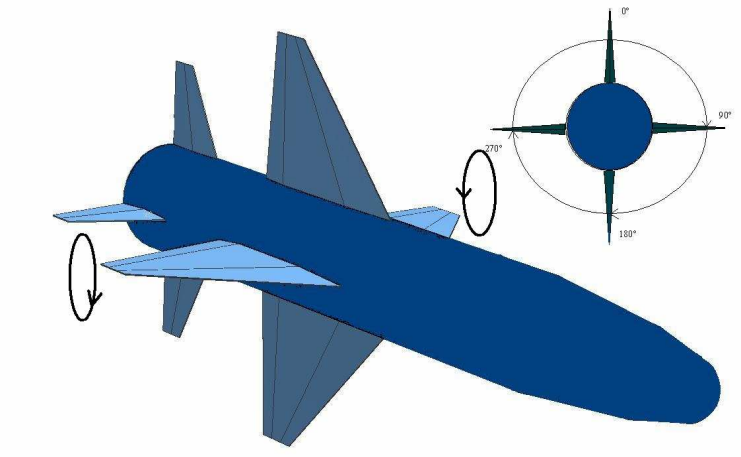

Figure 4-7 Aileron deflection rotation

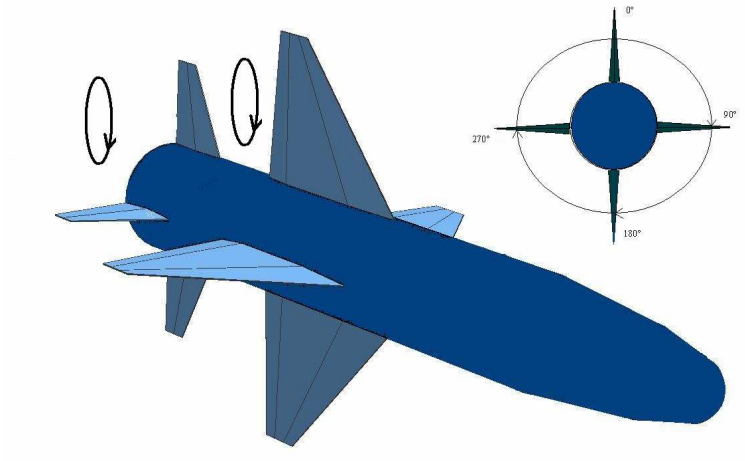

Figure 4-8 Elevator deflection angle

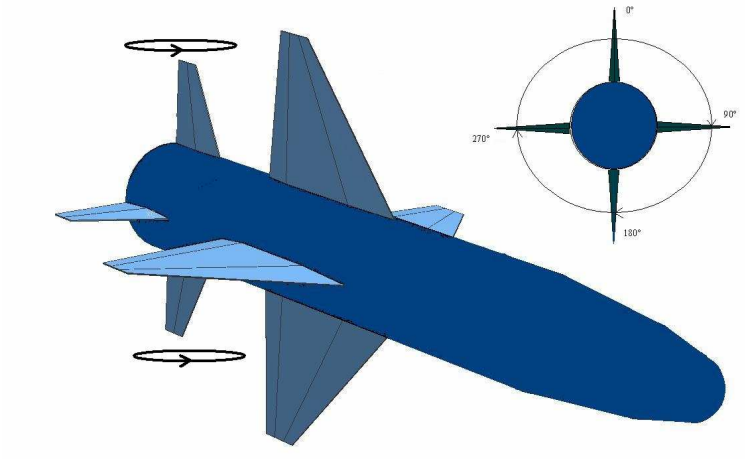

Figure 4-9 Rudder deflection angle

All control surfaces rotate around hinges, so they are all called moving panels. Rotation angle is described as incidence angle. Ranges the incidence angle to obtain the stability derivatives and aerodynamic coefficients are given for aileron, elevator, and rudder in Table 4-1. MISSILE DATCOM is used to acquire these derivatives and coefficients.

Table 4-1 Aileron, elevator, and rudder deflection ranges

Aileron(deg)	-20	-16	-12	-8	-4	0	4	8	12	16	20
Elevator (deg)	-20	-16	-12	-8	-4	0	4	8	12	16	20
Rudder (deg)	-20	-16	-12	-8	-4	0	4	8	12	16	20

4.3 Guidance

Guidance can be considered as the brain of the missile. It directs the missile, and therefore, directs its maneuvers via the control section to reach the target and be exploded at the target by means of the armament section and fuzing system. As affirmed before, the target is assumed to be fixed in this study. On the other hand, in the case that a seeker is mounted on the missile or that target coordinates are able to be updated in real time, missile can be guided to a moving target too. Assumptions for guidance are:

- Fixed target
- Missile has Global Positioning System (GPS)
- Missile has Inertial Navigation System (INS)
- Missile does not have a seeker

Given that the missile has GPS and INS, it does not need to have a seeker. Because, the target is fixed. This reduces the cost of the missile significantly. Terrain Counter Matching (TERCOM) can be integrated to the missile too. It is imperative at correcting errors in the inertial navigation system; predicted terrain profile data stored in the missile's computer are compared with the territory profile under the missile.

Figure 4-11 shows the longitudinal view of missile and target. Flight path angle γ is the angle between local horizon and velocity vector of the missile. The angle α between X coordinate of Body-fixed frame and velocity vector of the missile is the angle of attack. Moreover, the target is given as a circle on the Earth's surface with a radius equal to 50 m. The reason behind the predetermined radius of

the target is related to the warhead. The warhead is considered to be the payload of the missile. It changes from one target to another depending on the specific mission. They might carry two or three different types of explosives as well. This missile has an approximate capacity of 33 % of the overall mass of the missile reserved for warhead. The radius of the warhead's effective area is assumed to be 50 m. Accordingly, the adequate circular error of probability (CEP) can be assumed to be equal or less than 12 m.

Although, it is stated that the target is assumed on the Earth' surface, it may have an altitude. For the moment, it is important to load the predicted terrain profile data in the missile's computer to avoid the missile interception of other objects like a mountain, or a tower.

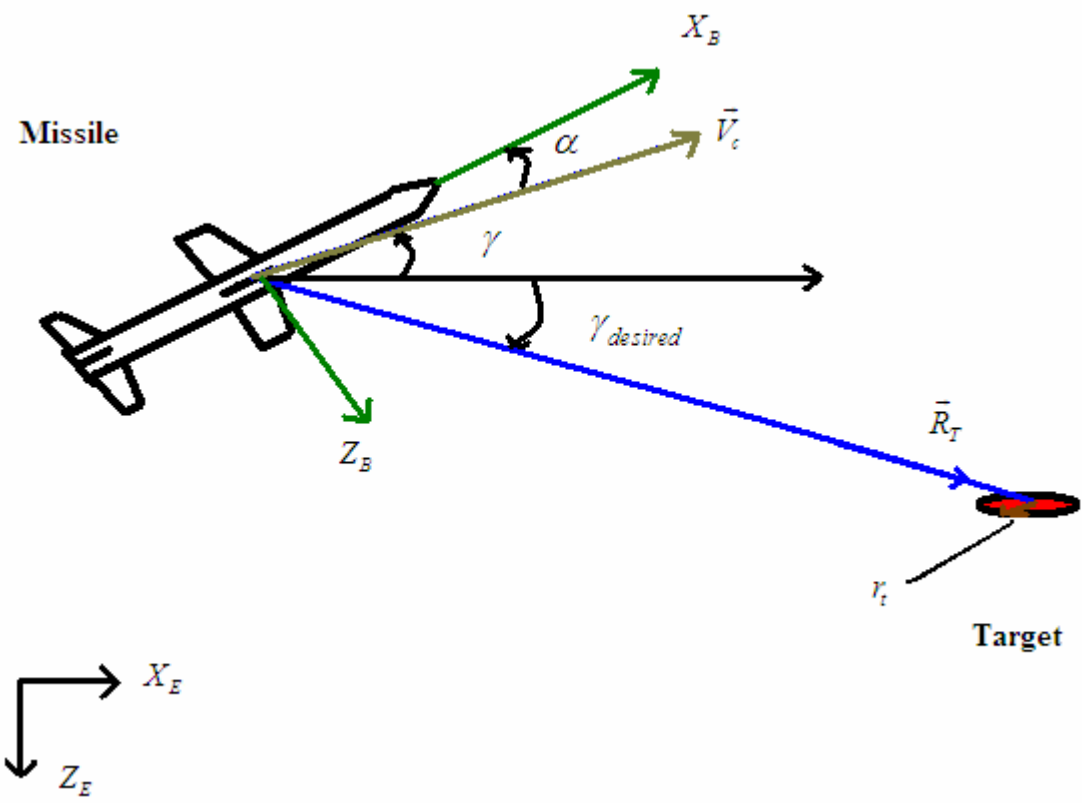

Figure 4-10 Longitudinal view of the missile and target

Velocity vector shows instantaneous direction of the missile (see Figure 4-10). From the Figure 4-10, it is obvious that to guide the missile to the target, a force needs to be applied so that missile alters its direction towards the target. Consequently, in order to hit the target, velocity vector should point target; in other words, it should coincides with the vector that origins at missile's center of mass and ends at the center of the target $\vec{R}_T$. This is the goal of the longitudinal guidance.

Figure 4-11 demonstrates the perfectly guided missile in longitudinal coordinates.

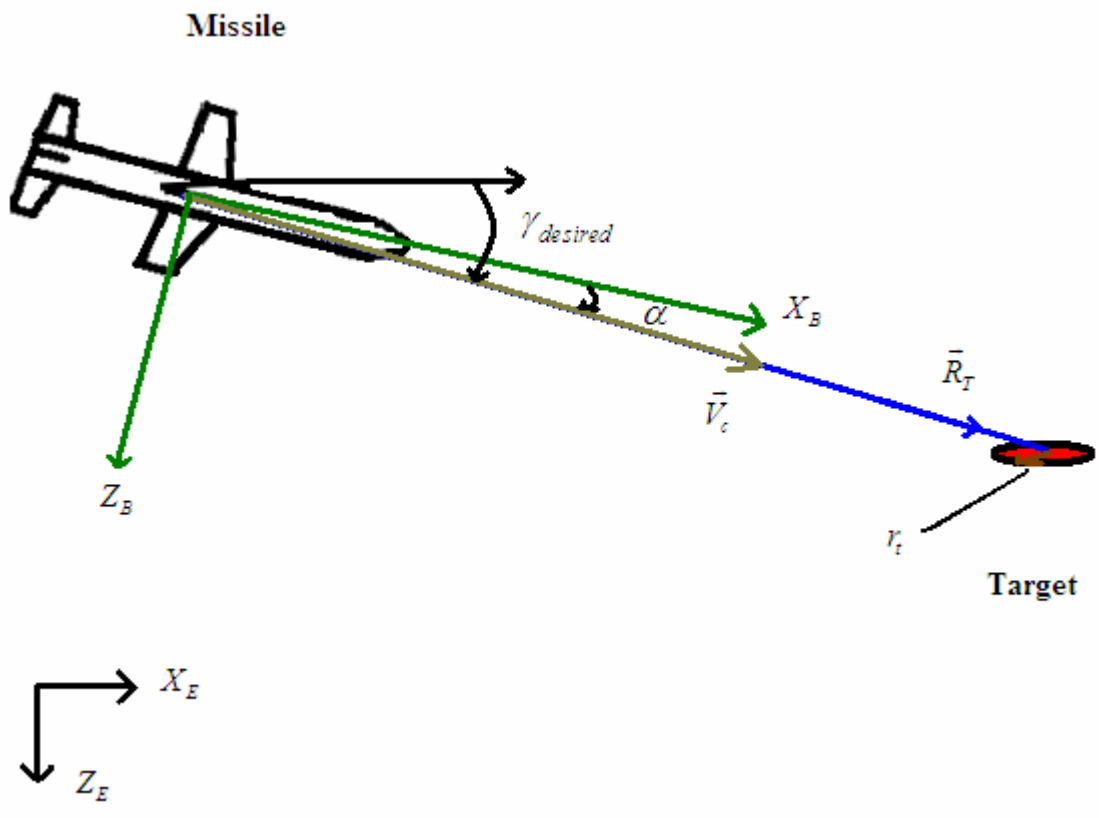

Figure 4-11 Longitudinal Guidance

In Figure 4-11 flight path angle of the missile is equal to desired flight path angle. In the view of that, velocity vector $\vec{V}_c$ coincides with target vector $\vec{R}_T$ as a

result of guidance. The realization of the guidance is performed by the nonlinear controller explained in the next chapter.

Figure 4-12 shows lateral view of the missile and the target. Yaw angle Ψ is the angle between X coordinate of Earth-fixed frame and the projection of the X coordinate of body-fixed frame of the missile on Earth surface plane. The angle β between X coordinate of Body-fixed frame and velocity vector of the missile is the side slip angle. Velocity vector shows instantaneous direction of the missile. Apart from this, the required side angle, $(\Psi+\beta)_{desired}$ so as to direct the missile to the path pointing the center of the target is seen in Figure 4-12.

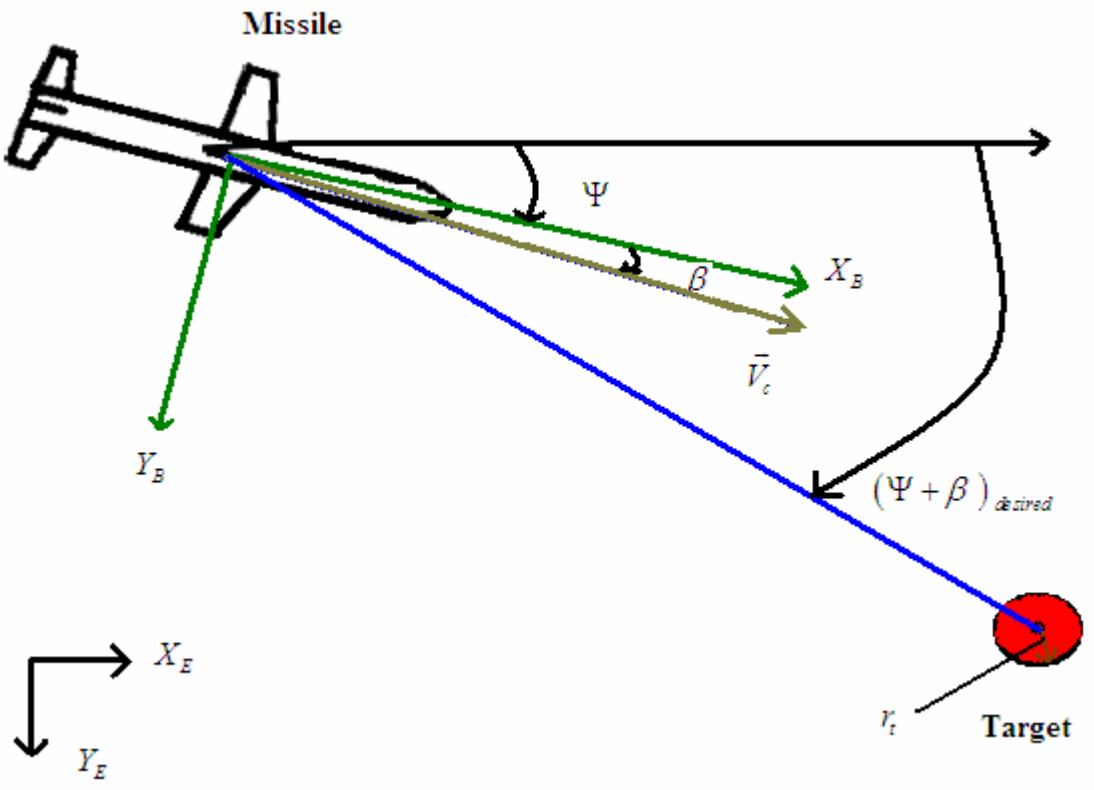

Figure 4-12 Lateral view of the missile and target

As a result, in order to hit the target, velocity vector should point target. This is the goal of the lateral guidance. Figure 4-13 displays the perfectly guided missile in

lateral coordinates. Hence, velocity vector $\vec{V}_c$ coincides with target vector $\vec{R}_T$ as a result of guidance.

It should be noted that while commanding yaw angle, side slip angle should be taken into account too. For the reason that, velocity vector should overlap on target vector rather than on X axis of the body-fixed frame.

This study assumes that atmosphere is at rest or to have a uniform velocity in space and constant. Therefore, small angle of side slip can be assumed. However, in turning maneuver, missile might have non-negligible side slip angle. This can be avoided by applying coordinated turn maneuver in which side force is kept zero so as to get zero side slip angle [13, 19].

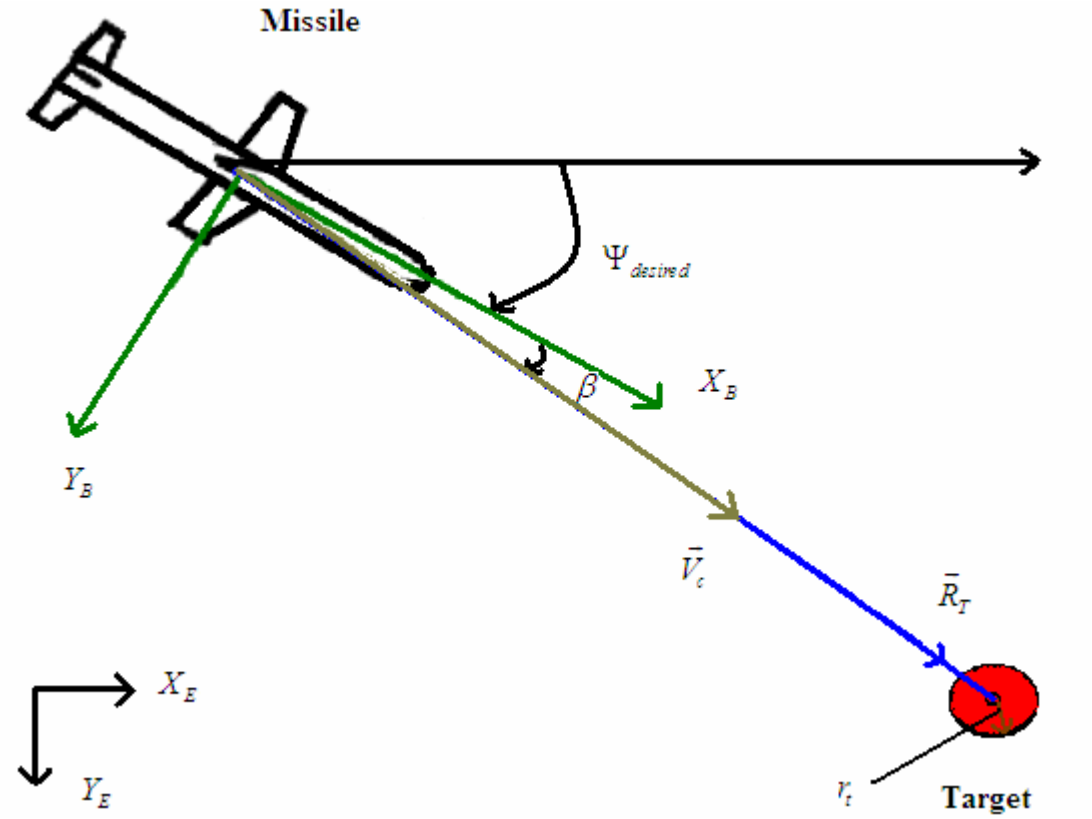

Figure 4-13 Lateral guidance

Assuming atmosphere is at rest or at uniform motion is a special case and not usual in real life. When there is wind, it needs to be added to calculations to obtain missile velocity terms with respect to Earth-fixed frame [13].

In this study both thrust vector and its magnitude are not controllable. Thrust is constant and available by propulsion section for approximately foremost 116 seconds. Afterwards, missile performs gravity-powered flight.

Above, guidance is explained in two subdivisions. This does not mean that longitudinal and lateral guidance are performed separately via controller. It is divided into two parts just to make the idea easier to follow.

Calculation of the yaw angle and flight path angle are geometrized in Figure 4-14.

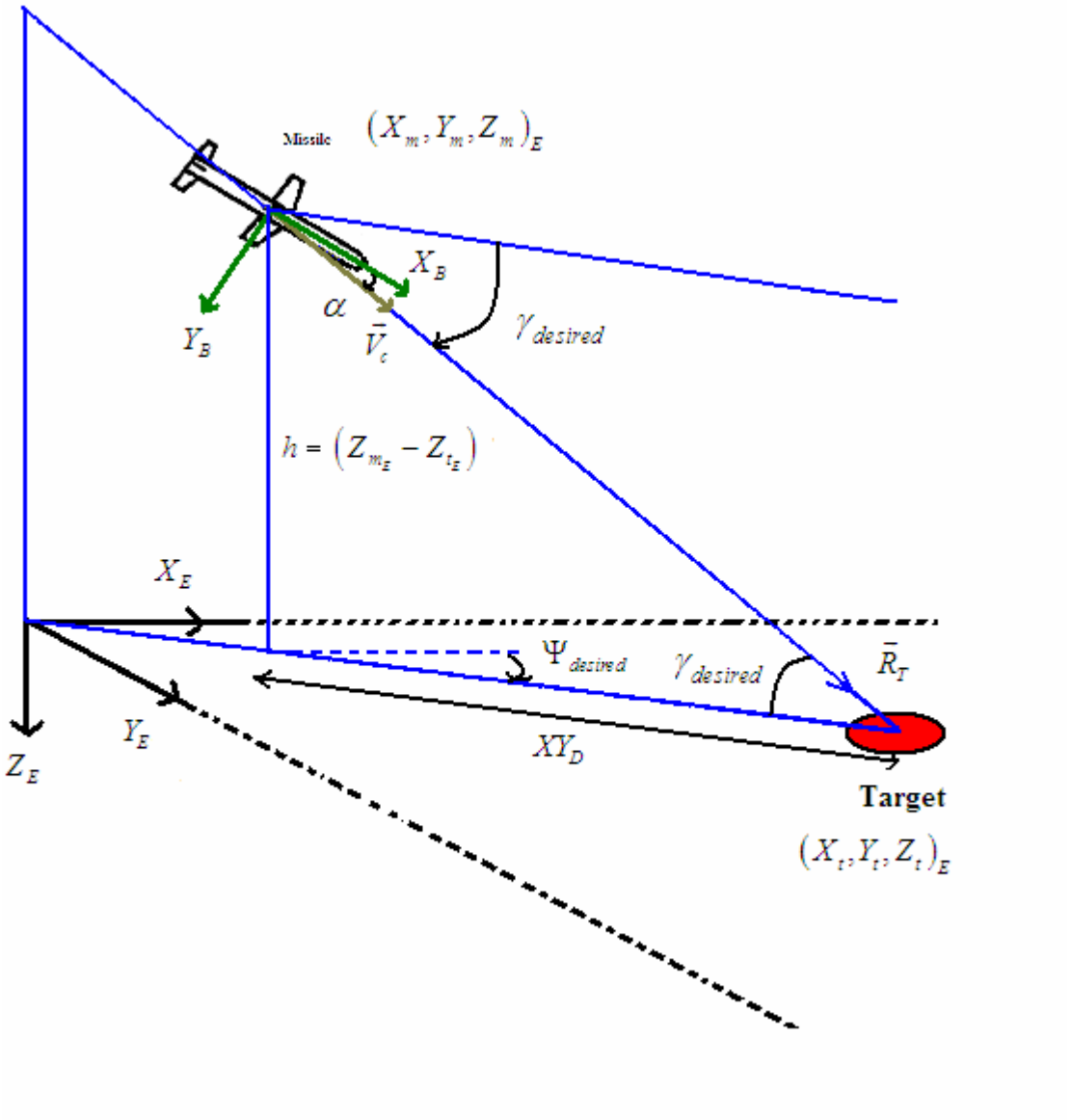

Figure 4-14 Desired yaw and flight path angle

Where, XY_D defines the distance from missile to target on XY plane of the Earth-fixed frame and h defines the altitude of the missile with respect to target. It is visible from the figure desired flight path angle is:

$$\gamma_{desired} = \tan^{-1} \frac{h}{XY_D} \tag{4.1}$$

and desired yaw angle is equal to:

$$\Psi_{desired} = \tan^{-1} \frac{\left(Y_{t_E} - Y_{m_E}\right)}{\left(X_{t_E} - X_{m_E}\right)} \tag{4.2}$$

In summary, the missile has Inertial Navigation System (INS) and Global Positioning System (GPS). INS has three accelerometers which measure accelerations along three mutually perpendicular axes. First integration of these accelerations give the velocities and second integration results in positions. INS is entirely contained in the missile and is programmed before launch. GPS's function is to correct the error in INS and so as to attain a high accuracy. To accomplish the explained guidance method, yaw angle and flight path angle are sent to the controller as the inputs and this is achieved in the next chapter.

CHAPTER 5

CONTROLLER

The guidance explained in previous chapter is achieved by nonlinear dynamics inverse controller. In this chapter, design of the correspondent controller is illustrated.

5.1 Missile flight control system

In guidance section, required control parameters are determined: flight path angle and yaw angle. Overall flight control system of the missile is composed of target, guidance, control variables modification, proportional-integral-derivative (PID) controller, inverse dynamic controller, actuators, and missile dynamics. A block diagram of the missile flight control system is given in Figure 5-1. Where, $(\gamma_{des}, \Psi_{des})$ is the pair of desired angles, flight path angle and yaw angle generated by guidance to orient missile velocity vector in the direction of the target. Guidance unit generates these angles via coordinates of missile and target in Earth-fixed frame represented by $(X_m, Y_m, Z_m)_E$ and $(X_t, Y_t, Z_t)_E$ respectively in the block diagram.

Guidance unit's output passes through modification. In this stage, control variables are modified either to achieve the desired trajectory or to moderate the control inputs to get preferred settling and transient responses. The control method, inverse dynamics control is implemented with PID feedback. Thrust's magnitude and direction is constant and non-controllable during the burning of propellant. Control is accomplished by aerodynamic surfaces: aileron, elevator and rudder. In figure, inverse dynamic controller in conjunction with PID is the autopilot of the system and it has the task of stabilizing of missile and tracking the guidance unit's outputs. $(\delta_{e\_cnd}, \delta_{a\_cnd}, \delta_{r\_cnd})$ are the respective commanded elevator, aileron, and rudder surface deflections by inverse dynamics controller. Actuators convert the commanded

elevator, aileron, and rudder surface deflections coming from the autopilot into achievable mechanical responses in order to deflect the fins to steer the missile towards the target.

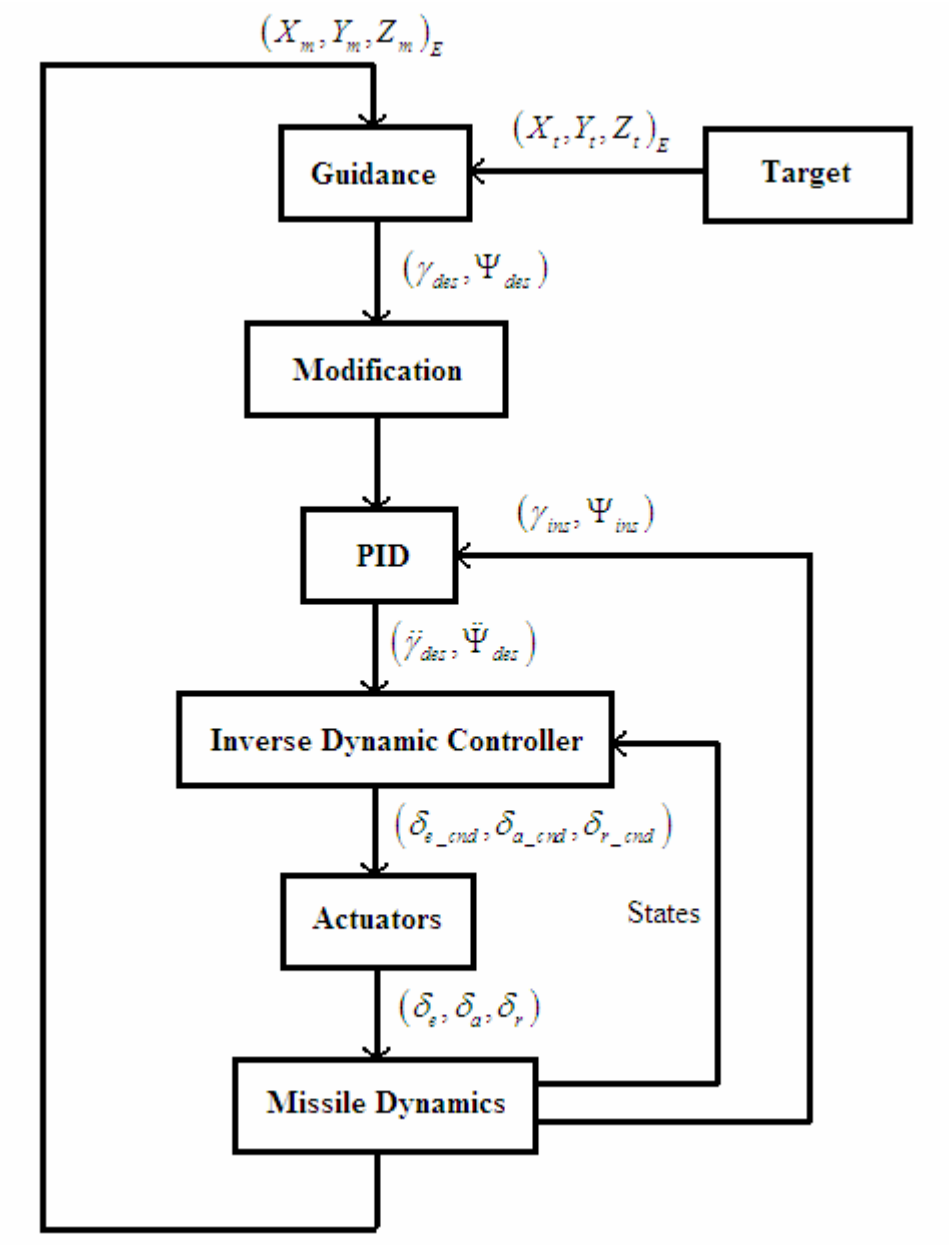

Figure 5-1 Missile flight control system

The transfer function of the actuators used in this missile is given in Equation (5.1).

$$\frac{\delta_{act}}{\delta_{cnd}} = \left(\frac{5}{5+s} \right)^2 \tag{5.1}$$

Where, the term δ_{cnd} stands for commanded surface deflection and δ_{act} stands for actual surface deflection attained by actuators. Missile dynamics in Figure 5-1 refers to the nonlinear 6 degrees of freedom model of the variable mass missile (see CHAPTER 2 for dynamics of the model).

5.2 PID

As affirmed previously, inverse dynamics control is executed with PID feedback. Consequently, the gradient of controller's response is adjusted by the proportional, integral and derivative gains. There are two PID controllers. One of which is for flight path angle feedback and another one is for heading angle feedback. That is, each PID controller is single input single output type. The dynamics of the inverse dynamics controller might be realized by PI or PD controller. Nonetheless, PI controller results in unsatisfactory overshoot performance and PD controller is not sufficient to overcome the steady state error. So, PID dynamic is preferred in this study. The steepness of the response is implemented by flight path angle and heading angle proportional gains respectively.

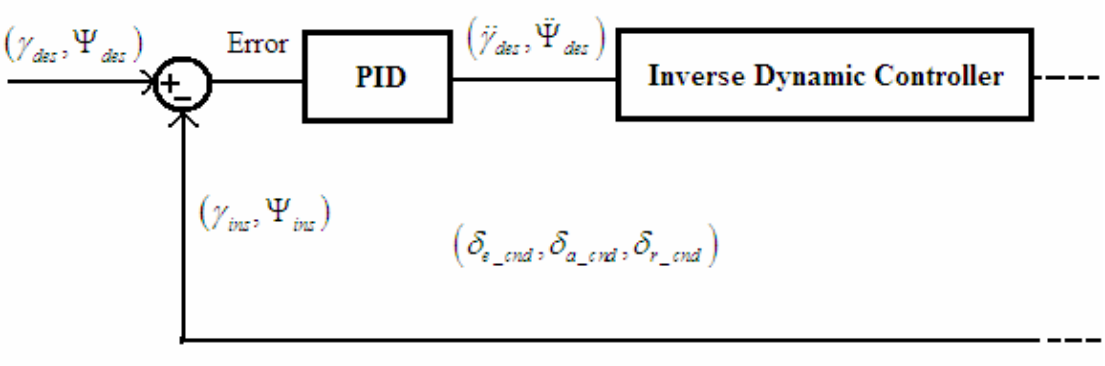

Figure 5-2 PID controller

Figure 5-2 illustrates the feedback loop involving PID controller. Actually this PID box consists of two PID controllers which are for flight path angle and heading angle. As seen from the figure, the inputs to the PID controllers are differences between desired angles coming from guidance unit and instantaneous true angles obtained from the missile dynamics. Outputs of the PID controllers are the second derivatives of the flight path angle and heading angle that are the inputs to the inverse dynamics controller.

5.3 Nonlinear inverse dynamic controller

Derivation method of the inverse dynamic is similar to the one in [12]. Equations of motion of the missile are derived in CHAPTER 2 and summarized through (2.123)-(2.137). They are re-summarized here for streamline of the derivation:

$$\dot{m}U + m\left(\dot{U} + QW - VR\right) = -mg\sin\Theta + F_{Ax} + F_{Tx} \tag{5.2}$$

$$\dot{m}V + m\left(\dot{V} + UR - PW\right) = mg\cos\Theta\sin\Phi + F_{Ay} \tag{5.3}$$

$$\dot{m}W + m\left(\dot{W} + PV - UQ\right) = mg\cos\Theta\cos\Phi + F_{Az} \tag{5.4}$$

$$\dot{I}_{xx}P + I_{xx}\dot{P} = L_A \tag{5.5}$$

$$\dot{I}_{yy}Q + I_{yy}\dot{Q} - \left(I_{zz} - I_{xx}\right)RP = M_A \tag{5.6}$$

$$\dot{I}_{zz}R + I_{zz}\dot{R} - \left(I_{xx} - I_{yy}\right)PQ = N_A \tag{5.7}$$

$$P = \dot{\Phi} - \dot{\Psi}\sin\Theta \tag{5.8}$$

$$Q = \dot{\Theta}\cos\Phi + \dot{\Psi}\cos\Theta\sin\Phi \tag{5.9}$$

$$R = \dot{\Psi}\cos\Theta\cos\Phi - \dot{\Theta}\sin\Phi \tag{5.10}$$

$$\begin{aligned}\dot{X}_E &= U\left(\cos\Theta\cos\Psi\right) + V\left(\sin\Phi\sin\Theta\cos\Psi - \cos\Phi\sin\Psi\right)\\ &+ W\left(\cos\Phi\sin\Theta\cos\Psi + \sin\Phi\sin\Psi\right)\end{aligned} \tag{5.11}$$

$$\begin{aligned}\dot{Y}_E &= U\left(\cos\Theta\sin\Psi\right) + V\left(\sin\Phi\sin\Theta\sin\Psi + \cos\Phi\cos\Psi\right)\\ &+ W\left(\cos\Phi\sin\Theta\sin\Psi - \sin\Phi\cos\Psi\right)\end{aligned} \tag{5.12}$$

$$\dot{Z}_E = U\left(-\sin\Theta\right) + V\left(\sin\Phi\cos\Theta\right) + W\left(\cos\Phi\cos\Theta\right) \tag{5.13}$$

$$\dot{\Psi} = \left(R\cos\Phi + Q\sin\Phi \right)\sec\Theta \tag{5.14}$$

$$\dot{\Theta} = Q\cos\Phi - R\sin\Phi \tag{5.15}$$

$$\dot{\Phi} = P + \left(R\cos\Phi + Q\sin\Phi \right)\tan\Theta \tag{5.16}$$

The inputs to the inverse dynamics controller are:

- $\ddot{\Psi}$
- $\ddot{\gamma}$

In other words, they are the commanded terms in the flight control system. Moment equations through (5.5)-(5.7) contains the rate of change of angular velocities of the missile in body-fixed frame which play the role of dictating required control surface deflections. Rate of change of angular velocities can be obtained by taking time derivative of Equations(5.8),(5.9) and (5.10). They include the terms:

- $\ddot{\Theta}$
- $\ddot{\Phi}$
- $\ddot{\Psi}$

These are the resultant commanded terms of the system. Therefore, it is needed to find $\ddot{\Phi}$ and $\ddot{\Theta}$, so two equations.

First one can be obtained from incorporation of Equations of (5.8) and (5.10) into Equation (5.3). Before this incorporation, it ought to be noted that in coordinated turn lateral acceleration is zero; as a result, F_{Ay} is zero in Equation (5.3) [13]. Consequently, after some manipulation, first equation is obtained as below:

$$\boxed{\dot{\Phi} = \frac{\frac{\dot{m}}{m}V + \dot{V} + \dot{\Psi}\left(U\cos\Theta\cos\Phi + W\sin\Theta \right) - U\dot{\Theta}\sin\Phi - g\cos\Theta\sin\Phi}{W}} \tag{5.17}$$

Second equation can be acquired from the Figure 5-3. It is observable from the figure that:

$$U = V_c\cos\beta\cos\alpha \tag{5.18}$$

$$V = V_c\sin\beta \tag{5.19}$$

$$W = V_c\cos\beta\sin\alpha \tag{5.20}$$

$$\sin\gamma = \frac{-W_E}{V_c} \tag{5.21}$$

where:

$$W_E = \dot{Z}_E \tag{5.22}$$

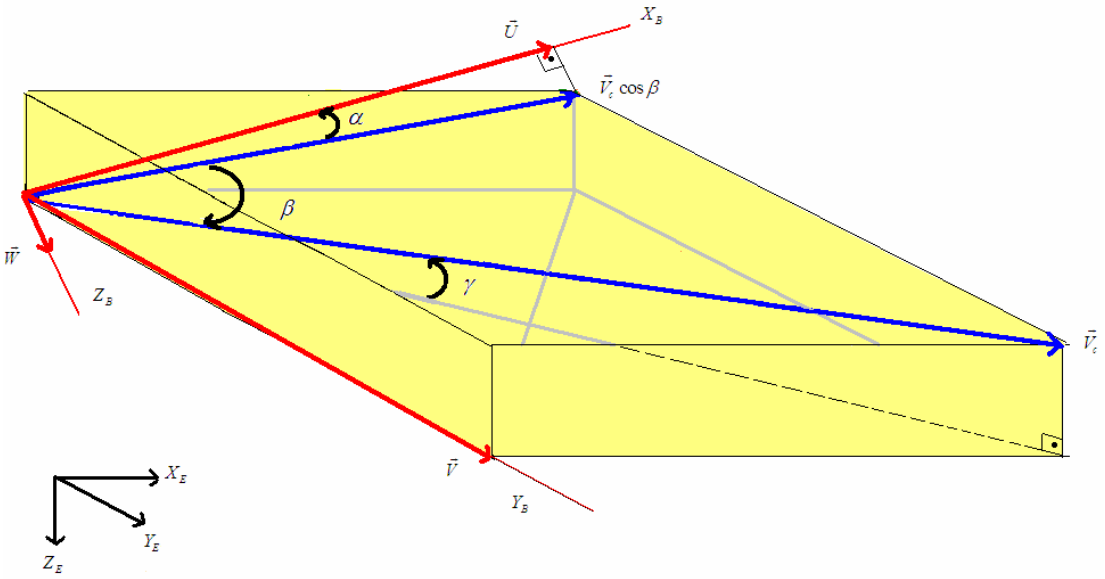

Figure 5-3 Flight path angle, side slip angle and angle of attack

Hence, when Equation (5.13) integrated in Equation (5.21), Equation (5.21) takes the form of:

$$\sin\gamma = \frac{U\left(\sin\Theta\right) - V\left(\sin\Phi\cos\Theta\right) - W\left(\cos\Phi\cos\Theta\right)}{V_c} \tag{5.23}$$

Via Equations from (5.18) to (5.20), $\sin\gamma$ is obtained as:

$$\boxed{\sin\gamma = \cos\beta\cos\alpha\sin\Theta - \sin\beta\sin\Phi\cos\Theta - \cos\beta\sin\alpha\cos\Phi\cos\Theta} \tag{5.24}$$

Finally, via some derivations and manipulations of the Equation (5.17) and Equation (5.24), expressions of $\ddot{\Phi}$ and $\ddot{\Theta}$ can be obtained.

Next step in the inverse dynamics controller is to get the rates of change of angular velocities, $\dot{P}$, $\dot{Q}$ and $\dot{R}$ by means of $\ddot{\Psi}$, $\ddot{\Theta}$ and $\ddot{\Phi}$. Afterward, these rates are put into force and moment equations to find the required control surface deflections.

Briefly, inverse dynamic controller first gets $\ddot{\gamma}$, $\ddot{\Psi}$ then finds corresponding $\ddot{\Phi}$ and $\ddot{\Theta}$, subsequently calculates related rates of change of angular velocities, $\dot{P}$, $\dot{Q}$ and $\dot{R}$ and lastly attains the required surface deflections via Equations throughout (5.2)-(5.7). This procedure is explained below.

To obtain the required elevator deflection, aerodynamic moment term, M_A, in Equation (5.25) needs to be expanded via moment coefficient, C_m (see Equation (5.27)).

$$\dot{I}_{yy}Q + I_{yy}\dot{Q} - \left(I_{zz} - I_{xx}\right)RP = M_A \tag{5.25}$$

$$M_A = C_m q_\infty Sd \tag{5.26}$$

$$C_m = C_{m_o} + C_{m_u}\frac{u}{V_\infty} + C_{m_\alpha}\alpha + C_{m_{\dot{\alpha}}}\dot{\alpha}\frac{d}{2V_\infty} + C_{m_q}q\frac{d}{2V_\infty} + C_{m_{\delta_e}}\delta_e \tag{5.27}$$

Therefore, elevator deflection is obtained as follow:

$$\delta_e = \frac{\dot{I}_{yy}Q + I_{yy}\dot{Q} - \left(I_{zz} - I_{xx}\right)RP}{q_\infty SdC_{m_{\delta_e}}} - \frac{C_{m_o} + C_{m_u}\frac{u}{V_\infty} + C_{m_\alpha}\alpha + C_{m_{\dot{\alpha}}}\dot{\alpha}\frac{d}{2V_\infty} + C_{m_q}q\frac{d}{2V_\infty}}{C_{m_{\delta_e}}} \tag{5.28}$$

Via the same way, aileron and rudder deflections can be obtained using the equations (5.29) to (5.37).

$$\dot{m}V + m\left(\dot{V} + UR - PW\right) = mg\cos\Theta\sin\Phi + F_{Ay} \tag{5.29}$$

$$\dot{I}_{xx}P + I_{xx}\dot{P} = L_A \tag{5.30}$$

$$\dot{I}_{zz}R + I_{zz}\dot{R} - \left(I_{xx} - I_{yy}\right)PQ = N_A \tag{5.31}$$

$$F_{A_y} = C_y q_\infty S \tag{5.32}$$

$$L_A = C_l q_\infty Sd \tag{5.33}$$

$$N_A = C_n q_\infty Sd \tag{5.34}$$

$$C_y = C_{y_o} + C_{y_\beta}\beta + C_{y_p} p\frac{d}{2V_\infty} + C_{y_r} r\frac{d}{2V_\infty} + C_{y_{\delta_a}}\delta_a + C_{y_{\delta_r}}\delta_r \tag{5.35}$$

$$C_l = C_{l_o} + C_{l_\beta}\beta + C_{l_p} p\frac{d}{2V_\infty} + C_{l_r} r\frac{d}{2V_\infty} + C_{l_{\delta_a}}\delta_a + C_{l_{\delta_r}}\delta_r \tag{5.36}$$

$$C_n = C_{n_o} + C_{n_\beta}\beta + C_{n_p} p\frac{d}{2V_\infty} + C_{n_r}\mathrm{r}\frac{d}{2V_\infty} + C_{n_{\delta_a}}\delta_a + C_{n_{\delta_r}}\delta_r \tag{5.37}$$

Resultant equation which shows the required aileron and rudder deflections apart from sideslip angle is obtained in Equation (5.38).

$$\begin{bmatrix}\beta\\ \delta_a\\ \delta_r\end{bmatrix} = \begin{bmatrix} C_{n_\beta} & C_{n_{\delta_a}} & C_{n_{\delta_r}} \\ C_{l_\beta} & C_{l_{\delta_a}} & C_{l_{\delta_r}} \\ C_{y_\beta} & C_{y_{\delta_a}} & C_{y_{\delta_r}} \end{bmatrix}^{-1} \begin{bmatrix} \dfrac{\dot{I}_{zz}R + I_{zz}\dot{R} - \left(I_{xx} - I_{yy}\right)PQ}{q_\infty Sd} - C_{n_o} - C_{n_p} p\dfrac{d}{2V_\infty} - C_{n_r}\mathrm{r}\dfrac{d}{2V_\infty} \\ \dfrac{\dot{I}_{xx}P + I_{xx}\dot{P}}{q_\infty Sd} - C_{l_o} - C_{l_p} p\dfrac{d}{2V_\infty} - C_{l_r} r\dfrac{d}{2V_\infty} \\ -C_{y_o} - C_{y_p} p\dfrac{d}{2V_\infty} - C_{y_r} r\dfrac{d}{2V_\infty} \end{bmatrix} \tag{5.38}$$

In this study, corresponding stability derivatives are calculated at correspondent angle of attack, sideslip angle, and Mach number; as a result, variation of C_n, C_y, and C_l with respect to sideslip angle can be included in C_{n_o}, C_{y_o}, and C_{l_o} terms. Thus, Equation (5.38) becomes:

$$\begin{bmatrix}\delta_a\\ \delta_r\end{bmatrix} = A^{-1}B \tag{5.39}$$

where:

$$A = \begin{bmatrix} C_{n_{\delta_a}} & C_{n_{\delta_r}} \\ C_{l_{\delta_a}} & C_{l_{\delta_r}} \\ C_{y_{\delta_a}} & C_{y_{\delta_r}} \end{bmatrix}^T \begin{bmatrix} C_{n_{\delta_a}} & C_{n_{\delta_r}} \\ C_{l_{\delta_a}} & C_{l_{\delta_r}} \\ C_{y_{\delta_a}} & C_{y_{\delta_r}} \end{bmatrix} \tag{5.40}$$

$$B = \begin{bmatrix} C_{n_{\delta_a}} & C_{n_{\delta_r}} \\ C_{l_{\delta_a}} & C_{l_{\delta_r}} \\ C_{y_{\delta_a}} & C_{y_{\delta_r}} \end{bmatrix}^T \begin{bmatrix} \dfrac{\dot{I}_{zz}R + I_{zz}\dot{R} - \left(I_{xx} - I_{yy}\right)PQ}{q_\infty Sd} - C_{n_o} - C_{n_p} p\dfrac{d}{2V_\infty} - C_{n_r} \mathrm{r}\dfrac{d}{2V_\infty} \\ \dfrac{\dot{I}_{xx}P + I_{xx}\dot{P}}{q_\infty Sd} - C_{l_o} - C_{l_p} p\dfrac{d}{2V_\infty} - C_{l_r} r\dfrac{d}{2V_\infty} \\ -C_{y_o} - C_{y_p} p\dfrac{d}{2V_\infty} - C_{y_r} r\dfrac{d}{2V_\infty} \end{bmatrix} \tag{5.41}$$

Where, superscript T shows the transpose operation of the corresponding matrix.

CHAPTER 6

RESULTS

This chapter is composed of the simulation results for inspection and verification of the missile design and principally missile dynamics, guidance and control. For this purpose more than a few cases corresponding to different trajectories were studied; nonetheless, for conciseness, decisive ones are presented here. In particular, the cases in which the missile completes its flight before burn-out are presented so that it enables us to scrutinize the control characteristics of the missile throughout the propulsion. Corresponding cases are:

- Case I : Cruise trajectory
- Case II : Arc trajectory
- Case III : Dive trajectory
- Case IV : Immediate dive trajectory
- Case V : High initial angle, 45 deg
- Case VI : Moving target with 8 m/s on X-axis in inertial frame

Table 6-1 summarizes the early positions of missile and target for each case. It includes the initial velocity of the missile at each case as well.

Table 6-1 Initial conditions and coordinates of the missile and target for cases

Case	Missile Initial Conditions				Target Coordinates			Initial Angle (deg)
	X (m)	Y (m)	Release Altitude (m)	Release Velocity (m/s)	X (m)	Y (m)	Z (m)	
I	0	0	4000	300	80000	25000	0	17.35
II	0	0	4000	300	140000	25000	0	10.12
III	0	0	4000	300	25000	3000	0	6.84
IV	0	0	4000	300	15000	1000	0	3.81
V	0	0	4000	300	50000	50000	0	45
VI	0	0	4000	300	80000	10000	0	7.13

Initial angle defines the angle between velocity vector of the missile and the target vector, $\vec{R}_T$ that connects the missile to the target, at separation of the missile from aircraft.

In trajectory plots, X, Y, Z axes correspond to Earth-fixed frame. It needs to be noted that –Z is equal to the altitude of the missile and positive Z points the center of Earth. The radius of the target is 50m for each case and it is observable in the correspondent XY plane flight path of each case.

Main difference in the last case is having moving target. In this case, target, which can be a warship, moves with velocity 8 m/s on X-axis of inertial frame.

6.1 Case I

This case is called cruise trajectory since it is kept at constant altitude before diving maneuver. However, it is different from general cruise in that its velocity is not constant. Therefore, it makes the trajectory more difficult to attain. Figure 6-1 and Figure 6-2 show the trajectory of the missile in XZ plane and Figure 6-3 and Figure 6-4 show that in XY plane. It is obvious from the figure that missile accomplishes to

keep the cruise altitude by an oscillation less than 140 m around the cruise altitude that is caused by the airspeed variation resulting in lift change. Meanwhile the airspeed of the missile increases up to 526 m/s (1.62 M) in which burn-out occurs and the airspeed starts decreasing till diving stage (see Figure 6-9 and Figure 6-10). In diving, via gravity, speed reaches to 313 m/s (0.92 M) in which termination of the target takes place.

Instead of using exact initial trim conditions, estimated trim point is used to test the adaptability of the missile and it is seen from Figure 6-7 that, the missile achieves its dynamic stability after a little period of time, 5 s. Sideslip angle remains very small throughout the flight; therefore, commanded heading angle steers the missile to the target with negligibly small error (see Figure 6-8). This steering is actualized at the beginning of the flight in order to maximize the effective range of the missile. Figure 6-6 demonstrates the commanded and actual heading angles where rise time is about 13 seconds. The settling time is not small because of the nonlinear aerodynamics of the missile wherein aerodynamic coefficients and stability derivatives change nonlinearly. Actually, this simulation reveals closer results to the real time applications. This steering is attained by coordinated turn. Required bank angle for this turn reaches up to 42 degrees (see Figure 6-11). Figure 6-13 and Figure 6-14 illustrate the correspondent aileron and rudder deflections for this turn. This is obtained by very small deflection angles owing to all moving fins. Figure 6-13 gives an idea about the stability about the longitudinal axis, X. It lacks of stability about X axis, so aileron continuously deflects to hold the zero bank angle. This stability is generally provided dihedral angle; nevertheless, they may cause more contact in shock wave and so heat dissipation problems. This is out of the scope of this thesis.

When the missile is as close to the target as desired to get aimed impact angle controller starts getting the flight path angle given in Figure 6-5. Elevator deflection range for this maneuver is quite reasonable (see Figure 6-12). Although, the rise time for flight path angle is not very fast, it is quite acceptable for fixed targets. In fact, the slow response can be improved by modifying the PID gains, especially modifying flight path angle proportional and derivative gains. Nonetheless, faster response

makes the pitch rate steeper and that results more severe inertial coupling (see Case II for inertial coupling) that may result in big circular error of probability owing to disturbance in dynamic stability.

Variation of mass, center of gravity, moments of inertia about X, Y, and Z axis are given throughout Figure 6-15 - Figure 6-19 .Furthermore, roll rate, pitch rate and yaw rate related to maneuvers are given through the Figure 6-20 - Figure 6-22.

Circular error of probabilities on XZ and XY planes can be obtained from Figure 6-2 and Figure 6-4 respectively. It is 1 m on XZ plane and less than 1 m on XY plane.

To sum up, even though the response of longitudinal maneuvers is sort of slow, the missile is able to achieve to terminate the target by less than 1 m circular error of probability.

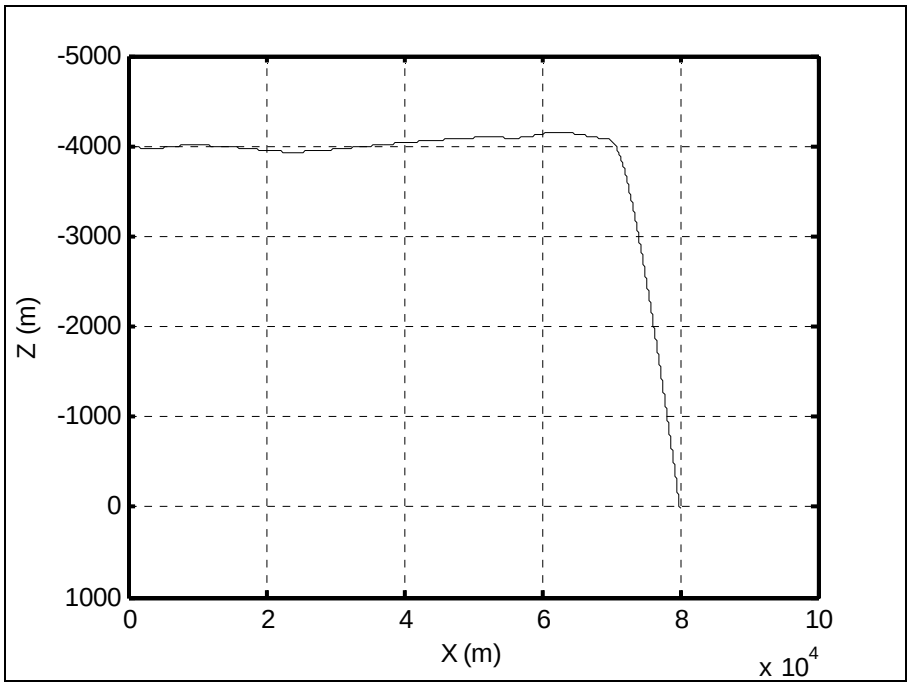

Figure 6-1 XZ plane flight path for case I

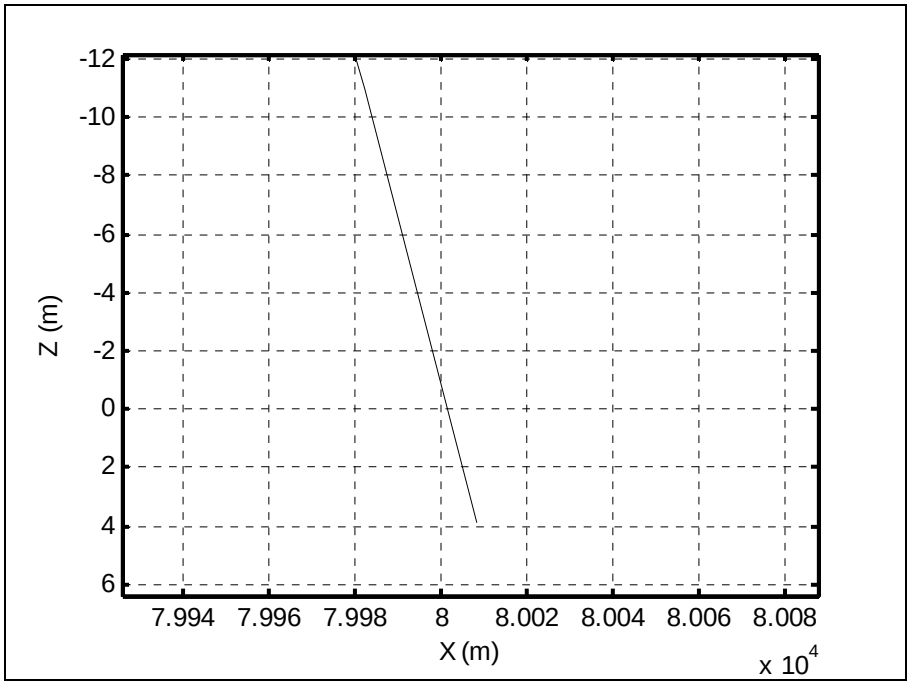

Figure 6-2 XZ plane missile-target interception for case I

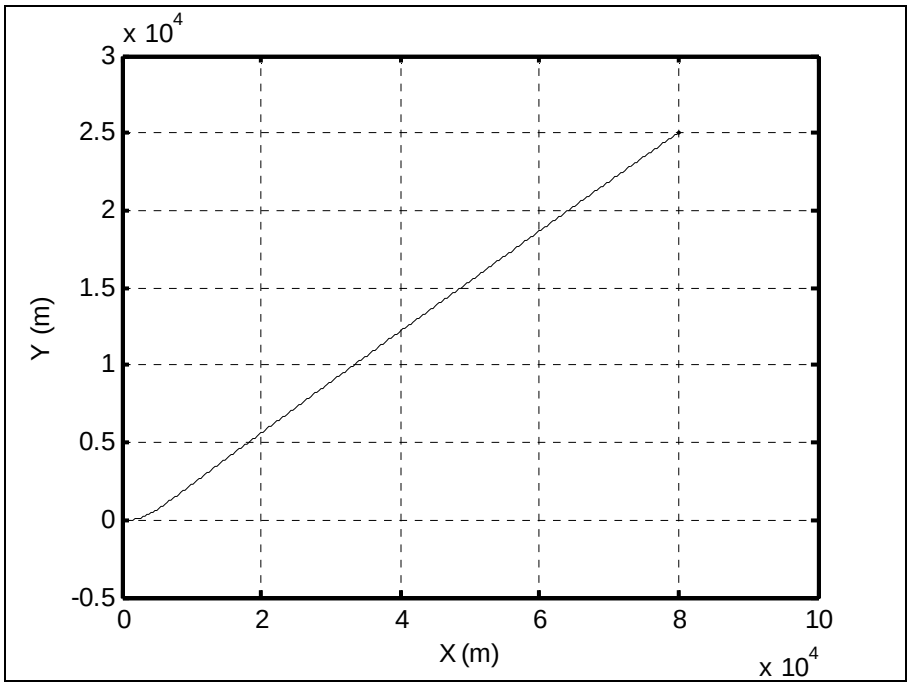

Figure 6-3 XY plane flight path for case I

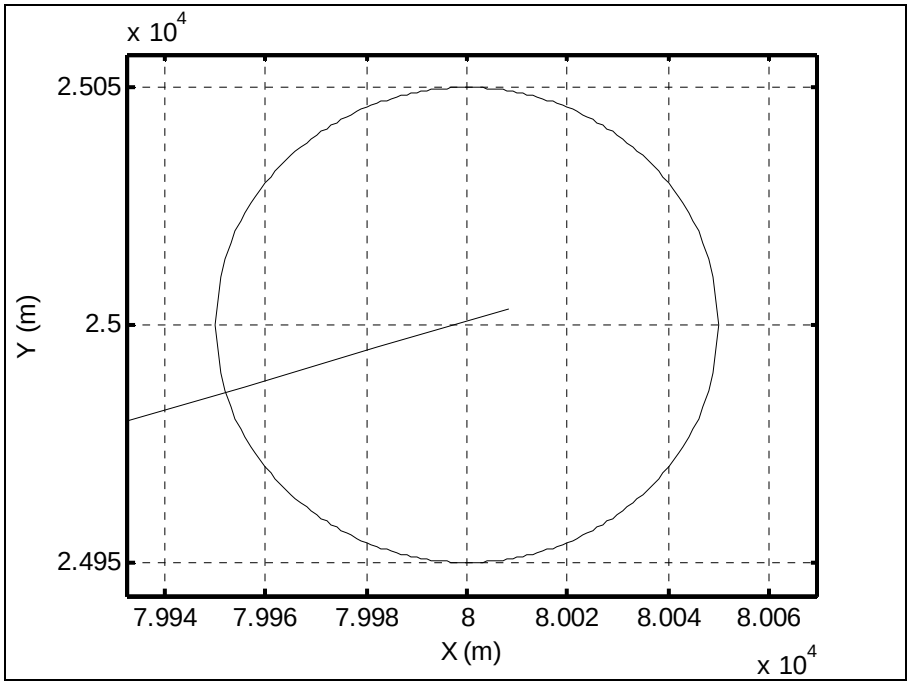

Figure 6-4 XY plane missile-target interception for case I

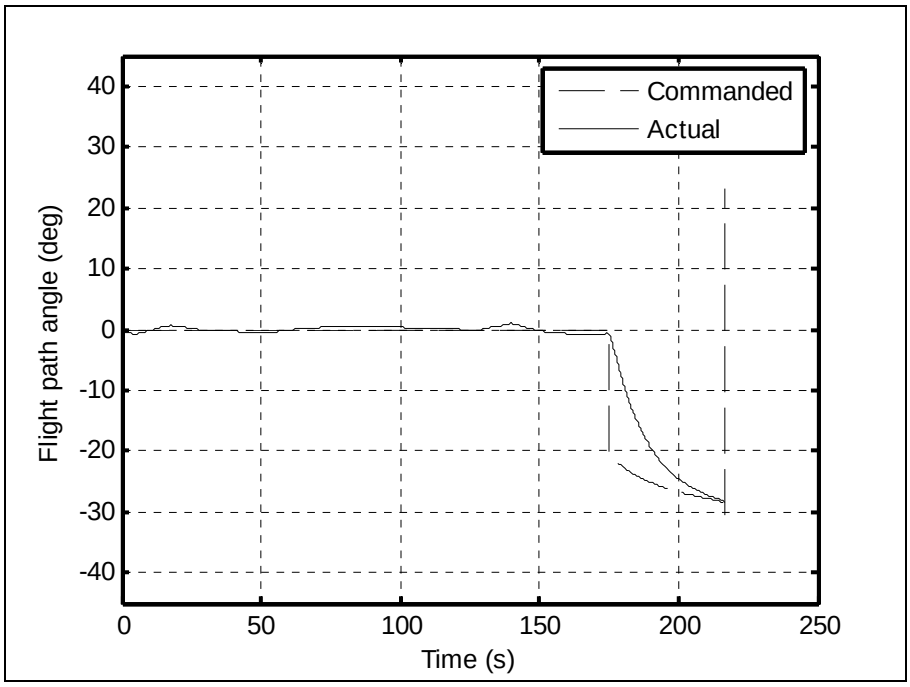

Figure 6-5 Flight path angle for case I

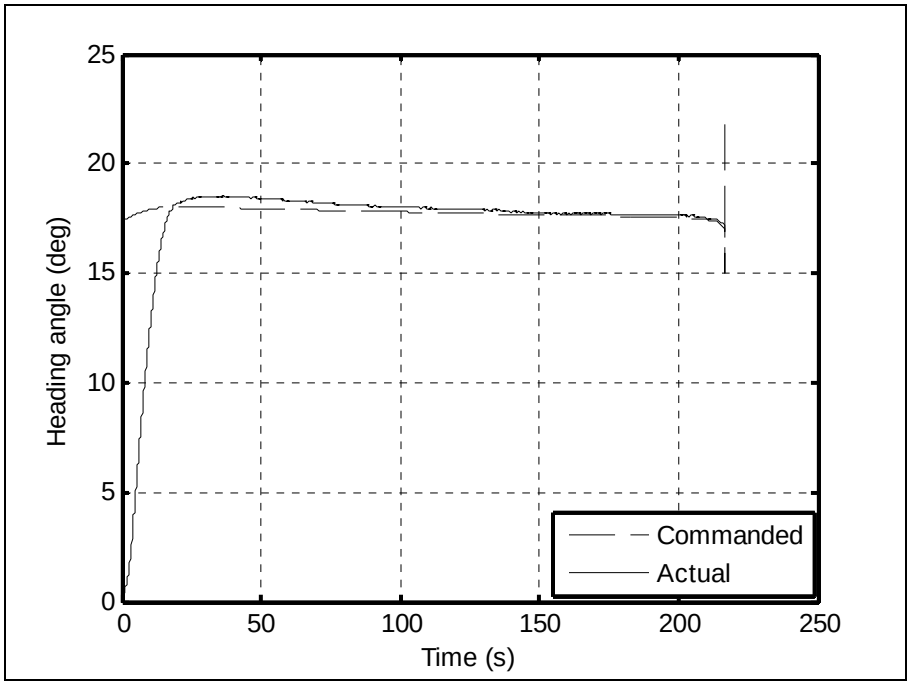

Figure 6-6 Heading angle for case I

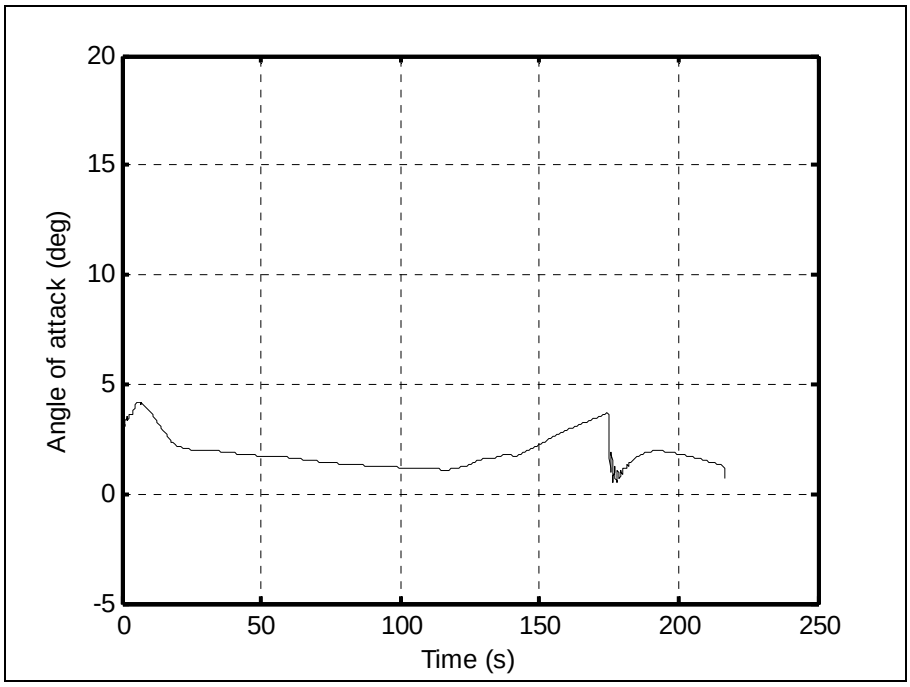

Figure 6-7 Angle of attack for case I

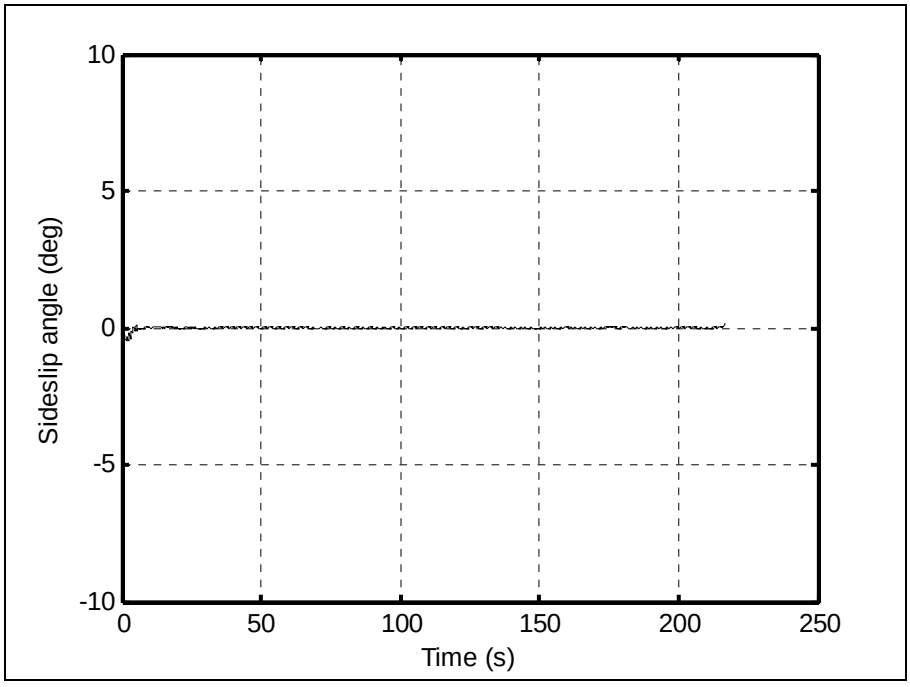

Figure 6-8 Sideslip angle for case I

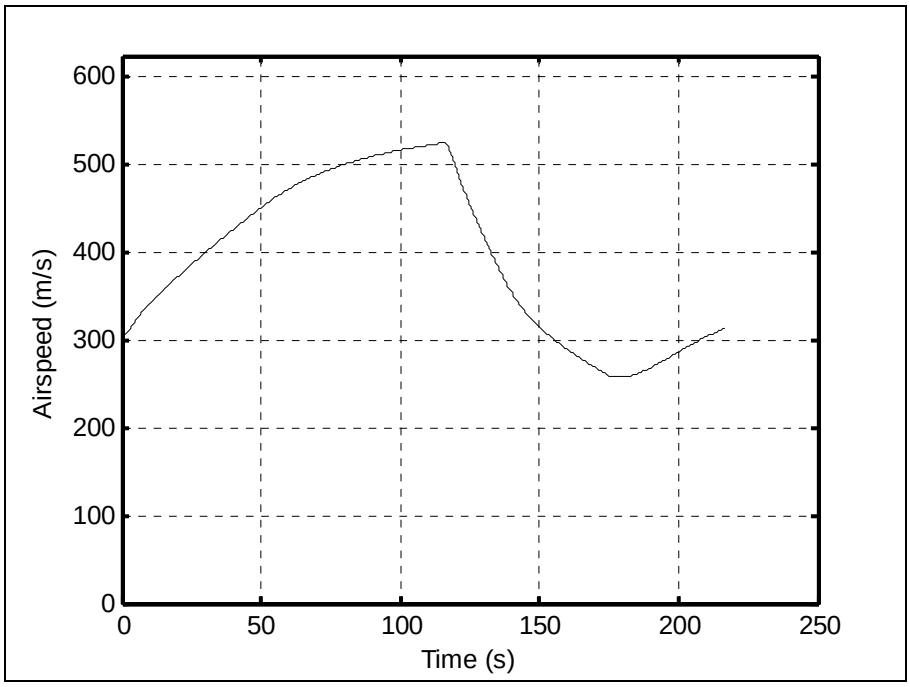

Figure 6-9 Airspeed for case I

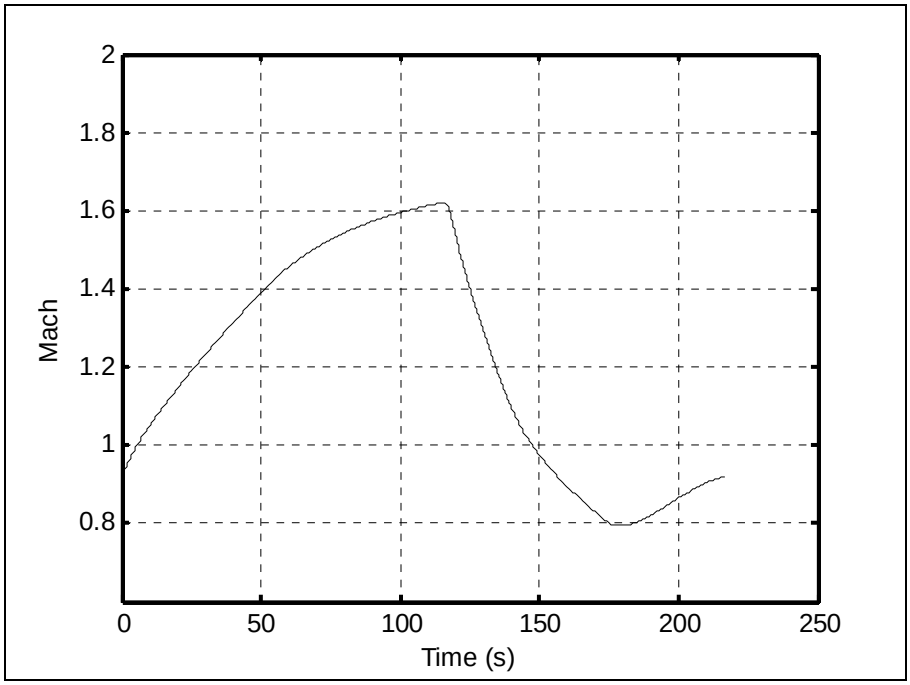

Figure 6-10 Mach number for case I

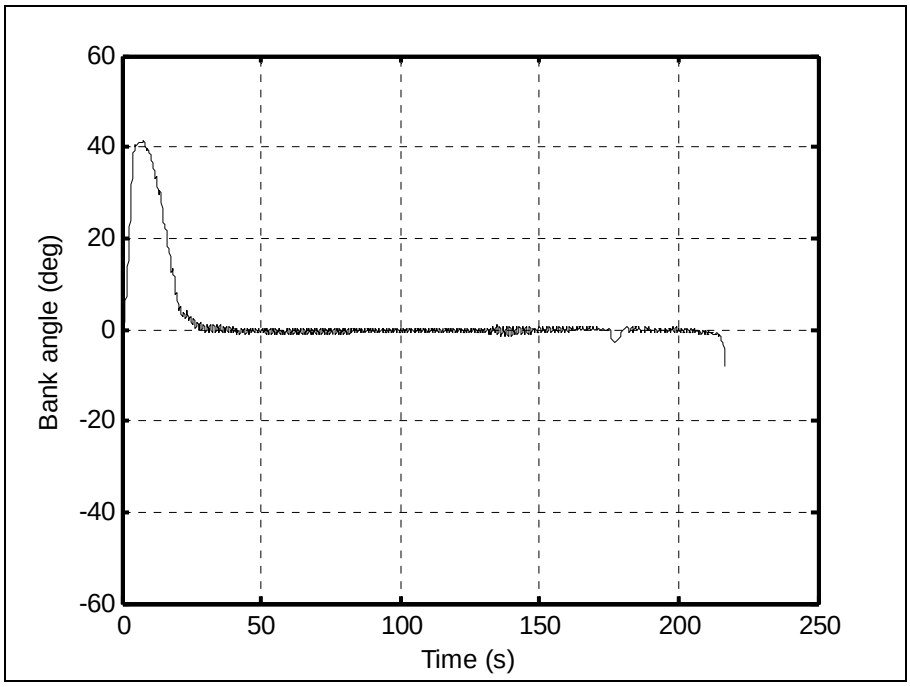

Figure 6-11 Bank angle for case I

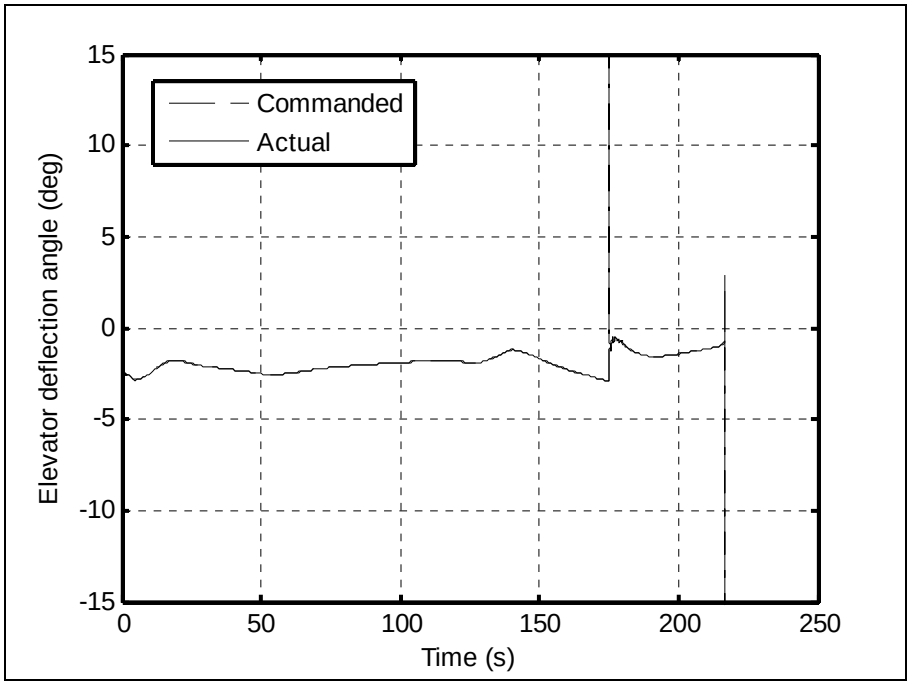

Figure 6-12 Elevator deflection angle for case I

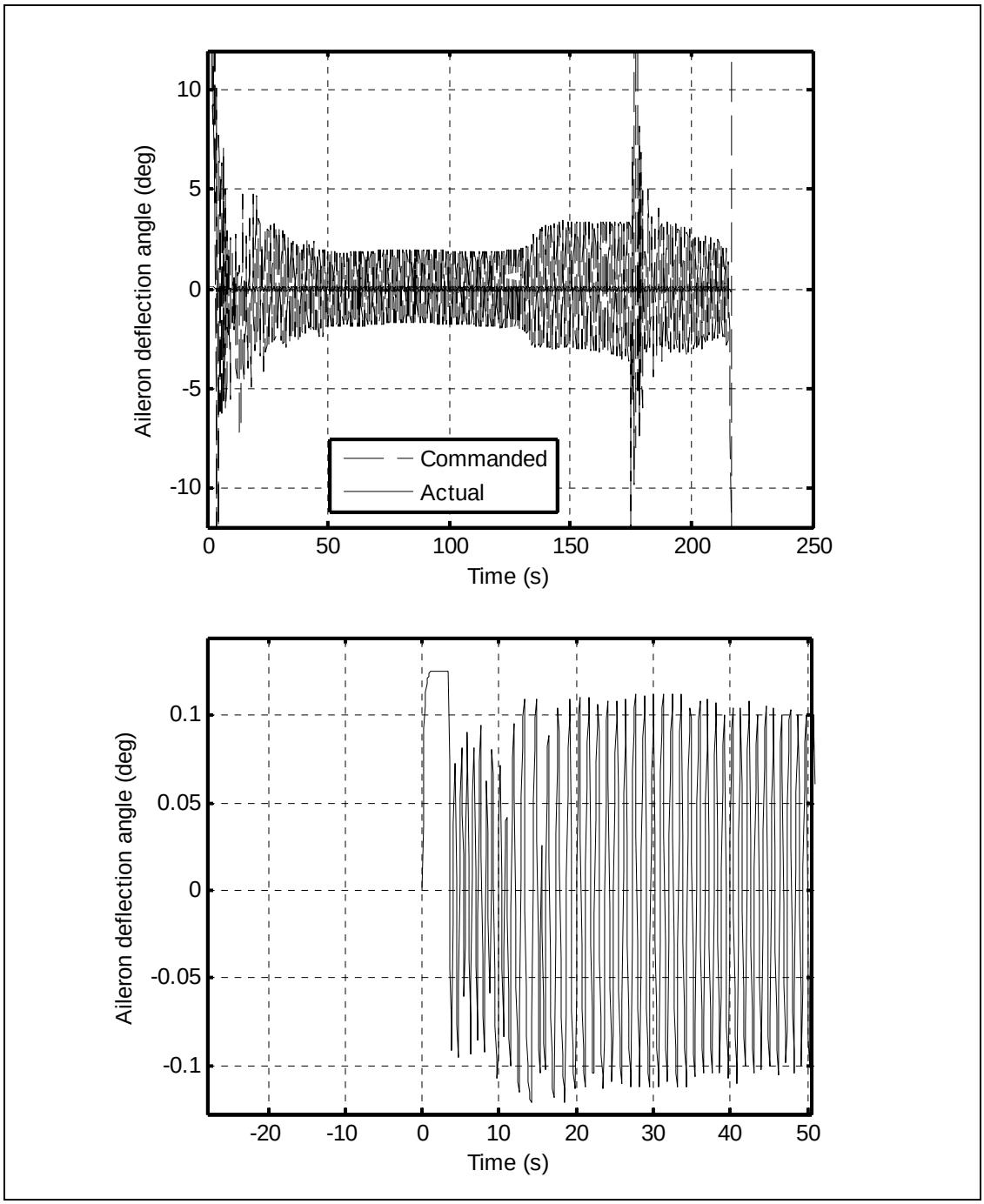

Figure 6-13 Aileron deflection angle for case I

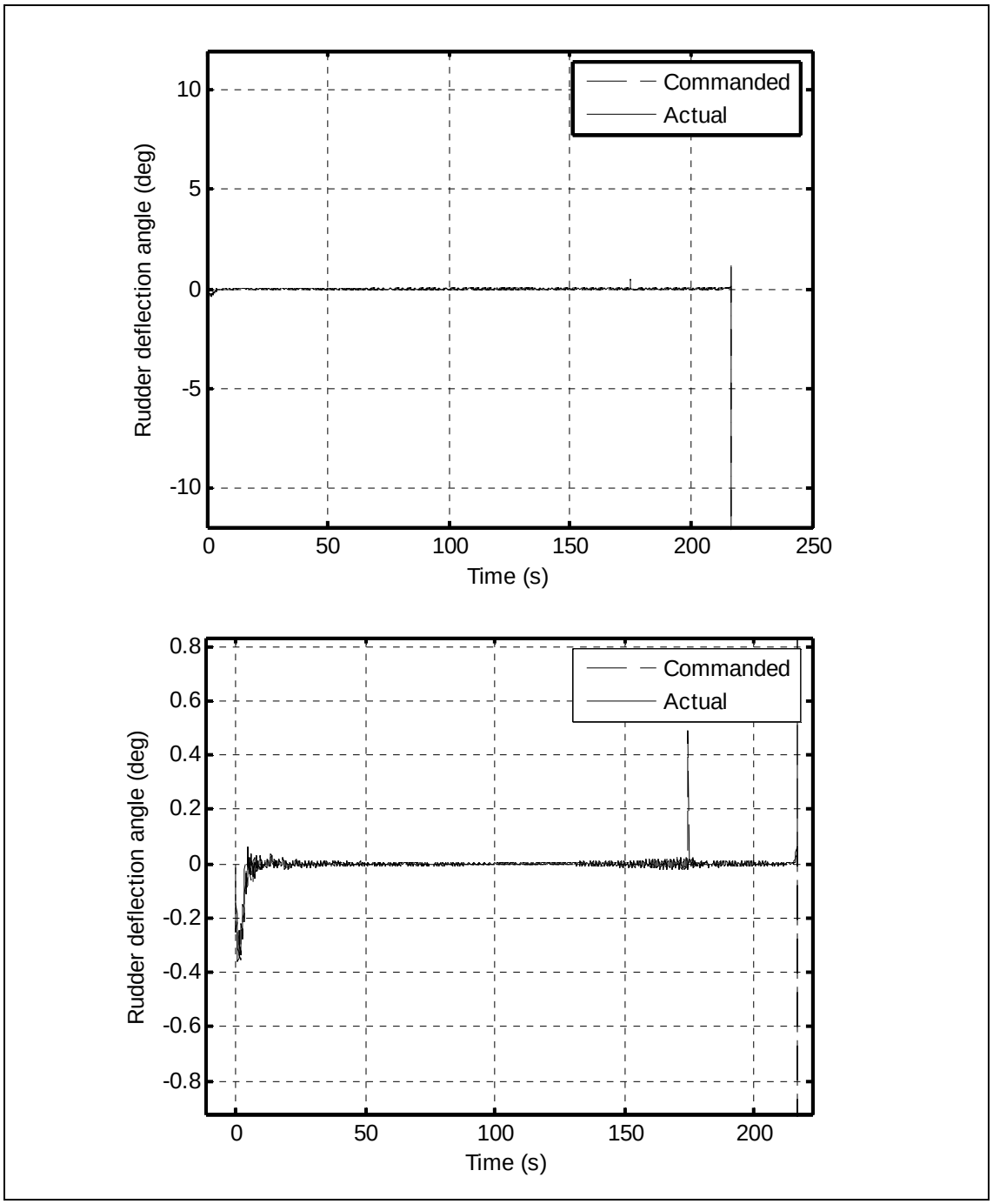

Figure 6-14 Rudder deflection angle for case I

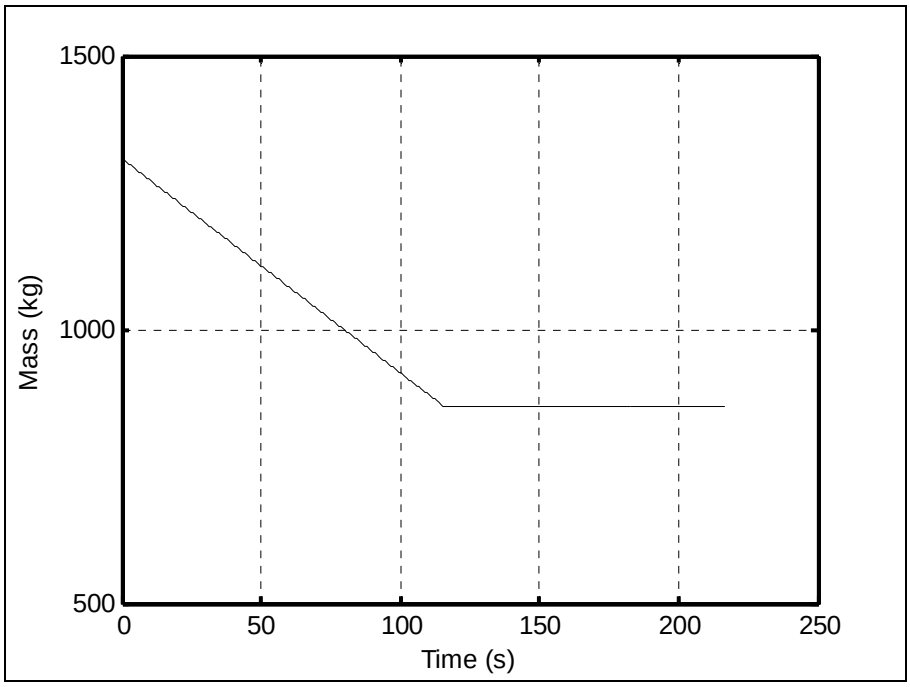

Figure 6-15 Variation of the missile's mass for case I

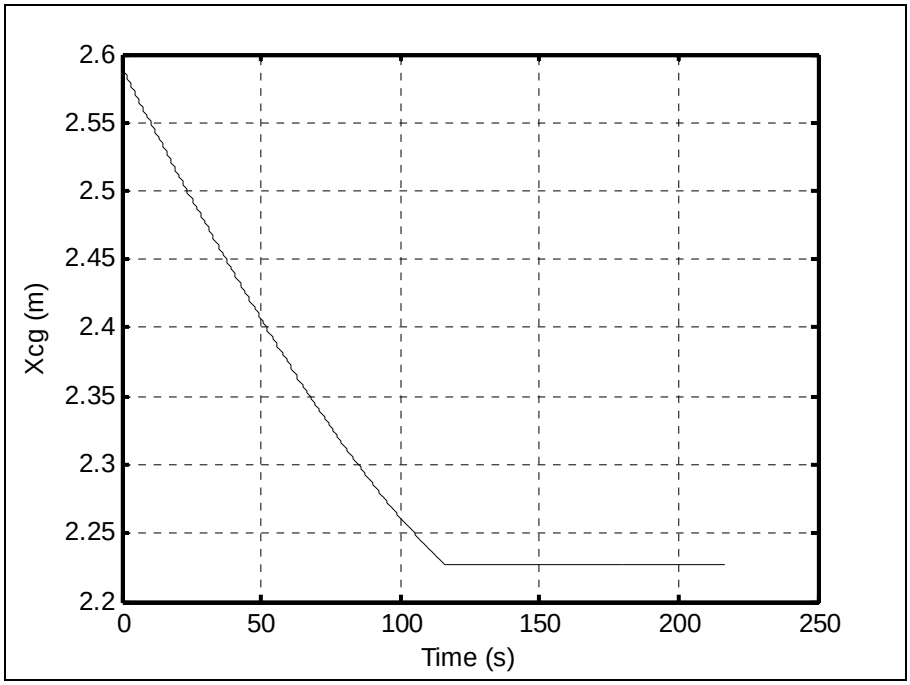

Figure 6-16 Center of gravity for case I

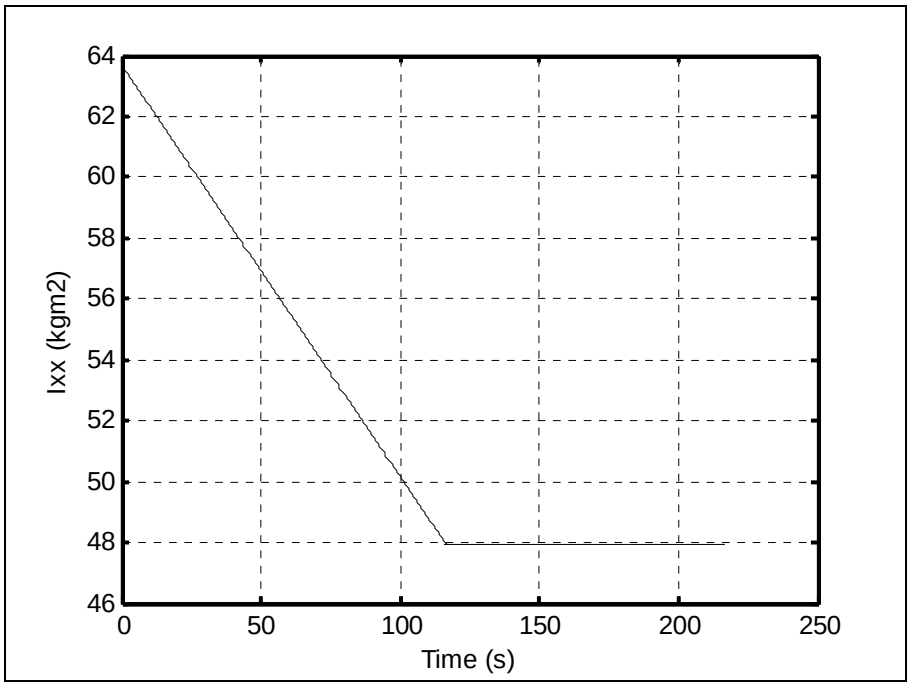

Figure 6-17 Moment of inertia about X axis for case I

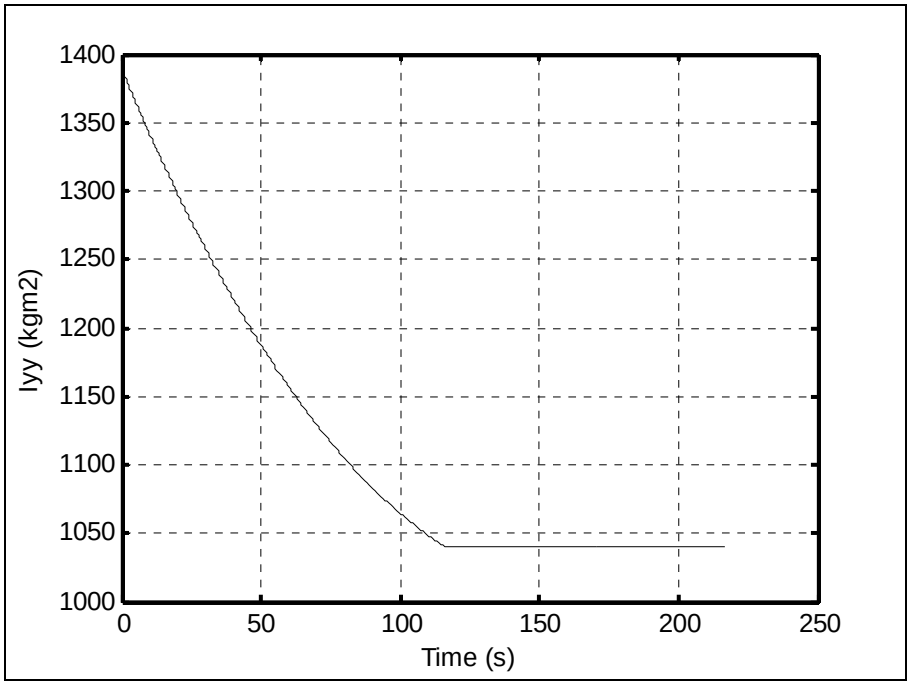

Figure 6-18 Moment of inertia about Y axis for case I

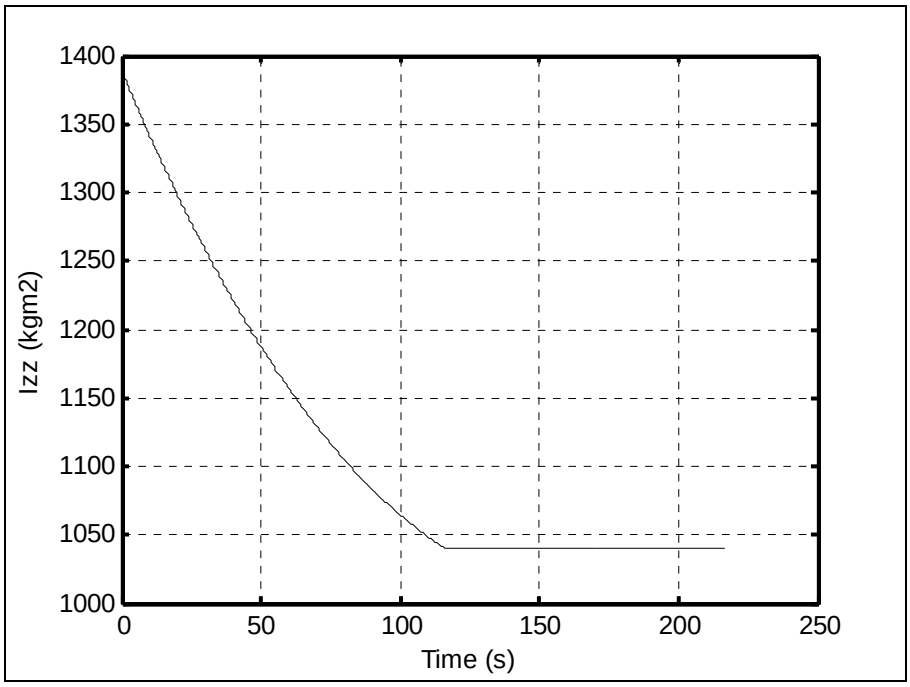

Figure 6-19 Moment of inertia about Z axis for case I

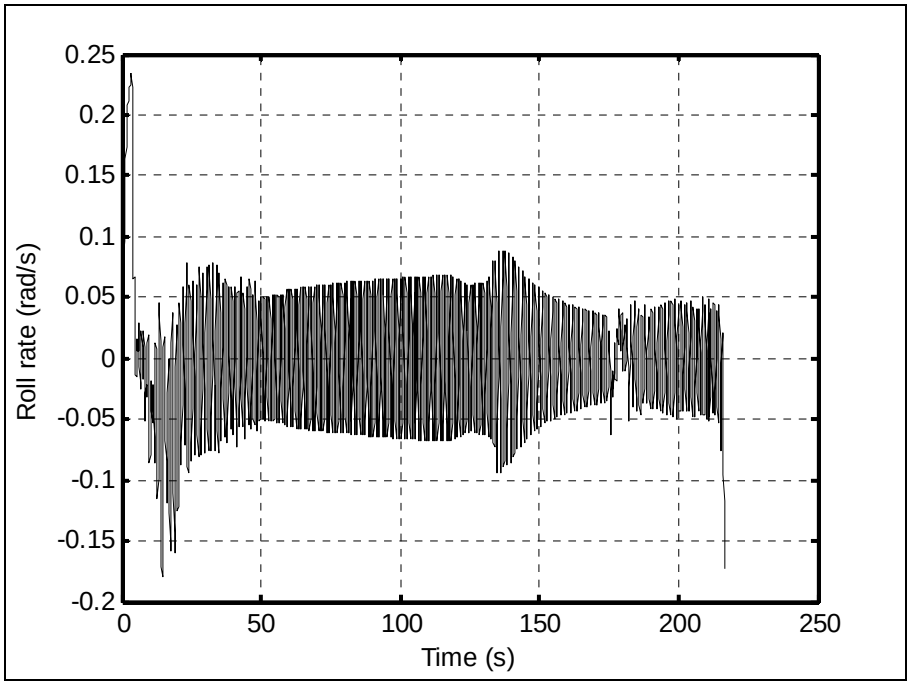

Figure 6-20 Roll rate for case I

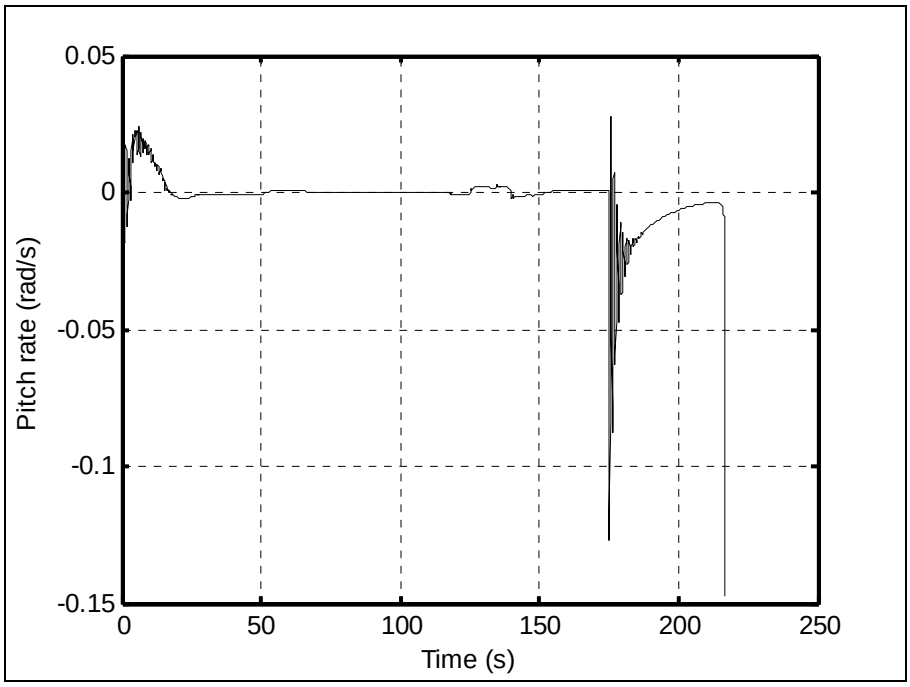

Figure 6-21 Pitch rate for case I

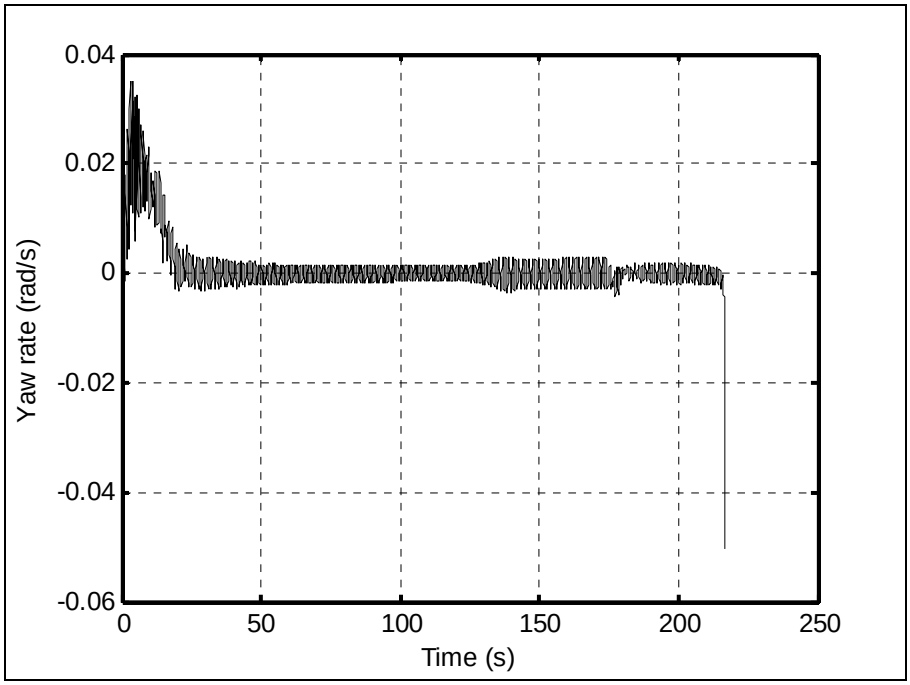

Figure 6-22 Yaw rate for case I

6.2 Case II

In this case, missile starts climbing whenever it is separated from the aircraft safely. The main advantage of the arc trajectory is to increase the range of the missile. First stage of this flight is thrust-powered flight and the second stage is powered by gravity. Missile almost reaches 12000 m altitude in this case.

Figure 6-23 and Figure 6-24 show the arc of the missile in XZ plane and Figure 6-25 and Figure 6-26 show it in XY plane. Trajectory initiates with increasing altitude and then ends by diving. Since, guidance unit first commands positive flight path angle and then commands the negative one to realize the trajectory and this is observable in Figure 6-27. Airspeed variation of the missile during arc trajectory is presented in Figure 6-31and in Figure 6-32. Differently from the first case, speed rises up to 595 m/s (2.02 M) owing to the fact that at higher altitude, air density decreases; so, drag decreases as well. This permits missile to fly faster.

When the burn-out occurs, missile is longitudinally steered directly to the target. On the other hand, lateral steering of the missile begins just after separation to make the use of propellant more efficiently towards target which is noticeable in Figure 6-28. Rise time is achieved about in 8 seconds and again the settling time is not small because of the nonlinear aerodynamics of the missile wherein aerodynamic coefficients and stability derivatives change nonlinearly. Where sideslip angle stays very small all over the flight; consequently, commanded heading angle steers the missile to the target with negligibly small error (see Figure 6-30). Steering is achieved by means of coordinated turn which corresponds to 35 degrees bank angle as shown in Figure 6-33. History of the aileron and rudder control surface deflections is available in

Figure 6-35 and Figure 6-36. These figures reveal the quite small deflection angles are adequate for this turn on account of all moving fins.

At the beginning of the flight, the missile achieves its dynamic stability after a little period of time, 6 seconds (see Figure 6-29 and Figure 6-34).

As affirmed in the case I, aileron deflection history gives an idea about the stability about the longitudinal axis, X. It does not have stability about X axis; so, aileron continuously deflects to hold the zero bank angle.

Another crucial thing that is salient in Figure 6-27 and Figure 6-33 is the immediate bank angle disturbance as the missile instantaneously pitches down about at 117^{th} second. This is also noticeable as a disturbance in heading angle history (Figure 6-28). This is because of the inertial coupling that comes from the PQ and PR in moment equations (2.127) and (2.128) [18]. This is observable in roll, pitch and yaw rates in Figure 6-42, Figure 6-43, and Figure 6-44 respectively. Rapid pitch down rate results in instantaneous positive yaw and roll rates; as a result, positive bank angle and yaw angle disturbances. The controller manages to re-stabilize the missile after this inertial coupling though. This might be alleviated by modifying wing and tail area or with additional improved control systems. Therefore, more studies need to be conducted to solve this issue.

Variation of mass, center of gravity, moments of inertia about X, Y, and Z axis are given right through Figure 6-37 - Figure 6-41.

Circular error of probabilities on XZ and XY planes can be obtained from Figure 6-24 and Figure 6-26 in that order. It is about 1 m on XZ plane and XY plane.

To sum up, the missile is able to achieve to terminate the target by less than 1 m circular error of probability. Moreover, the range of the missile is increased % 75 with respect to first case.

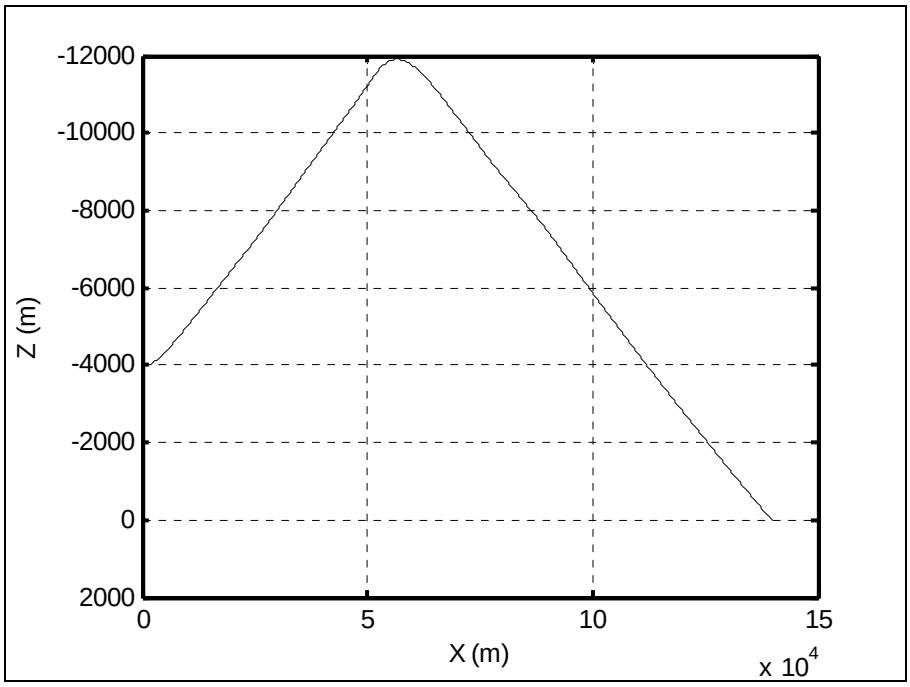

Figure 6-23 XZ plane flight path for case II

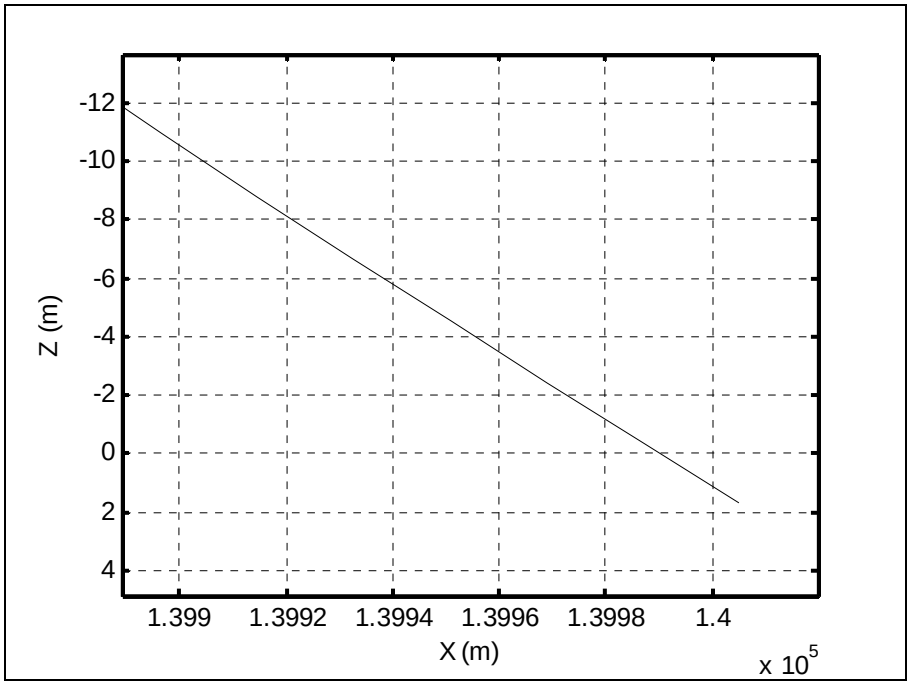

Figure 6-24 XZ plane missile-target interception for case II

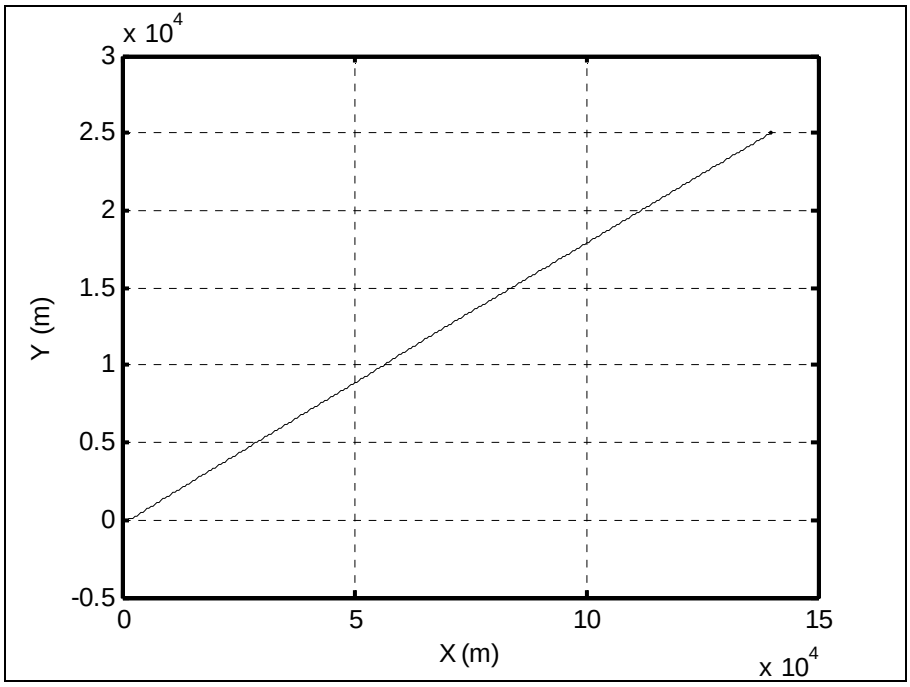

Figure 6-25 XY plane flight path for case II

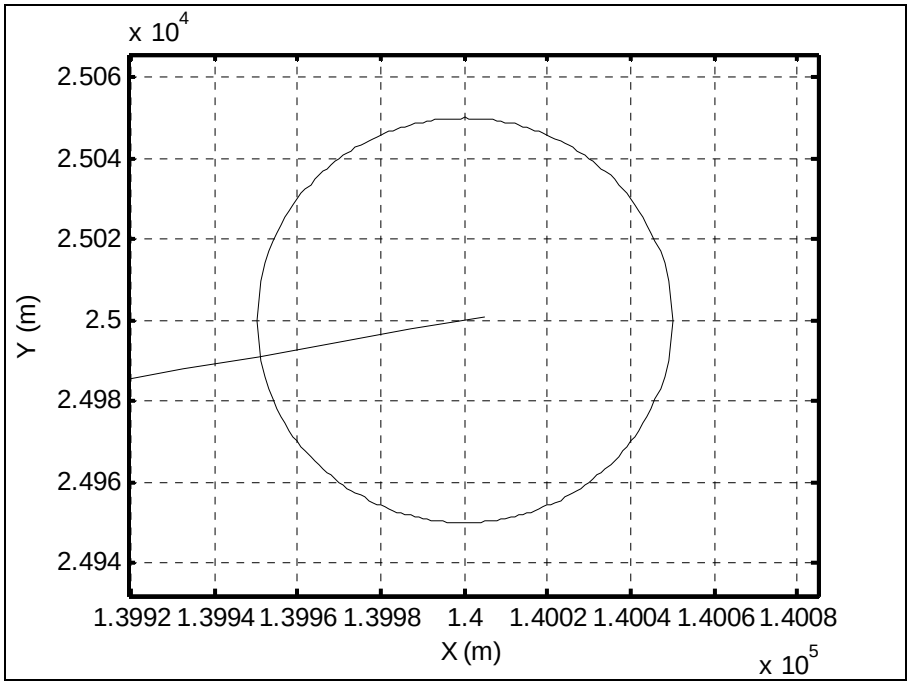

Figure 6-26 XY plane missile-target interception for case II

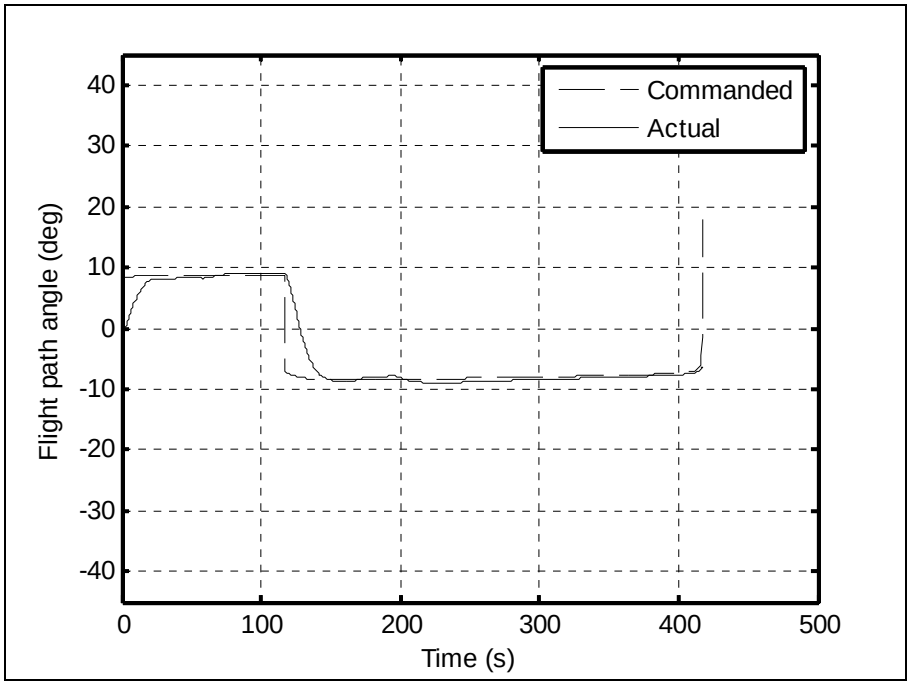

Figure 6-27 Flight path angle for case II

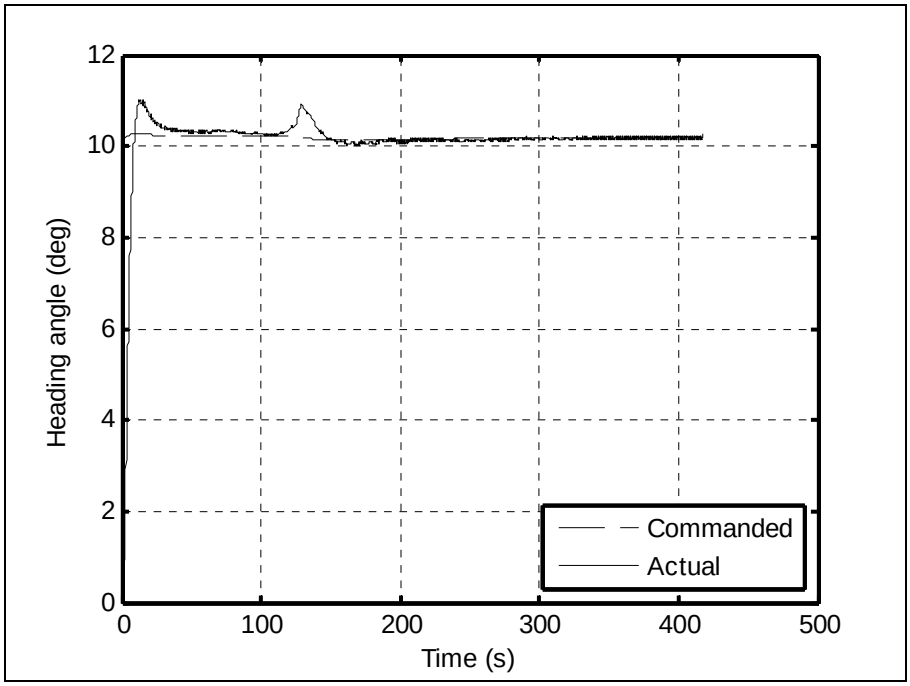

Figure 6-28 Heading angle for case II

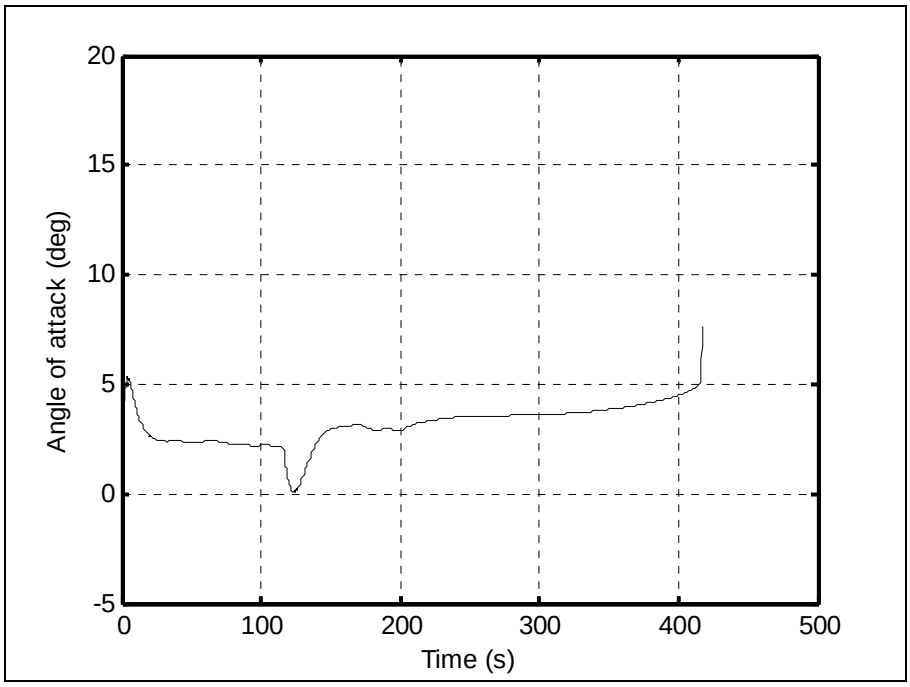

Figure 6-29 Angle of attack for case II

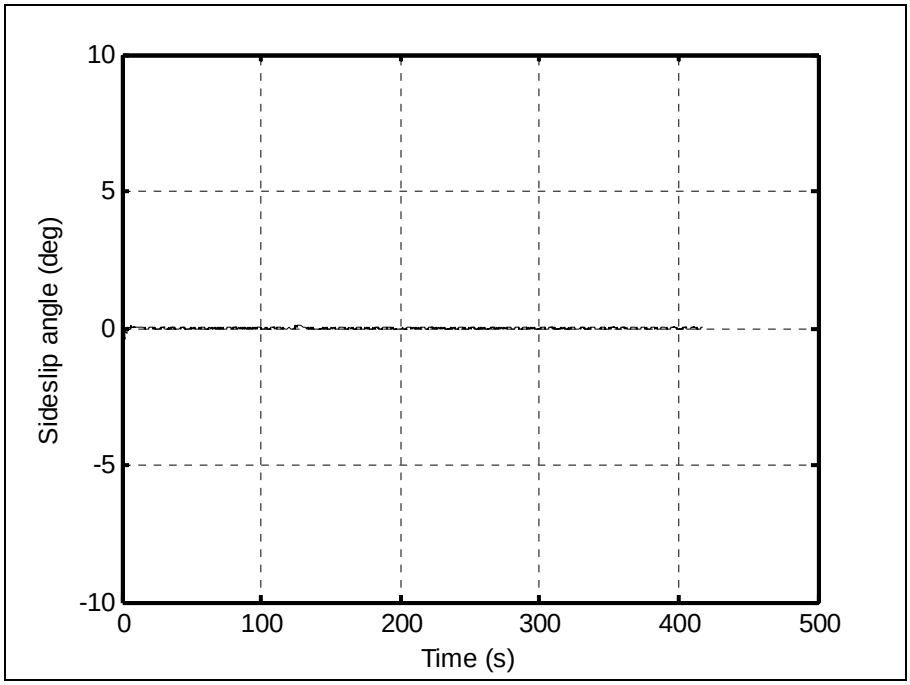

Figure 6-30 Sideslip angle for case II

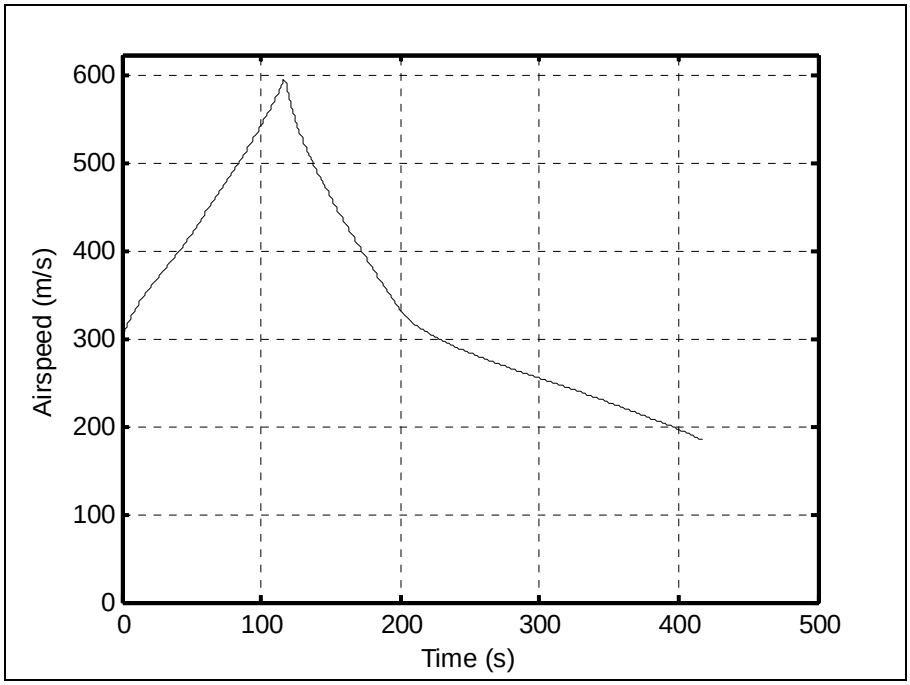

Figure 6-31 Airspeed for case II

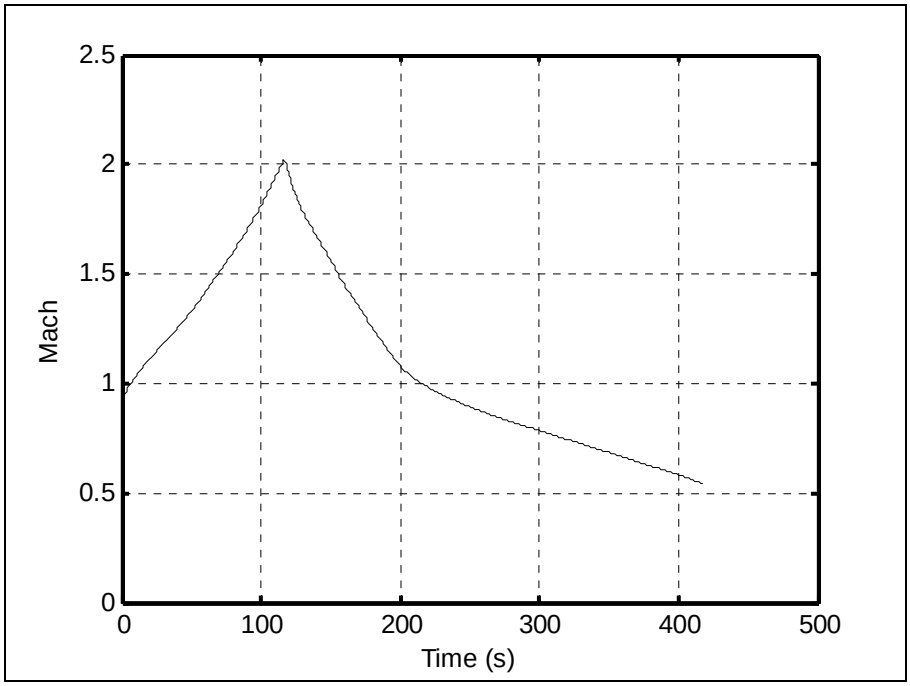

Figure 6-32 Mach number for case II

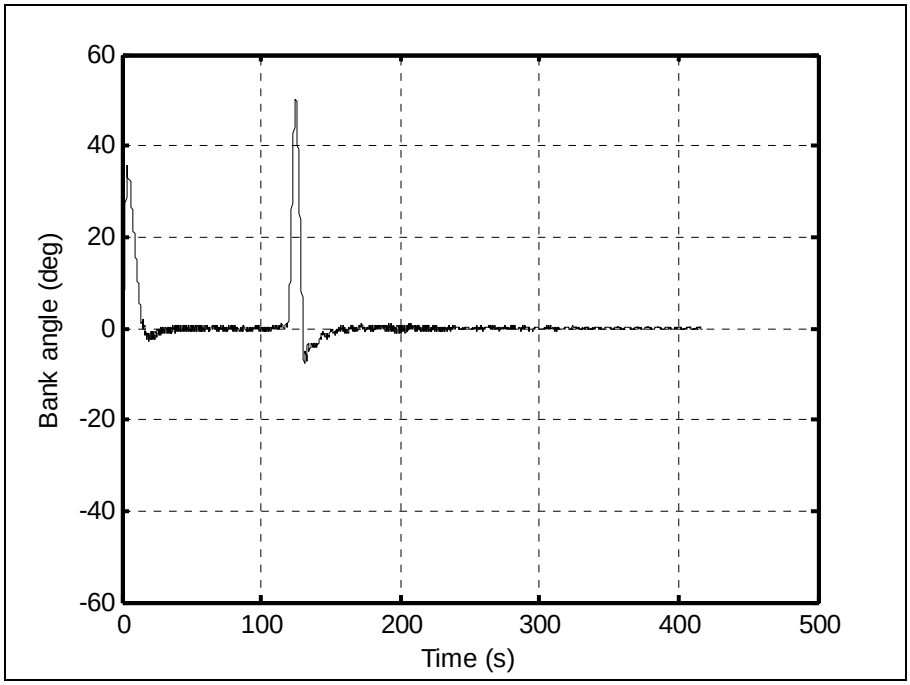

Figure 6-33 Bank angle for case II

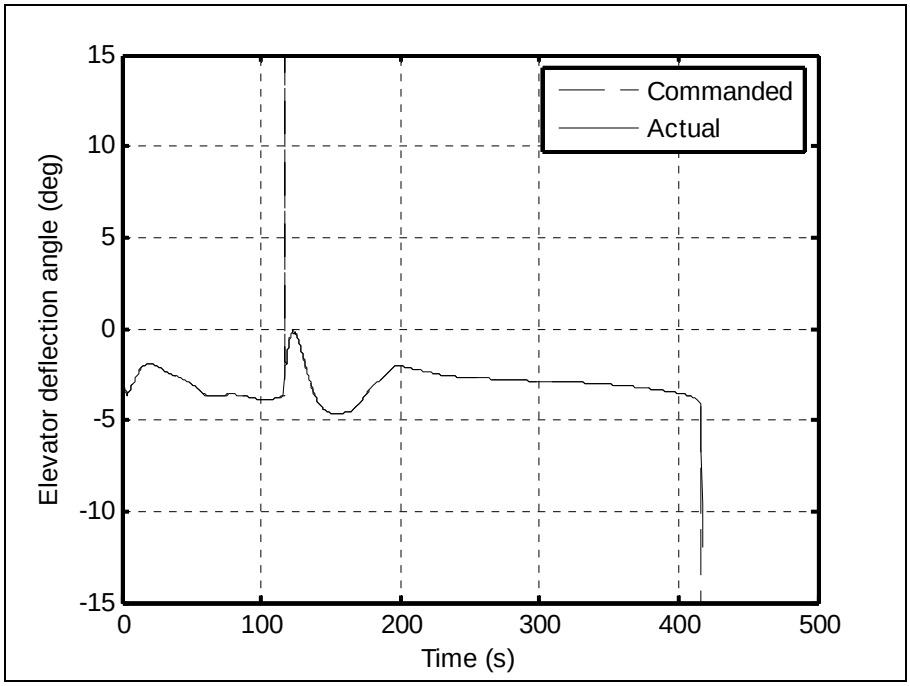

Figure 6-34 Elevator deflection angle for case II

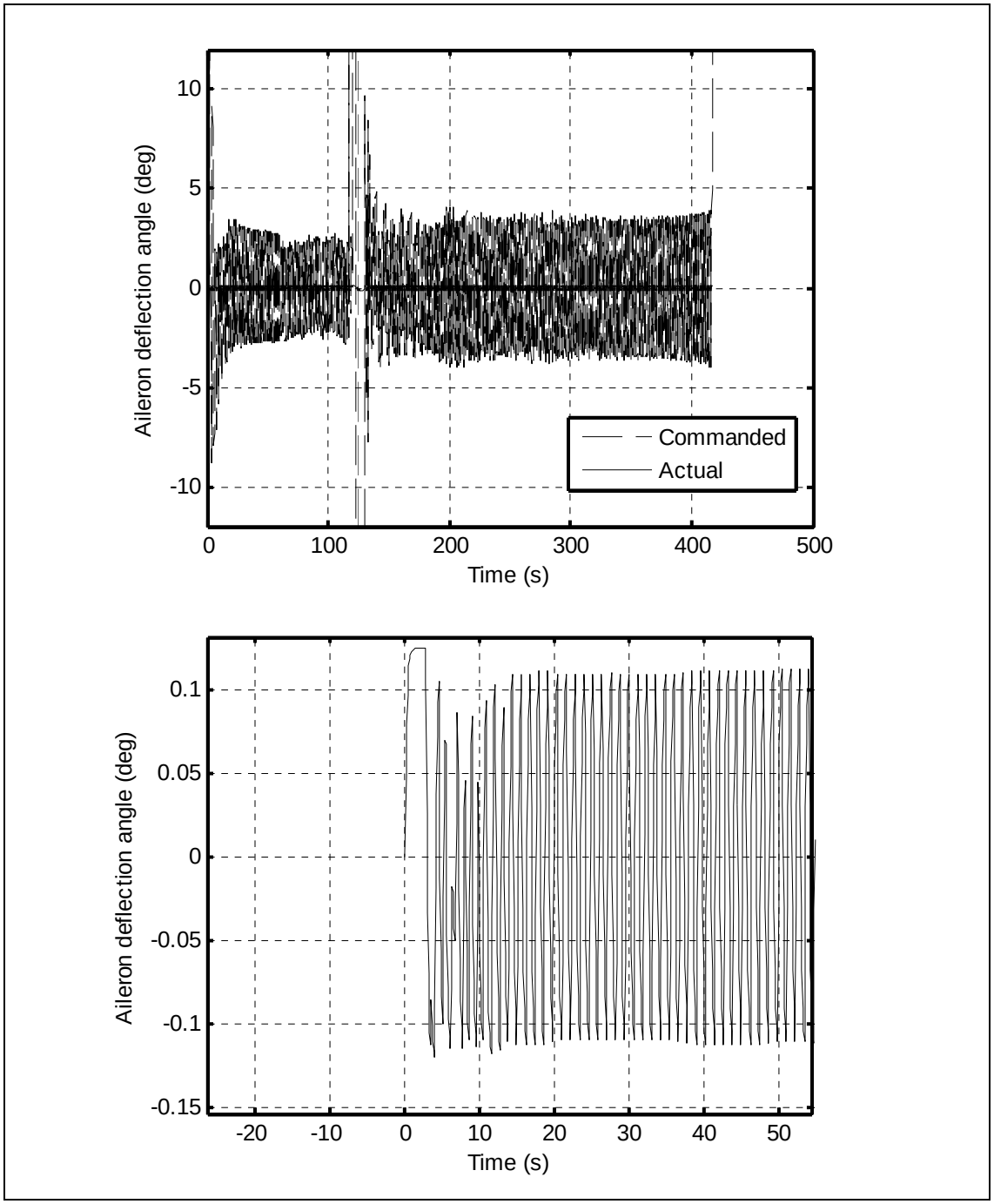

Figure 6-35 Aileron deflection angle for case II

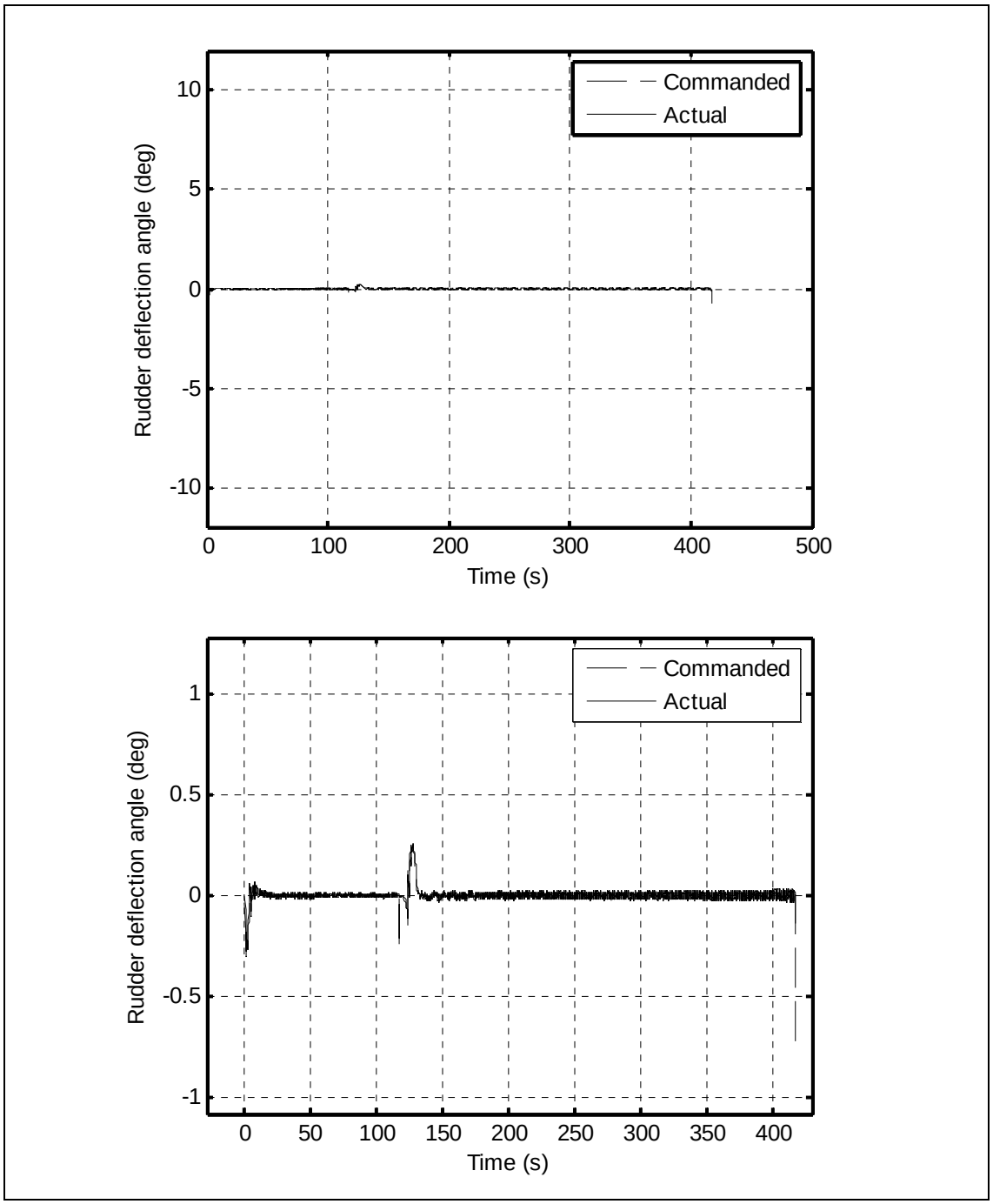

Figure 6-36 Rudder deflection angle for case II

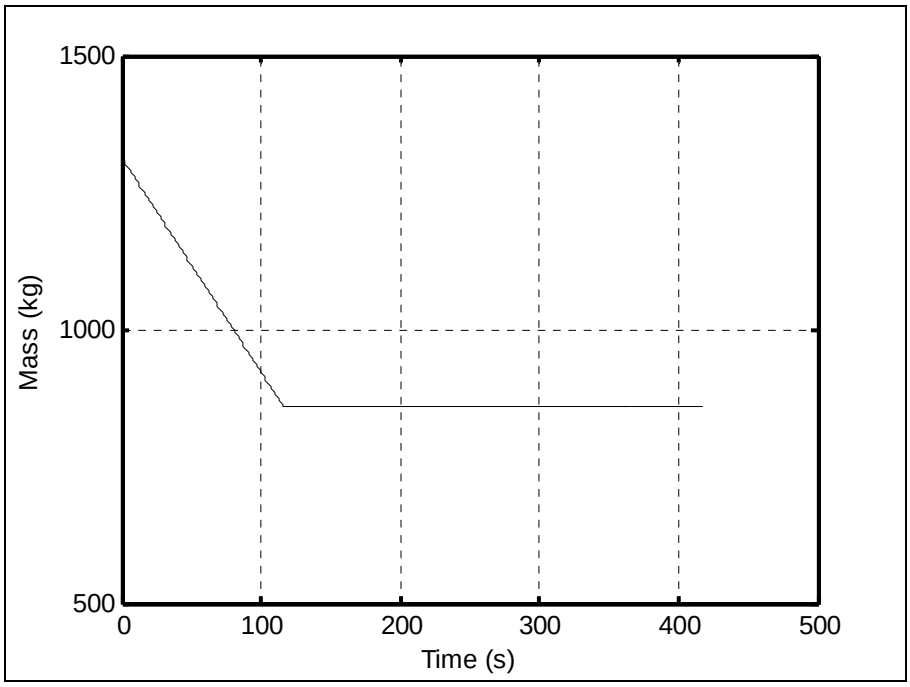

Figure 6-37 Variation of the missile's mass for case II

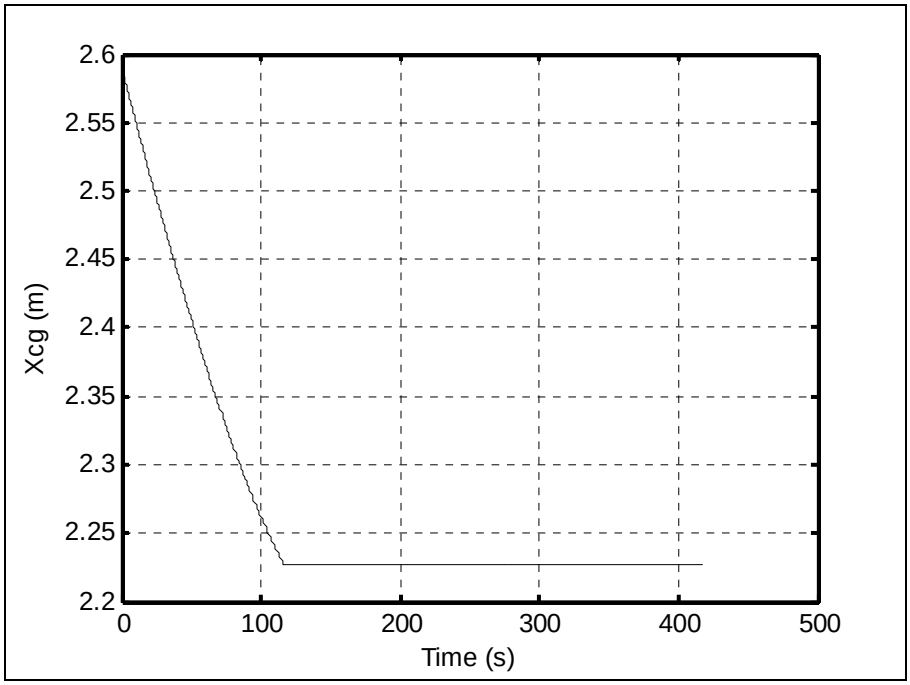

Figure 6-38 Center of gravity for case II

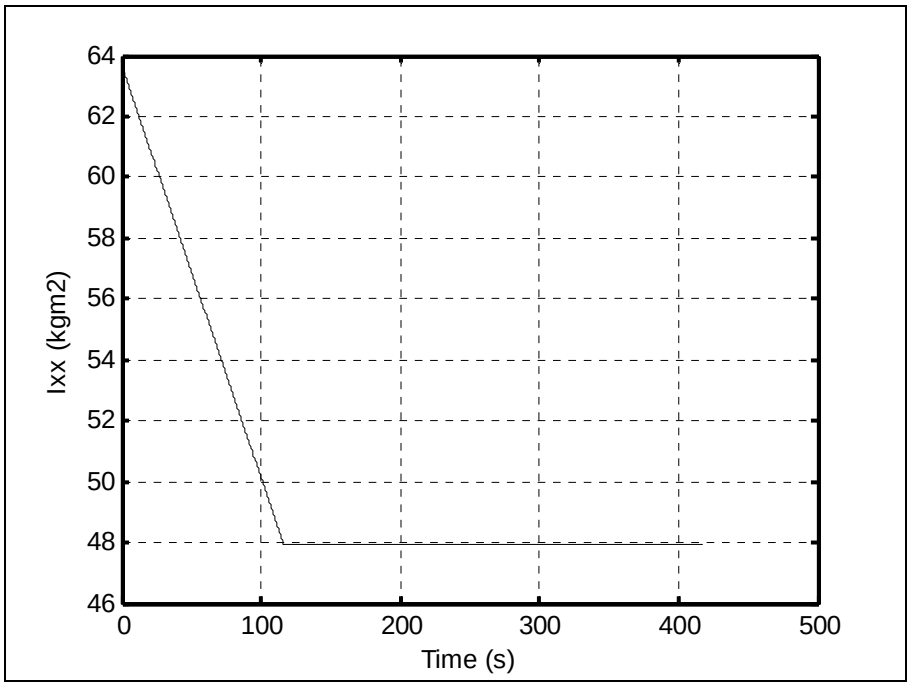

Figure 6-39 Moment of inertia about X axis for case II

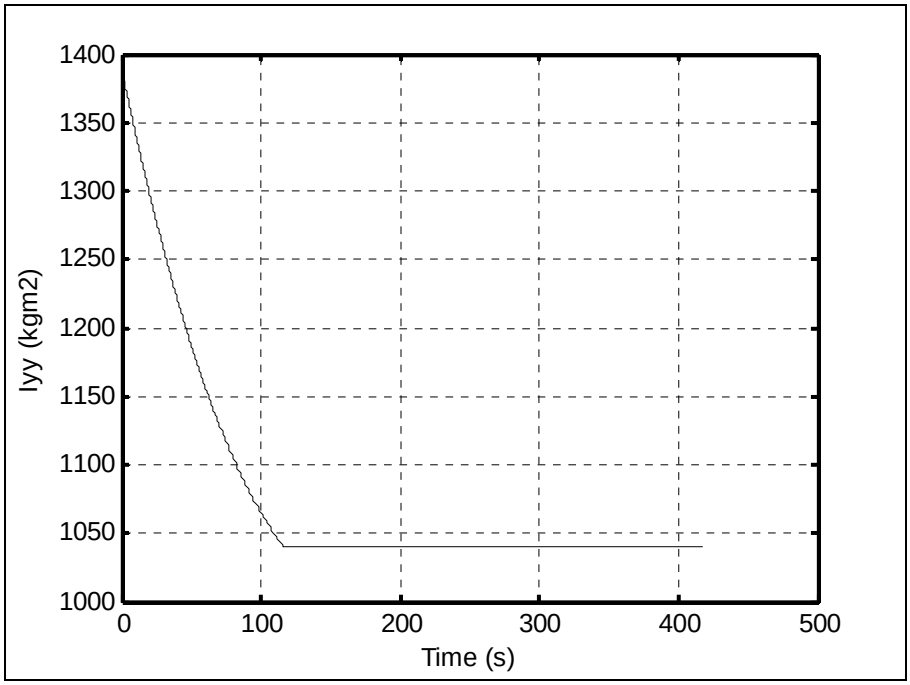

Figure 6-40 Moment of inertia about Y axis for case II

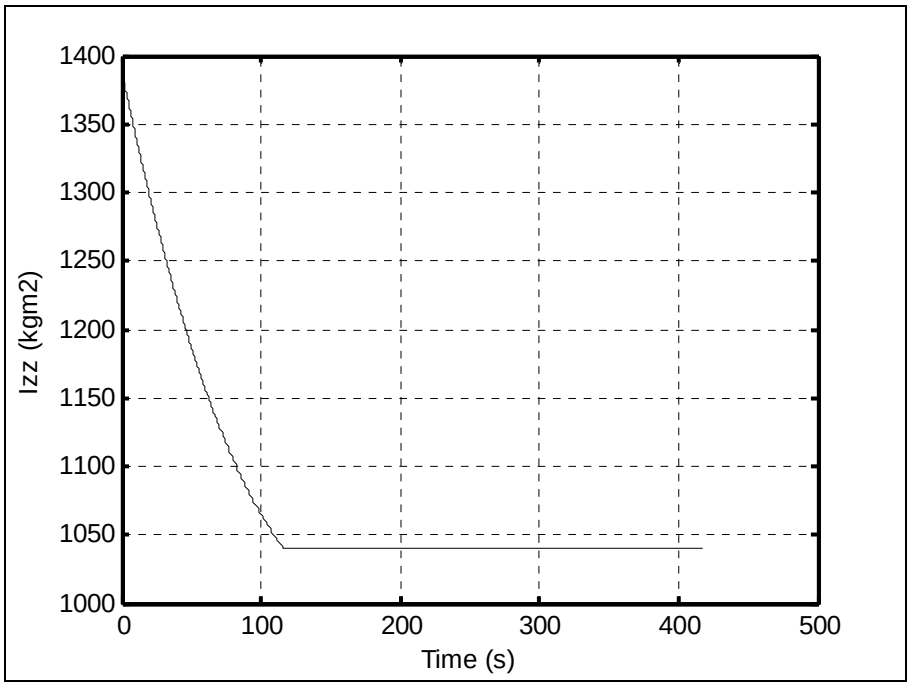

Figure 6-41 Moment of inertia about Z axis for case II

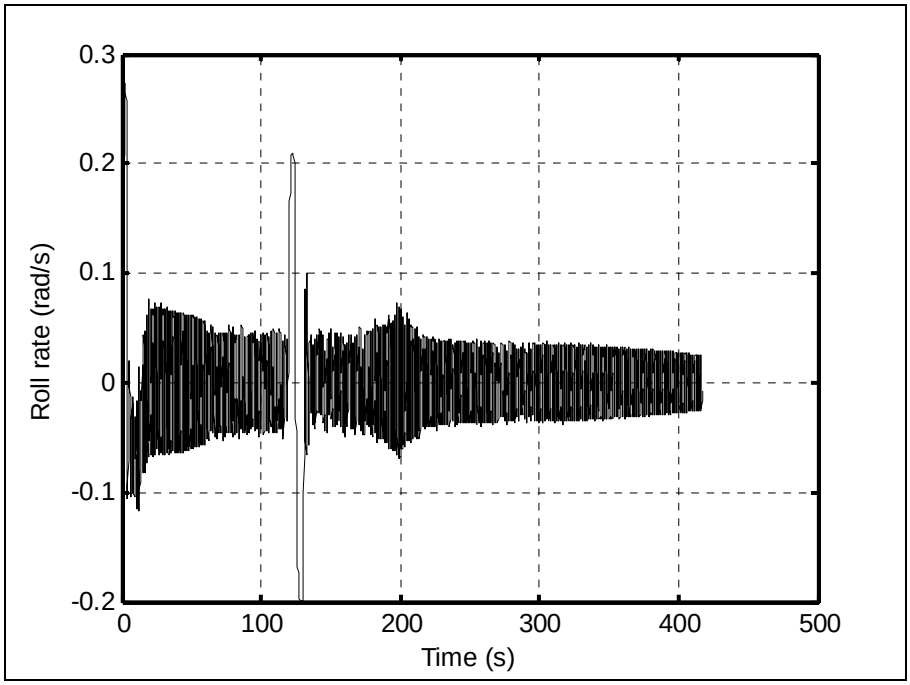

Figure 6-42 Roll rate for case II

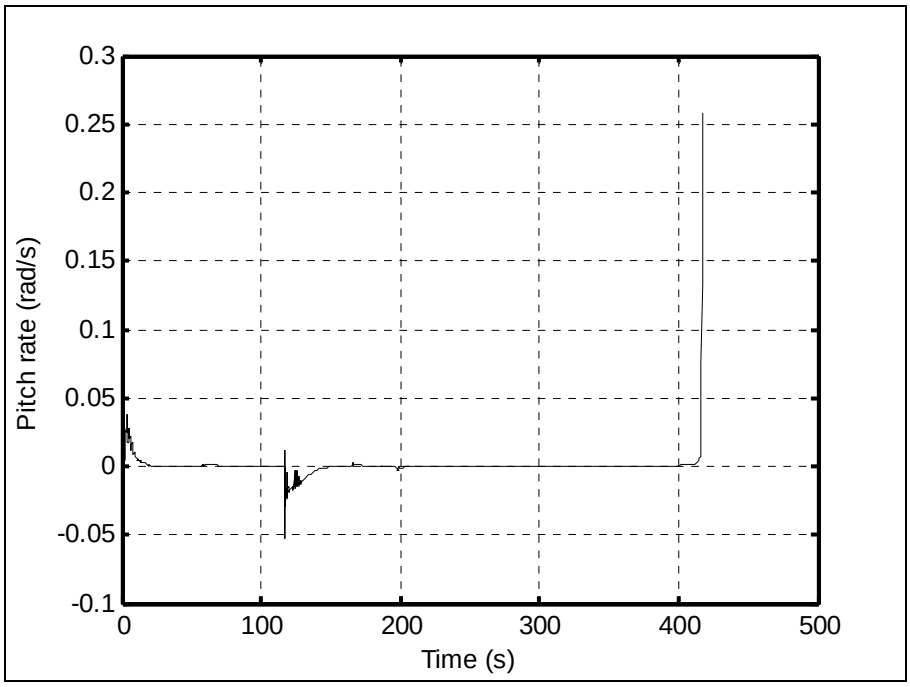

Figure 6-43 Pitch rate for case II

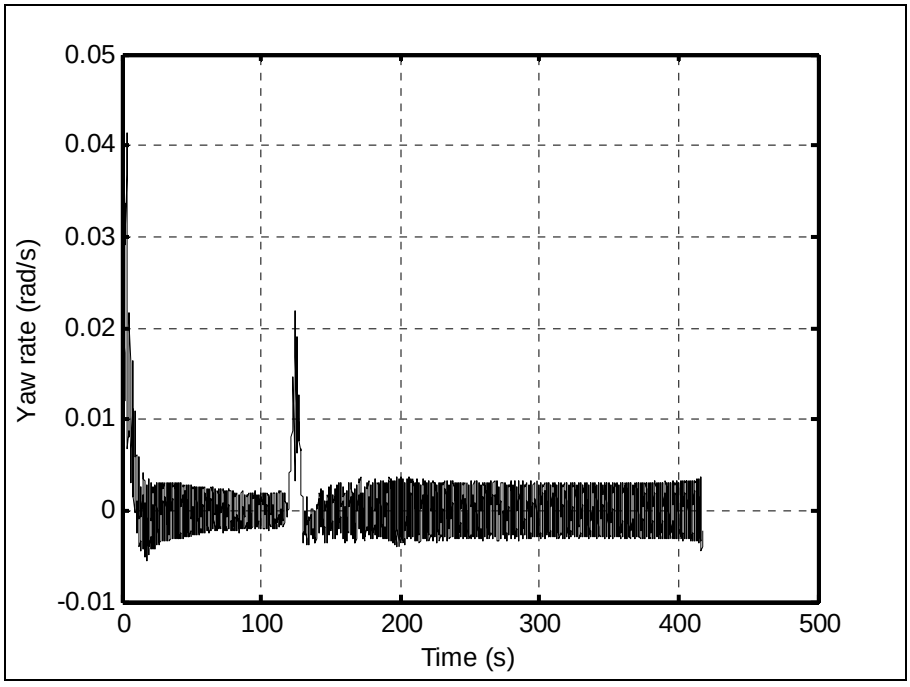

Figure 6-44 Yaw rate for case II

6.3 Case III

Unlike the first two cases, in this case convergence of the missile's trajectory to the target takes place before burn-out. Next case, case IV, is also similar to this case. Verification of these cases makes terminations of close targets possible. That is, even though the missile is designed for stand-off, short-ballistic (~100 km) ranges, confirmation of these cases enable the missile to launch so as to wipe out unexpectedly arising targets; such as ships, buried or hidden artillery or bases. In this respect, validation of those may contribute significantly.

Since, the most portion of the trajectory is composed of diving maneuver; this case is called dive trajectory. Figure 6-45, Figure 6-46, Figure 6-47, and Figure 6-48 show the trajectory of the missile on XZ plane and XY plane respectively. From the figures, it is seen that first 11000 m is traveled at the altitude of 4000 m and then diving phase commences. Along through the combination of constant altitude diving paths, airspeed of the missile continuously increases for the reason that the thrust-powered flight happens. Figure 6-53 and Figure 6-54 present the speed record wherein maximum speed is acquired at the overlap of the target as 516 m/s (1.51 M). It is the maximum striking speed among the first three cases. This is preferred owing to the fact that it appreciably boosts the effect of strike. Plus, remaining propellant may well behave like warhead that provides the missile with more efficient strike (see Figure 6-59).

Figure 6-51, the record of angle of attack shows how efficient the missile achieves dynamic stability in a short period of less than 5 seconds. As stated before, the missile does not start at a predetermined trim point. Moreover, it is apparent while the speed of the missile rises the angle of attack diminishes because required lift is obtained at a lower angle of attack.

Sideslip angle remains very small throughout the flight; therefore, commanded heading angle steers the missile to the target with negligibly small error (see Figure 6-52). This steering is accomplished at the beginning of the flight alike in

previous cases. Figure 6-50 reveals the commanded and actual heading angles. From this figure, rise time is read about 8 seconds. Nonetheless, heading angle is disturbed at 30th second owing to the rapid push down (nose down pitch rate). High airspeed plays an important role at making the pitch steeper. Minor unwanted-inertial-coupling consequences are observable in Figure 6-55, and necessitated control surface deflections to minimize the disturbance are observed in Figure 6-57 and
Figure 6-58. This is the same issue faced in the case II.

Diving maneuver to obtain -20 degrees flight path angle is shown in Figure 6-49. The corresponding elevator deflection history is given in Figure 6-56. Where, extremely steep commanded elevator deflection angle for pitch down maneuver is noticeable. As declared in the case II, to prevent the missile from having unwanted-inertial-coupling outcome, smoothing the steep pitch-down or pitch-up maneuvers will be investigated in the following studies.

Center of gravity, moments of inertia about X, Y, and Z axis are available through Figure 6-60 - Figure 6-63 . .Besides, roll rate, pitch rate and yaw rate related to maneuvers are given in Figure 6-64, Figure 6-65, and Figure 6-66.

Circular error of probabilities on XZ and XY planes are 6 m and 2 m respectively (see Figure 6-46 and Figure 6-48).

To sum up, even though the response of longitudinal maneuvers is again kind of slow, the missile is able to accomplish to terminate the target by less than 8 m circular error of probability.

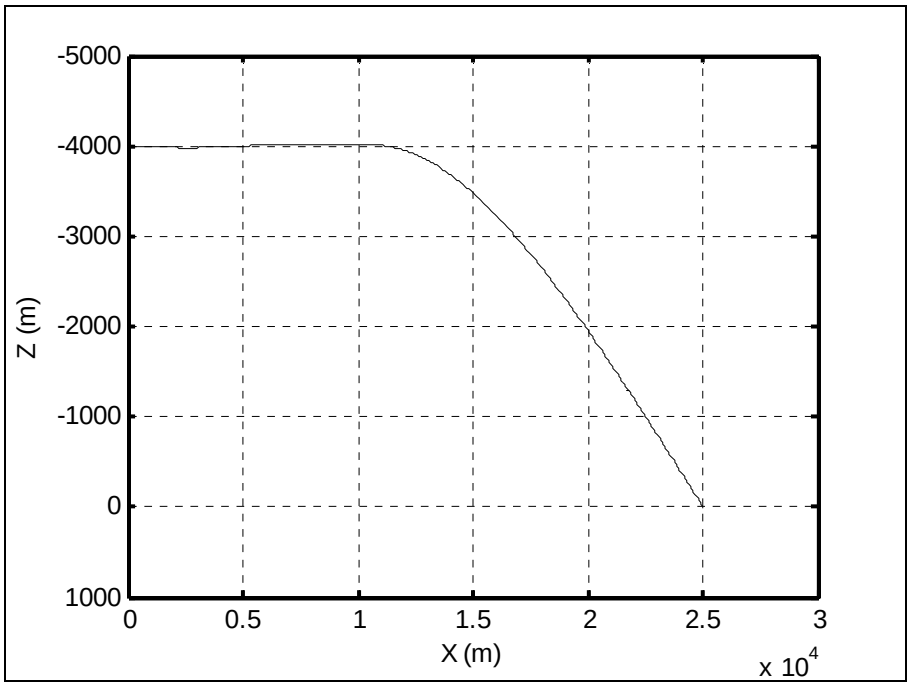

Figure 6-45 XZ plane flight path for case III

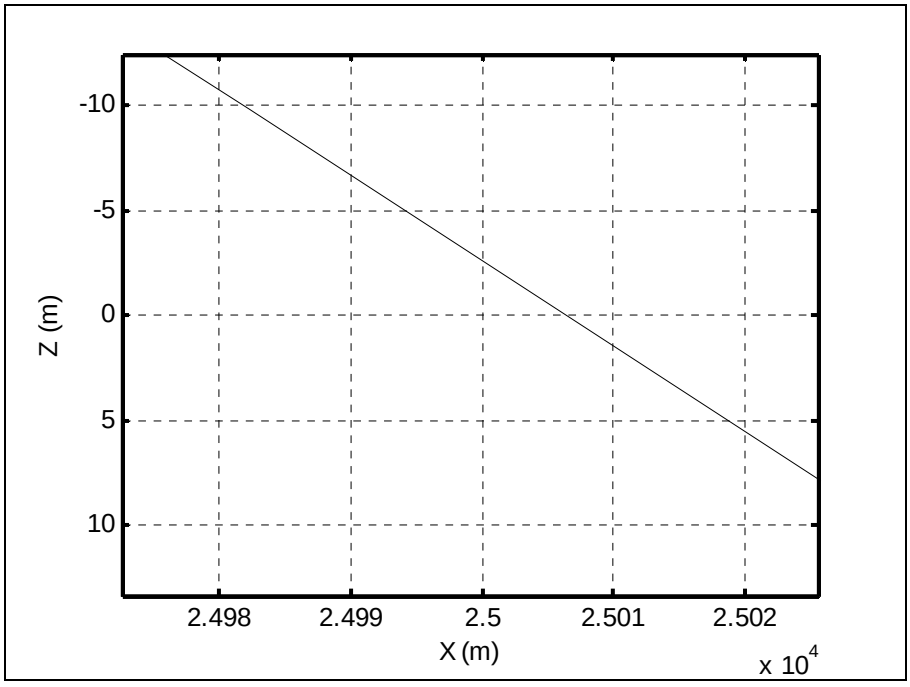

Figure 6-46 XZ plane missile-target interception for case III

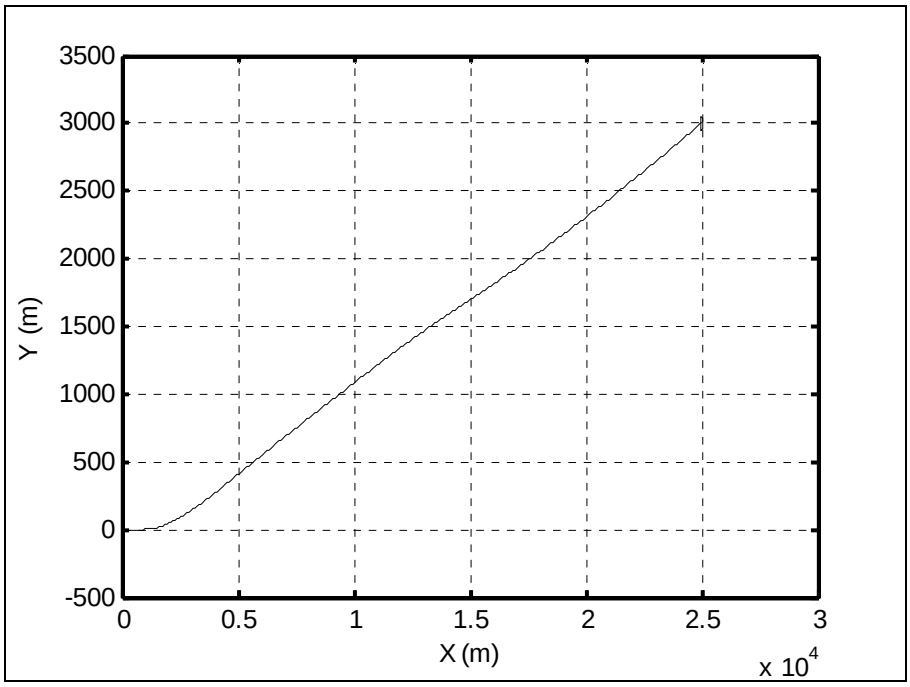

Figure 6-47 XY plane flight path for case III

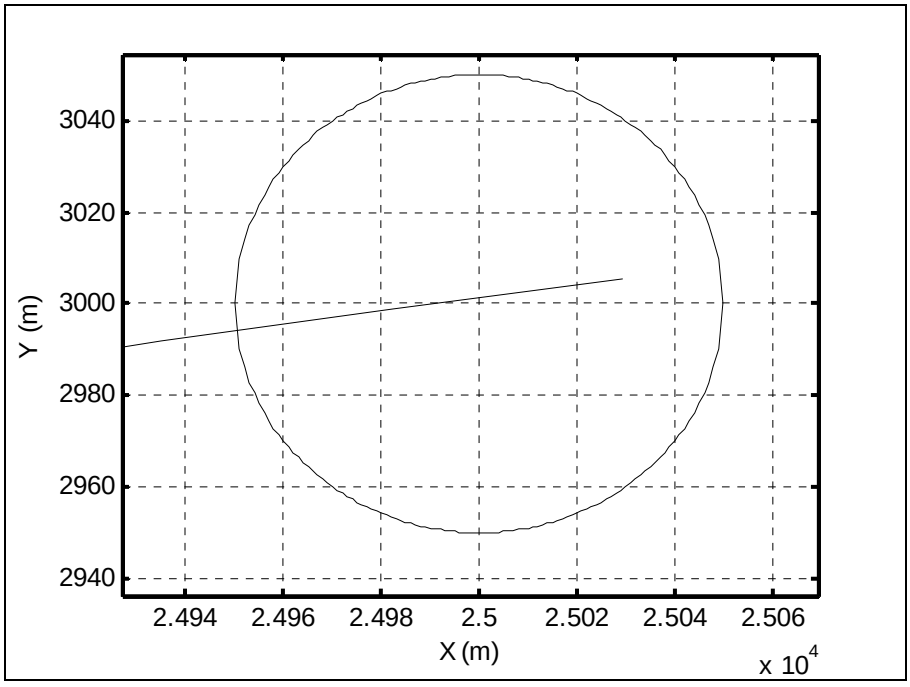

Figure 6-48 XY plane missile-target interception for case III

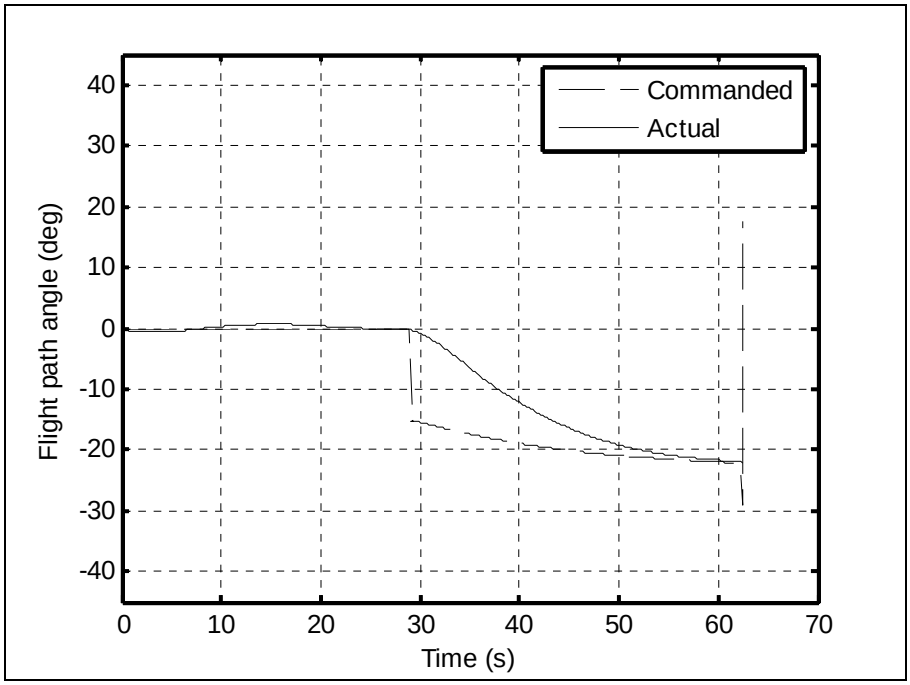

Figure 6-49 Flight path angle for case III

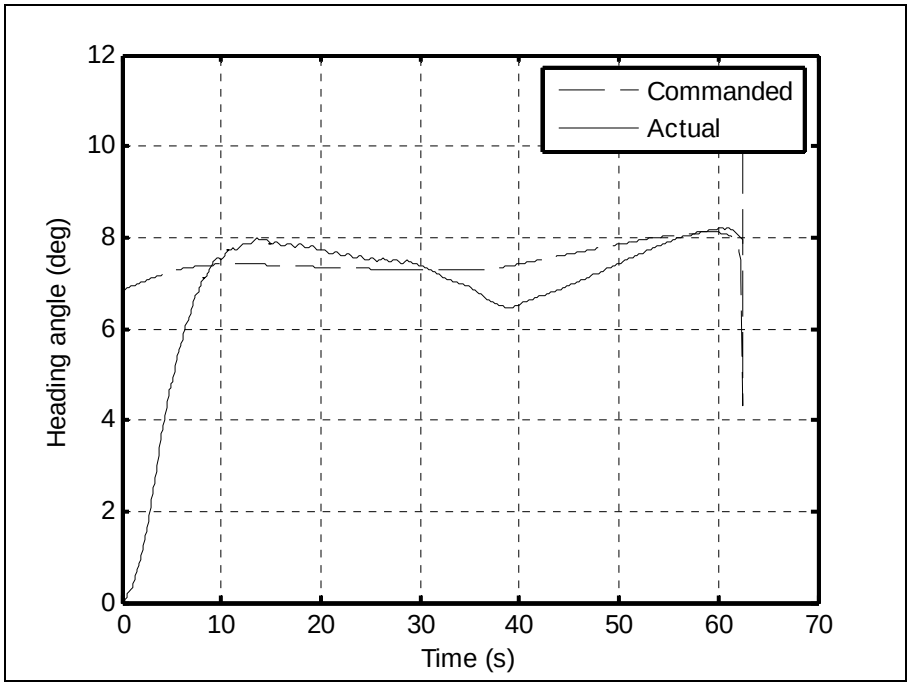

Figure 6-50 Heading angle for case III

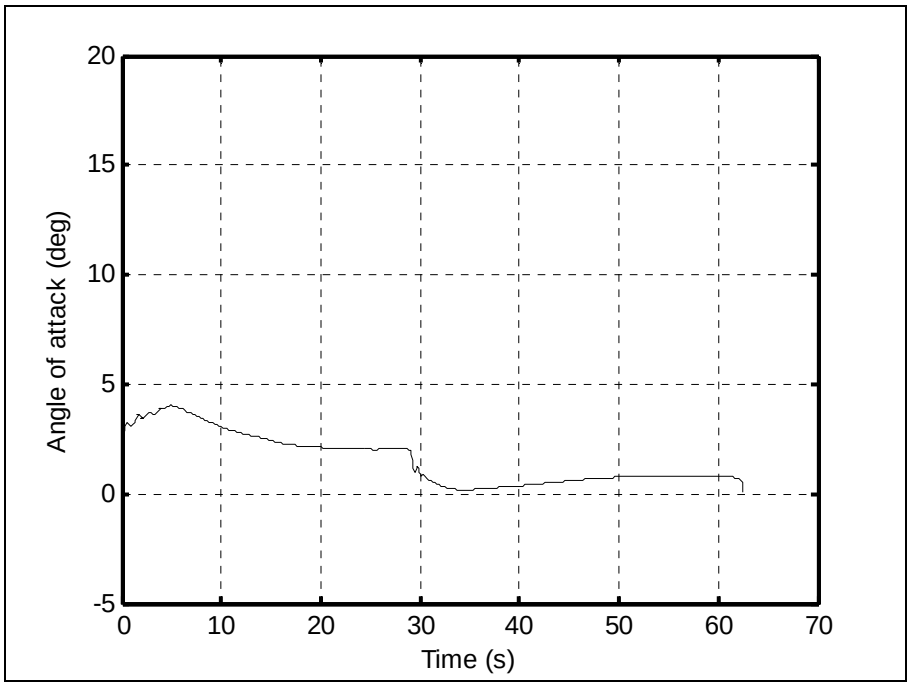

Figure 6-51 Angle of attack for case III

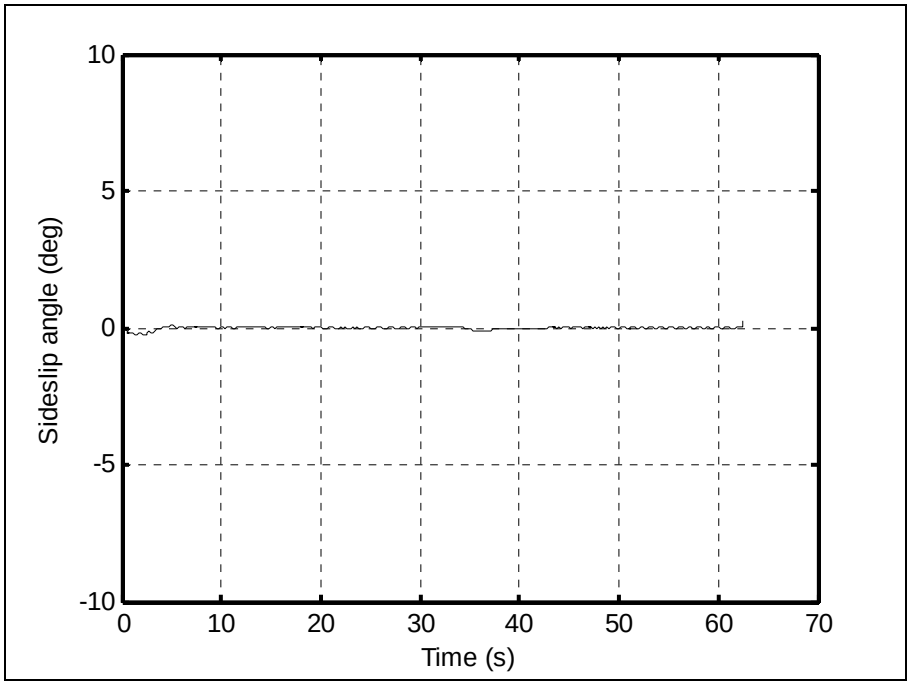

Figure 6-52 Sideslip angle for case III

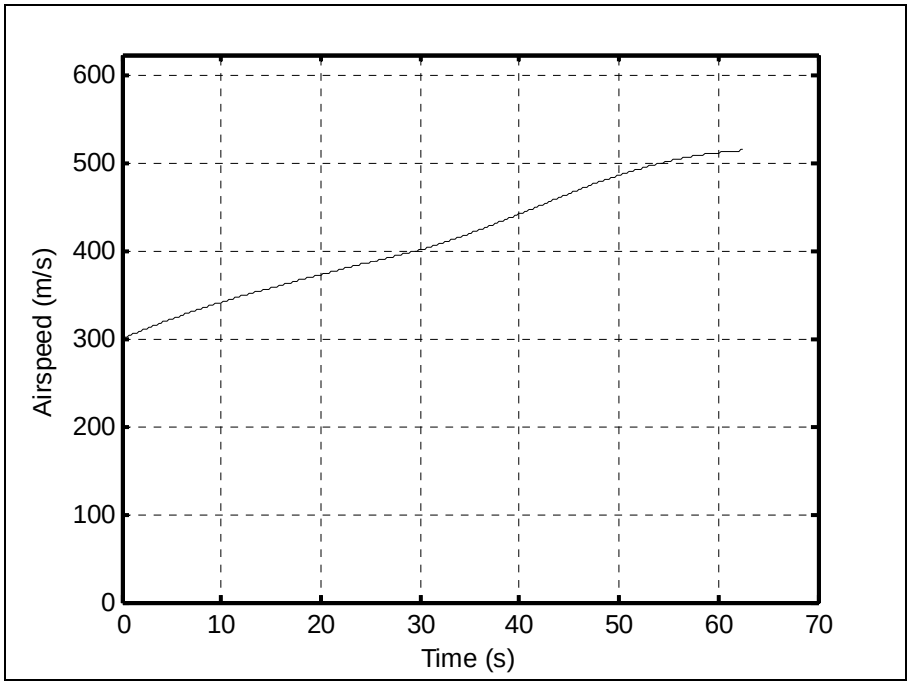

Figure 6-53 Airspeed for case III

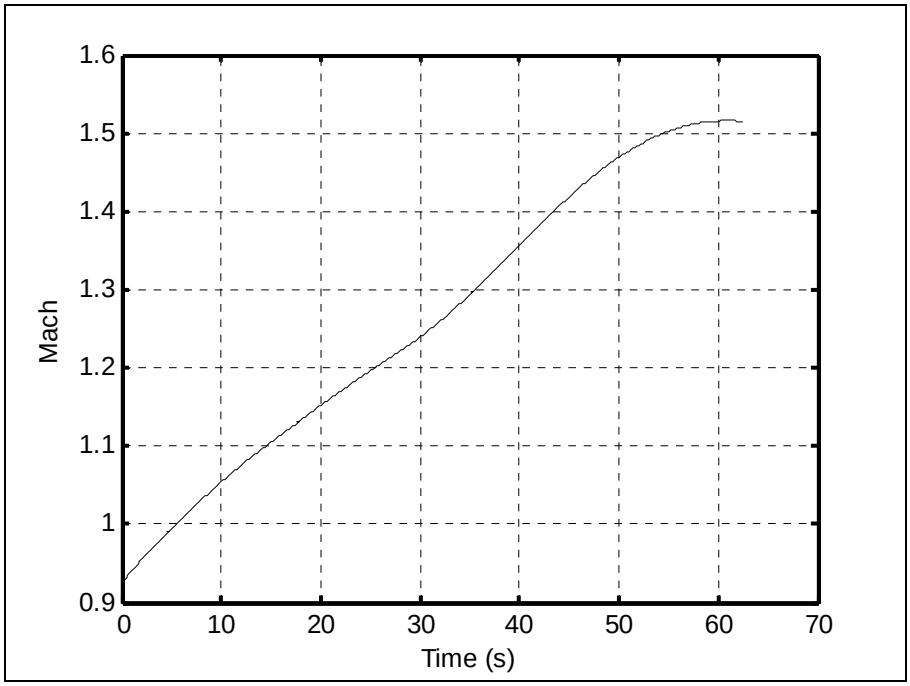

Figure 6-54 Mach number for case III

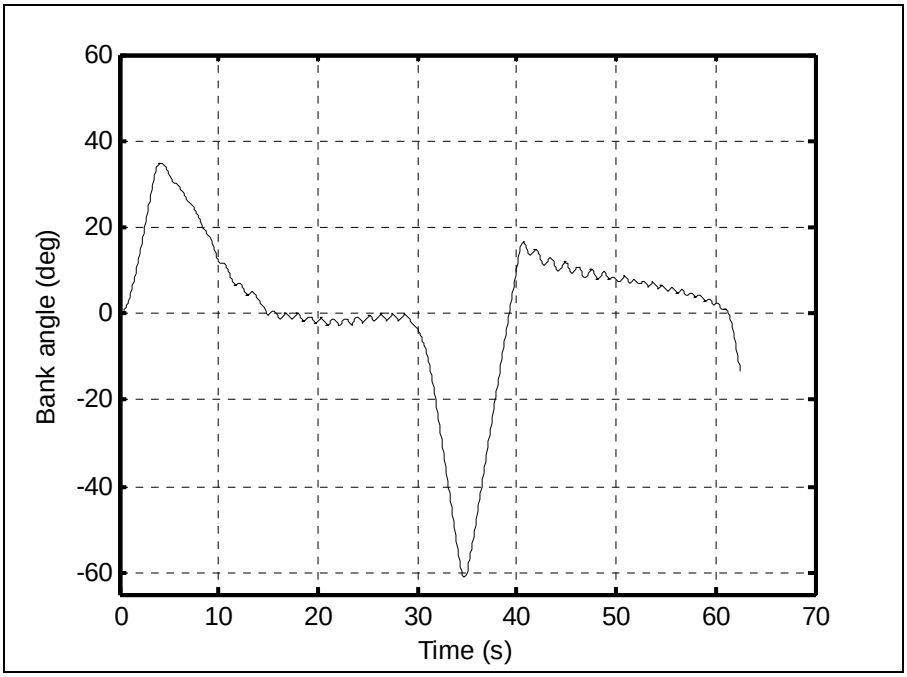

Figure 6-55 Bank angle for case III

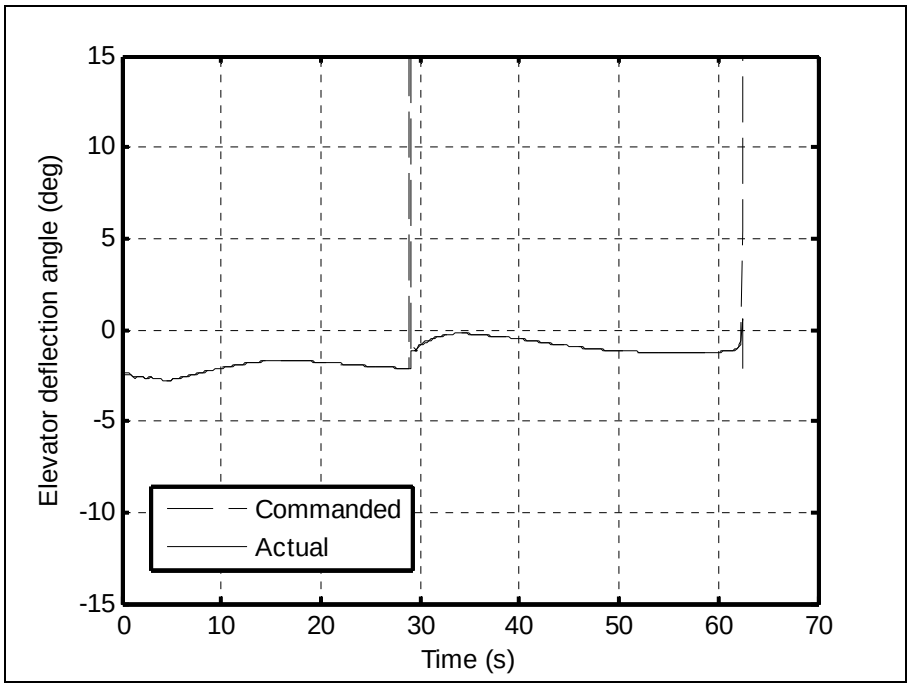

Figure 6-56 Elevator deflection angle for case III

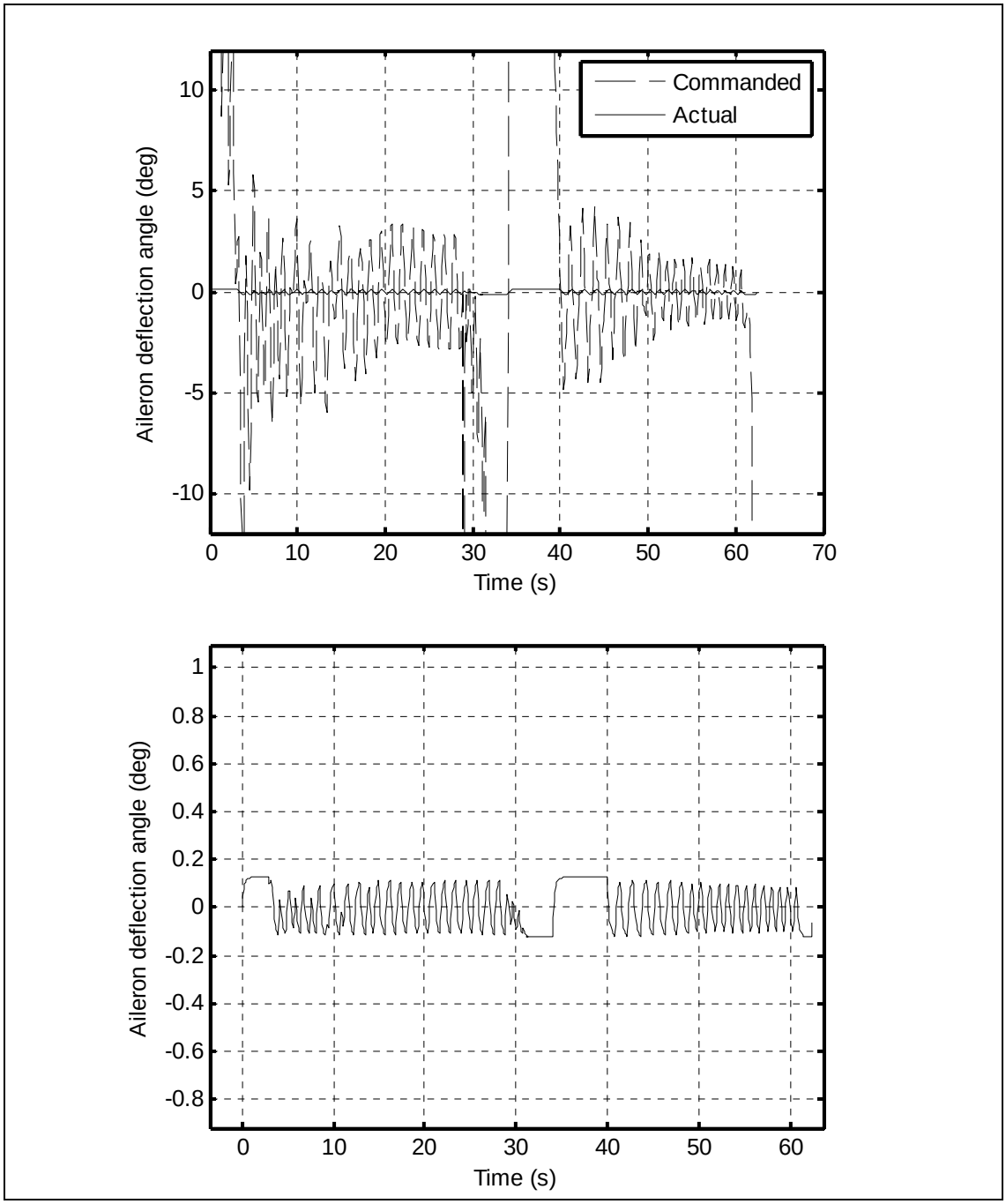

Figure 6-57 Aileron deflection angle for case III

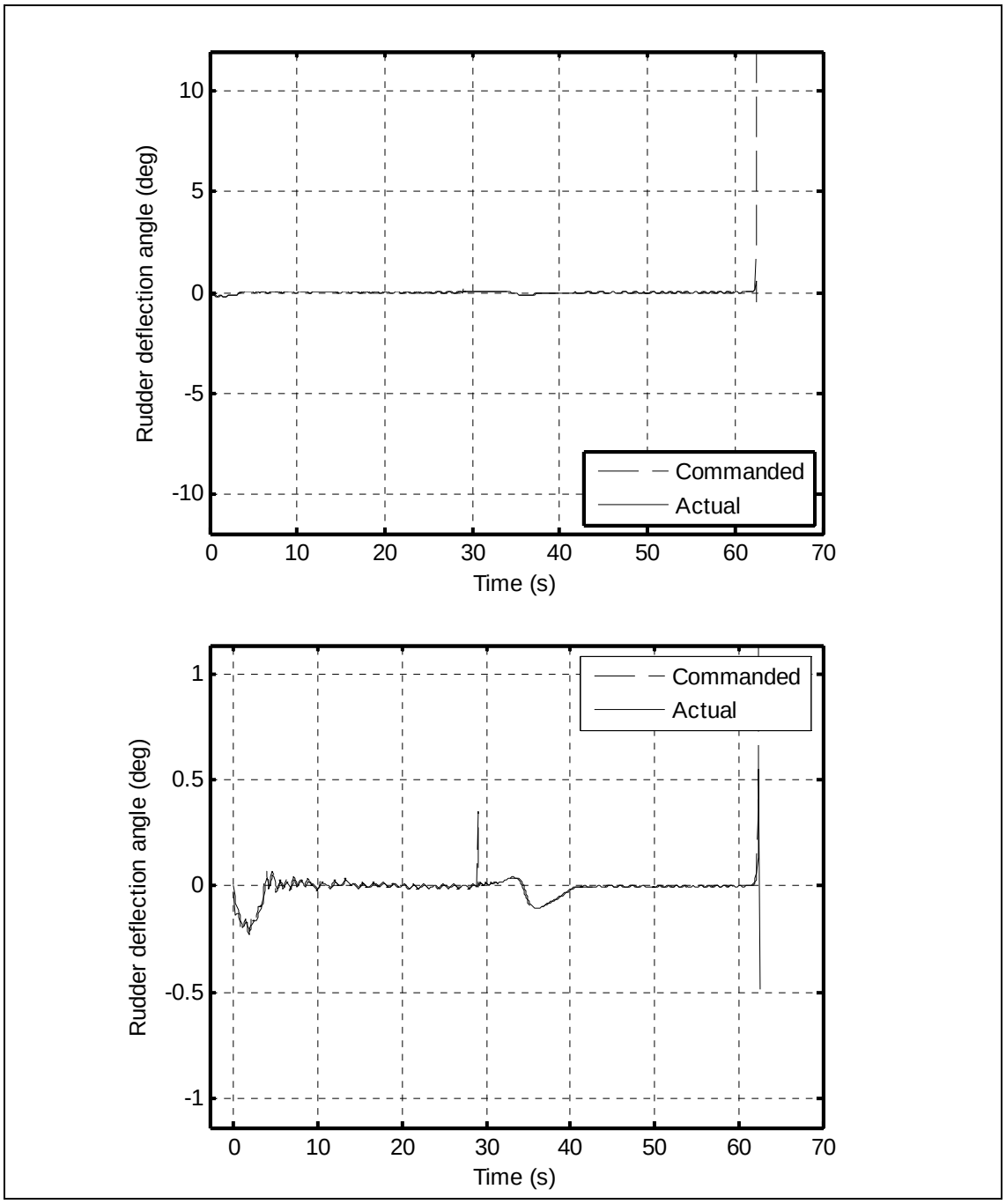

Figure 6-58 Rudder deflection angle for case III

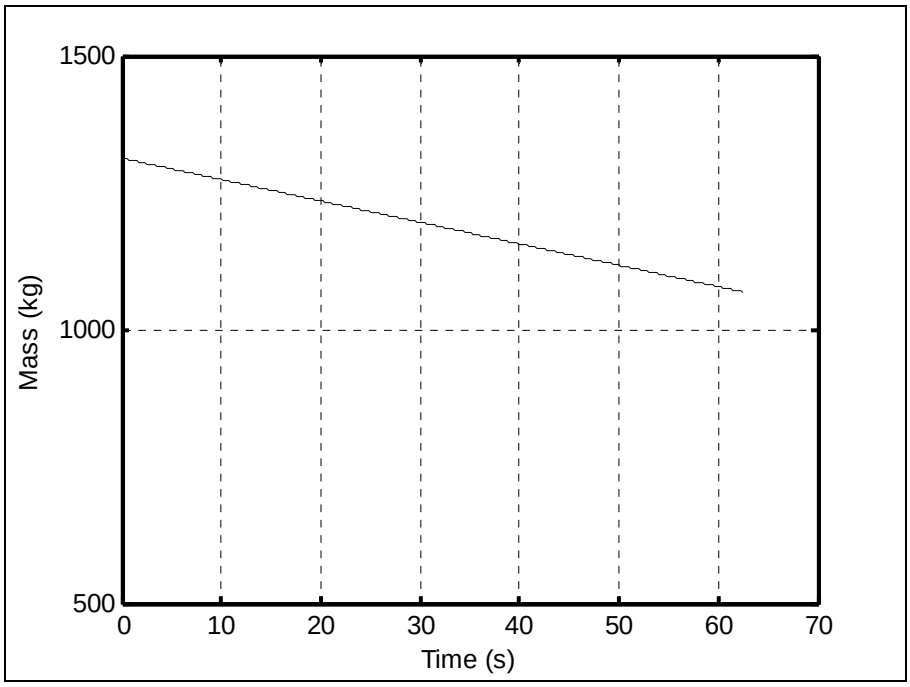

Figure 6-59 Variation of the missile's mass for case III

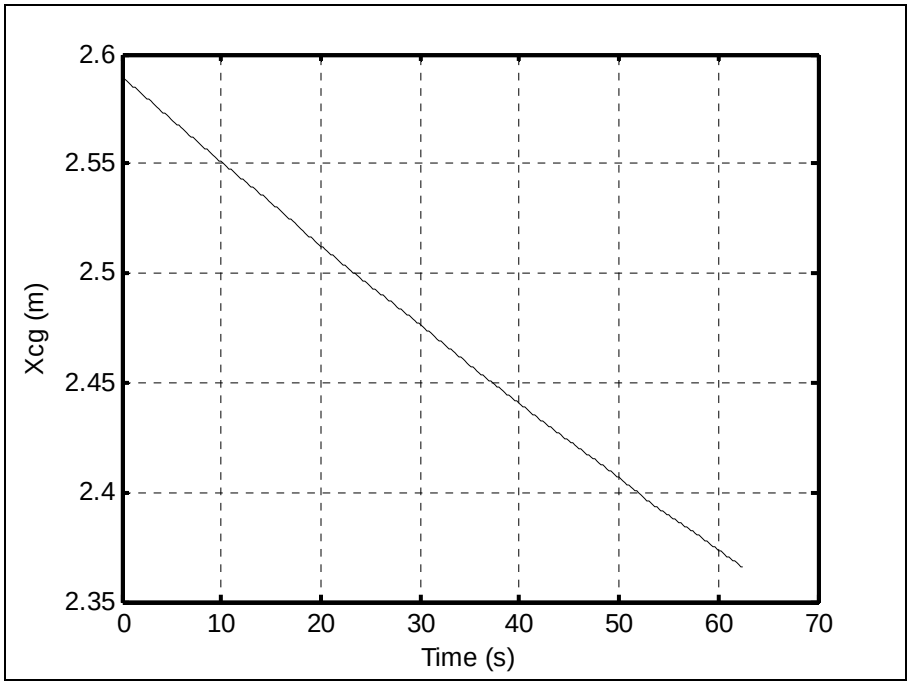

Figure 6-60 Center of gravity for case III

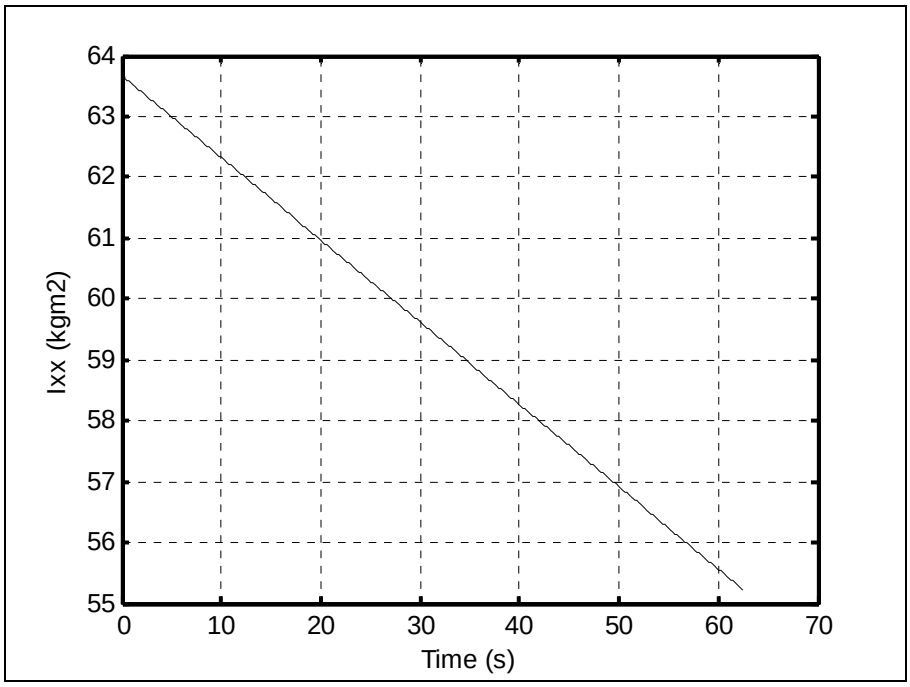

Figure 6-61 Moment of inertia about X axis for case III

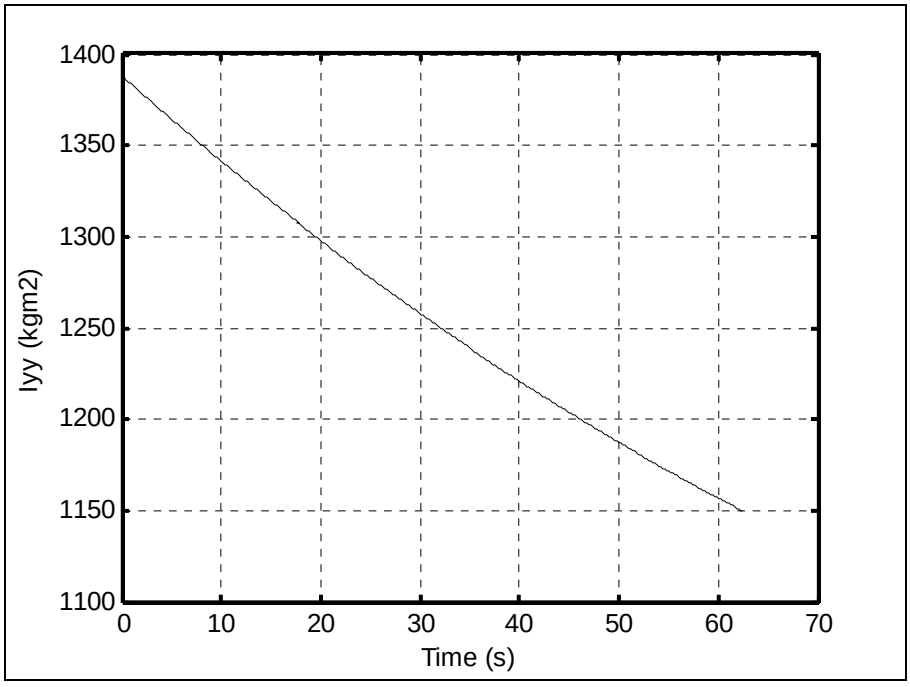

Figure 6-62 Moment of inertia about Y axis for case III

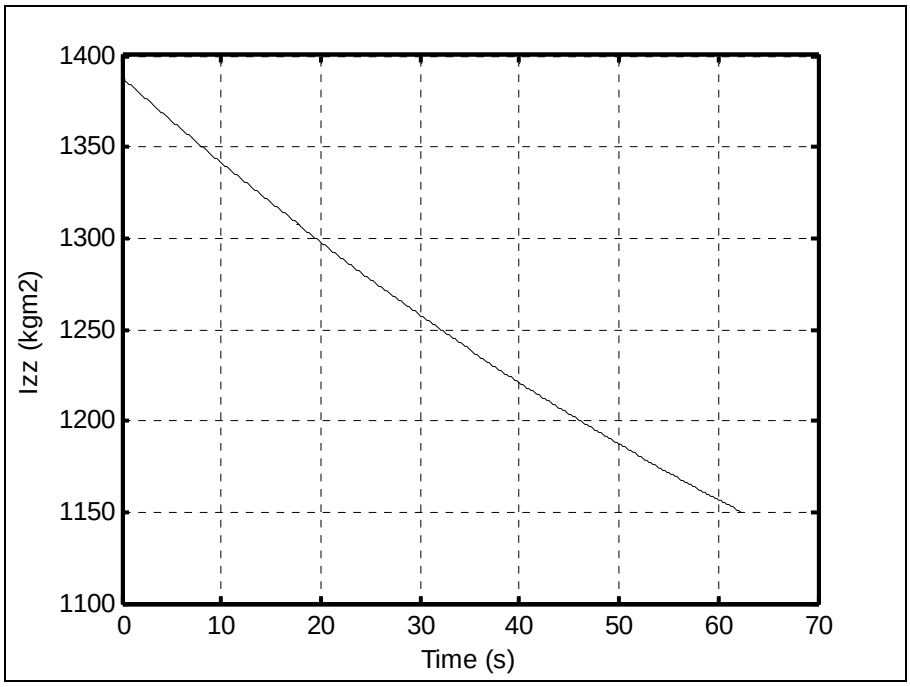

Figure 6-63 Moment of inertia about Z axis for case III

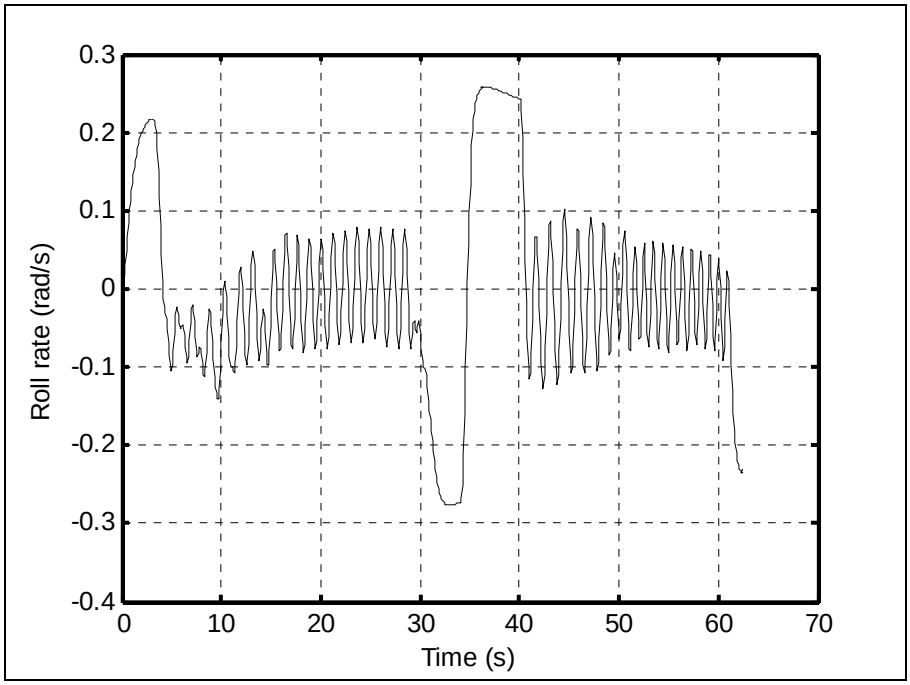

Figure 6-64 Roll rate for case III

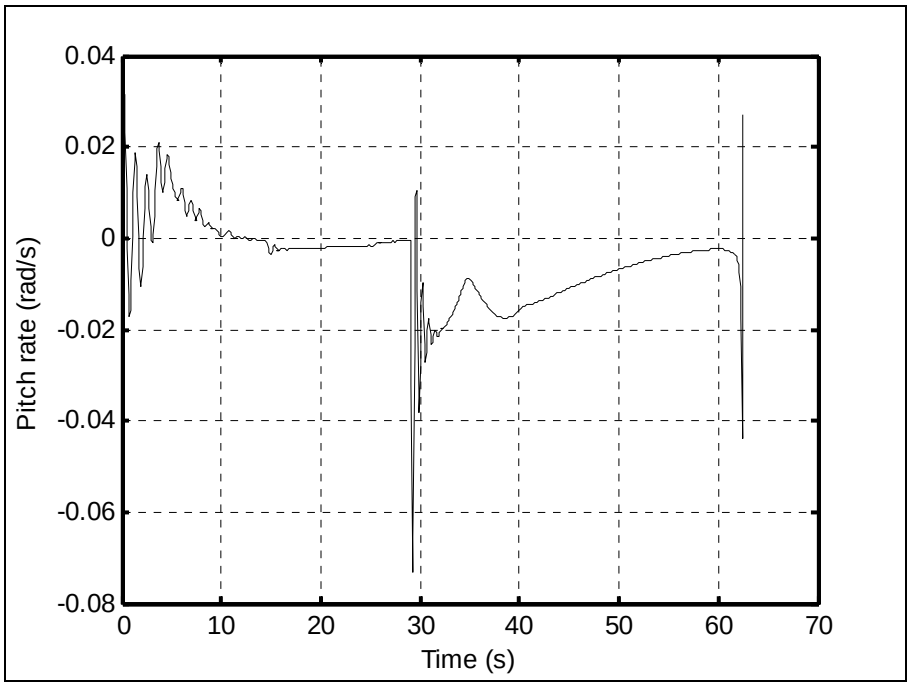

Figure 6-65 Pitch rate for case III

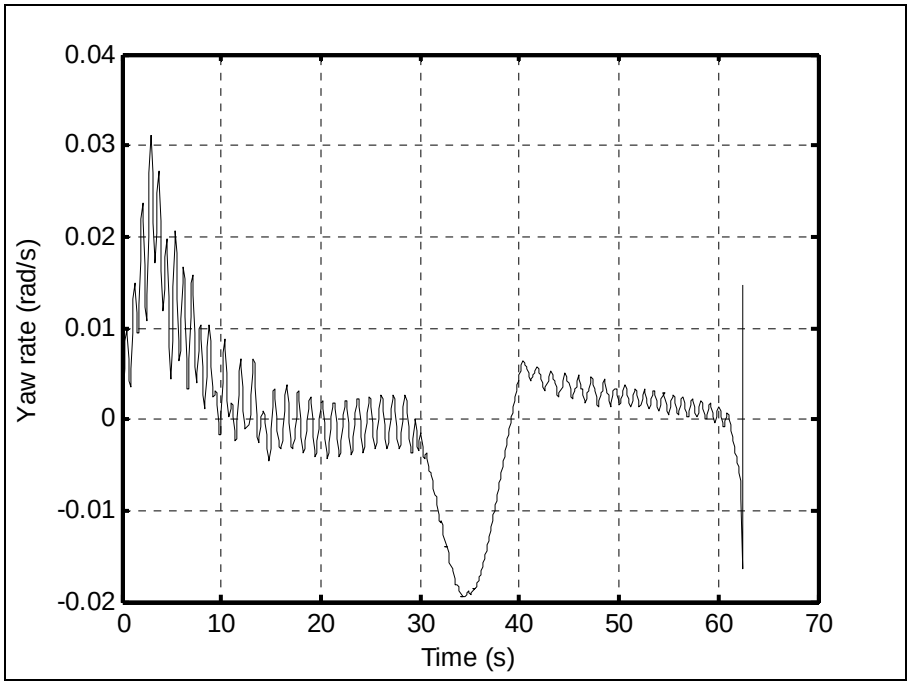

Figure 6-66 Yaw rate for case III

6.4 Case IV

In this case, the target is at the closest position, so this case is called immediate dive trajectory. Trajectory directly begins with dive maneuver and it is completed at target before burn-out. Therefore this case has the same verification role like case III. Yet, it is different from case III in that trajectory does not have a constant altitude stage.

Figure 6-67 and Figure 6-68 show the missile's path on XZ plane. Figure 6-69 and Figure 6-70 demonstrate the path of the missile on XY plane. Through the diving path, airspeed of the missile increases continuously; however, owing to the shorter flight distance, it is not as high as in case III. Figure 6-75 and Figure 6-76 illustrate the airspeed history of the missile. Highest speed is obtained when the missile strikes the target and it is equal to 480 m/s (1.41 M). It is the second maximum striking speed among the all cases. Consequently, it has more efficient strike than first two cases, if impact angle does not make a big difference. It may even have more effective strike than 3rd case because of the fact that it has more propellant remained (see Figure 6-81).

All over the flight, as seen in Figure 6-74 sideslip angle variation and its magnitude are ignorable. Thus, heading angle control guides the missile to the target with negligible inaccuracy. Guidance is managed by the use of coordinated turn to obtain required heading angle. History of heading angle and bank angle is plotted in Figure 6-72 and Figure 6-77. Corresponding rise time for heading angle is about 16 seconds. Aileron and rudder surface deflections are recorded in Figure 6-79 and Figure 6-80 for equivalent heading command.

Figure 6-73 shows the history of angle of attack that proves how the missile realizes dynamic stability in a short period of time less than 5 seconds.

Pitching down maneuver to get about -20 degrees flight path angle is shown in Figure 6-71. The related elevator deflection history is given in Figure 6-78.

Center of gravity, moments of inertia about X, Y, and Z axis are available through Figure 6-82 - Figure 6-85. What's more, roll rate, pitch rate and yaw rate

related to maneuvers are given in figures through Figure 6-86, Figure 6-87, and Figure 6-88.

Circular error of probabilities on XZ and XY planes are 11 m and 3.5 m respectively (see Figure 6-68 and Figure 6-70).

Briefly, even if target is very close and control and guidance of the missile is performed before burn-out, missile is able to hit the target with a CEP less than 12 m.

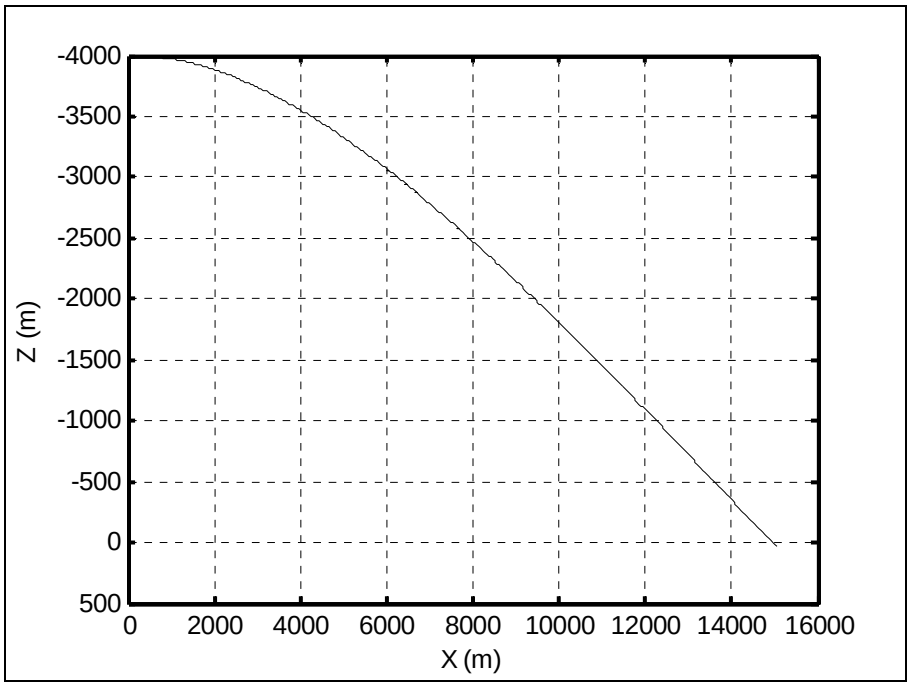

Figure 6-67 XZ plane flight path for case IV

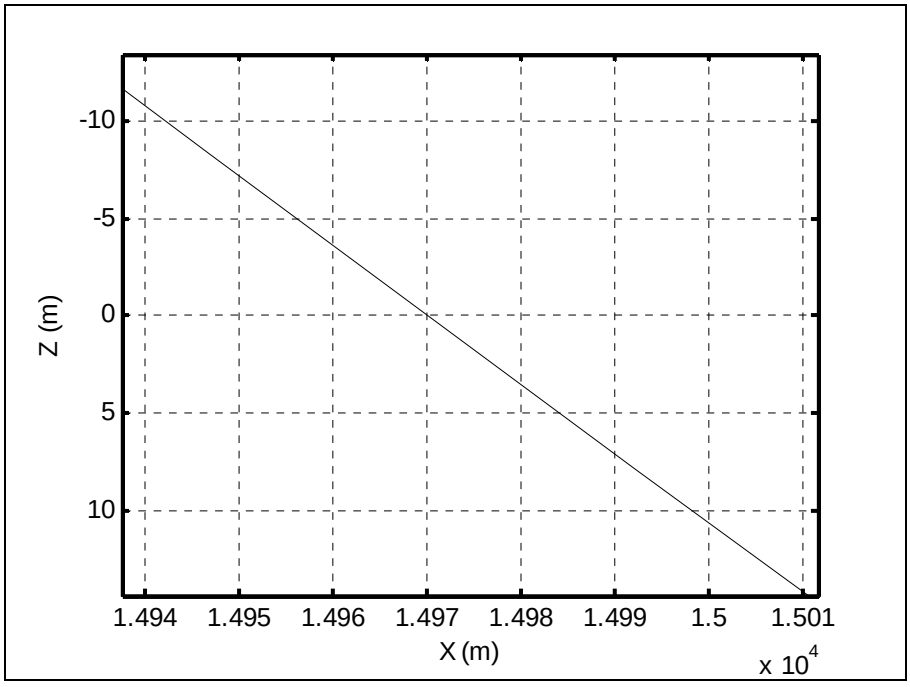

Figure 6-68 XZ plane missile-target interception for case IV

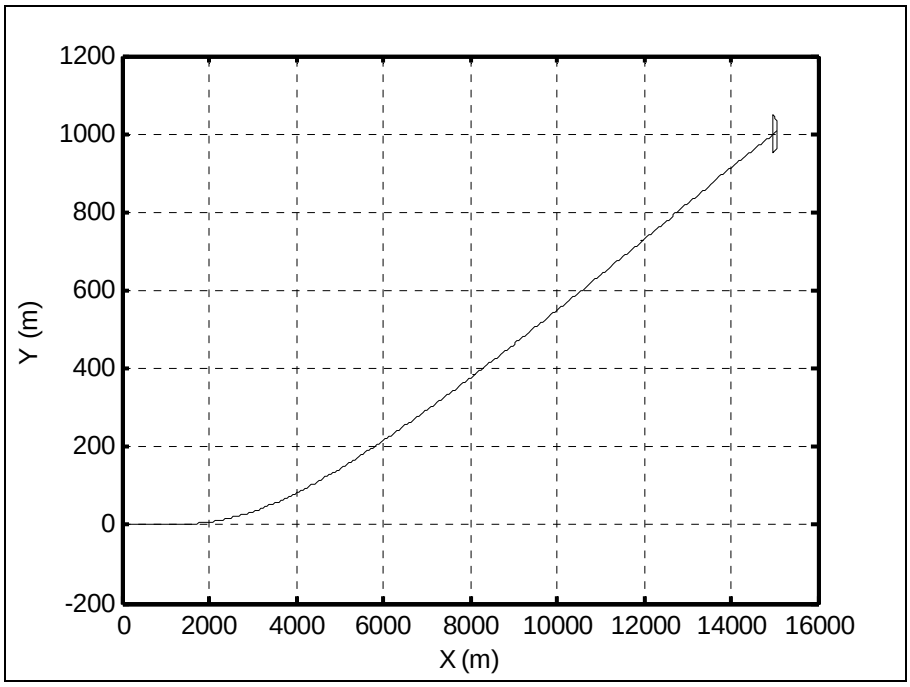

Figure 6-69 XY plane flight path for case IV

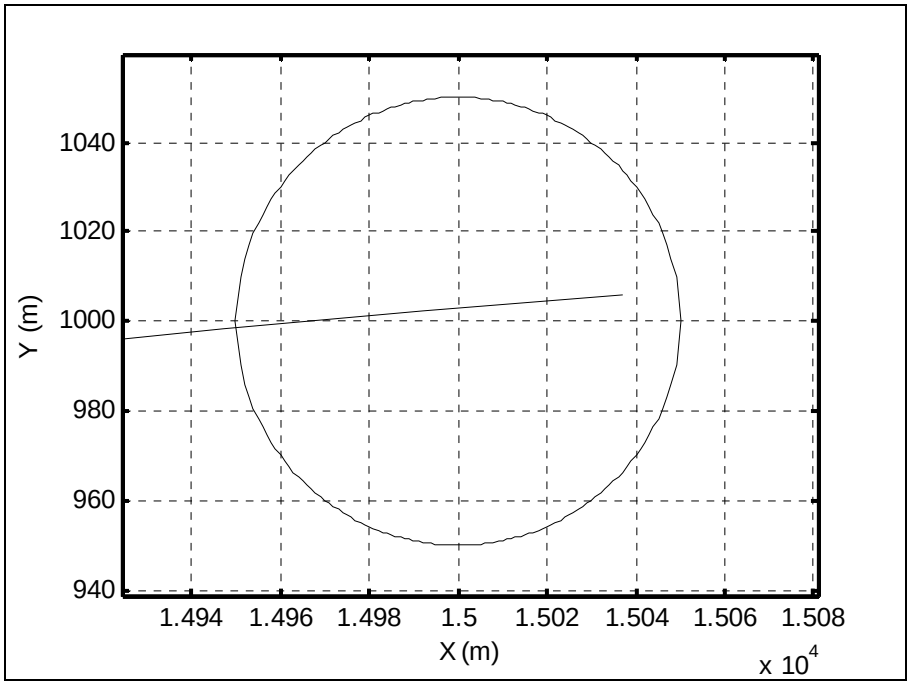

Figure 6-70 XY plane missile-target interception for case IV

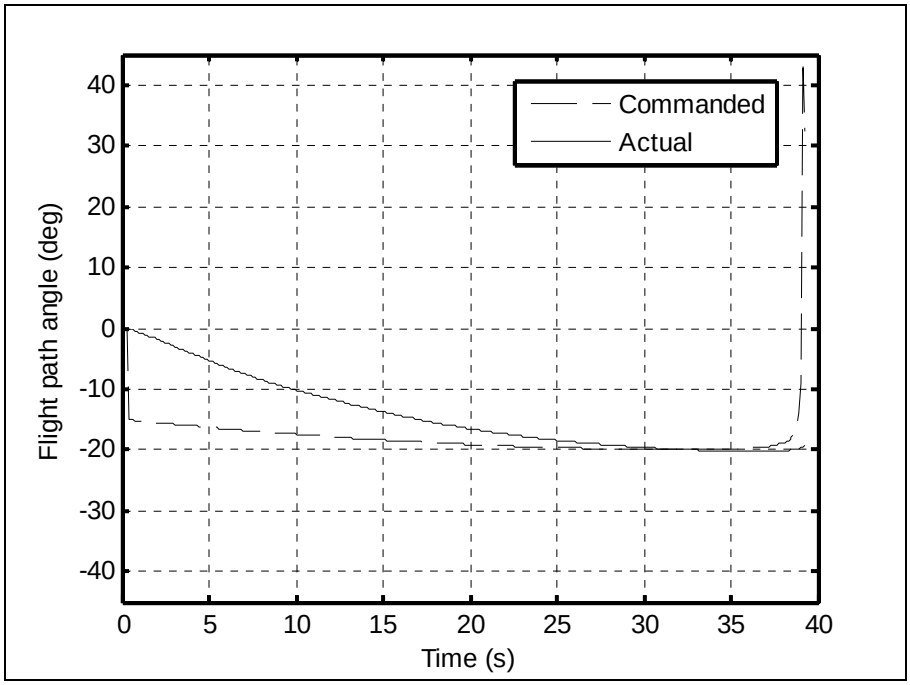

Figure 6-71 Flight path angle for case IV

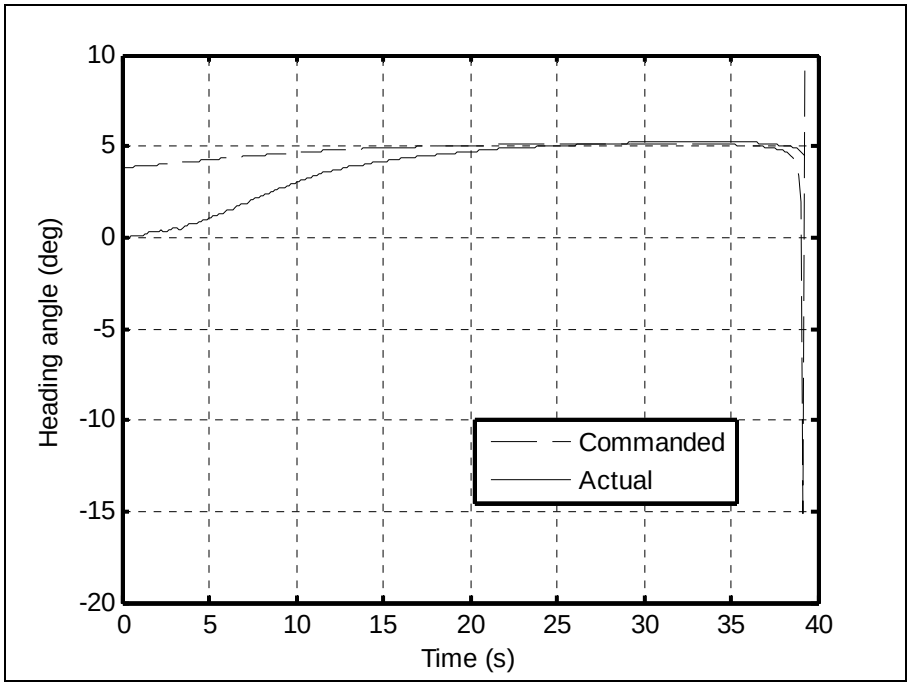

Figure 6-72 Heading angle for case IV

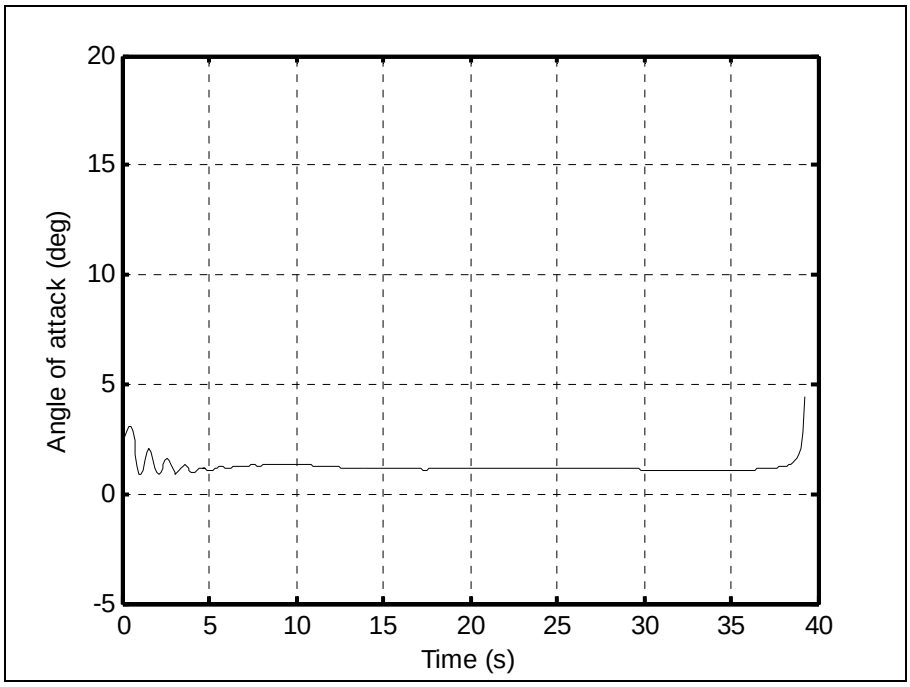

Figure 6-73 Angle of attack for case IV

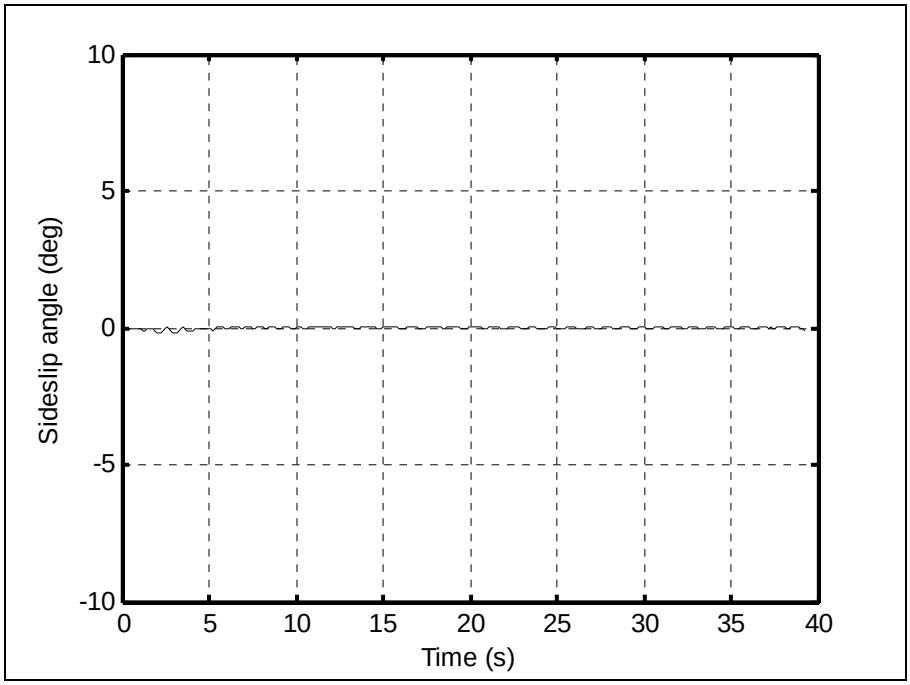

Figure 6-74 Sideslip angle for case IV

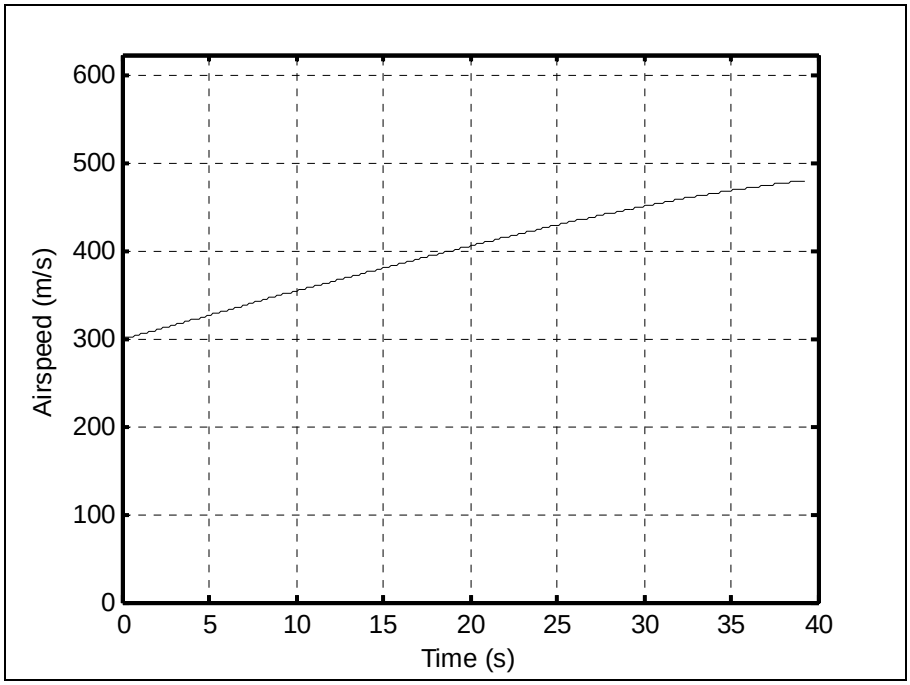

Figure 6-75 Airspeed for case IV

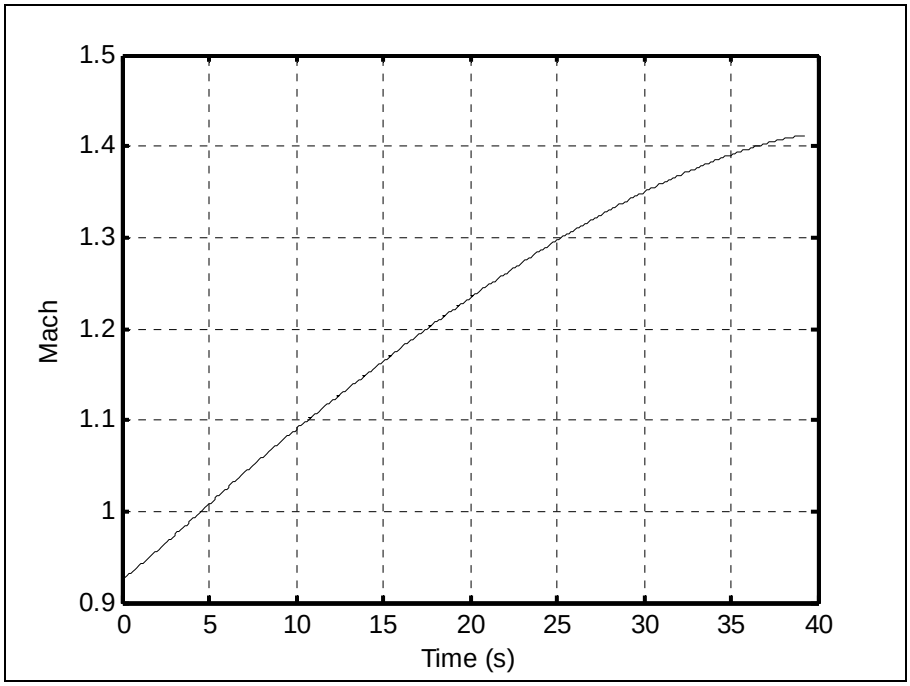

Figure 6-76 Mach number for case IV

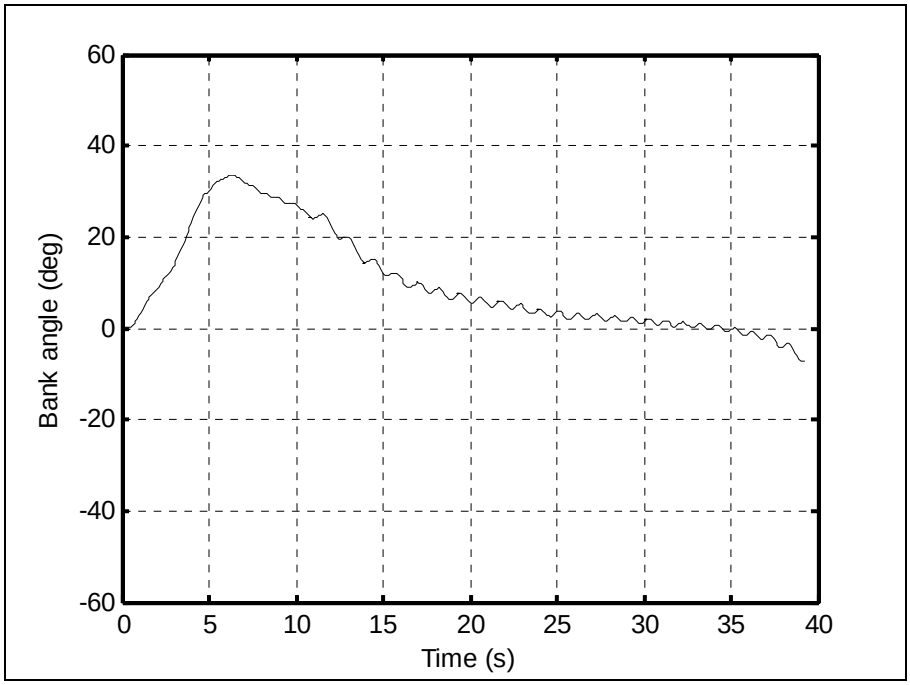

Figure 6-77 Bank angle for case IV

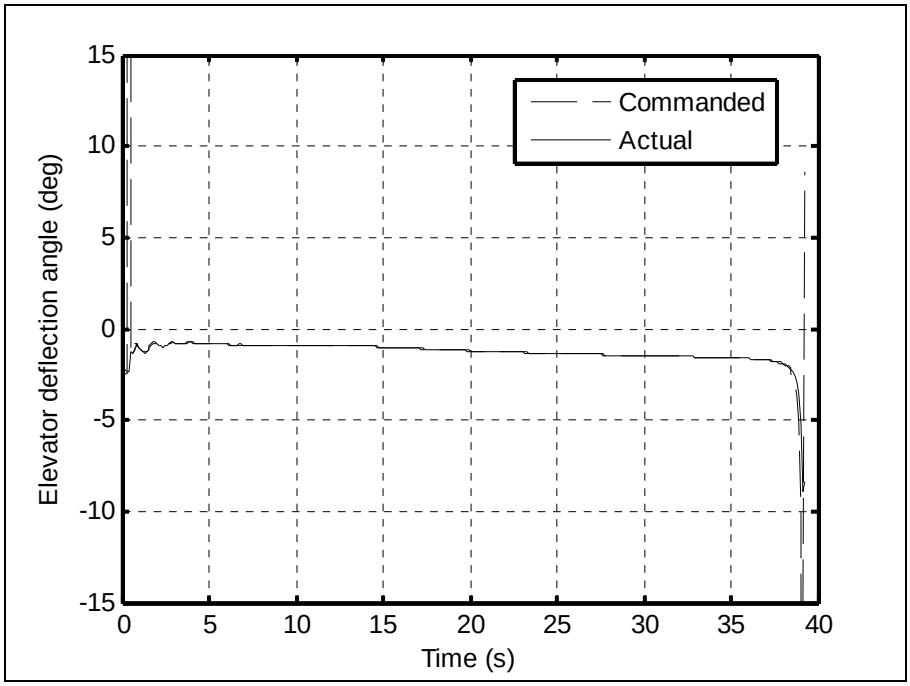

Figure 6-78 Elevator deflection angle for case IV

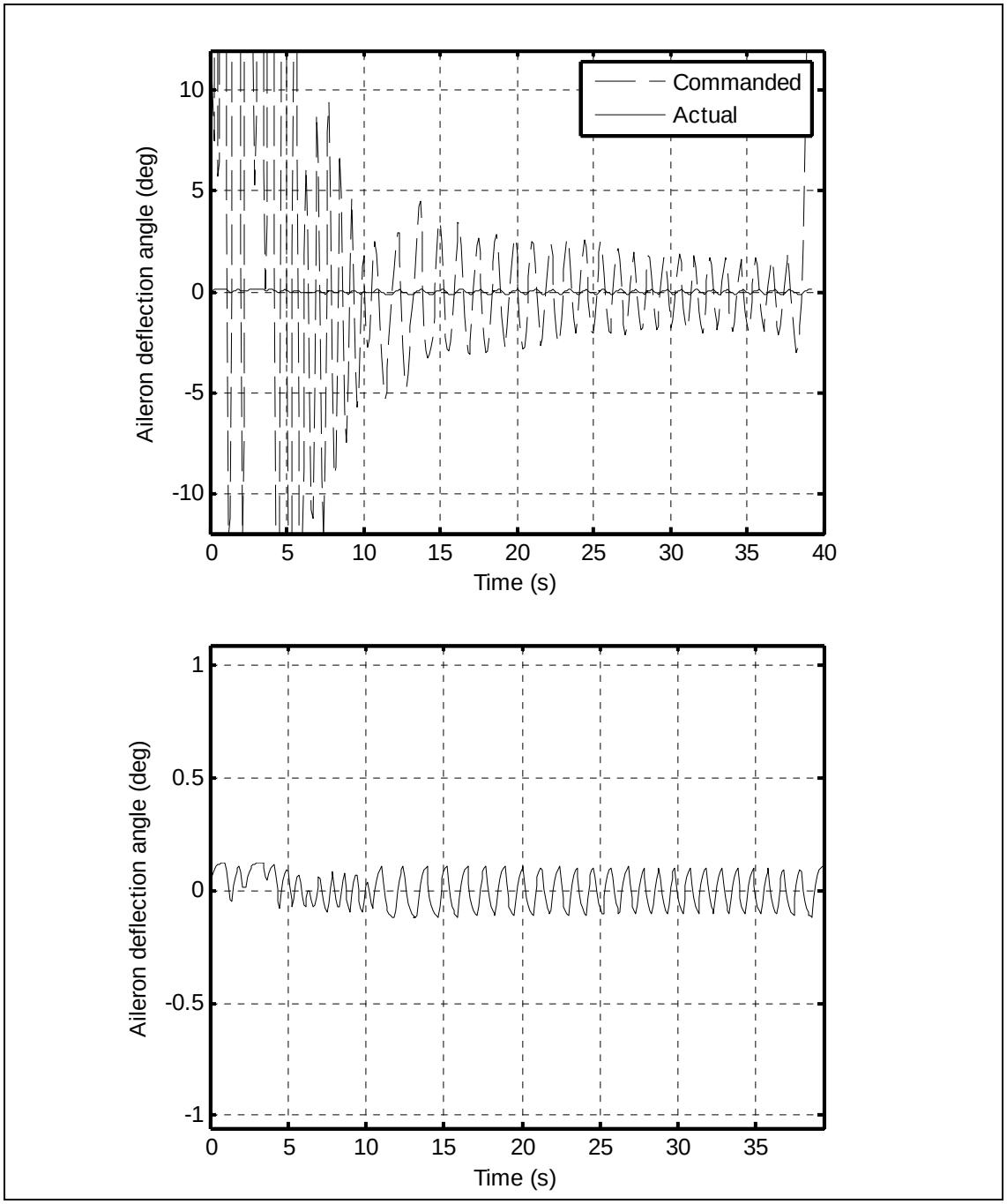

Figure 6-79 Aileron deflection angle for case IV

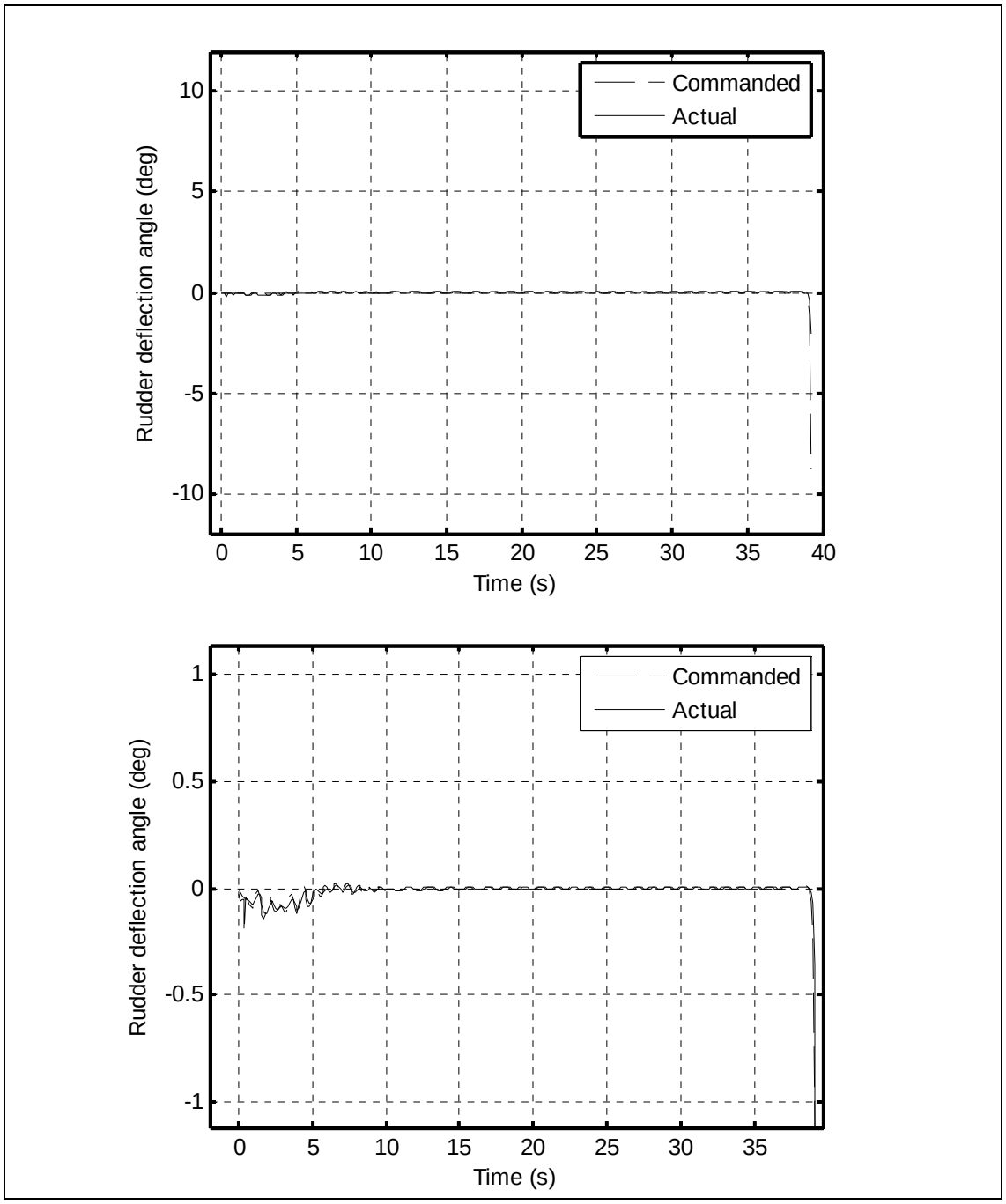

Figure 6-80 Rudder deflection angle for case IV

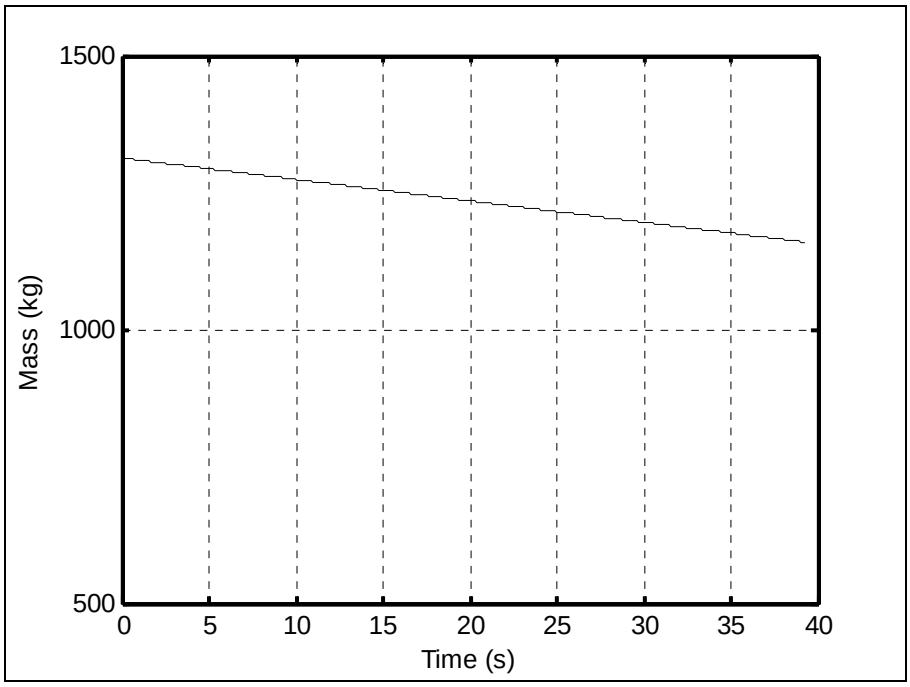

Figure 6-81 Variation of the missile's mass for case IV

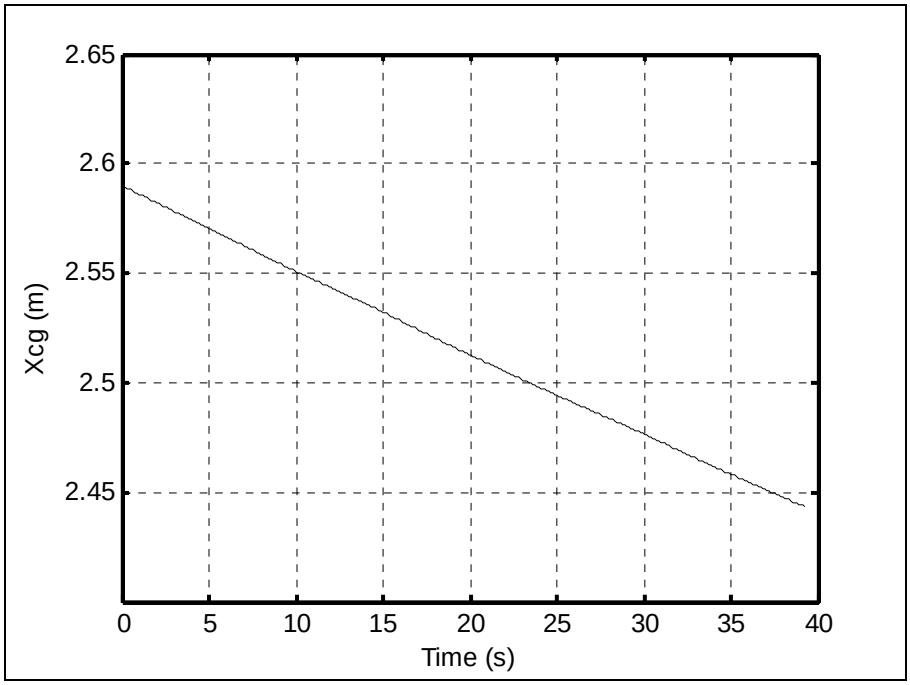

Figure 6-82 Center of gravity for case IV

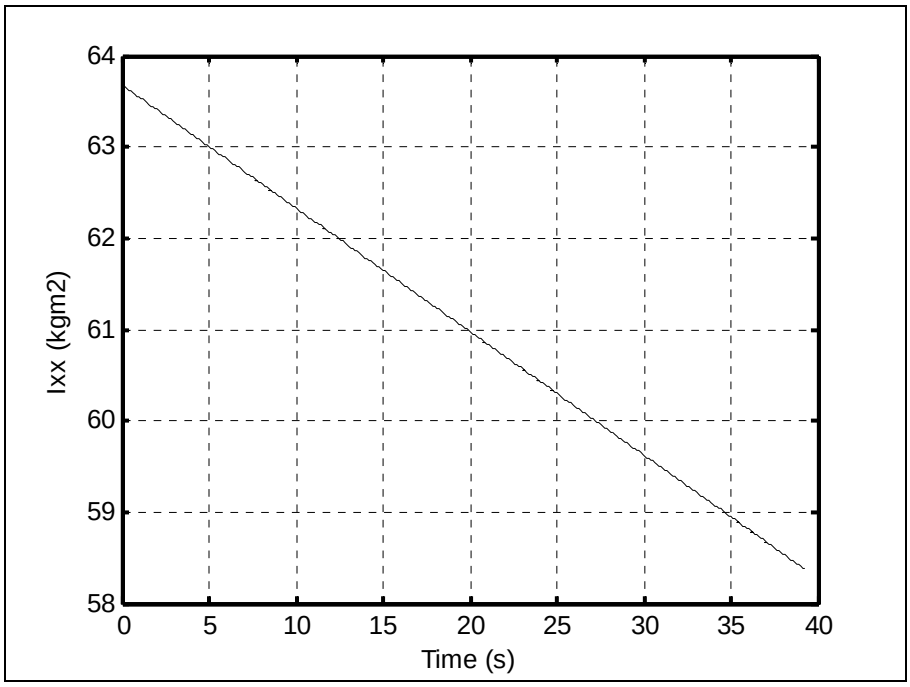

Figure 6-83 Moment of inertia about X axis for case IV

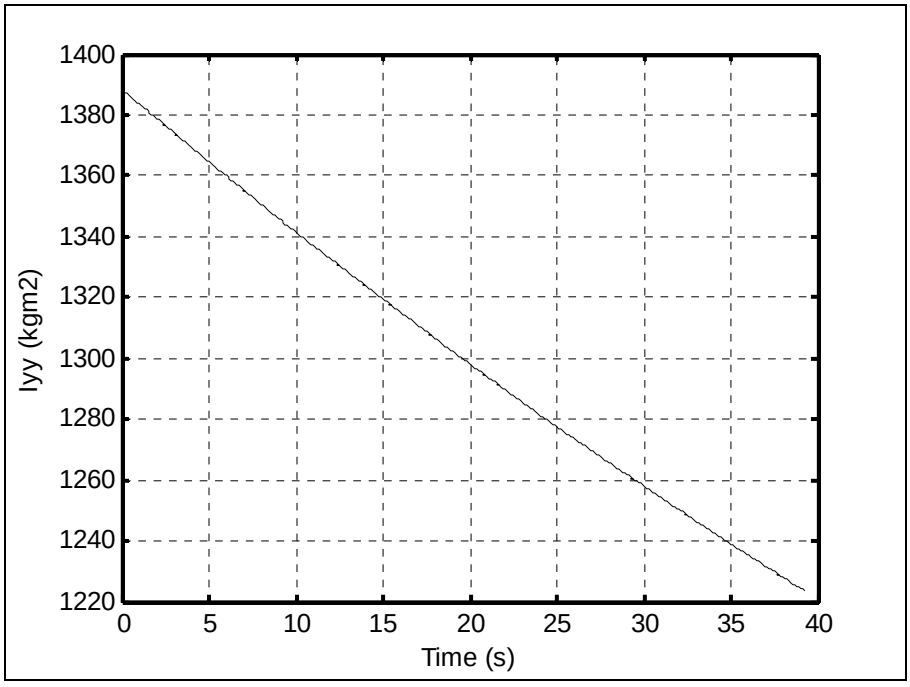

Figure 6-84 Moment of inertia about Y axis for case IV

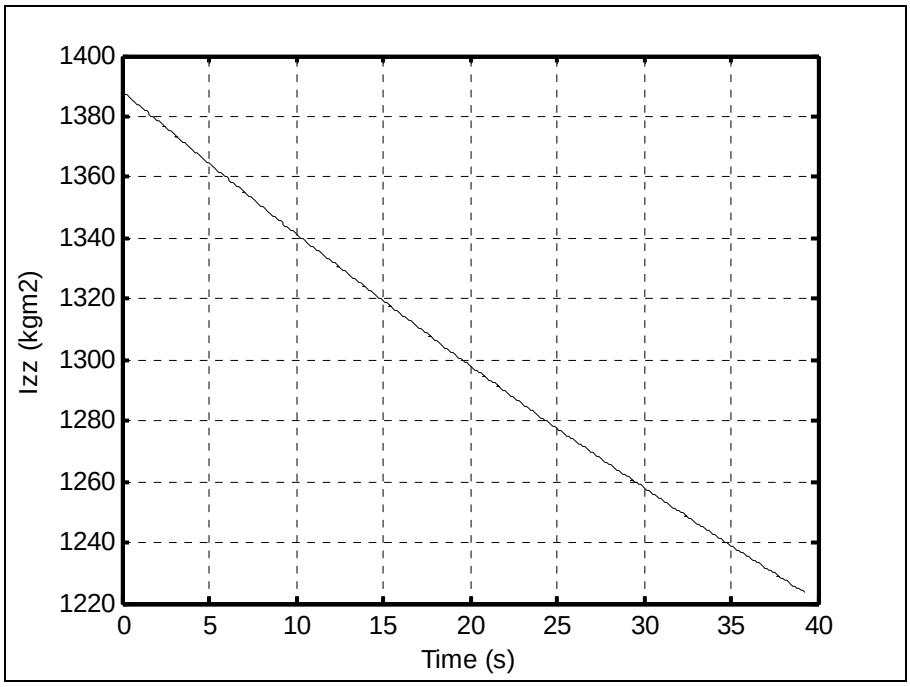

Figure 6-85 Moment of inertia about Z axis for case IV

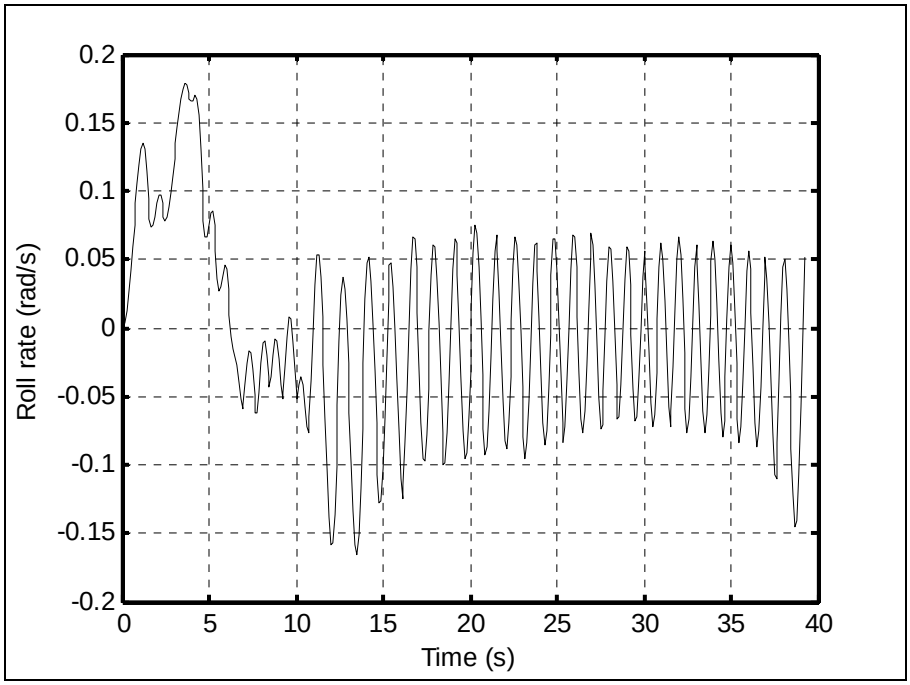

Figure 6-86 Roll rate for case IV

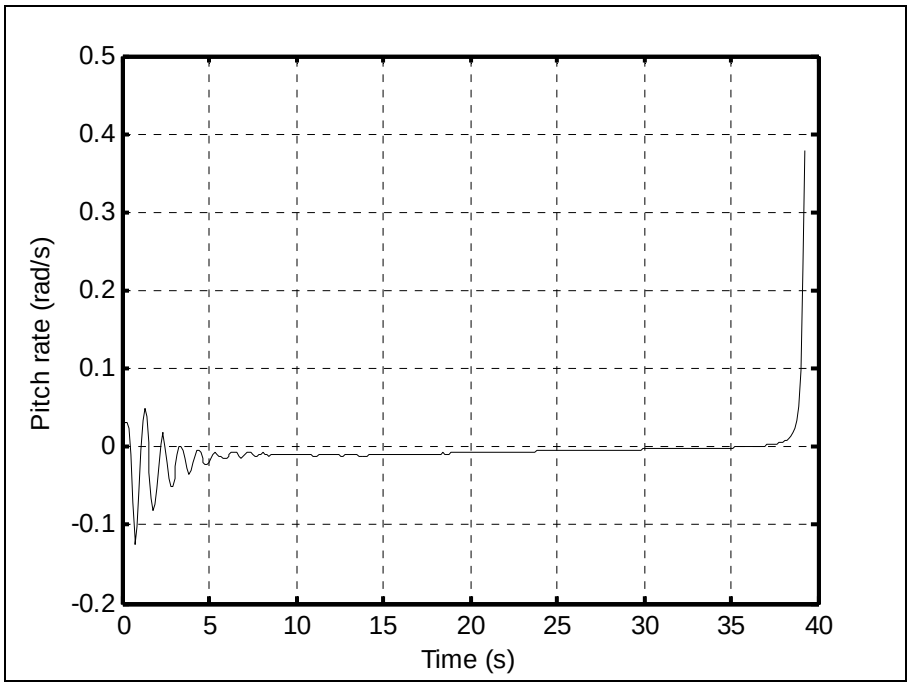

Figure 6-87 Pitch rate for case IV

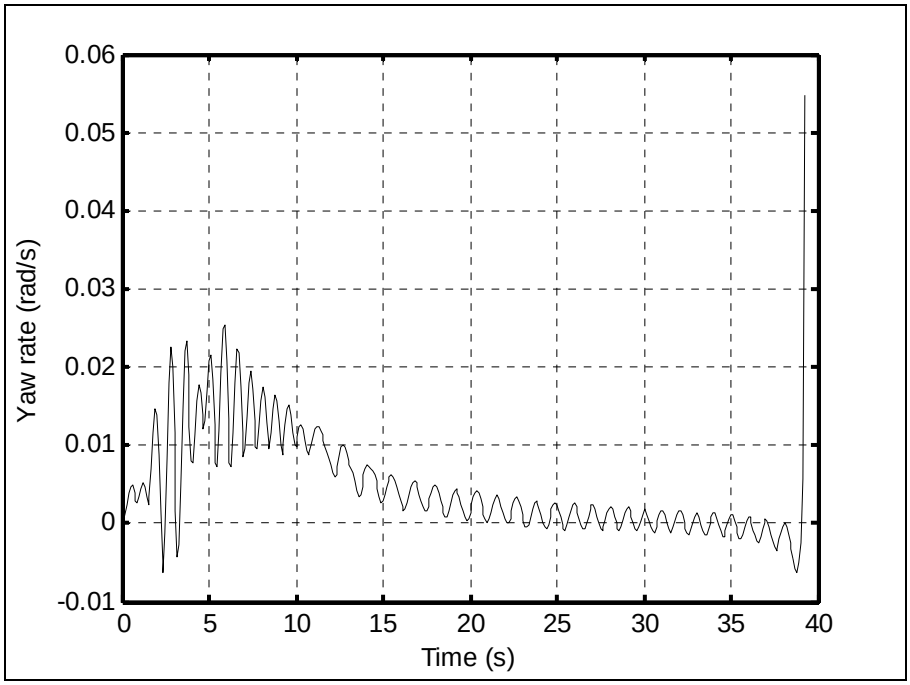

Figure 6-88 Yaw rate for case IV

6.5 Case V

This case is similar to the first case. However, it has higher initial angle which is defined as the angle between velocity vector of the missile and the target vector, $\vec{R}_T$ that connects the missile to the target, at separation of the missile from aircraft. Initial angle is 45 degrees in this case and it is observable from Figure 6-94

Figure 6-89 and Figure 6-90 show the trajectory of the missile in XZ plane and Figure 6-91 and Figure 6-92 show that in XY plane. It is noticeable from Figure 6-89 that missile achieves to keep the cruise altitude by an oscillation less than 130 m around the cruise altitude that is caused by the airspeed variation resulting in lift change. Performed coordinated turn to obtain the required heading angle is observable from Figure 6-91. Required heading angle is high compare to other cases since the initial angle is high as defined previously. Commanded and actual heading angles through the flight are given in Figure 6-94. As it is seen in the figure the missile achieves to reach and sustain the desired heading angle through the flight. Sideslip angle remains very little throughout the flight; consequently, commanded heading angle steers the missile to the target with negligibly small error (see Figure 6-96). This steering is achieved by coordinated turn. Necessary bank angle for this turn reaches up to 50 degrees as observable in Figure 6-99. Corresponding aileron and rudder deflections to perform this turn are quite reasonable (see Figure 6-101 and Figure 6-102). This is obtained by very small deflection angles because of all moving fins.

As mentioned previously, the missile lacks of stability about X axis, so aileron continuously deflects to hold the zero bank angle as observable in Figure 6-101.

The flight path angle history is given in Figure 6-93. The variation of the elevator deflection to obtain the commanded flight path angle is given in Figure 6-100.

Variation of mass, center of gravity, moments of inertia about X, Y, and Z axis are given throughout Figure 6-103 - Figure 6-107. In addition, roll rate, pitch rate and yaw rate related to maneuvers are given through the Figure 6-108 - Figure 6-110.

Circular error of probabilities on XZ and XY planes can be found from Figure 6-90 and Figure 6-92 respectively. It is less than 6 m on XZ plane and less than 4 m on XY plane.

To sum up, even the initial angle between velocity vector of the missile and the target vector at separation is high, the missile is able to steer itself starting from separation and terminate the target by less than 6 m circular error of probability.

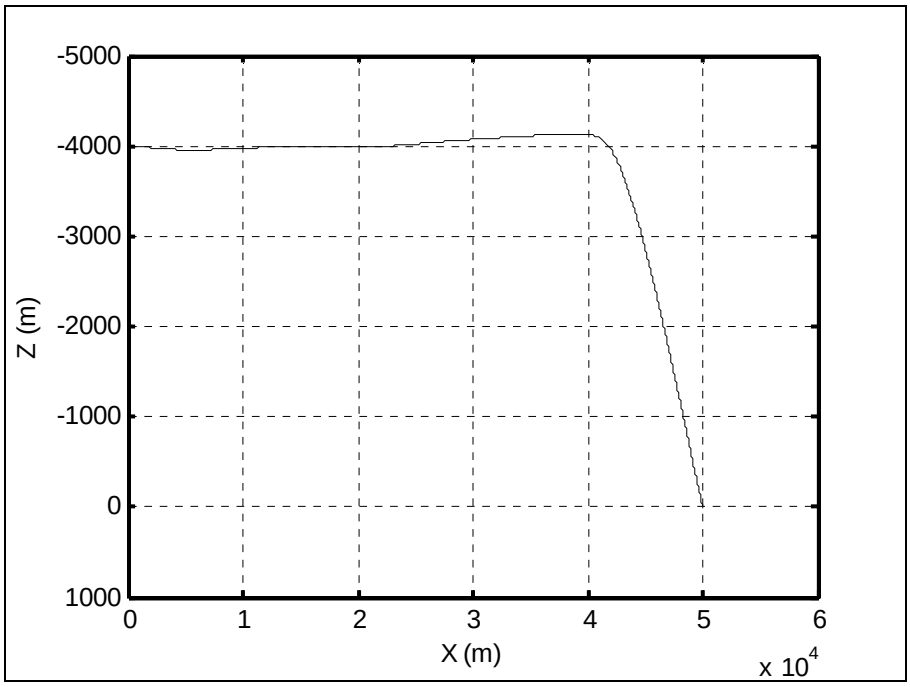

Figure 6-89 XZ plane flight path for case V

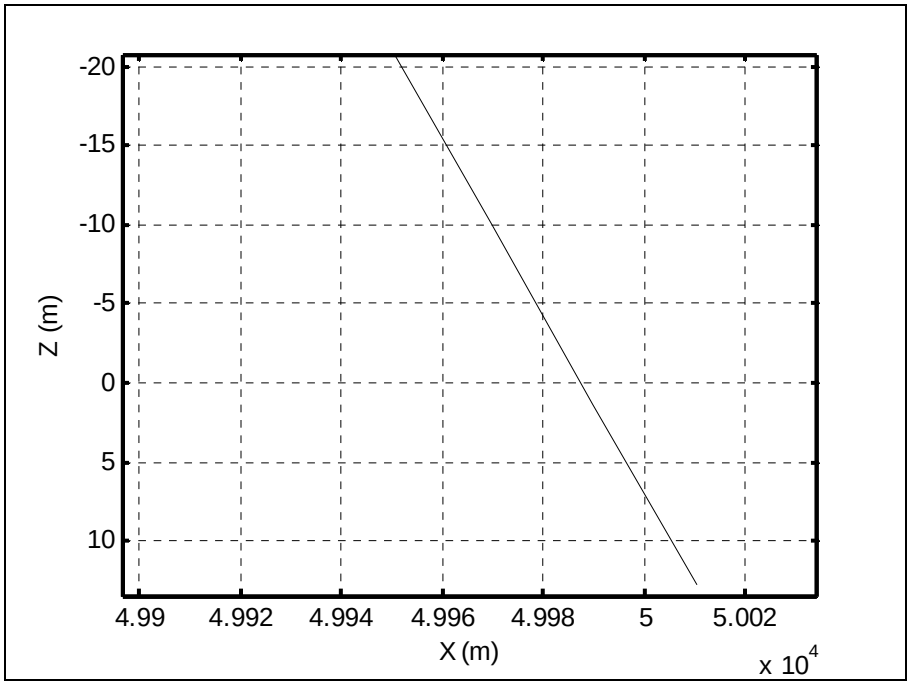

Figure 6-90 XZ plane missile-target interception for case V

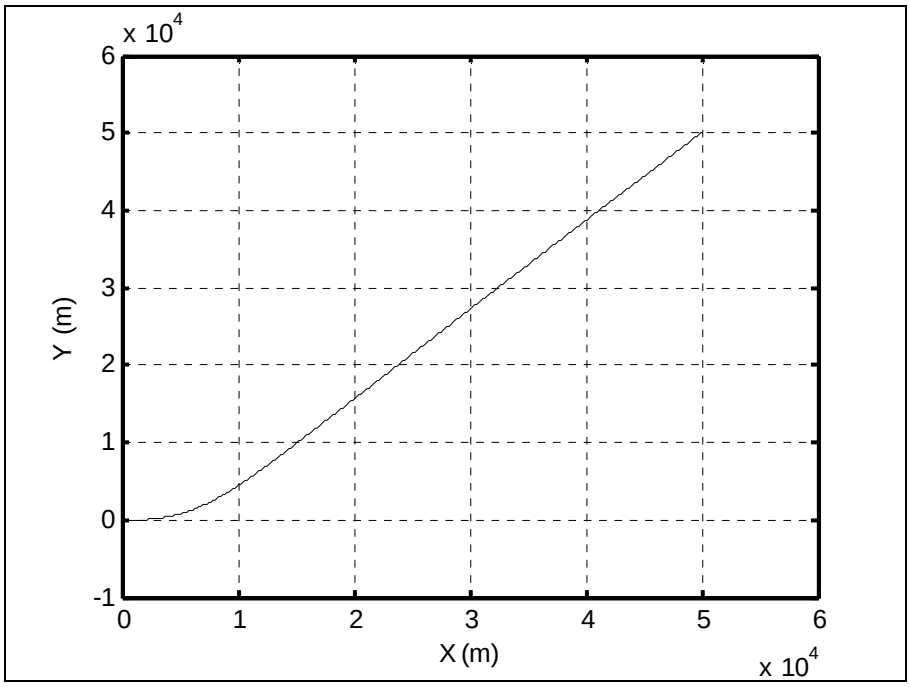

Figure 6-91 XY plane flight path for case V

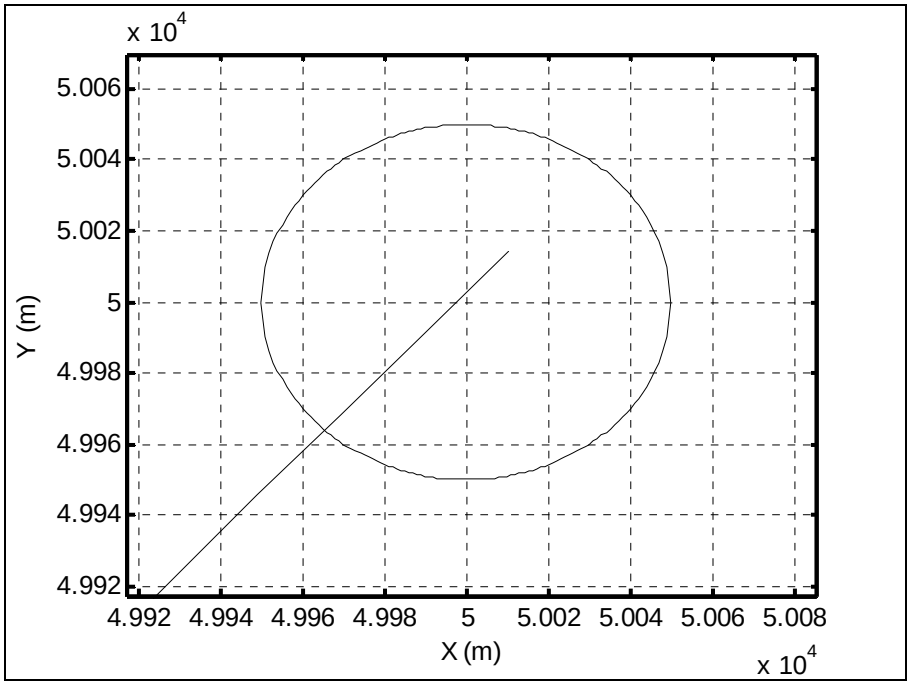

Figure 6-92 XY plane missile-target interception for case V

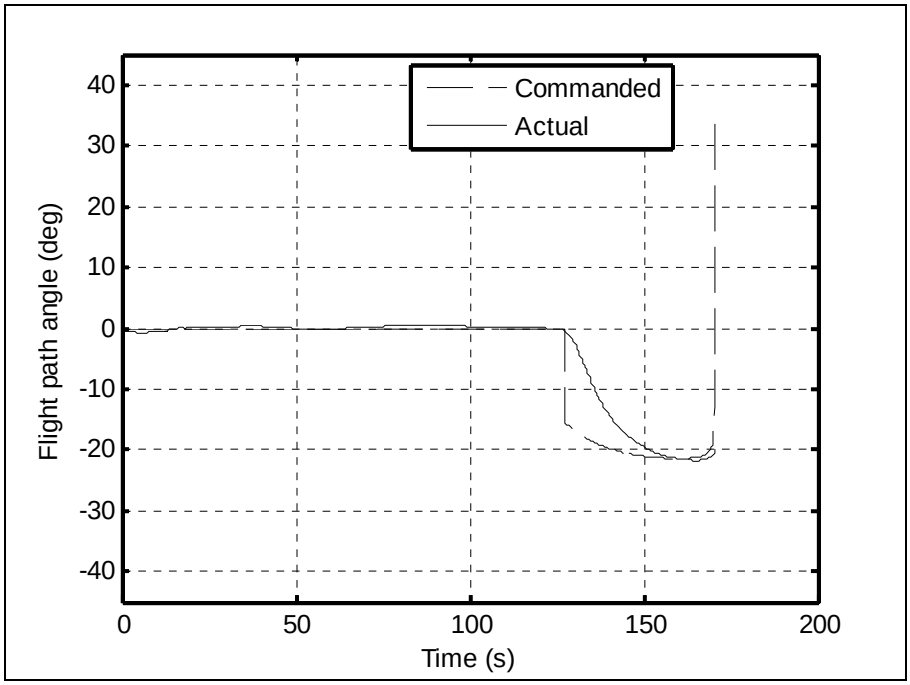

Figure 6-93 Flight path angle for case V

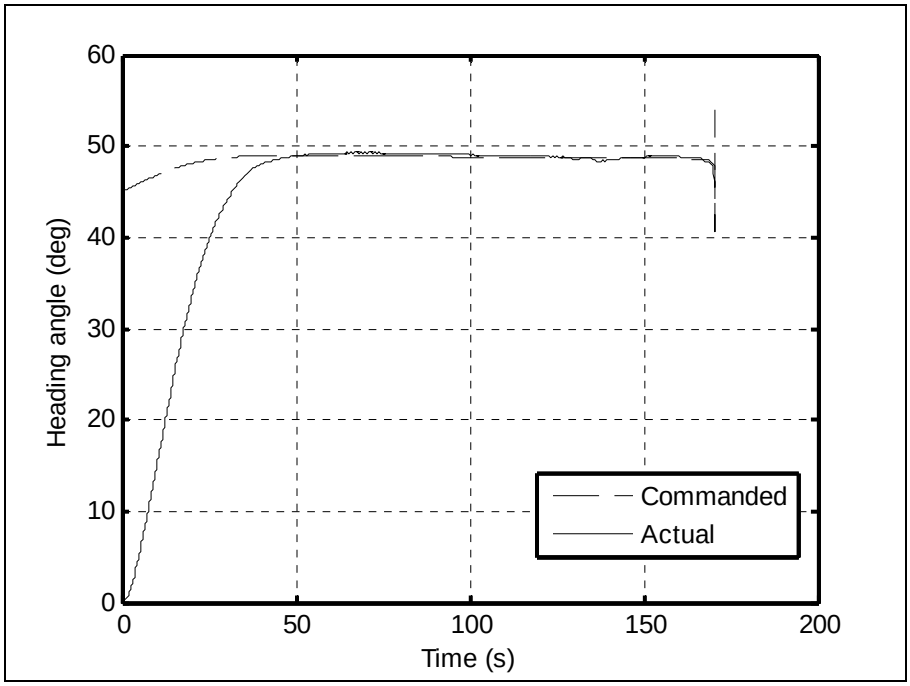

Figure 6-94 Heading angle for case V

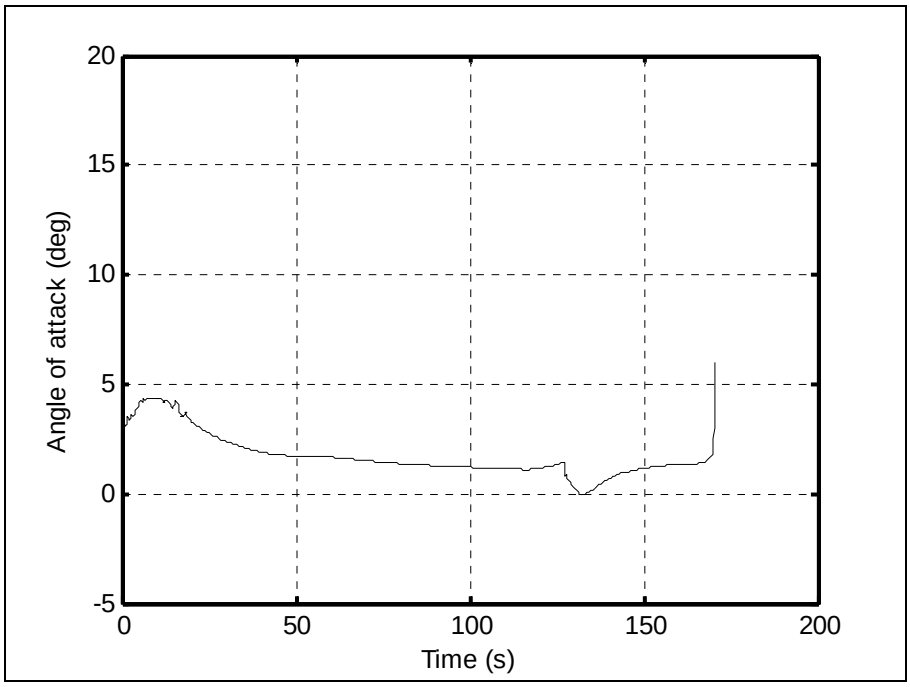

Figure 6-95 Angle of attack for case V

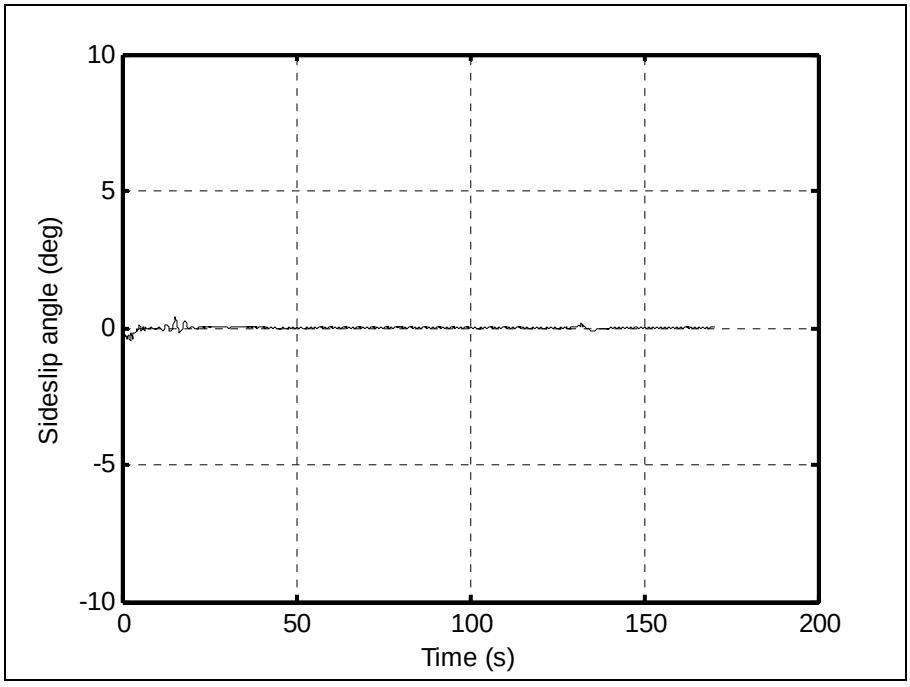

Figure 6-96 Sideslip angle for case V

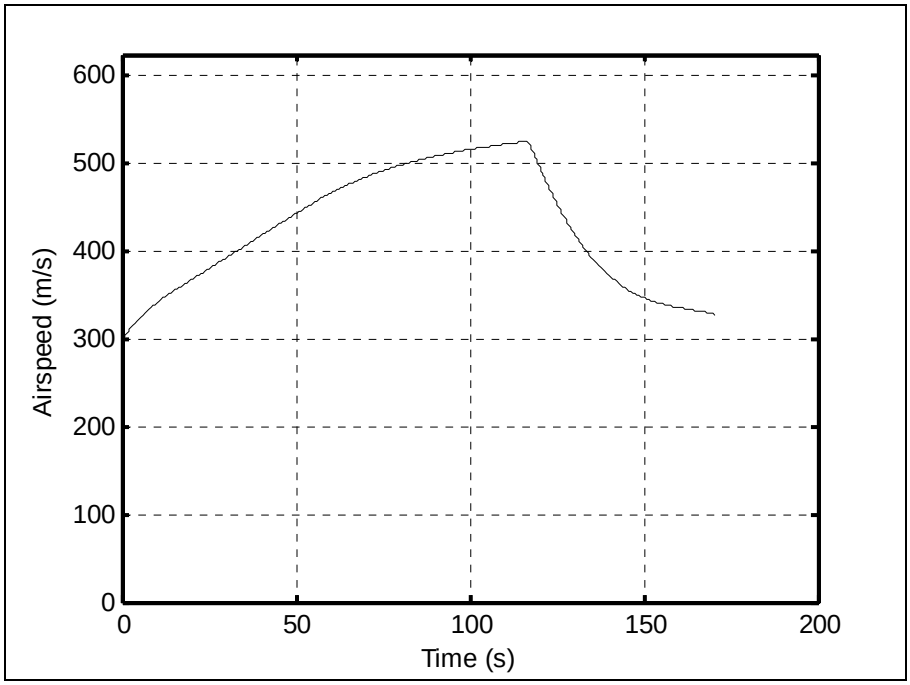

Figure 6-97 Airspeed for case V

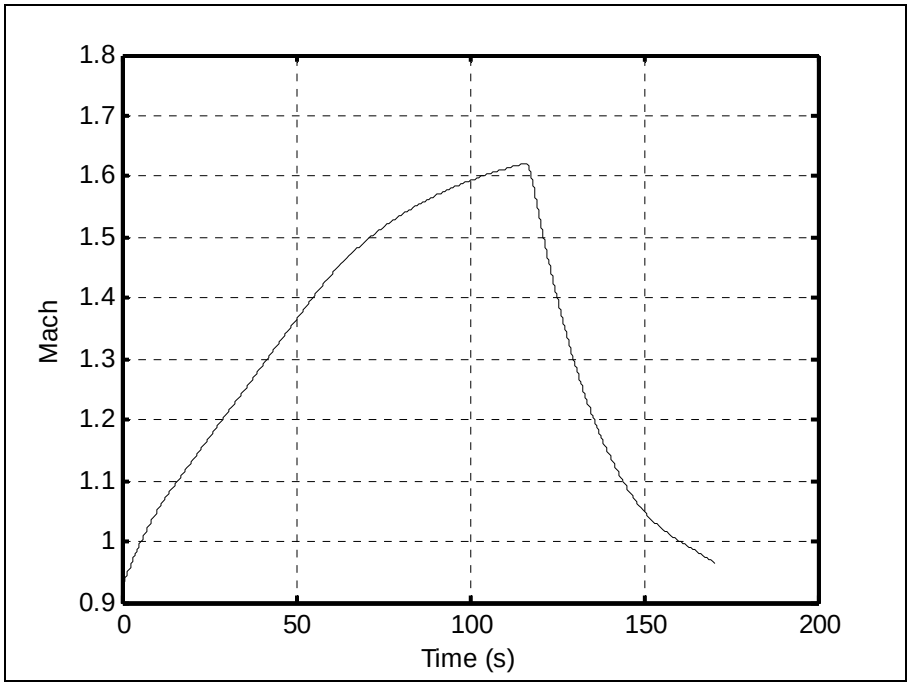

Figure 6-98 Mach number for case V

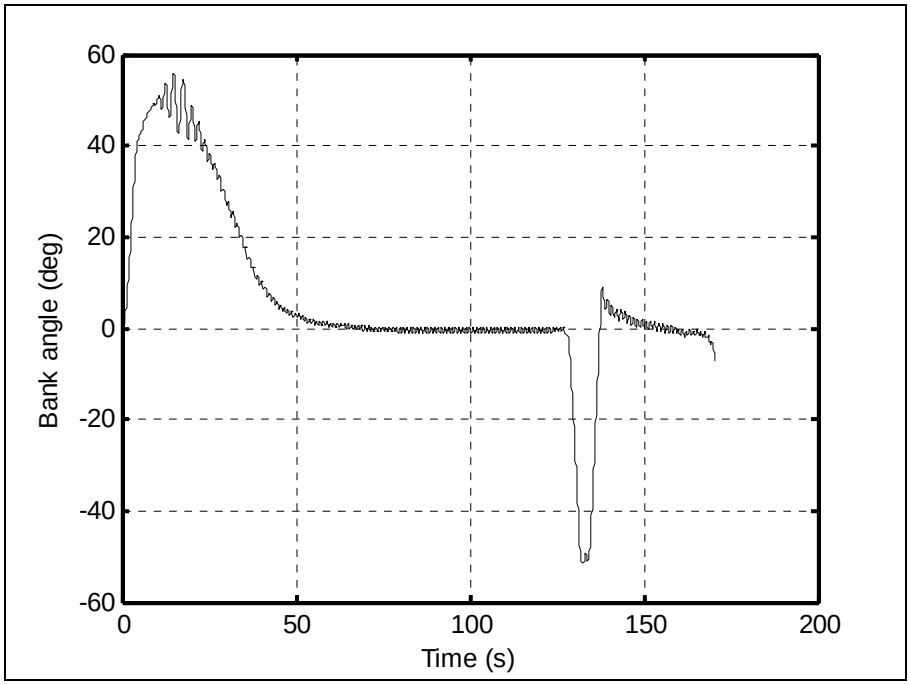

Figure 6-99 Bank angle for case V

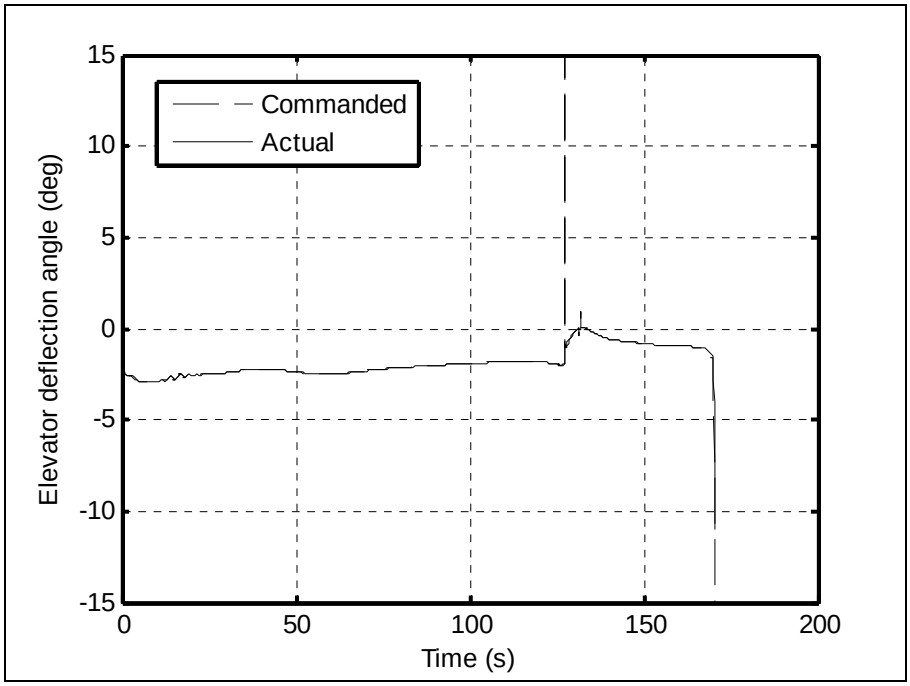

Figure 6-100 Elevator deflection angle for case V

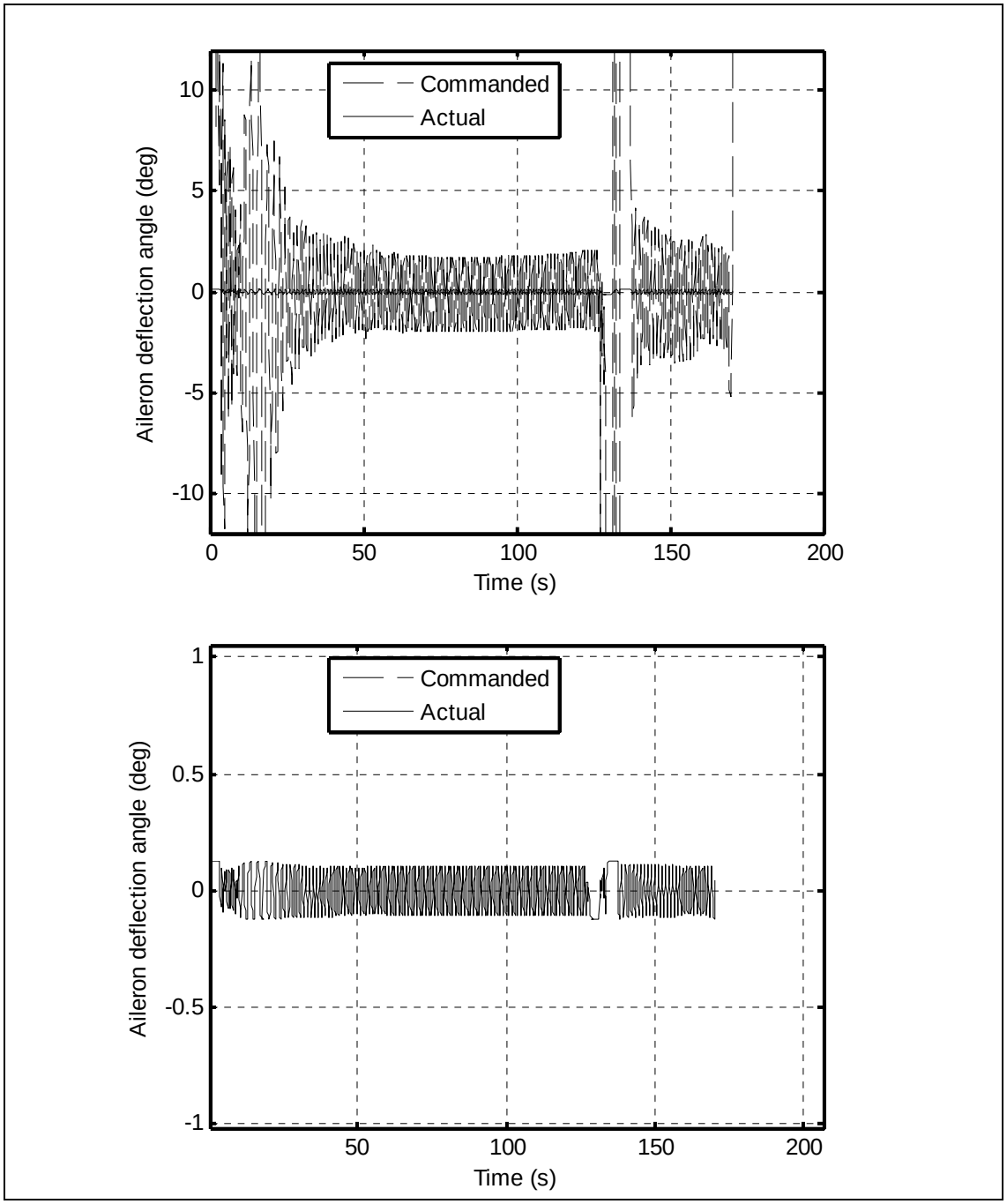

Figure 6-101 Aileron deflection angle for case V

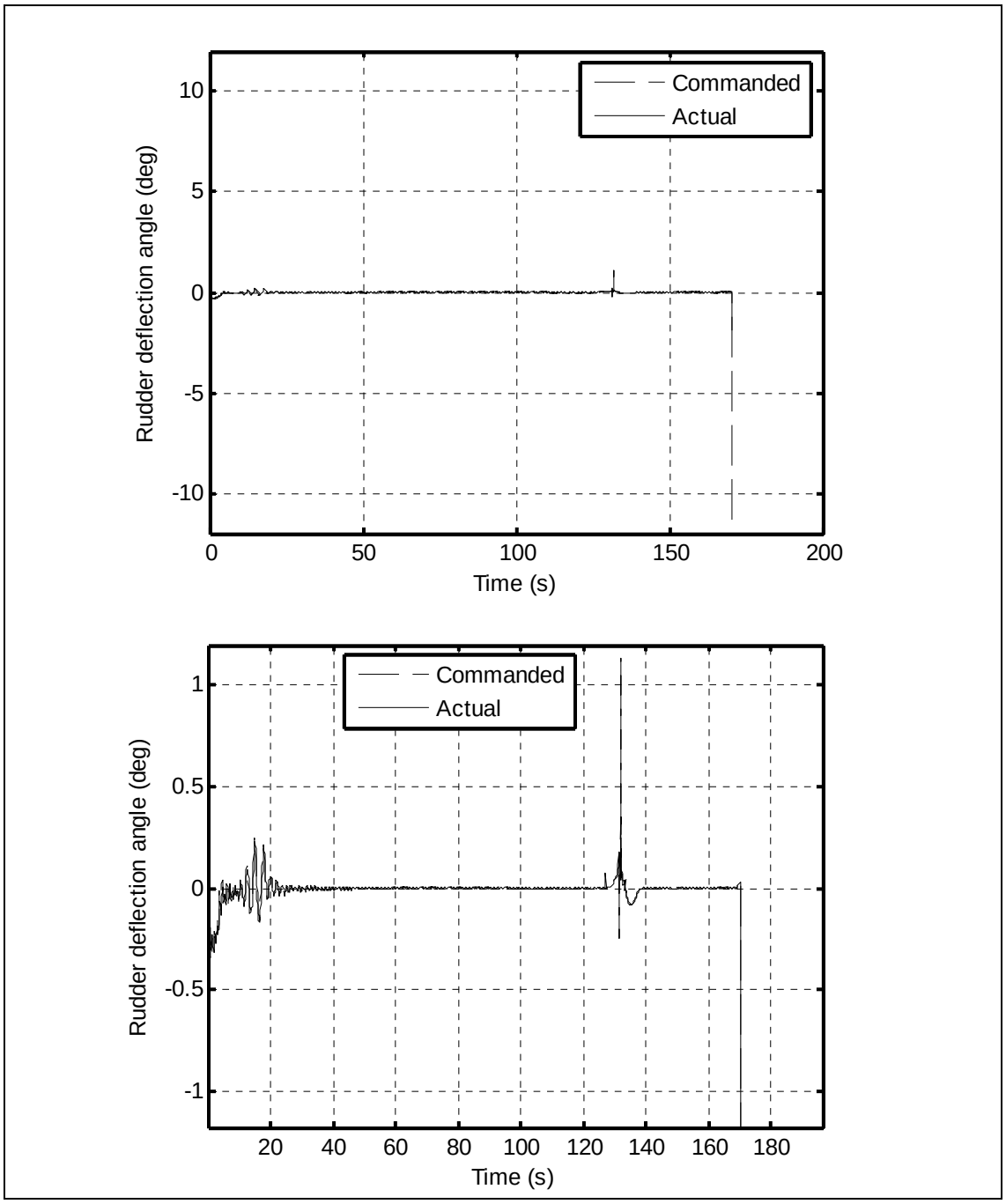

Figure 6-102 Rudder deflection angle for case V

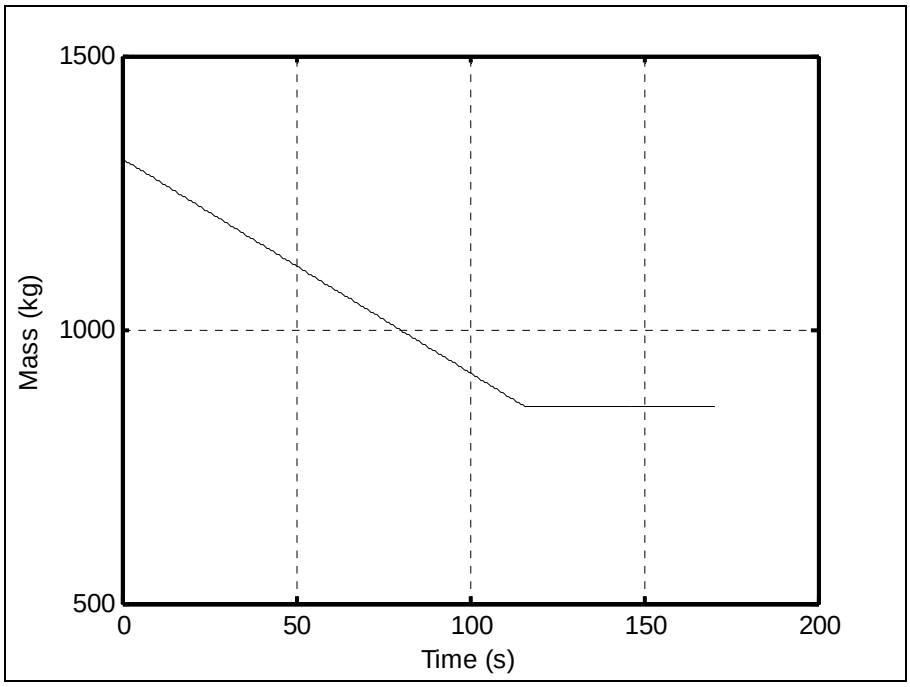

Figure 6-103 Variation of the missile's mass for case V

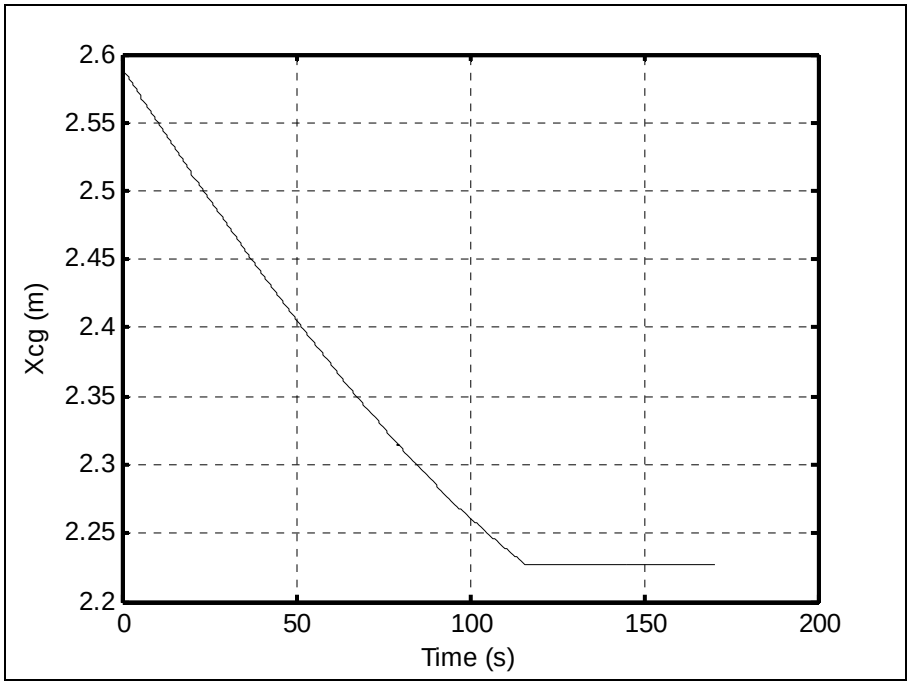

Figure 6-104 Center of gravity for case V

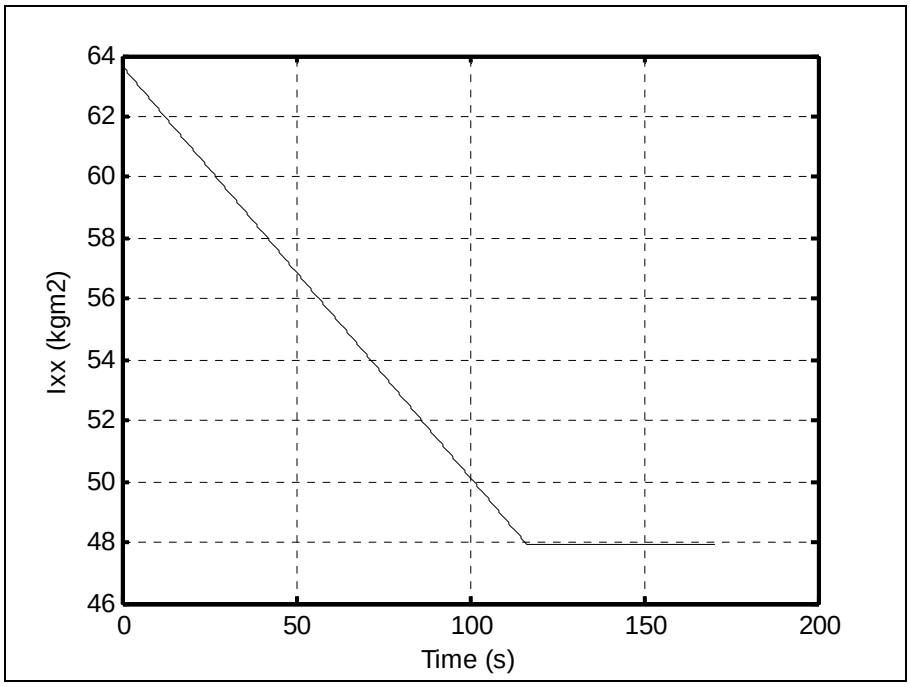

Figure 6-105 Moment of inertia about X axis for case V

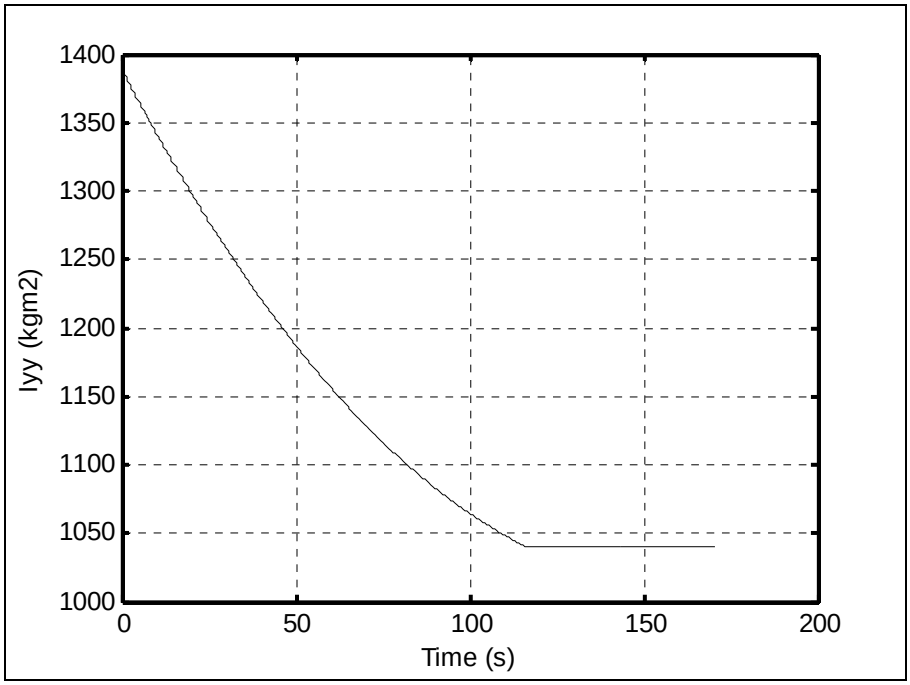

Figure 6-106 Moment of inertia about Y axis for case V

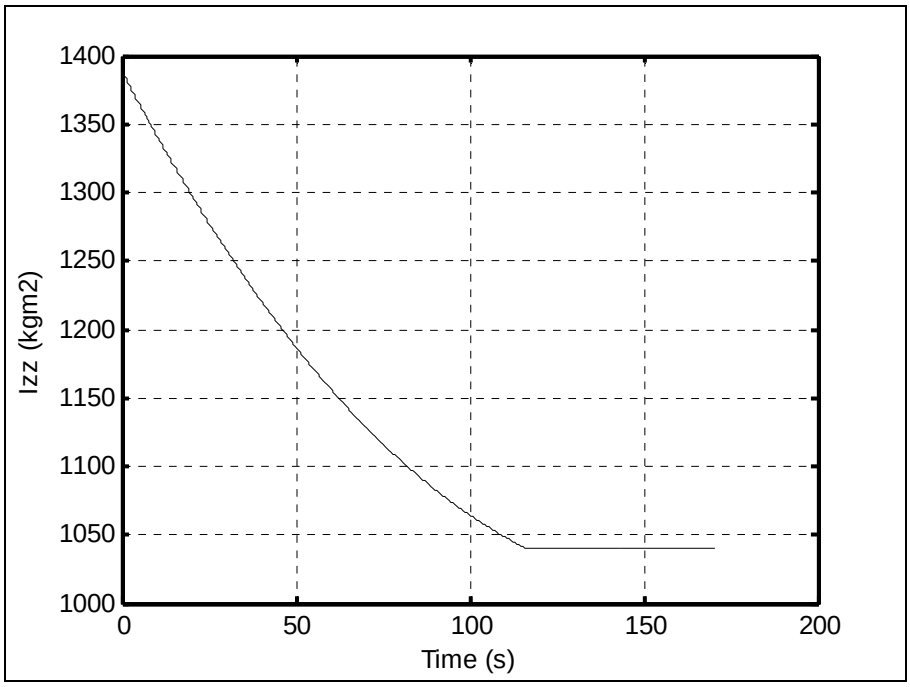

Figure 6-107 Moment of inertia about Z axis for case V

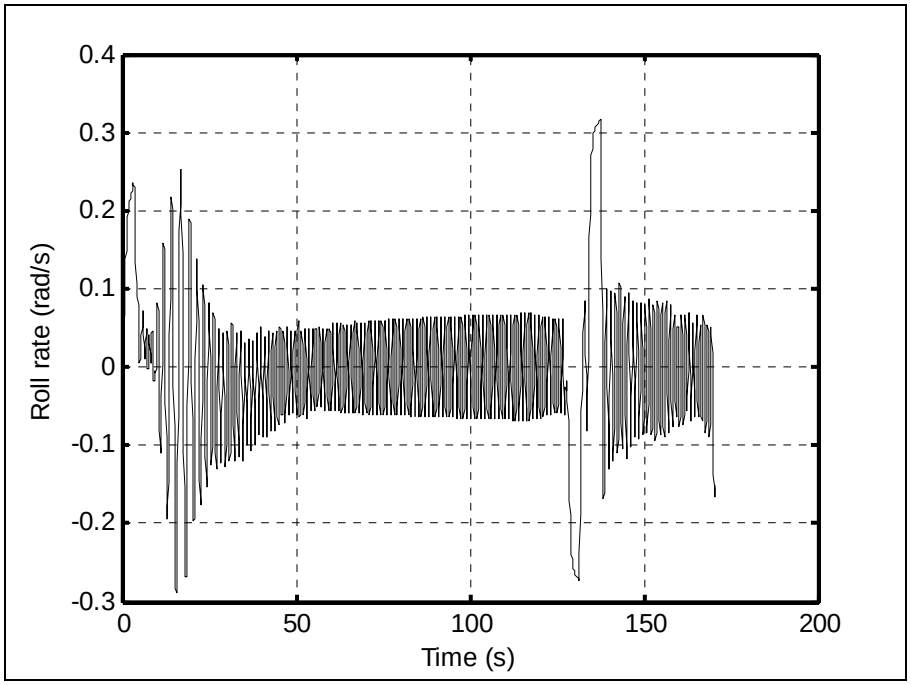

Figure 6-108 Roll rate for case V

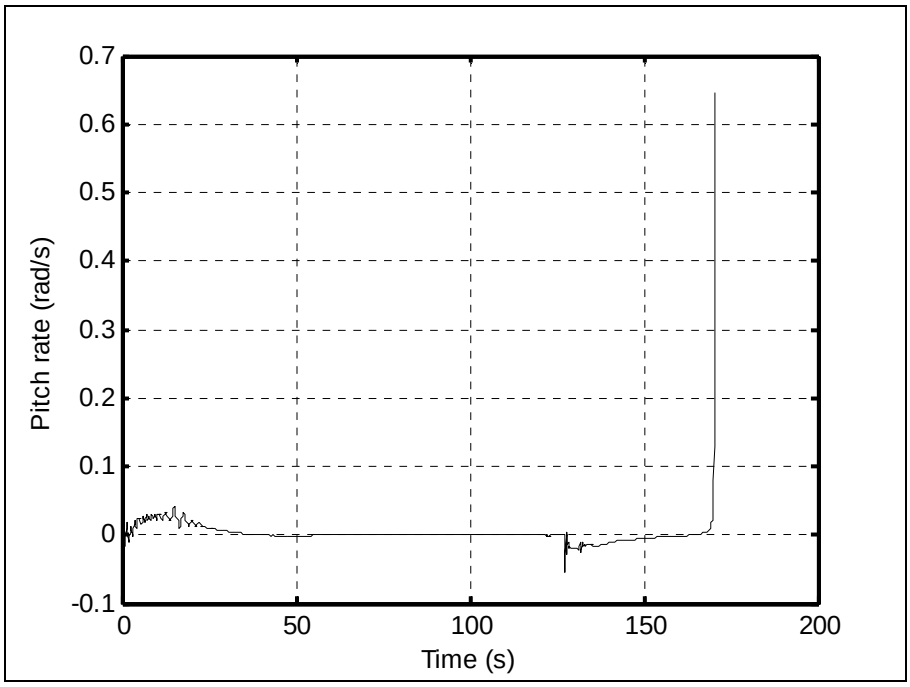

Figure 6-109 Pitch rate for case V

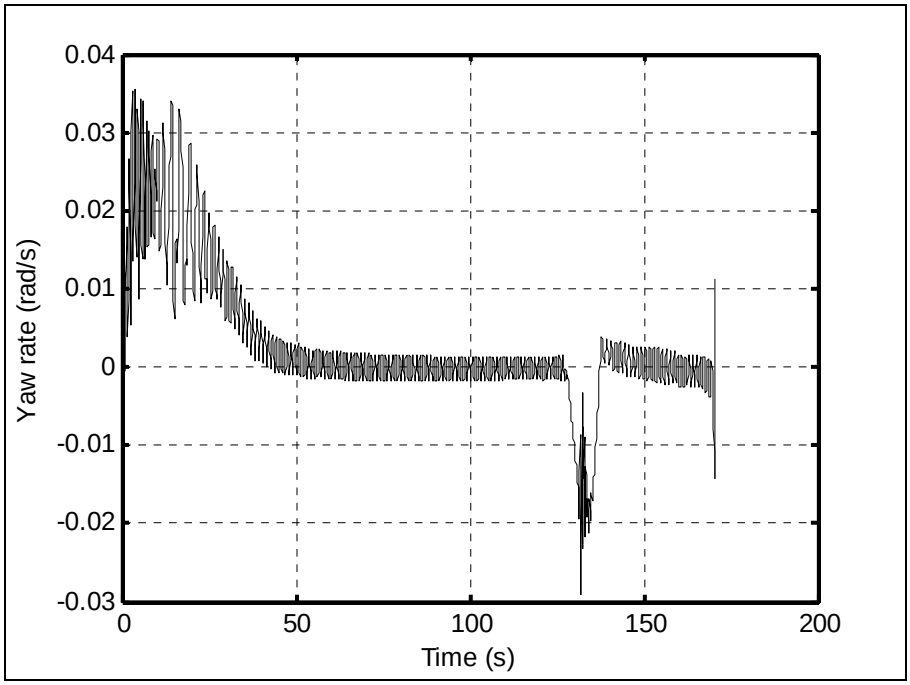

Figure 6-110 Yaw rate for case V

6.6 Case VI

In the first five cases, the target is assumed to be fixed. A warships is also among the possible targets of this type of missile. Therefore, in this case the target is assumed to have a constant velocity along the X-axis of inertial frame. Its velocity is taken as the average warship velocity which is about 16 knots equal to 8 m/s.

The initial coordinates of the target are given as 80000 m on X-axis and 10000 m on Y-axis of the inertial frame. Figure 6-111 and Figure 6-112 illustrate the trajectory of the missile in XZ plane and Figure 6-113 and Figure 6-114 illustrate that in XY plane. It is clear from Figure 6-114 that the target reaches to the X coordinate equal to 81648 m. Since the flight takes about 206 seconds and meanwhile target moves 206 seconds with the velocity 8 m/s. So, it travels 1648 m during the missile's flight. In the Figure 6-112, it is apparent that the missile hits the target's center by about 8 m error on XZ plane. According to the Figure 6-114, the missile hits the target's center by about 3 m error on XY plane. Therefore, circular error of probabilities on XZ and XY planes are not more than 10 m and 5 m respectively.

The variation of missile states are given through Figure 6-115 - Figure 6-124 and Figure 6-130 - Figure 6-132 and they vary in quite reasonable ranges. Moreover, variation of mass, center of gravity, moments of inertia about X, Y, and Z axis are given throughout Figure 6-127- Figure 6-129.

In summary, the designed controller and guidance unit of the missile enable the missile to hit the moving target with the accuracy less than 8 m.

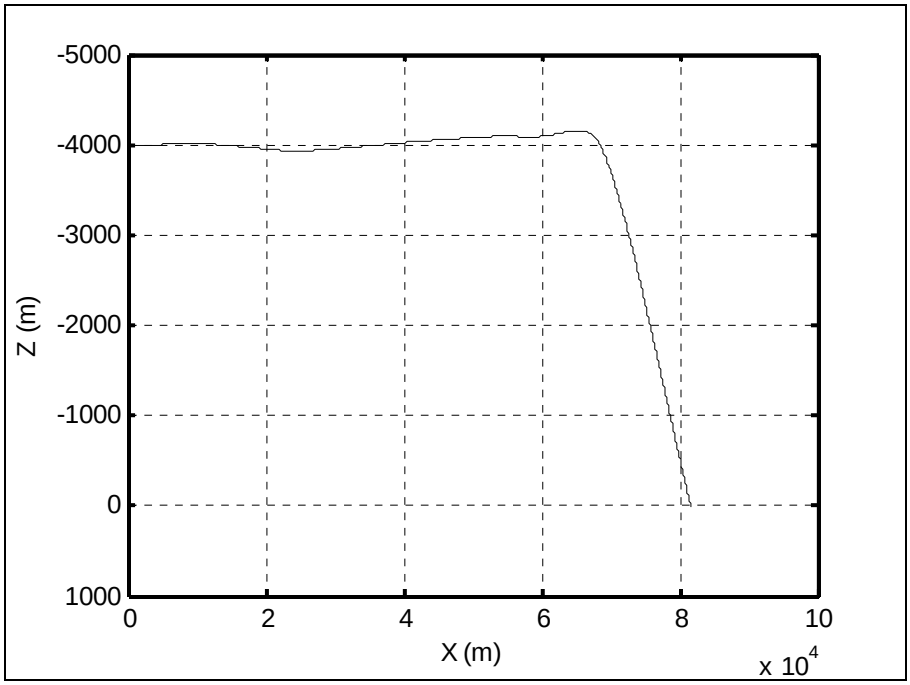

Figure 6-111 XZ plane flight path for case VI

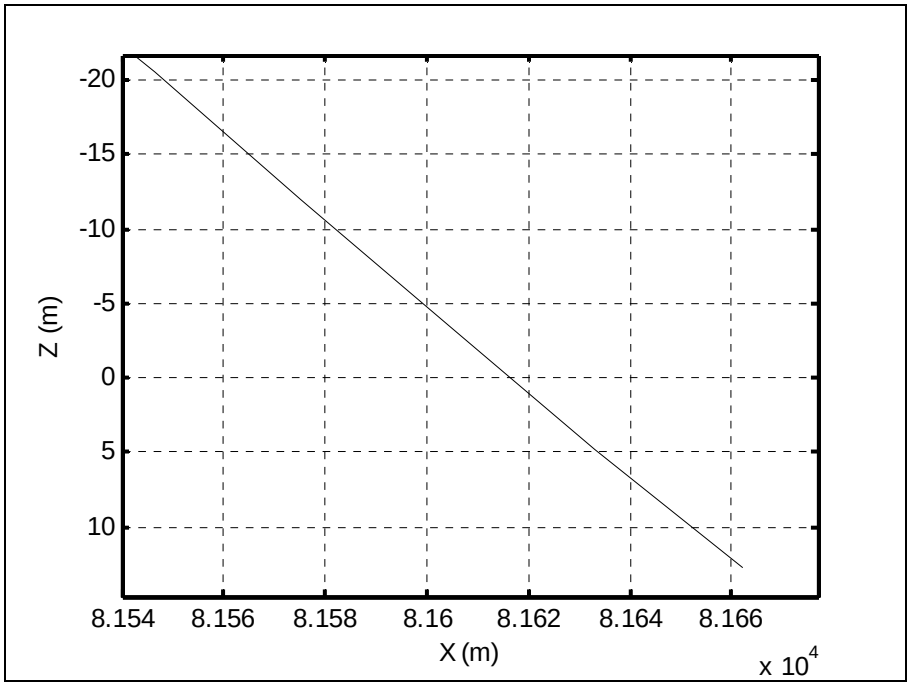

Figure 6-112 XZ plane missile-target interception for case VI

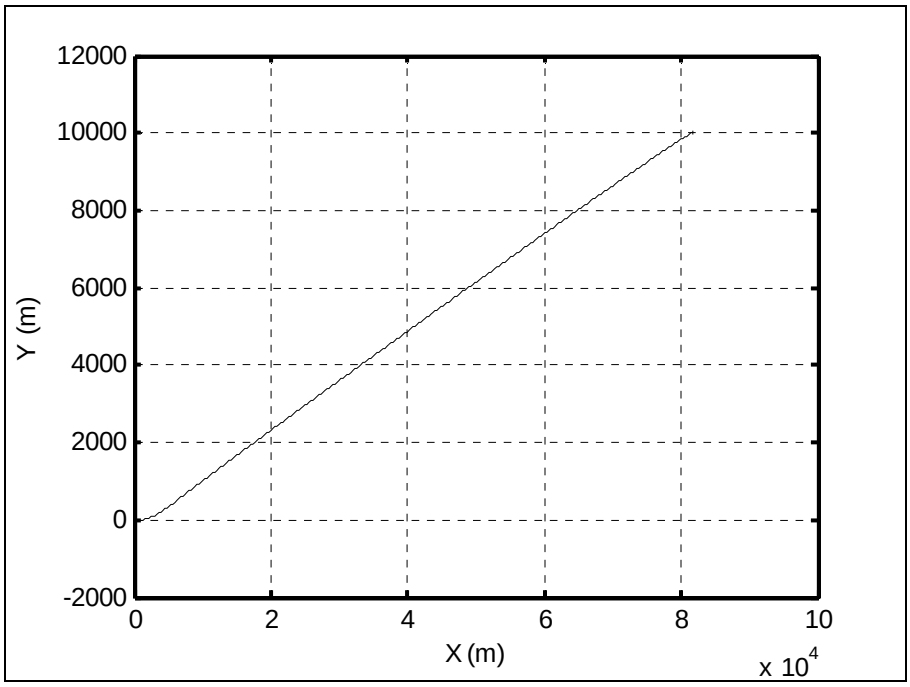

Figure 6-113 XY plane flight path for case VI

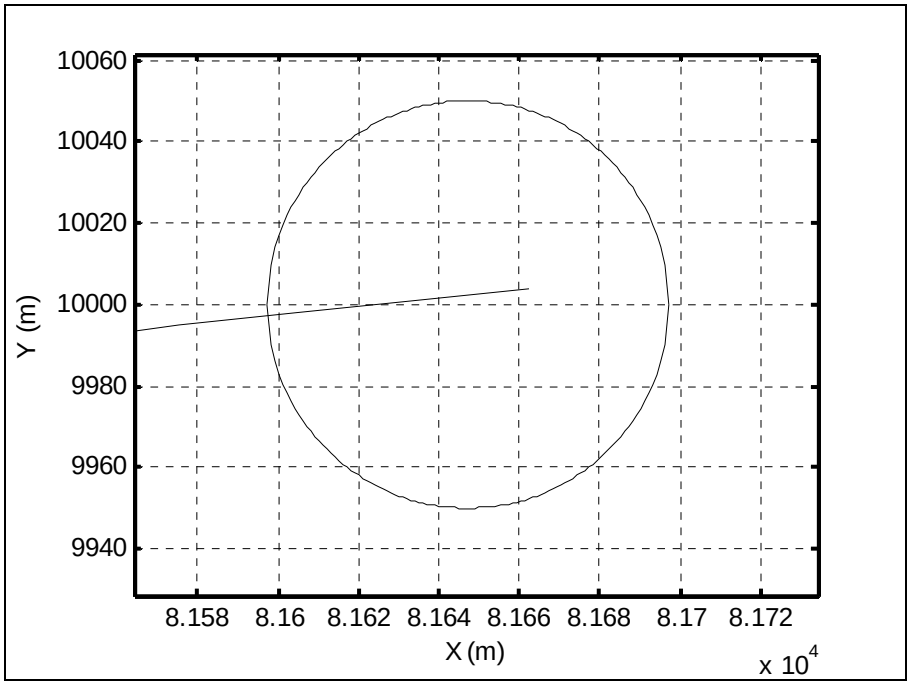

Figure 6-114 XY plane missile-target interception for case VI

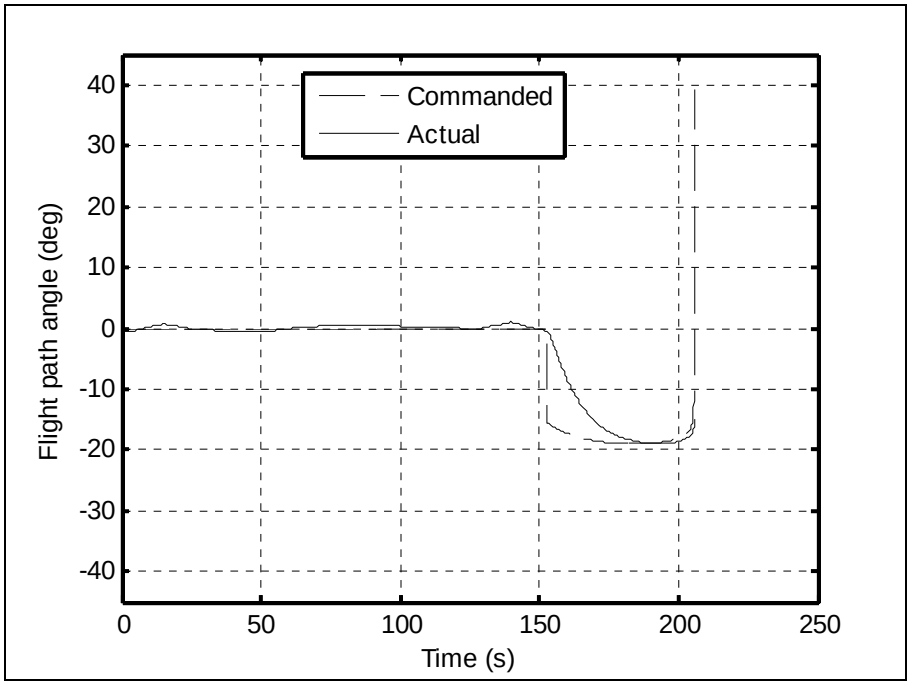

Figure 6-115 Flight path angle for case VI

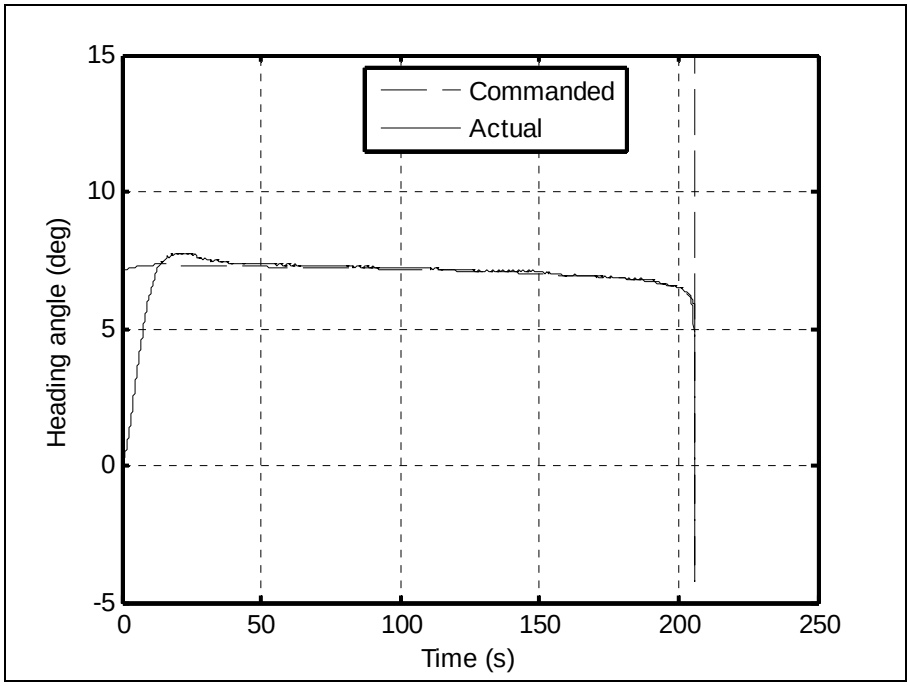

Figure 6-116 Heading angle for case VI

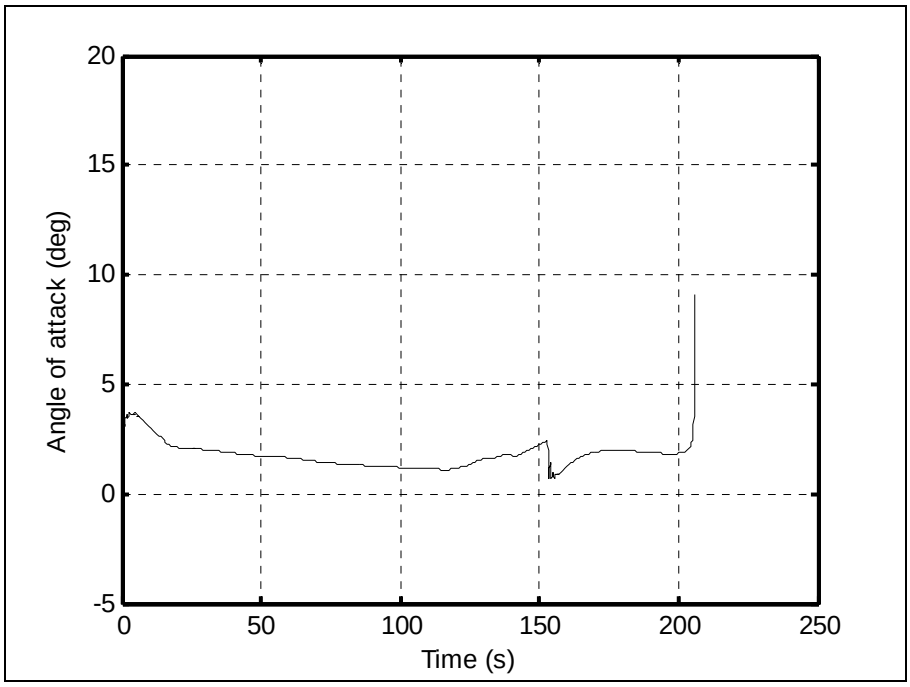

Figure 6-117 Angle of attack for case VI

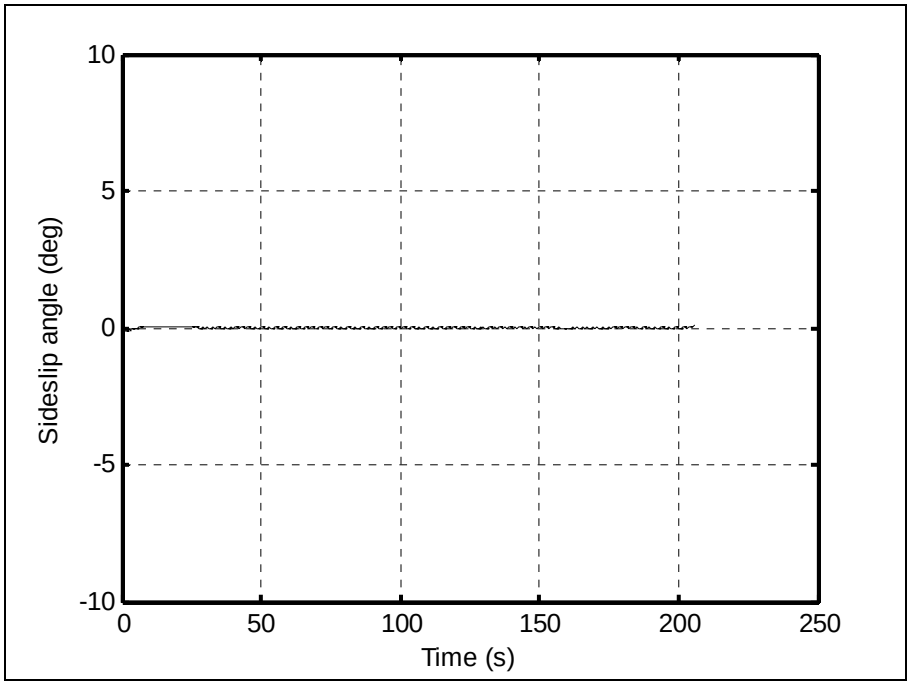

Figure 6-118 Sideslip angle for case VI

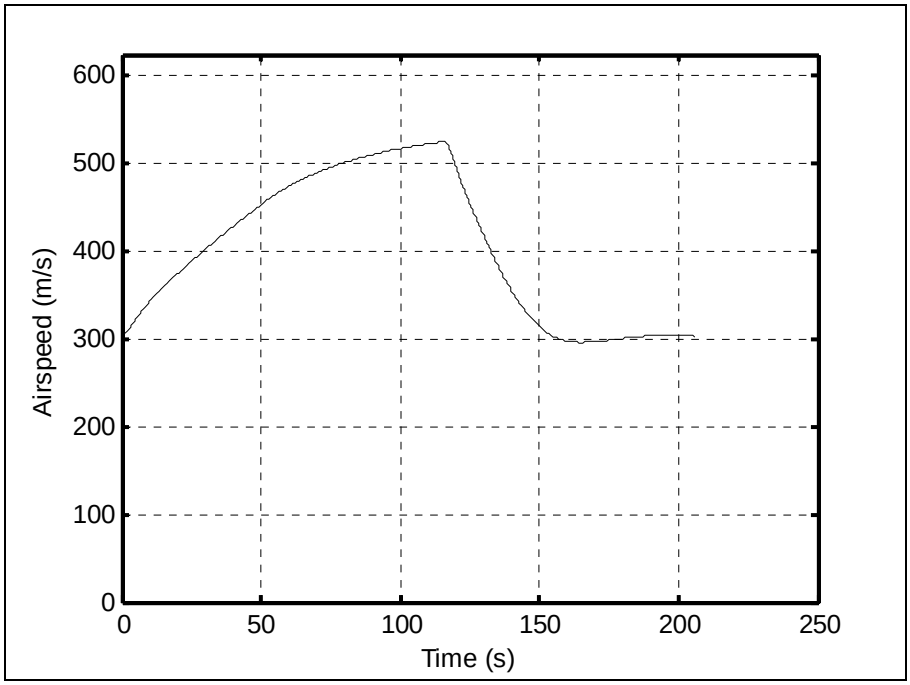

Figure 6-119 Airspeed for case VI

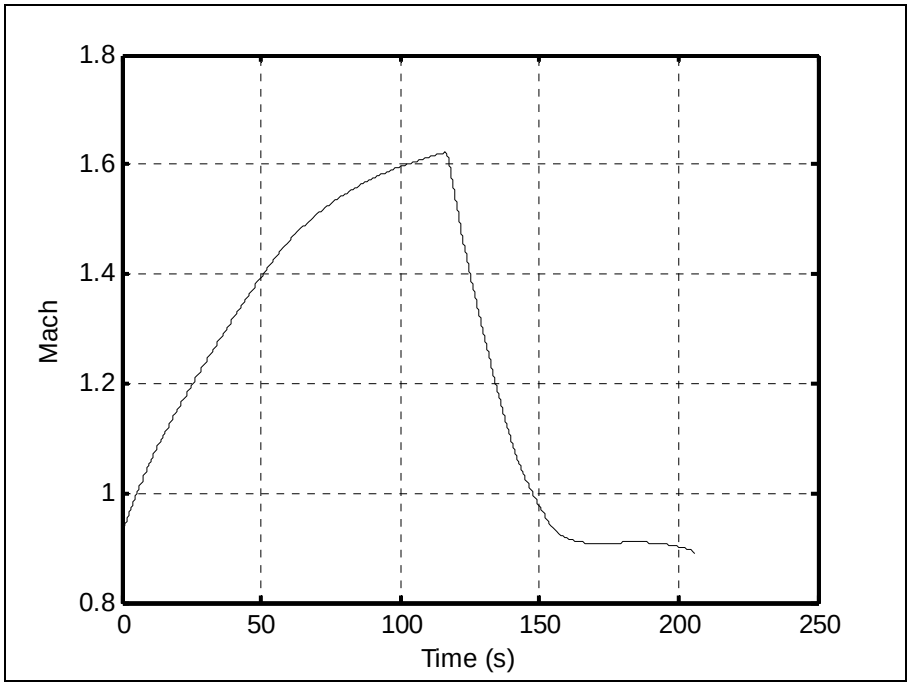

Figure 6-120 Mach number for case VI

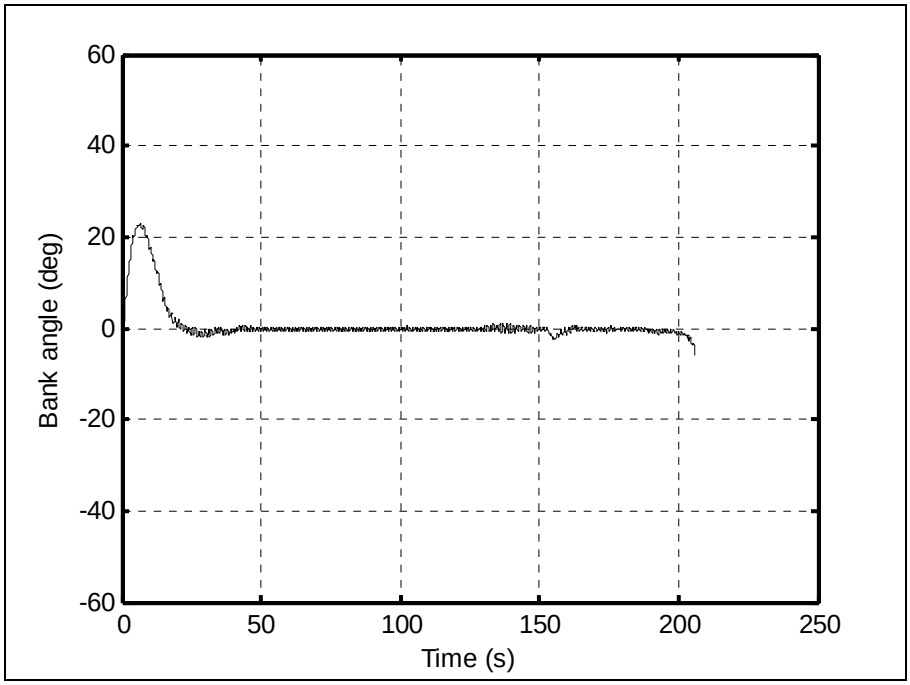

Figure 6-121 Bank angle for case VI

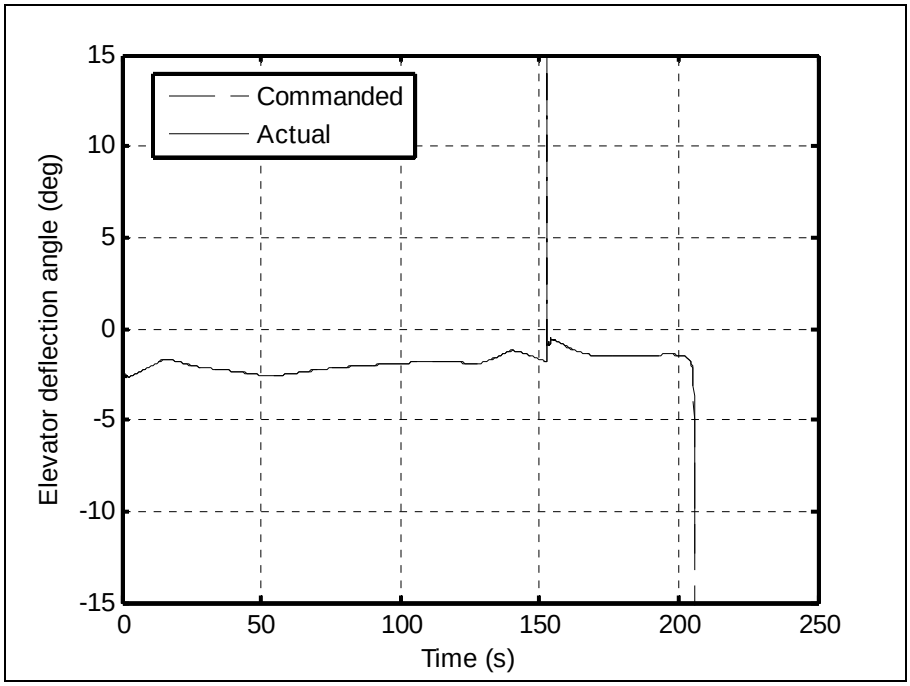

Figure 6-122 Elevator deflection angle for case VI

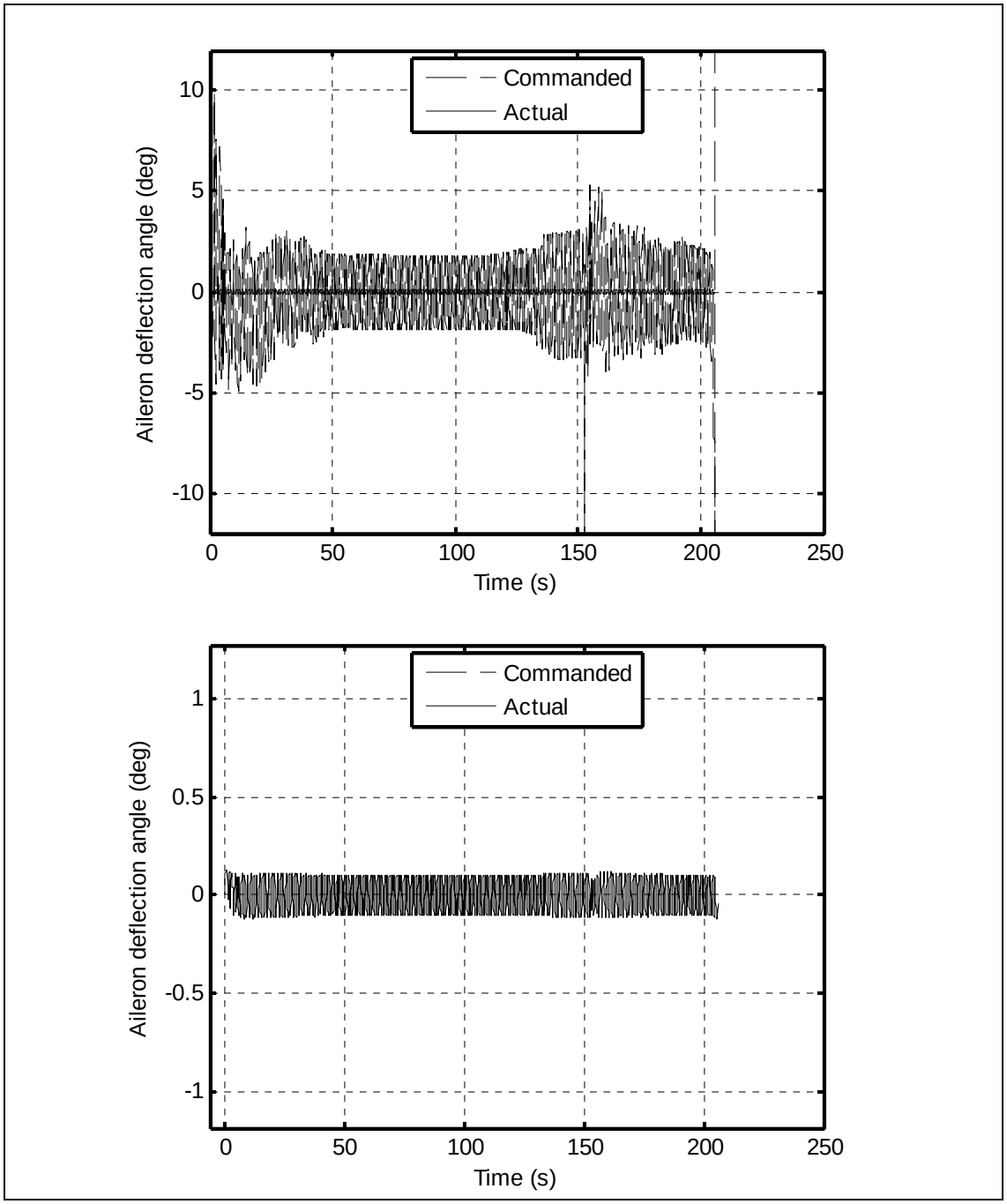

Figure 6-123 Aileron deflection angle for case VI

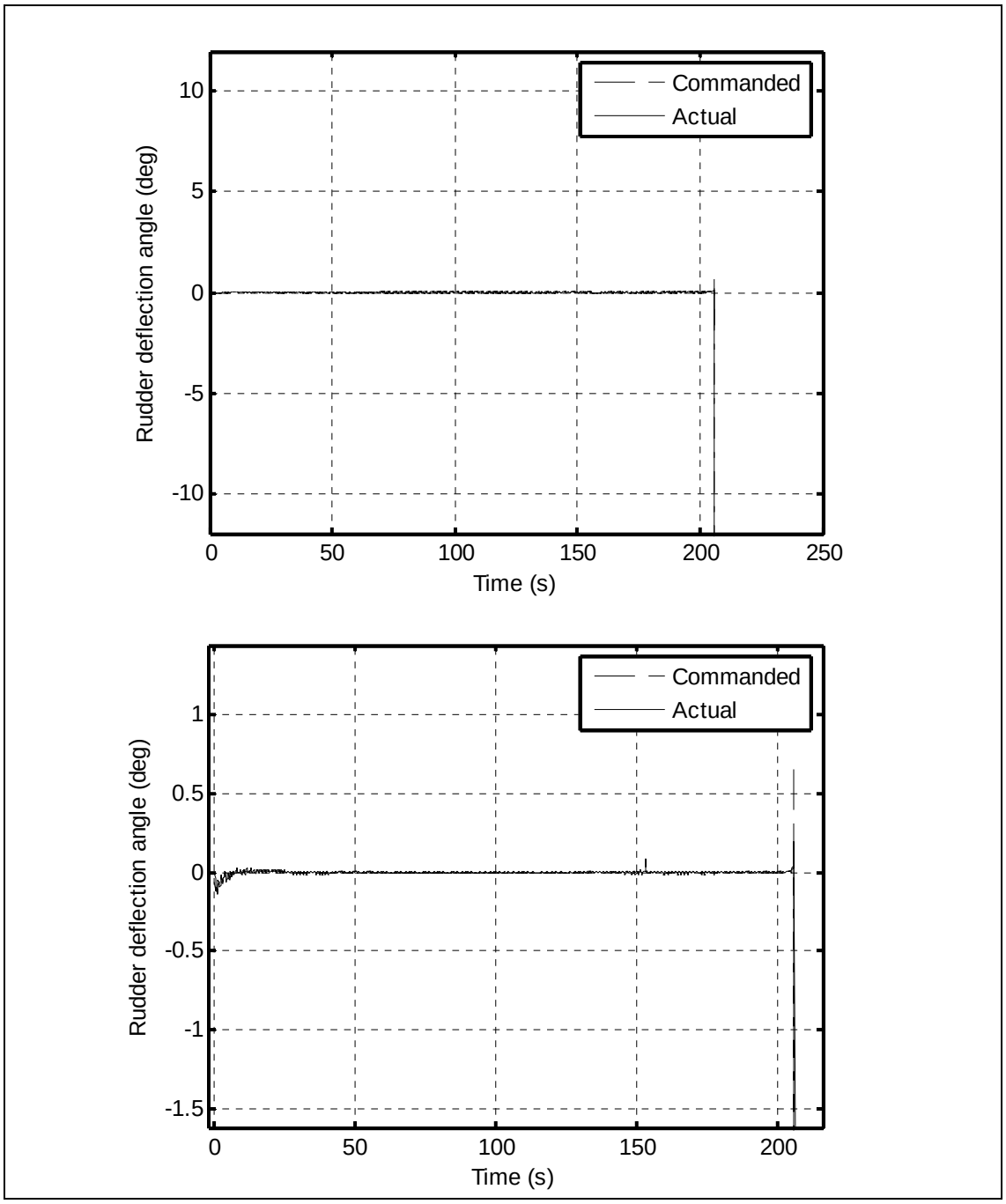

Figure 6-124 Rudder deflection angle for case VI

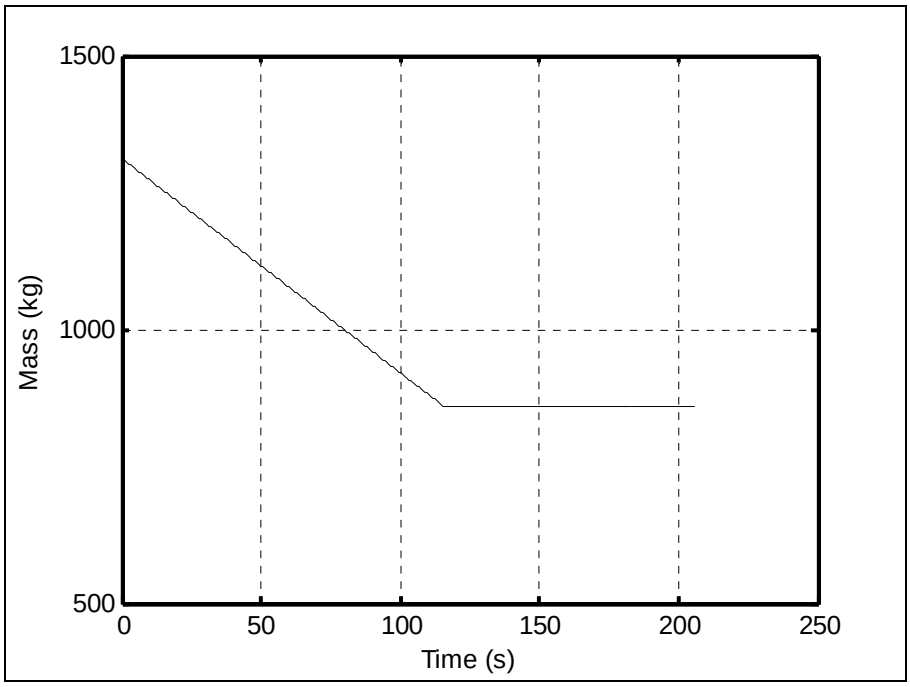

Figure 6-125 Variation of the missile's mass for case VI

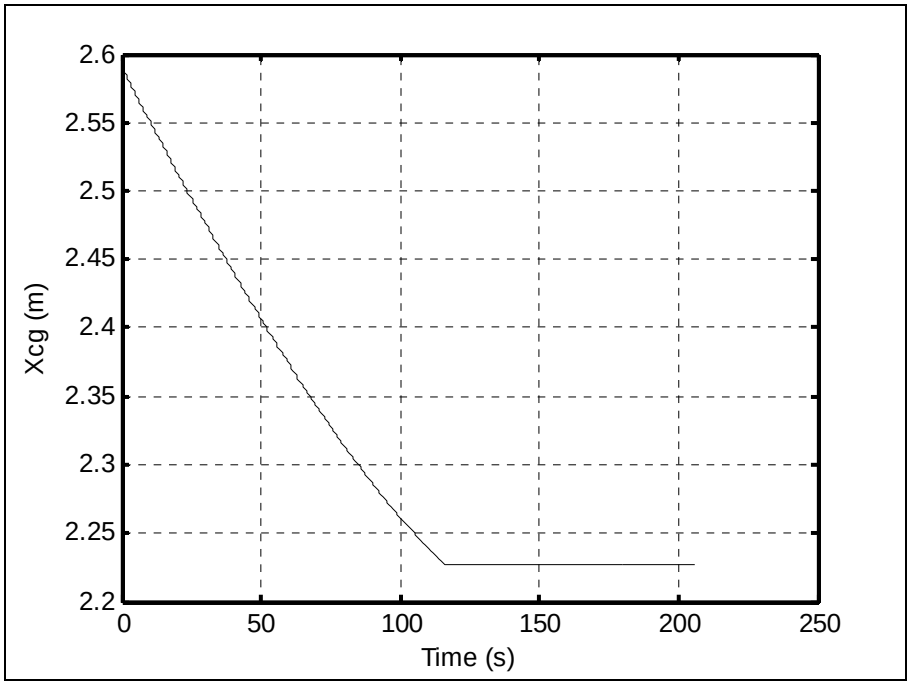

Figure 6-126 Center of gravity for case VI

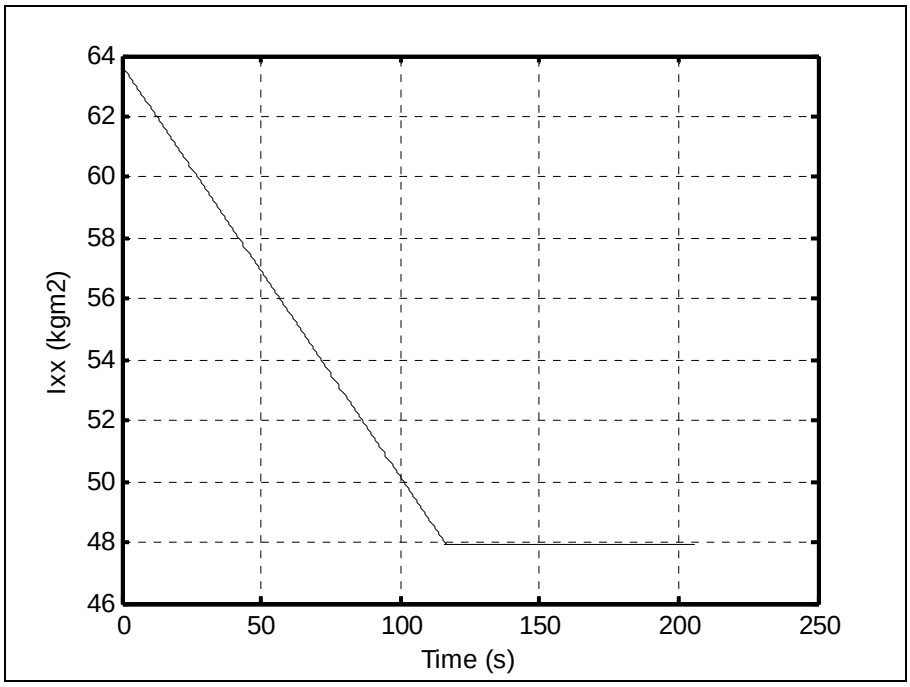

Figure 6-127 Moment of inertia about X axis for case VI

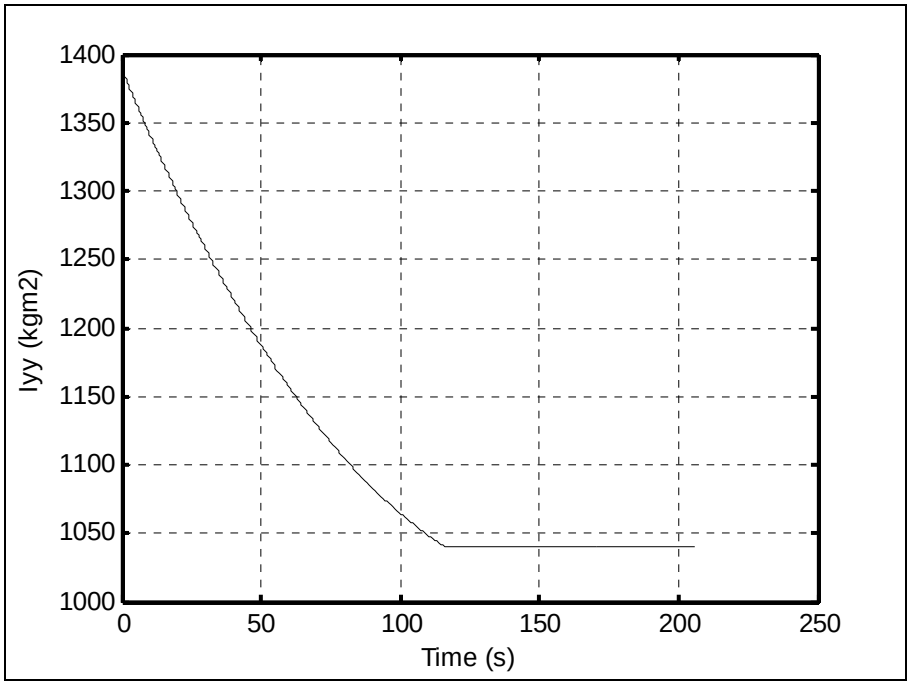

Figure 6-128 Moment of inertia about Y axis for case VI

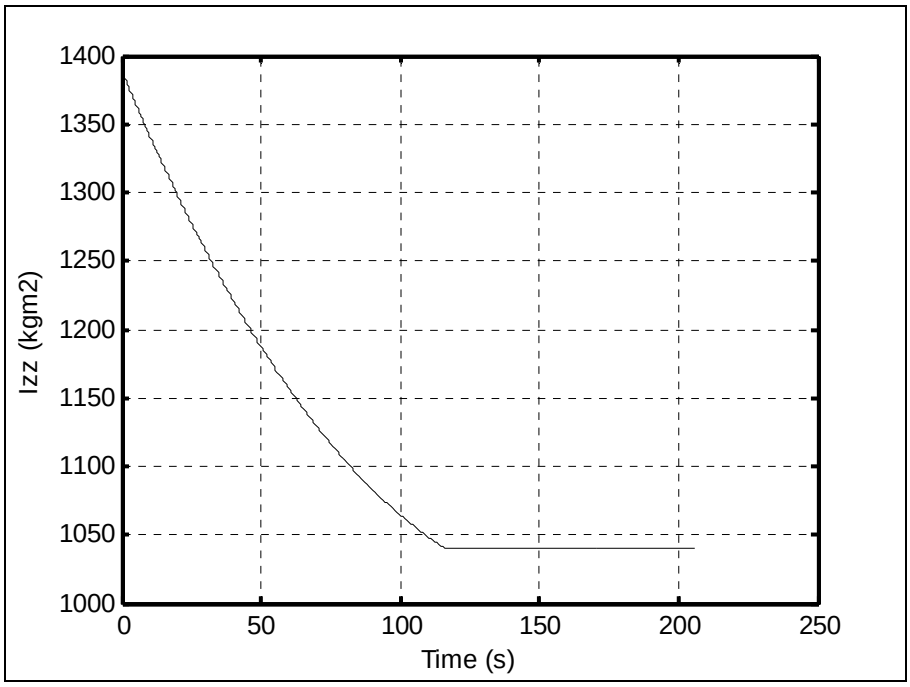

Figure 6-129 Moment of inertia about Z axis for case VI

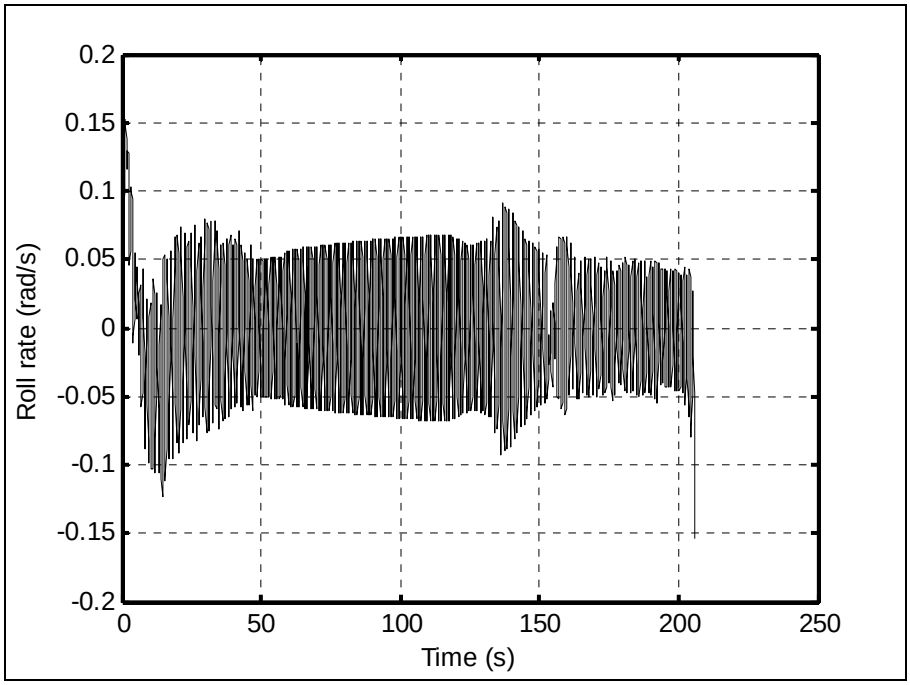

Figure 6-130 Roll rate for case VI

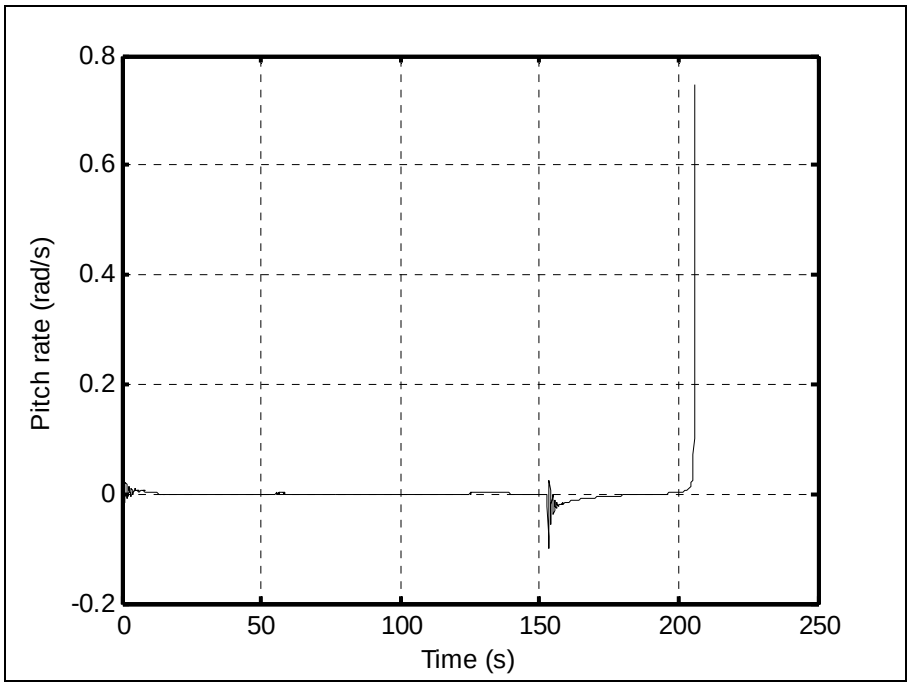

Figure 6-131 Pitch rate for case VI

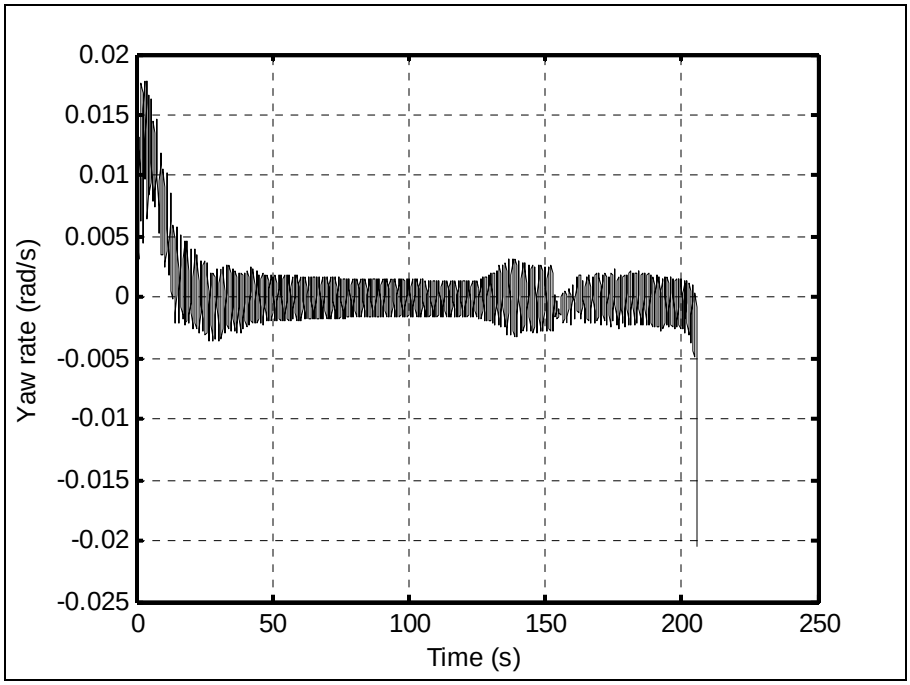

Figure 6-132 Yaw rate for case VI

CHAPTER 7

CONCLUSION

Equations of motion covering the variation of mass and moment of inertias were derived and modified for the conceptually designed air-to-surface missile, studied in this thesis. The forces and moments in the equations of motions were represented by stability derivatives. Using MISSILE DATCOM, stability derivatives and aerodynamic coefficients were obtained at different angle of attack, speed and sideslip angle. For a fixed target with 50 m radius on the Earth's flat surface, guidance method was developed. Furthermore, possible trajectories were explored. Then, nonlinear inverse dynamics controller, which is in conjunction with guidance section, was designed. Finally, the missile was modeled in six degrees of freedom and the implementation of the developed dynamics, guidance and controller method was tested on this model. Simulations were carried out in Matlab/Simulink™ environment. Simulation results were presented for six cases: cruise, arc, dive, and immediate dive trajectories and high initial angle and moving target cases.

In the first two cases, cruise and arc trajectories, target and missile interception took place after burn-out. For both cases, less than 1 m circular error of probability was obtained. In the third case, circular error of probabilities on XZ and XY planes were recorded as 6 m and 2 m correspondingly. Similar to first two cases, interception of the target and the missile also took place after burn-out in fifth case and missile hit the target with accuracy less than 6 m. Circular error of probabilities

for the fourth case, which had the closest target, on XZ and XY planes were found as 11 m and 3.5 m respectively. In brief, albeit target was very close, missile accomplished to hit the target with a CEP less than 11 m. Case six illustrated that the missile was also able to hit the moving targets. For this case, an accuracy, circular error of probability less than 8 m was obtained. Results show that the varying mass missile dynamics, guidance and control were successfully developed and deployed so that the missile is capable of hitting the target through all flight regime.

This study explores the response of the missile that is close to the real time response since the coupling between longitudinal and lateral dynamics of the missile in nonlinear inverse dynamics controller is not ignored. That is, there is no linearization involved in the controller design. The gains, proportional, derivative and integral constants of the PID controller, are kept same through the all the flight. With the gains used in this study, response is not very fast; however, it is quite acceptable for the fixed targets. What is definite from the results of this study is the necessity of resolving inertial coupling challenge. Because the corresponding solution will enable the missile be capable of achieving high maneuvers during propulsion phase. Following, the developed control design can be adapted to other missiles. For instance, a 2.75” missile can be steered to the targets which are closer than burn-out distance. Therefore, incorporation of the dynamics and controller, developed in this study, to any other missile may exactly enlarge the effective strike range.

REFERENCES

[1] I. Kaminer, A. Pascoal, P. Khargonekar, and C. Thompson, “A Velocity Algorithm for the Implementation of Gain Scheduled Controllers,” *Automatica,* Vol. 31, No. 8, 1995, pp. 1185-1191.

[2] G. Gu, J. R Cloutier, and G. Kim, “Gain Scheduled Missile Autopilot Design Using Observer-Based *H*∞ Control,” *Proceedings of the American Control Conference,* 1995, pp. 1951-1955.

[3] C. Schumacher, and P. Khargonekar, “Missile Autopilot Designs Using H∞ Control with Gain Scheduling and Dynamic Inversion,” *Journal Of Guidance, Control, And Dynamics* Vol. 21, No. 2, March–April 1998, pp. 243-243.

[4] R. A. Nichols, R. T. Reichert, and W. J. Rugh, "Gain Scheduling for H-Infinity Controllers: A Flight Control Example," *IEEE Transactions on Control Systems Technology,* Vol. 1, No. 2, 1993, pp. 69-79.

[5] G. J. Balas, R. Lind, and A. Packard, "Optimally Scaled *H*∞ Full Information Control Synthesis With Real Uncertainty," *AIAA Journal of Guidance, Control, and Dynamics,* vol. 19, no. 4, 1996, pp. 854-862.

[6] S. M. Yang and N. H. Huang, "Application of *H*∞ Control to Pitch Autopilot of Missiles," *IEEE Transactions on Aerospace and Electronic Systems,* vol. 32, no.1, 1996, pp. 426-433.

[7] D. A. Lawrence, J. H. Kelly, and J. H. Evers, “Gain Scheduled Missile Autopilot Design Using A Control Signal Interpolation Technique," *AIAA*, 1998. pp. 1394-1402.

[8] L. R. Hunt, R. Su, and G. Meyer, "Global Transformations of Nonlinear Systems," *IEEE Transactions on Automatic Control*, Vol. 28, 1983, pp. 24-31.

[9] S. H. Lane and R. F. Stengel, "Flight Control Design Using Non-linear Inverse Dynamics," *Automatica*, Vol. 24, No. 4, 1988, pp. 471-483.

[10] M. Azam and S. N. Singh, "Invertibility and Trajectory Control for Nonlinear Maneuvers of Aircraft," *Journal of Guidance, Control, and Dynamics*, Vol. 17, No. 1, 1994, pp. 192-200.

[11] Wise and J. L. Sedwick, "Nonlinear $H\infty$ Optimal Control For Agile Missiles", *AIAA Journal of Guidance, Control, and Dynamics*, vol. 19, no. 1, pp. 157-165, 1996.

[12] T. W. McLain and R.W. Beard, "Nonlinear Optimal Control Design of A Missile Autopilot", *AIAA*, 1998. pp. 1209-1216.

[13] Y. Gunbatar, *Automatic Airspace Avoidance Using Advanced Flight Control System*, M. S. Thesis, Department of Aerospace Engineering, Wichita State University, July 2006

[14] U. J. Pesonen, J. E Steck, K. Rokhsaz, S. Bruner, and N. Duerksen, Adaptive Neural Network Inverse Controller for General Aviation Safety," *AIAA Journal of Guidance, Control, and Dynamics*, Vol. 27, No. 3, 2004

[15] J. Roskam, *Airplane Flight Dynamics and Automatic Flight Controls – Second Edition*, DARcorporation, 1995, pp 3. .

[16] M. K. Özgören, *Lecture Notes on Principles of Robotics*, Department of Mechanical Engineering, Middle East Technical University, Spring 2004

[17] J. Roskam, *Airplane Flight Dynamics and Automatic Flight Controls – Second Edition,* DARcorporation, 1995, pp. 125-130 .

[18] J. H. Blakelock, *Automatic Control of Aircraft and Missiles – Second Edition*, John Wiley & Sons, Inc 1991. pp. 203.

[19] J. D. Anderson, *Introduction to Flight – Fifth Edition*, McGraw Hill, 2005, pp. 467.